PhD degree in Molecular Medicine (curriculum in Computational Biology)

European School of Molecular Medicine (SEMM),

University of Milan and University of Naples "Federico II"

Settore disciplinare: Bio/11

Genomic landscape and transcriptional regulation by YAP and Myc in the liver

Ottavio Croci

Center for Genomic Science of IIT@SEMM, Milan

Matricola n. R10752

Supervisor:

Dr. Bruno Amati

IEO, Milan

Added supervisor:

Dr. Stefano Campaner

Center for Genomic Science of IIT@SEMM, Milan

Anno accademico 2017-2018

Table of contents

List of abbreviations

4-sU
: 4-thioUridine

AML
: Acute Myeloid Leukemia

AMOT
: Angiomotin

BET
: Bromodomain and Extraterminal domain

BL
: Burkitt's Lymphoma

CDK9
: Cyclin Dependent Kinase 9

CHi-C
: Capture Hi-C

ChIP-Seq
: Chromatin Immunoprecipitation Sequencing

CK1
: Casein-Kinase 1

CTD
: C-terminal Domain

DEG
: Differentially Expressed Genes

DMSO
: Dimethyl Sulfoxide

DNase-Seq
: DNase Sequencing

Dox
: Doxycycline

ES
: Enrichment Score

GEO
: Gene Expression Omnibus

GSEA
: Geneset Enrichment Analysis

HCC
: Hepatocellular Carcinoma

HIF1A
: Hipoxia Inducible Factor 1A

HNF1A
: Hepatocyte Nuclear Factor 1 A

HNF4A
: Hepatocyte Nuclear Factor 4 A

Hpo
: *Hippo*

ID
: Identifier

IgH
: Immunoglobulin Heavy chain

MM
: Multiple Myeloma

mRNA
: messenger RNA

NELF
: Negative Elongation Factor

NGS
: Next Generation Sequencing

OHT
: 4-Hydroxytamoxifen

PFK1
: Phosphofructokinase

PRC
: Polycomb Repressive Complex

RNA Pol2
: RNA Polymerase 2

RNA-Seq
: RNA Sequencing

ROI
: Region Of Interest

S1P
: Sphingosine-1-Phosphate

Sav
: *Salvador*

Scrib
: *Scribble*

SREBP
: Steroid Regulatory Element-Binding Protein

TEAD
: TEA Domain family

TES
: Transcription End Site

Trr
: *Trithorax*

TSS
: Transcription Start Site

WT
: Wild Type

Wts
: *Warts*

YAP
: YES Associated Protein

Yki
: *Yorkie*

eRPKM
: Reads Per Million per Kb normalized on exons

Figure Index

I Abstract

This thesis is divided in three sections; the main project is described in the first part, while additional projects are developed in two appendixes.

In the main project we studied YAP, the downstream effector of the Hippo pathway, a transcriptional co-factor that plays a fundamental role in de-differentiation, cell proliferation and transformation. While its upstream regulation has been extensively studied, its role as transcriptional co-factor is still poorly understood. We show that YAP co-adjuvates the transcriptional responses of Myc oncogene to promote cell proliferation and transformation; when both YAP and Myc are overexpressed, YAP is recruited on genomic sites pre-marked by Myc, TEAD and active chromatin and potentiate the expression of cell cycle genes regulated by Myc. In addition, we show that YAP promotes cell de-differentiation by antagonizing *in cis* the expression of liver-specific genes controlled by HNF4A master regulator, thus providing a mechanism on how YAP can revert the phenotype of a differentiated hepatocyte into a progenitor cell.

In the first appendix we explain the mechanism of BRD4 inhibition, a promising strategy for the treatment of Myc-driven tumors. The efficacy of this strategy relies on the control of transcriptional elongation mediated by BRD4 on gene promoters, independently of the downregulation of Myc oncogene. Although the inhibition of BRD4 causes its genome-wide displacement on promoters, the effects on transcription are restricted to a subset of sensitive genes. This specificity relies on the fact that while most genes compensate the drop in elongation caused by BRD4 inhibition with further recruitment of RNA Pol2 on promoters and maintain a

proficient mRNA transcription, vulnerable genes are not able to promote these compensatory effects, because RNA Pol2 recruitment on these promoters is already maximized. Our results show how the impairment of elongation genome-wide can affect specific transcriptional programs.

In the second appendix we describe a new web application, Chrokit, aimed at analyzing genomic data in a fast and intuitive way. Chrokit handles a set of genomic regions of interest and performs several tasks on them, such as selecting particular subsets, computing overlaps and visualize reads enrichment of specific chromatin features interactively. The application is multiplatform and can be run on dedicated servers to maximize computational power and provide accessibility to multiple users simultaneously.

II Introduction

1 Overview of the Hippo pathway

The core of the Hippo pathway was first characterized in *Drosophila Melanogaster* and is composed of a kinase cascade that ultimately leads to the control of cell division, cell differentiation and stem cell properties (Wu et al., 2003). This pathway is apically regulated by the *Hippo* (Hpo) Ser/Thr kinase, which interacts and phosphorylate the *Salvador* (Sav) adaptor protein (Tapon et al., 2002); this leads to the phosphorylation of *Warts* (Wts) kinase and its co-activator, *Mats* (Justice et al., 1995), which in turn phosphorylates the final effector of the pathway, the *Yorkie* transcriptional co-factor (Yki) (Huang et al., 2005). If Yki is phosphorylated, it binds 14-3-3 proteins and is sequestered in the cytoplasm (Oh and Irvine, 2008). The core components of the Hippo pathway are conserved in mammals. In particular, the homologous of Hpo, Sav, Wts, *Mats* and Yki are Mst1/2, WW45, Lats1/2, Mob a/b, and YAP (YES associated protein), respectively (Zhao et al., 2010a). TAZ (transcriptional co-activator with PDZ-binding motif), the YAP paralogue, was discovered later and shares largely redundant functions with YAP (Kanai et al., 2000).

When the Hippo pathway is switched "on", YAP and TAZ are phosphorylated by Lats1/2 and inactivated, either because they are sequestrated in the cytoplasm (Hao et al., 2008; Kanai et al., 2000) and destabilized through ubiquitination and degradation by the proteasome (Zhao et al., 2010b; Liu et al., 2010). If the Hippo pathway is in an "off" state, YAP/TAZ are free to translocate into the nucleus to regulate transcriptional programs controlling cell growth, organ development, de-differentiation and tumorigenesis (Varelas, 2014). YAP/TAZ in the nucleus function as transcriptional co-activators (Kanai et al., 2000; Yagi et al., 1999) (Figure 1); being devoid of DNA binding capability, they require the interaction with transcription

factors partners in order to regulate gene transcription. Some of these transcription factors have been characterized, the most prominent being proteins of the TEA domain family member (TEAD) (Hansen et al., 2015; Ota and Sasaki, 2008).

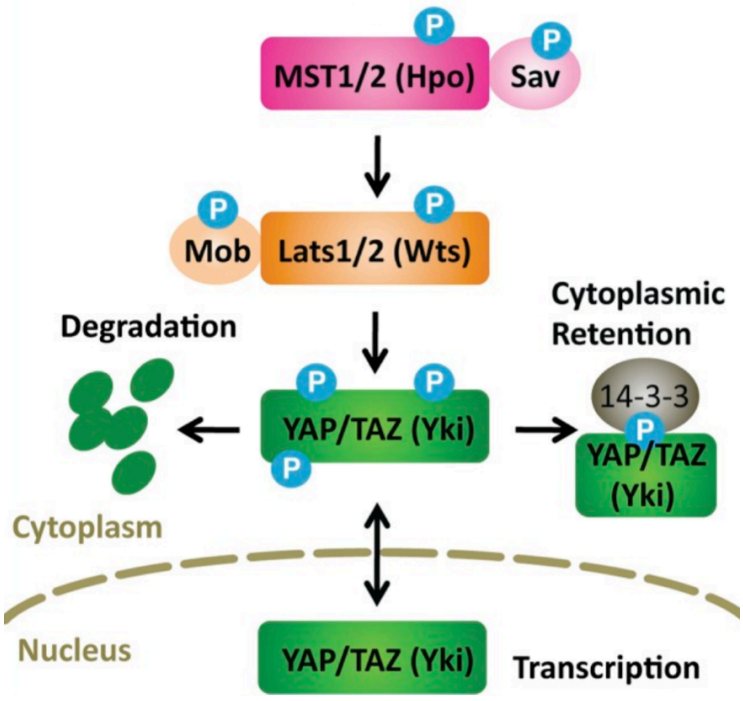

Figure 1: Overview of the Hippo pathway. Mst1/2 proteins (together with Sav adaptor protein) promote the phosphorylation of Lats1/2 proteins, which, in turn, phosphorylate of YAP and TAZ co-activators. When phosphorylated, they are retained in the cytoplasm by 14-3-3 proteins or degraded. When the Hippo pathway is "off", YAP and TAZ can translocate into the nucleus to promote transcription of target genes.

2 Upstream regulation of YAP/TAZ

Multiple external stimuli can modulate the activity of YAP/TAZ by regulating the activity of the Hippo pathway (Meng et al., 2016); in addition, Hippo pathway-independent mechanism can directly regulate YAP/TAZ activity (Meng et al., 2016; Feng et al., 2014). Below we provide a summary of the main stimuli identified so far, which are represented in Figure 2.

2.1 Mechanical forces and extracellular matrix

YAP/TAZ nuclear localization is induced in conditions of high cytoskeletal tension and when stress fibers are present, conditions that can be experimentally controlled by tweaking the stiffness of the extracellular matrix. This mechanism of regulation is dependent on the activity of Rho GTPases, actomyosin cytoskeleton (Dupont et al., 2011) and JNK1/2 kinases (Meng et al., 2016). Cell adhesion to fibronectin promotes the activation of focal adhesion kinases and the SRC-PI3K-PDK1 signaling pathway, thus inhibiting Lats1/2 (Kim and Gumbiner, 2015). Pulling mechanical forces can act on cells and induce YAP/TAZ activity via F-actin. Inhibition of its polymerization (mediated by actin capping proteins) correlates with cytoplasmic retention of YAP/TAZ; this mechanism is independent on and dominates over Hippo pathway-dependent YAP/TAZ regulation (Aragona et al., 2013). In tissues, cell growth and differentiation can be induced or inhibited by applying mechanical cues that regulate YAP/TAZ activity. The biochemical components of this mechanically induced signal transduction pathway are still poorly understood (Dupont, 2016).

2.2 Cell polarity and cell-cell contacts

Physical contact between cells is required for a correct tissue organization and involves the formation of tight and adherens junctions (Niessen et al., 2011). Some of the components in these junctions have been described as Hippo pathway regulators. Angiomotin (AMOT) is one of the essential components of tight junctions (Wells et al., 2006); it can interact with the WW motif of both YAP and TAZ proteins, thus promoting their sequestration both at tight junctions and on the plasma membrane (Zhao et al., 2011). As such, AMOT is a putative tumor suppressor, which restricts YAP/TAZ activity.

KIBRA, a protein involved in cell polarity which localizes on the apical domain in epithelial cells (Yoshihama et al., 2012) can activate Lats1 protein thus indirectly promoting the phosphorylation and inactivation of YAP (Wilson et al., 2014). In addition, KIBRA binds the PTPN14 phosphatase (Wilson et al., 2014), which, in turn, dephosphorylate YAP and inhibit its activity (Liu et al., 2013b).

Studies on skin cells revealed that α-catenin can recognize and associate to 14-3-3 protein bound by phospho-YAP: this interaction inhibits YAP activity by preventing YAP dephosphorylation mediated by PP2A phosphatase (Schlegelmilch et al., 2011).

Another regulator is Scribble (SCRIB), a determinant of cell polarity (Rodriguez-Boulan and Macara, 2014). In mammary epithelial cells, this protein forms a membrane associated complex with Mst, Lats and TAZ and promotes the phosphorylation of Lats, thereby inhibiting TAZ. During the epithelial-to-mesenchimal transition, Scribble is released into the cytoplasm and looses its binding with the Mst/ Lats /TAZ complex, as a results TAZ is also released and free to translocate into the nucleus where it controls the expression of genes controlling self-renewal of breast (cancer) stem cells (Cordenonsi et al., 2011).

2.3 Signaling through G-protein coupled receptors

Many stimuli that lead to cell growth involve soluble molecules, such as hormones and growth factors; some of these factors can also regulate the Hippo pathway activity. Sphingosine-1-phosphate (S1P) can activate S1P receptors and Rho GTPases, therefore activating YAP in a Hippo-independent manner (Miller et al., 2012).

YAP activation is important for the survival of podocytes and kidney function; in podocytes, angiotensin II binds to its G-protein coupled receptor, AT1R, inhibits Lats phosphorylation and promotes YAP nuclear translocation in an actin-dependent manner (Wennmann et al., 2014).

In general, activation of $G\alpha_s$ proteins leads to phosphorylation and inhibition of Lats and YAP, while the activation of G11/13, q11 can promote YAP nuclear translocation. In the first scenario, $G\alpha_s$ can activate cAMP and PKA, which in turn leads to the phosphorylation of Lats /YAP (Yu et al., 2013), while in the latter case, other stimuli such as S1P, LPA (Yu et al., 2012) or thrombin (Mo et al., 2012) can activate Gq11/13 and activate YAP. In both cases, Rho GTPases transduce external signals to Lats kinases.

2.4 Metabolic stress conditions

Several evidences indicate that YAP/TAZ activity can be modulated by energy stress conditions. During glucose deprivation cellular ATP levels decrease, the AMPK protein is activated and phosphorylates and stabilizes AMOTL1 protein; this, in turn, promotes the phosphorylation and cytoplasmic retention of YAP (deRan et al., 2014). AMPK can also directly inactivate YAP by phosphorylation on multiple sites (see paragraph 4.1, page 11) (Wang et al., 2015) and can phosphorylate Lats1/2, which leads to YAP cytoplasmic retention and degradation (Meng et al., 2016). In homeotic conditions, YAP is active and can promote glycolysis and GLUT3 expression, indicating a role for glucose uptake and utilization (Wang et al., 2015). High concentrations of glucose are responsible for phosphofructokinase (PFK1) activation, an enzyme involved in the gluconeogenic pathway. Other than its enzymatic activity, PFK1 can bind TEAD, and this binding promote YAP/TAZ-TEAD stabilization and activity (Enzo et al., 2015).

Lipid metabolism can also affect YAP/TAZ activity in a Hippo-independent manner. Rho GTPases require geranylgeranylpyrophosphate, a product of mevalonate pathway, for their localization on cell membrane. The mevalonate pathway is activated by SREBP1/2 transcription factors and is important for cholesterol and lipid

metabolism. Inhibition of this pathway prevents the localization of Rho GTPases on the cell membrane thus impairing YAP/TAZ activation (Sorrentino et al., 2014).

Cell proliferation and growth are processes that require a large amount of energy; when cells run out of metabolites, these processes must be terminated, and YAP and TAZ inactivation can work as a switch between high usage and low usage of nutrients (Yu et al., 2015).

While glucose deprivation and energy stress can inhibit YAP/TAZ activity, hypoxia can lead to the opposite effect in two different ways. When O_2 pressure is lowered, Lats 1/2 are ubiquitilated by the SIAH2 ubiquitin ligase and degraded, thus activating YAP (Ma et al., 2014). Moreover, in low oxygen condition, the master transcription factor Hipoxia inducible factor 1A (HIF1A) is also activated (Semenza, 2001). This factor can then bind the TAZ promoter and induce its expression (Xiang et al., 2014). HIF1A also promotes the expression of SIAH1, which in turn further stimulates TAZ activity by degrading Lats 2 kinase through ubiquitination (Xiang et al., 2014).

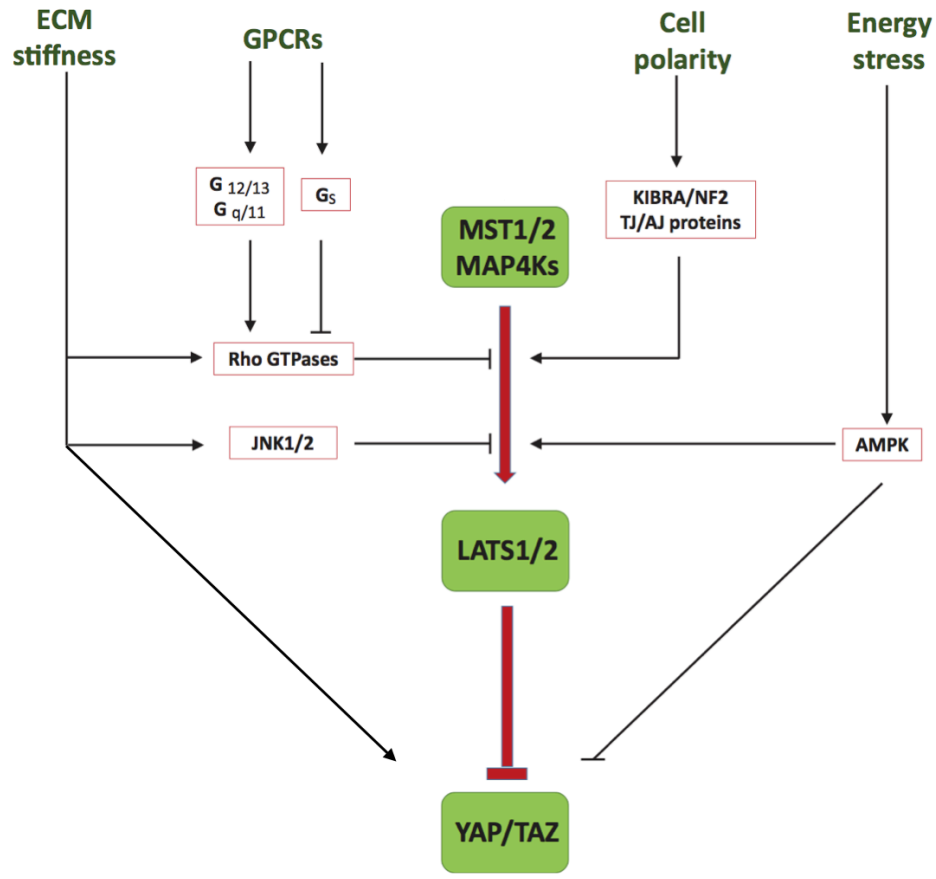

Figure 2: Different external stimuli can regulate YAP and TAZ activity. The stiffness of extracellular matrix (ECM) can activate Rho GTPases and JNK1/2 kinases, which, in turn, inhibit the phosphorylation of Lats1/2 and indirectly activate YAP and TAZ; these can be activated also by Hippo-independent mechanisms. Soluble factors can bind to G protein- coupled receptors (GPCRs); depending on which kind of G protein is activated ($G_{12/13}$, G_q or G_s), Rho GTPases can be activated or inhibited, and YAP and TAZ can be activated or inhibited, respectively. Proteins involved in cell polarity (KIBRA/NF2, adherens and tight junctions proteins) can promote the phosphorylation of Lats1/2 and YAP/TAZ inactivation. In energy stress condition, AMPK is activated: it can phosphorylate and inhibit YAP and TAZ directly or promote the phosphorylation of Lats1/2 proteins.
Figure adapted from "Mechanisms of Hippo pathway regulation" (Meng et al., 2016) Copyright © 2016 Meng et al.; Published by Cold Spring Harbor Laboratory Press.

3 Transcriptional complexes that cooperate with YAP/TAZ

YAP and TAZ, as transcription co-factors, cannot bind directly DNA, but require the presence of a transcription factor binding partner to associate to chromatin.

TEADs are the key mediators of YAP/TAZ activity in many biological systems. In NIH3T3 cells and 3D cultures of MCF10A cells, YAP effect on cell proliferation is impaired in the absence of this transcription factor. In *Drosophila*, *Scalloped* (the

TEAD homolog) is required for tissue overgrowth induced by Yki overexpression (Zhao et al., 2008). *In vitro* studies on 293T cells or in 3D cultures of MCF10A cells showed that disruption of TEAD/TAZ interaction inhibits cell growth (Zhang et al., 2009a). This applies also for YAP: pharmacological inhibition of YAP/TEAD binding with verteporfin in mouse liver reduces the hepatomegaly caused by YAP overexpression and VGLL4, a TEAD binding partner, is able to inhibit YAP/TEAD interaction and block lung cancer progression *in vivo* (Liu-Chittenden et al., 2012; Zhang et al., 2014). Recent experiments in breast cancer cells showed that TEAD is always present in YAP and TAZ genomic binding sites (Zanconato et al., 2015), suggesting that TEADs may be required for YAP/TAZ functions in this biological system.

Emerging evidence suggesting that TEADs are not the only binding partners of YAP/TAZ comes from recent studies that identified other transcription factors as mediators of YAP/TAZ co-activation.

SMAD transcription factors mediate the TGF-β signaling, leading to cell growth, differentiation or apoptosis; activation of this pathway triggers nuclear translocation of SMAD proteins and activation of their target genes (Moustakas et al., 2001). It has been demonstrated that both TAZ (Varelas et al., 2008) and YAP (Varelas et al., 2010) bind to SMAD 2/3 proteins and contribute to their nuclear accumulation and transcriptional activity. TEADs can also bind to SMAD2/3 proteins, and their knockdown leads to a reduced TGF-β signaling activity (Hiemer et al., 2014), indicating that TEADs are required for YAP/TAZ/SMAD-mediated transcriptional activation.

WW domain of YAP protein mediates the interaction with the PY motif present in the RUNX transcription factor, thus promoting the expression of its target genes (Yagi et al., 1999) and inhibiting apoptosis (Levy et al., 2008b).

YAP/TAZ binding to Pax3 is required for co-activation of Pax3 target gens, which are important for the development of the neural crest. This mechanism is independent of TEAD binding (Manderfield et al., 2014), suggesting that, depending on the biological system, TEAD may or may not be necessary for YAP/TAZ activity.

Interaction with TBX5 and β-catenin transcription factor is required for proliferation of cells of β-catenin-driven cancers (Rosenbluh et al., 2012); the assembly of this complex is promoted by a specific YAP phosphorylation (He et al., 2016). YAP can bind to and cooperate with Klf4 to induce the differentiation of the intestinal stem cells into Goblet cells (Imajo et al., 2014).

Finally, following stimulation, the tyrosine kinase receptor ERBB4 can be processed by proteolysis (such as neuregulin 1) into a soluble intracellular form (Ni, 2001); this molecule can then bind to the WW-domain of YAP through its PPxY domain (Komuro et al., 2003), and promote the YAP nuclear translocation and target gene expression, by forming the ternary complex YAP/TEAD/ERBB4 (Haskins et al., 2014).

4 Regulation of YAP/TAZ activity by post-translational modification

4.1 Post-translational modifications affecting YAP activity

YAP localization, stability or activity can be modulated by post-translational modifications that can occur on different residues (He et al., 2016).

Ser-127 is important for YAP inactivation: either Lats- or Akt-dependent phosphorylation of this residue promotes YAP cytoplasmic retention through interaction with 14-3-3 proteins (Hao et al., 2008; Basu et al., 2003).

Ser-397 phosphorylation by Lats, instead, is a pre-requisite for Ser-400 phosphorylation by casein-kinase 1 (CK1), which mediates the recruitment of ubiquitin ligases targeting YAP for proteasomal degradation (Zhao et al., 2010b). During energy stress condition, AMPK kinase can phosphorylate YAP in multiple sites

(Ser-61, Ser-94, Thr-119). Ser-61 phosphorylation inhibits YAP transcriptional activity, while Ser-94 phosphorylation impairs its binding to TEADs (Wang et al., 2015). Ser-109 residue can be phosphorylated by PKC (delta), decreasing YAP stability (Llado et al., 2015). DNA damage can activate c-Abl kinase, which can also phosphorylate YAP on Tyr-407. In this scenario YAP increases its affinity for the p73 transcription factor, promoting the expression of pro-apoptotic genes (Levy et al., 2008a) and inhibiting the expression of anti-apoptotic gene (Keshet et al., 2015). When Tyr-407 is not phosphorylated, YAP increase its affinity for RUNX and potentiate the expression of the *Itch* gene, a ubiquitin ligase which induces p73 degradation (Levy et al., 2008b). Thus the Tyr-407 phosphorylation, by acting on the regulation of p73 activity, is a switch between the pro-apoptotic and the anti-apoptotic YAP function. Tyr-407 can also be phosphorylated by other tyrosine kinases, such as YES1 and SRC kinases, to promote the assembly of the YAP-TBX5-β-catenin transcriptional complex which is essential for the proliferation of β-catenin driven cancer cells (Rosenbluh et al., 2012).

Other post-translational modifications, able to modulate YAP activity, have been discovered in the last few years.

The Set7 methyltransferase can methylate Lys-494 in YAP protein, leading to cytoplasmic localization of YAP. It is still unknown which is/are the proteins that keeps the methyleted-YAP in the cytoplasm, nor if Ser-127 phosphorylation is required (Oudhoff et al., 2013).

Lys-494, together with Lys-497, can be also a target for acetylation/deacetylation by CBP/p300 and SIRT1 proteins, respectively. This modifications can occur under specific DNA-damaging conditions, increase YAP transcriptional activity and regulate cellular responses to alkylating agents (Hata et al., 2012).

YAP protein levels can also be regulated by modifying Lys-97 and Lys-280: these residues can be either sumoylated by PML protein or ubiquitinated, increasing or decreasing its half-life, respectively (Lapi et al., 2008).

4.2 Post-translational modifications affecting TAZ activity

TAZ activity regulation is very similar to that of YAP. Its nuclear/cytoplasmic shuttling is mediated by phosphorylation of Ser-89, the homologous of YAP S127 (Kanai et al., 2000). With this modification, TAZ can bind to 14-3-3 proteins and is sequestered in the cytoplasm. Furthermore, phosphorylated Ser-311 can form a binding site for CK1 kinase, which in turn phosphorylates Ser-314, thus flagging TAZ for ubiquitination and proteasomal degradation (Liu et al., 2010).

Similarly, TAZ can be targeted for proteasomal dependent degradation if Ser-58 and Ser-62 are phosphorylated by GSK3 kinase (Huang et al., 2012). These phosphorylations can be reversed by PP1A phosphatase (Liu et al., 2011).

TAZ can also be phosphorylated on Ser-90, Ser-105, Thr-326, Thr-346 during mitosis by CDK1, preventing epithelial-to-mesenchimal transition (Zhang et al., 2015a). TAZ can be phosphorylated by c-Abl in the Tyr-316 residue, in conditions of hyperosmotic stress (Jang et al., 2012); phospho-TAZ can then associate to NFAT5 and inhibit TAZ DNA-binding and target genes expression.

Whether post-translational modifications, other than phosphorylations, may regulate TAZ activity is at the present unknown.

5 YAP/TAZ control tissue development, regeneration and cell differentiation

5.1 YAP/TAZ are required for the development of many tissues

Genetic experiments in animal models revealed a relevant role of YAP/TAZ in tissue development.

In *Drosophila*, Yki is required for eyes growth: when Yki expression was abolished, eyes showed remarkable reduced size (Huang et al., 2005). In mice, YAP is required for proper neuromuscular junction formation: mice that lack YAP expression in muscle cells show decreased muscle strength because of impaired acetylcholine receptor clustering (Zhao et al., 2017).

YAP and TAZ expression are required in nephrogenic lineage for proper kidney development (Reginensi et al., 2013), independently of their pro-proliferative functions. Cranial neural crest development also requires YAP and TAZ activation: mice in which they have been knocked out have impaired vascular development of the neural tube and craniofacial abnormalities (Wang et al., 2016). Additional evidence of their role in the nervous system comes from studies in *Zebrafish*: when YAP expression is knocked down, the size of brain and eyes is reduced, and the development of craniofacial cartilage is impaired (Jiang et al., 2009). A temporal fine regulation of Hippo-dependent YAP activation is required in post natal mammary gland development: YAP-deficient mice undergo defects in the formation of the structure of the gland during pregnancy, because of apoptosis of mammary epithelial cells (Chen et al., 2014).

5.2 YAP promotes tissue regeneration

Emerging evidence *in vivo* also pointed out a role for YAP in mediating tissue regeneration.

YAP plays an important role in the regeneration of cardiac tissue: mice in which it has been knocked out in cardiomyocytes show defects in heart functions from 6 weeks of age (Xin et al., 2013). Moreover, the overexpression of the activated mutant-form of YAP (YAP^{S127A}) in cardiomyocytes promotes regeneration of the heart (Xin et al., 2013). YAP expression is also required to maintain the intestinal stem cell pool and to promote crypt regeneration, after irradiation-induced damage (Gregorieff et al., 2015). YAP expression was also found to be correlated to the regeneration of airway epithelial cells after exposure to either naphthalene or diphtheria toxin A (Lange et al., 2015). Proper muscle formation depends on YAP expression (Zhao et al., 2017) and TEAD4 is required for muscle regeneration after notexin treatment, a drug that damage muscle cells, suggesting that YAP could play a role also in regeneration of skeletal muscles (Joshi et al., 2017).

5.3 YAP/TAZ promote de-differentiation

It is known that the Hippo pathway plays an important role in the determination of cell fate in different tissues. YAP expression is essential to sustain pluripotency in mouse embryonic stem cells, and TEADs are required to mediate this effect (Lian et al., 2010). Moreover, YAP protein binds to promoters and induce the expression of genes important for embryonic stem cells identity, such as Nanog, Oct4 and Sox2 (Lian et al., 2010). In the lung, the balance between nuclear and cytoplasmic YAP regulates the differentiation of the airway epithelium (Mahoney et al., 2014); here both Mst1/2 deletion and the ectopic expression of YAP^{S127A} result in the activation of genes regulating proliferation and migration and the concomitant repression of genes involved in metabolism and differentiation (Lange et al., 2015). In the intestine, YAP and TAZ can exert two different functions; if they interact with Klf4, they promote the differentiation of progenitor cells into Goblet cells, while if they cooperate with TEAD,

they induce intestinal stem cells proliferation. This indicates that YAP and TAZ can promote either differentiation or proliferation, depending on the context (Imajo et al., 2014). TEAD and YAP regulate the expression of pancreatic progenitor cells specific genes, while Mst1/2 activation and the consequent YAP inactivation promote the differentiation to acinar or endocrine cells (Cebola et al., 2015).

6 Pathological consequences of YAP/TAZ activation

If not properly regulated, the Hippo pathway can lead to pathological conditions (Cacemiro et al., 2017; Li and Gumbiner, 2016). Initial experiments carried out in *Drosophila* showed that if components of the Hippo pathway are inhibited (i.e. boosted Yki activity), tissues increase in size in a significant way. In particular, Wts deficiency leads to an overgrowth of different tissues, such as wings and legs (Justice et al., 1995), while *Mats* mutations leads to tumor formation in various organs of *Drosophila*. *Mats* has also a role in promoting apoptosis, and when its function is impaired, programmed cell death cannot be activated properly (Lai et al., 2005). The same phenotypes can be obtained when *Hippo* and *Salvador* proteins functions are compromised. Sav has a dual role in both promoting cell cycle exit and apoptosis, and its human ortholog (WW45) is found mutated in some cancer cell lines (Tapon et al., 2002). *Hippo* is also required for cell cycle exit, modulating the expression of cyclin E (Harvey et al., 2003).

In mammals, Hippo pathway alteration can lead to overgrowth of different tissues and cancer development as shown for *Drosophila* (Zanconato et al., 2016).

Experiments carried out in mouse models showed that conditional knock out of WW45 in the liver induces the activation of YAP, expansion of oval cells and liver tumor formation (Lee et al., 2010; Lu et al., 2010). Other *in vivo* experiments demonstrated that also Mst1/2 proteins are strong tumor suppressors: when these

two proteins are conditionally deleted in hepatocytes, mice develop focal tumors in liver parenchima (Lu et al., 2010; Song et al., 2010; Zhou et al., 2009). Single inactivation of either Mst1 or Mst2 did not result in organ overgrowth, indicating their redundant role in regulating liver size. Mst1 and 2 are also required for the correct function of the intestine: when they are deleted, YAP relocalizes in the nuclei, the differentiation of intestine epithelium is affected and adenomas start to appear in the colon (Zhou et al., 2011). In the muscles, activation of YAP is able to cooperate with TEAD and promotes rabdomyosarcoma development from satellite cells (Tremblay et al., 2014).

Clinical data further indicates the association of YAP activation in a wide variety of cancers (Zanconato et al., 2016). In the reproductive system, the ERG oncogene induces YAP activation and the development of prostate cancer; ERG and YAP are thus both expressed in prostate cancer tissues, and the expression of YAP is correlated with poor prognosis (Nguyen et al., 2015). TAZ was also found upregulated in endometrial carcinoma (Romero-Pérez et al., 2015) while YAP is over-expressed in cervical cancer tissues (He et al., 2015); here it is also stabilized by E6 HPV oncogenic protein, indicating that also viral agents can interfere with YAP function. Elevated YAP/TAZ activity has been reported in cancers of central nervous system, such as neuroblastoma (Li et al., 2015), meningioma (Baia et al., 2012) and schwannoma (Boin et al., 2014). YAP/TAZ nuclear staining and their activation is correlated also with poor patients prognosis in non-small-cell lung cancer (Lau et al., 2014), breast cancer (Di Agostino et al., 2015), and osteosarcoma (Chan et al., 2014), indicating that Hippo pathway activity can be impaired also in tumors arising from different organs.

Unexpectedly, YAP seems to have an opposite effect in hematological malignancies, such as multiple myelomas, lymphomas and leukemias. In malignant cells, which harbor extended DNA damage due to oncogene driven replicative stress, Abl1 is

localized in the nucleus but alone is not sufficient to trigger apoptosis. When YAP is activated, it interacts with Abl1, which, in turn, is able to translocate in the nucleus and induce apoptosis. Therefore, depending on the tissue, YAP can act also as a tumor suppressor (Cottini et al., 2014).

YAP dysregulation can also lead to developmental defects, without promoting tumor formation. Mst1/2 proteins suppress cell proliferation in the pancreas and are required for proper tissue differentiation; their loss leads to structural defects and impaired function of the organ (George et al., 2012). The same is true for heart: Hippo pathway inactivation (either by ablating Sav, Mst1/2, Lats2 proteins) provokes cardiomegaly and postnatal mice death (Heallen et al., 2011). Developmental defects and hyperproliferation were also observed when Hippo pathway components are deleted in lung (Lin et al., 2015) and skin (Schlegelmilch et al., 2011). These data suggest that YAP activation may or may not promote tumorigenesis depending on other factors, such as the biological system or the environment.

7 The role of YAP in the liver

In the liver, YAP plays key roles in regulating embryonic development, cell differentiation and tissue regeneration; moreover its dysregulated activity is responsible for tumorigenesis (Yimlamai et al., 2014; Hong et al., 2015; Yimlamai et al., 2015).

During embryonic development, the Hippo pathway is involved in the transition from fetal hepatoblasts to adult hepatocytes. In fetal liver, YAP and TEAD bind a specific subset of enhancers and promote expression of embryonic-specific genes in cooperation with HNF4A and FOXA2 (Alder et al., 2014), two transcription factors that play a role in lipid metabolism, bile acid biosynthesis and hepatocyte identity (Martinez-Jimenez et al., 2010; Inoue et al., 2004; Wolfrum et al., 2004; Babeu and

Boudreau, 2014; Bonzo et al., 2012; Bochkis et al., 2008). These authors suggested that upon hepatocyte differentiation, an enhancer switch can occur: HNF4A and FOXA2 can be evicted from a subset of TEAD bound enhancers and relocate on a new set of enhancers not bound by TEAD: this should promote the expression of adult hepatocytes genes (Alder et al., 2014).

YAP ectopic activation is able to de-differentiate adult hepatocytes into progenitor cells (Yimlamai et al., 2014). Moreover, Mst1/2 double knocked out represses HNF4A and FOXA2 transcriptional program, promoting de-differentiation, hepatocyte proliferation and oval cell expansion (Fitamant et al., 2015). This process is reversible, since YAP inhibition is able to restore hepatocyte differentiation (Fitamant et al., 2015).

YAP is also involved liver regeneration. Rats in which 70% of the liver was resected through partial hepatectomy can regenerate the tissue within one week. During regeneration, YAP is activated, localized in the nuclei and its target genes are expressed (Grijalva et al., 2014). In this setting TAZ cannot compensate for loss of YAP.

Finally, YAP plays an important role as oncogenic driver in the liver; when its activation is prolonged (8 weeks), tumor nodules start to appear (Dong et al., 2007). YAP-dependent liver overgrowth and tumor development strongly depend on TEAD interaction: if YAP/TEAD interaction is genetically or pharmacologically inhibited, liver cancer growth is reduced (Liu-Chittenden et al., 2012).

Clinical observations indicate that both YAP and TAZ are prognostic markers for hepatocellular carcinoma (HCC). TAZ expression in HCC correlates with poor patient outcome; its expression is required for hepatocellular carcinoma cell proliferation, invasiveness and epithelial-to-mesenchimal transition (Xiao et al., 2015). YAP was found upregulated in about 62% of HCC samples; where it displays nuclear

localization and its expression is correlated with poor tumor differentiation and prognosis (Xu et al., 2009).

III Materials and methods

Materials and methods of this project were published (Croci et al., 2017).

1 Biological experiments

1.1 Mice strains and cells

Tet-YAP mice (Col1A1-YAP^{S127A} transgenic mice) were provided by Jonas Larsson and tet-MYC transgenic mice from Martin Eilers (Van Riggelen et al., 2010). Liver-specific transgene expression was repressed in LAP-tTA transgenic mice by continuous administration of food supplemented with 625mg/Kg of doxycycline. For long-term activation, 8 weeks old mice were shifted to a regular diet (i.e. doxycycline free) at 4 or 13 weeks. For short-term transgene activation (which was under the control of Rosa26 ubiquitous promoter) (Kisseberth et al., 1999), mice were fed with doxycycline-supplemented food for 2 days.

MycER was activated in 3T9MycER murine fibroblasts (Sabò et al., 2014) by the addition of 4-hydroxytamoxifen (OHT, 20-400nM), while YAP^{S127A} was induced by 2 µg/ml doxycycline and ethanol was used as control.

1.2 Chromatin immunoprecipitation

For Myc, TEAD, Histone Marks and RNA Pol2 ChIP, 3T9 fibroblasts or dissected liver/tumors were fixed with 1% formaldehyde in PBS and quenched with 0.125M of Glycine. For YAP ChIP, fixation was performed by a double step approach with 0.5 M DSG (Di-(N-succinimidyl)-glutarate) for 45 min and then 1% formaldehyde (FA) in PBS 12 min. Fixed cells or tissues were further processed as previously described (Sabò et al. 2014).

Cells or liver tissue/tumoral nodules were lysed with RIPA buffer (20 mM HEPES pH7.5, 300 mM NaCl, 5 mM EDTA, 10% Glycerol, 1% Triton X-100) supplemented with MINI-complete Protease Inhibitor Cocktail Tablets (Roche) and phosphatase inhibition (0.4 mM ortovanadate, 10 mM NaF) and sonicated (Branson). Cleared lysates were quantified by Bradford assay, run on a SDS-page and immunoblotted with the indicated primary antibodies. Chemiluminescent detection after incubation of the membranes with the appropriate secondary antibody, was done through a CCD camera using the ChemiDoc System (Bio-Rad).

1.3 Antibodies

The following Antibodies were used for ChIP: H3K4me1 (Abcam, ab8895), H3K27ac (Abcam, ab4729), H3K4me3 (Active Motif, #39159), MycN262 (Santa Cruz, sc 764) and RNA Pol2 N20-X (Santa Cruz, sc-899), YAP 63.7 (Santa Cruz, sc101199), TEAD (ARP38276_P050, Aviva Systems Biology). Normal rabbit IgG (Santa Cruz, sc-2027) was used as background control.

2 Data analysis

2.1 Read filtering

ChIP-Seq and RNA-Seq libraries were sequenced using Illumina HiSeq 2000 instrument, to produce 50 bp reads, which were filtered using fastQC program v. 0.9.3 (Andrews, 2010).

PCR artefacts can occur in every NGS experiment, leading to high reads duplication levels; in order to overcome this problem, unique reads were kept, while duplicate reads were thrown.

Depending on the quality of the experiment, each base pair of sequenced reads comes with a score (the Phred score) that represents the probability of a base call in a given position; this score is defined as – 10*log10 (p), where p is the estimated probability of the base-call (Ewing et al., 1998). Base pairs at the 3' end of the read have, on average, lower scores than those on the 5' end; this is because the sequencing carried out by Illumina sequencer involves synthesis of oligonucleotides, that is not synchronous for all the reads (Fuller et al., 2009). For that reason, nucleotide that came with a score lower than 20 were considered as not determined, and were considered as "N"; this process, known as "masking", was carried out using fastqMasker (with options –Q 33 –q 20 –r –N –v -i), that is part of FASTX toolkit v. 0.0.13.2 (http://hannonlab.cshl.edu/fastx_toolkit/). Then, a read was discarded if 3 or more nucleotide were marked as "uncertain".

2.2 Primary analyses: reads alignment

Upon the filtering step, reads were aligned on the mm9 genome assembly (Meyer et al., 2013). Single-end or paired-end sequencing reads were obtained if a Chip-Seq or RNA-Seq experiment was carried out, respectively.

Single-end reads alignment (ChIP-Seq). ChIP-Seq single end reads were aligned using BWA program v. 0.6.2 (Li and Durbin, 2009), to find the position of each read in the genome. This program implements the Burrows-Wheeler transform algorithm (BWT) (Burrows and Wheeler, 1994) and the backward search (Ferragina and Manzini, 2000). These algorithms are fundamental for read mapping, since a brute force search for each read on the genome would be infeasible from a computational point of view. Briefly, the BWT algorithm takes the string on which the mapping should be carried out (in this case the sequence of the genome) and find all possible

combinations by rotating the string. All the rotations of the string are sort in lexicographical order, and the last column of the matrix obtained is the BWT of the original string; this is finally used in the backward search to find the position of each read.

Paired-end reads alignment (RNA-Seq). This algorithm uses the BWT of the genome and the backward search as before, to map each read in an efficient way. For paired end read mapping (RNA-Seq experiments), tophat v. 2.0.8 software (Trapnell et al., 2009) was used. This program can map the reads taking into account the splicing of the genes. In a first step, tophat align the reads that can be mapped in a contiguous way. In a second step, the program uses the first alignment to find possible combinations of exon-exon junctions and carries out a second alignment using these junctions as a template (https://ccb.jhu.edu/software/tophat/manual.shtml).
On average, after filtering and alignment steps, about 1/5-1/4 of successfully mapped reads were obtained from the original reads from the instrument.

2.3 Secondary analyses: peak calling, DEG calling and expression quantification

*ChIP-Seq peak calling***.** In order to find the genomic locations that are enriched in mapped reads of a particular transcription factor or histone marks in ChIP-Seq experiments, a peak calling analysis was carried out. For this purpose, the Model-based Analysis of ChIP-Seq (MACS) software v. 2.0.9 was used (Zhang et al., 2008). The aligned reads mapped on the "+" strand and "-" strand are generally concentrated on the edges of the ChIP-Seq fragments, which are more accessible, compared to the centre of the fragment that is occupied by the transcription factor and is not accessible. The length (d) calculated by MACS is used to shift the reads on the 3' end by d/2, improving the prediction of the transcription factor-DNA interaction site.

Then, the program scans the genome to find genomic locations that are particularly enriched in shifted reads, and are thus marked as "bound" by the transcription factor. An input ChIP-Seq (a ChIP-Seq in which no antibody was used or immunoprecipitating the transcription factor of interest, i.e. the entire genome) is subtracted for each step of the scanning, to remove the background noise.

Statistically significant peaks were defined if their p value was < 10^{-5} for transcription factors and 10^{-8} for histone marks. The enrichment of reads inside defined genomic regions (for example, ChIP-Seq peaks) was calculated using the functions implemented in compEpiTools package (Huber et al., 2015; Kishore et al., 2015). Briefly, the enrichment was defined as the sum of the number of the reads for each base pair of a genomic range; then, this number was normalized by the number of aligned reads (obtaining rpm, reads per million). To calculate read density, this number was further normalized by the width of the genomic regions (obtaining rpm/bp, reads per million/base pair).

RNA-Seq differential gene expression and quantification. In RNA-Seq experiment, finding the number of reads that fall into exons of the genes of a particular genome is a required step. To this aim, featureCounts v. 1.4.5 program was used (Liao et al., 2014). Count files obtained were used for clustering analyses and for downstream analyses: differential gene expression and expression quantification.

To find genes that were differentially expressed in two different conditions, DESeq2 R package was used (Love et al., 2014). This program takes as input the count files from the previous step and finds the genes whose expression differs significantly. DESeq2 fits a negative binomial distribution to model RNA-Seq count data, and finds the genes whose log2 fold change in gene expression deviates from this distribution. The log2 fold change given by DESeq2 of a specific gene is shrunken according to the mean

level of the expression among replicates and to the variability of the expression. Thus, the less a gene is expressed, as well as the more variable the expression of a gene is, the more the log2 fold change is shrunken.

Expression was quantified as eRPKM (reads per million per Kb normalized on exons). Genes were defined as deregulated if their p adjusted was < 0.05 and their absolute value of log2 fold change calculated by DESeq2 was >0.5 for 2d liver and 3T9 cells, while >1 for pre-tumoral liver and liver tumors.

All primary and secondary alignments were carried out using HTS-flow (Bianchi et al., 2016).

2.4 Motif finding analysis

Motif finding analysis was required to find transcription factors that could cooperate *in cis* with a given ChIP-ed transcription factor. This was carried out using PscanChIP tool (Zambelli et al., 2013). This tool finds the over-represented sequences under ChIP-Seq peaks summits, and compare them with Jaspar 2016 database (Mathelier et al., 2016), to find which transcription factor the motif corresponds to. PscanChIP outputs two p values in motif finding analysis, one global and one local.

The global p-value represents the probability of finding a specific motif in a subset of query regions relatively to all the regions accessible by transcription factors in a given cell line; low global p values are found when the ChIP-ed factor act as a dimer with another transcription factor binding partner.

The local p-value represents the probability of finding a specific motif in a query genomic region compared to the flanking regions. This can happen when two transcription factors interact together but only in a specific subset of promoters with specific functions.

For motif finding analysis a window around [-75; +75] from the peaks summits was used, and the average of local/global p value was shown.

2.5 Gene set enrichment analysis

The function of a given group of genes was determined through a geneset enrichment analysis (GSEA) (Subramanian et al., 2005) using the java GSEA application (http://software.broadinstitute.org/gsea/index.jsp). Briefly, a set of genes sorted by a specific feature (in this case, log2 fold change in gene expression between two conditions) is given in input to the algorithm. Then, for each gene in the ranked list, the programs finds if that gene is present also in the geneset of the database, and, if present, an enrichment score (ES) is increased, otherwise is decreased. To address whether a geneset found is statistically significant or not, the same walk through the genes of the query is done by shuffling randomly the order of these genes multiple times (10^4), forming a null distribution by which is possible to calculate a p value. In the analyses, top 10 hits of GSEA results were considered, if the absolute value of their enrichment score was higher than 2 and their p adjusted was lower than 0.01.

2.6 Definition of promoters/genebody/intergenic regions and super-enhancers

The location of a genomic region (i.e. ChIP-Seq peak) was assigned as follows. Genomic regions overlapping with at least 1 base pair (bp) with any annotated promoter (defined as [-2000; +1000] genomic window from TSS) were defined as belonging to promoters. The rest of the regions were considered part of genebodies if they overlapped with at least 1 bp with any transcript. All genomic regions not assigned were defined as "intergenic". Annotations were performed with the R annotation packages of Bioconductor TxDb.Mmusculus.UCS*C*.mm9.knownGene (Meyer et al., 2013) for all mouse experiments (liver and 3T9 cells).

2.7 RNA Pol2 stalling index

The RNA Pol2 stalling index (Rahl et al., 2010) was defined as SI=reads Prom/reads GB, where "reads Prom" are the library-normalized reads at promoters, defined as [-300; +300] interval from TSS, while "reads GB" are the library-normalized reads at genebodies, defined as [TSS+300; TES+300] interval. Genes shorter than 600 bp were excluded from the analysis, and only genes with an RNA Pol2 peak onto their promoters were considered. For average profile plots, genes were expanded 20% before TSS and above TES, divided into 150 bins and the reads were normalized by both library size and gene length. The function to calculate SI was implemented in compEpiTools package (Kishore et al., 2015).

2.8 Public datasets

External data were retrieved from GEO database (Edgar, 2002). Adult and embryonic HNF4A ChIP-Seq data were retrieved from GEO accession IDs GSM2055887 and GSM1318181.

Chip-Seq and expression data of mouse liver data (ChIP-Seq, RNA-Seq) were deposited under the accession ID GSE83869.

IV Results

The results are divided in two sections. In the first part (Results part 1, page 29) we describe the binding of YAP and TEAD to the genome and how they regulate chromatin and transcriptional programs. In the second part (Result part 2, page 67) we show the mechanism of YAP and Myc cooperation in promoting cell proliferation.

1 Results part 1: Genomic analysis of YAP and TEAD in the liver

1.1 Design and rationale of the study

The Hippo pathway plays an important role in liver function: when this pathway is deregulated, YAP activation can promote hepatocyte de-differentiation, proliferation and tumor formation (Camargo et al., 2007). Moreover, clinical data showed that YAP is overexpressed in >50% of hepatocellular carcinoma samples (Xu et al., 2009) (see paragraph II7, page 18).

In the recent years, many efforts focused on the study of the upstream regulation of this pathway, in particular how soluble factors and mechanical cues could modulate the activity of YAP and TEAD (Yu et al., 2015). However, the mechanisms by which YAP and TEAD activation translate these external stimuli into transcriptional regulation are poorly known. To better investigate these aspects, we took advantage of mouse models that expressed the constitutively active form of YAP (YAP^{S127A}) and we focused our attention on the effects of YAP activation in the liver.

The R26-rtTA; tet-YAP^{S127A} mouse model was used to evaluate the short-term response upon YAP activation; in this model the rtTA element is in the Rosa26 locus, ensuring a ubiquitous YAP expression by feeding mice with doxycycline for 2 days. Unfortunately, this model could not be exploited to perform long-term analyses, since prolonged ubiquitous activation of YAP caused mice death, due to intestinal problems.

The long-term effects of YAP activation were evaluated using LAP-tTA; tet-YAP^{S127A} mice; in this model, ectopic YAP transcription is restricted to the liver, because it is under the control of liver-specific LAP promoter (Descombes et al., 1990). YAP expression could be switched on by removing doxycycline from the mouse diet. Using this model we analyzed the effects of YAP induction for 4 weeks and 13 weeks.

In the lab, we observed that short-term YAP induction (i.e. 2 days) did not alter significantly the liver tissue (De Fazio, personal communication); however, 4 weeks YAP induction led to a massive cell proliferation and hepatomegaly, characterized by hyperplasia of poorly differentiated hepatocytes, as previously reported (De Fazio, personal communication) (Camargo et al., 2007).

Examination of livers of LAP-tTA; tet-YAP^{S127A} after 13 weeks of doxycycline free diet revealed the appearance of focal tumoral lesions (De Fazio, personal communication).

Here by using ChIP-Seq and RNA-Seq experiments we profiled the genomic landscape of YAP and TEAD following YAP activation in the liver. In particular, we asked which were the genomic loci occupied by YAP and TEAD, how YAP and TEAD binding can influence chromatin modifications at both promoters and distal sites, which were the transcriptional programs regulated by either short- and long-term YAP induction and whether other transcription factors cooperate or compete with YAP to regulate gene expression.

1.2 TEAD binds chromatin mainly at distal sites

To examine genome wide chromatin occupancy following YAP activation we carried out ChIP-Seq experiments in the mouse adult liver either in wild type animals (WT) or in LAP-tTA; tet-YAP^{S127A} mice after 4 weeks of YAP^{S127A} expression (henceforth pre-tumoral stage or 4W liver).

TEAD bound 33417 genomic sites in WT liver and its occupancy was further increased upon YAP activation, when 81682 ChIP peaks were detected (Figure 3, left). TEAD genomic occupancy was mainly distal, since only 29.1% of the peaks were located at promoters in WT liver and 17.7% in pre-tumoral liver (Figure 3, right).

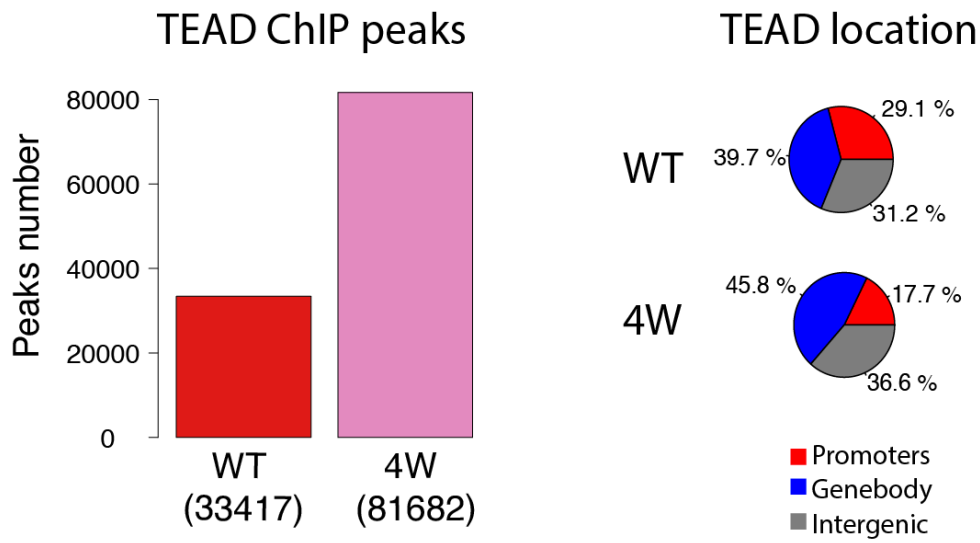

Figure 3: TEAD genomic occupancy is increased upon YAP activation and mainly involves distal sites. Left: barplot representing TEAD peaks number in WT liver (red) and upon 4 weeks of YAP induction (4W, pink); number of peaks is shown inside parenthesis. The number of peaks was dramatically increased in pre-tumoral stage. Right: piecharts showing the fraction of TEAD peaks in WT and 4W liver located at promoters (red), genebodies (blue) and intergenic regions (grey); the majority of peaks were detected at distal sites in both conditions.

Virtually all TEAD peaks found in WT liver were consistently detected also in pre-tumoral liver, both at promoters (Figure 4a) and distal sites (Figure 4d). Upon closer inspection, the additional binding sites detected in 4W livers appeared as already bound by low levels of TEAD in WT liver (Figure 4c, f; subset III), thus suggesting that their low enrichment may have prevented their detection by the peak caller algorithm.

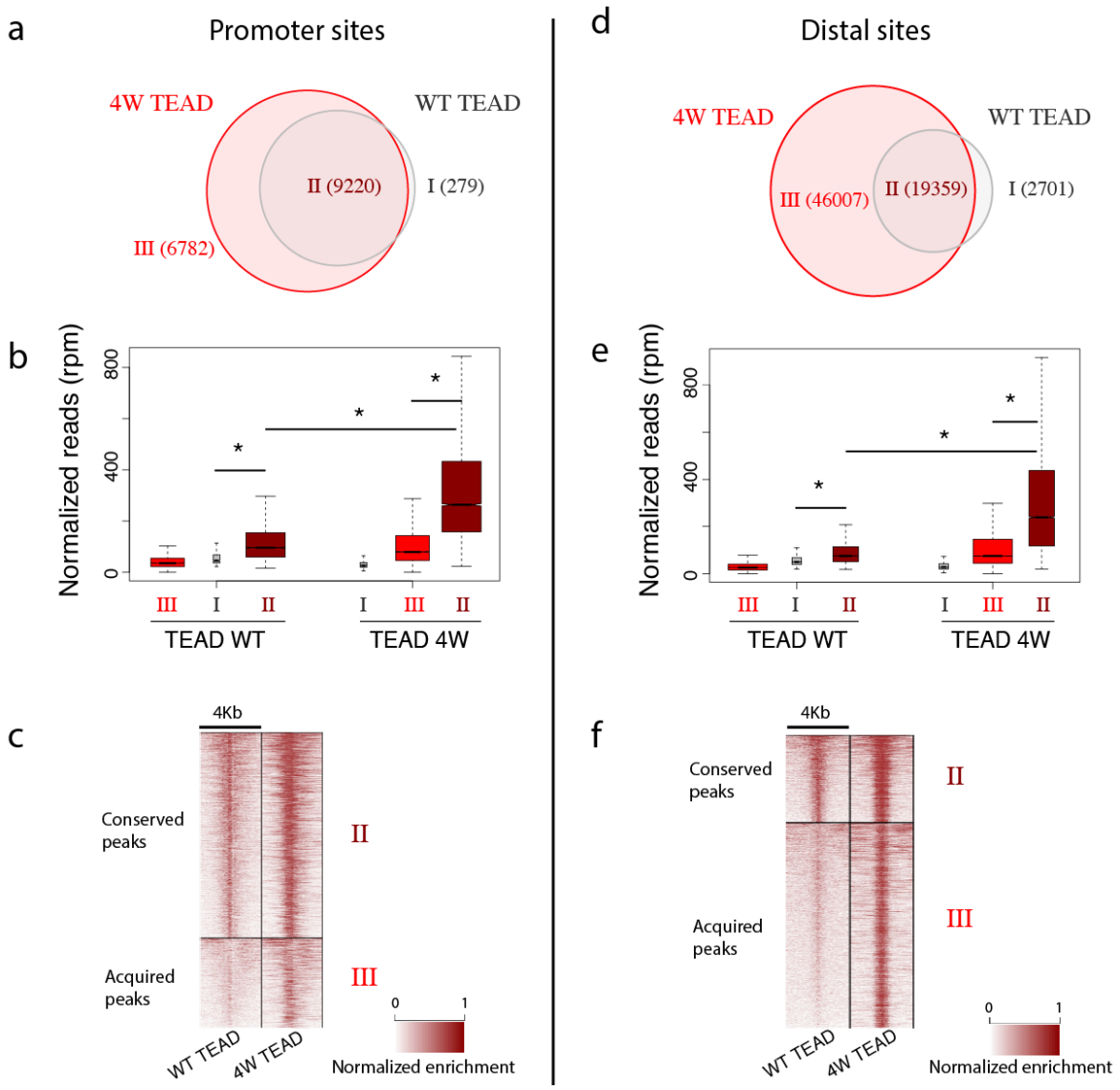

Figure 4: TEAD chromatin binding is increased upon YAP activation. (a, d) Venn diagrams showing the overlap between TEAD peaks detected in WT and pre-tumoral liver both at promoters (a) and distal sites (d), the number of genomic regions is shown in parenthesis; (b, e) Boxplot of the TEAD enrichment in the subsets of TEAD peaks represented in the Venn diagrams above (I, II and III), at promoters (b) and distal sites (e); common peaks were more enriched compared to other subsets, and the increase in TEAD binding was global, but stronger in common peaks (subset II); (c, f) heatmaps showing TEAD enrichments in conserved peaks and peaks acquired upon YAP activation, both at promoters (c) and distal sites (f). (* $p<2.2*10^{-16}$, Student's t-test).

The higher number of TEAD peaks upon YAP activation was also accompanied by a genome-wide increase in their enrichment (Figure 4b, e). This global raise in TEAD genomic occupancy could be due to its increased expression induced by YAP activation.

RNA-Seq experiments showed that 3 out of the 4 TEAD genes (TEAD 1,2,4) increased their expression upon YAP induction (Figure 5a); moreover, both YAP and TEAD peaks were detected on the promoter of TEAD 1 and 4 (Figure 5b). These data suggest that YAP induction may promote the expression of TEAD 1 and 4 through a direct regulation.

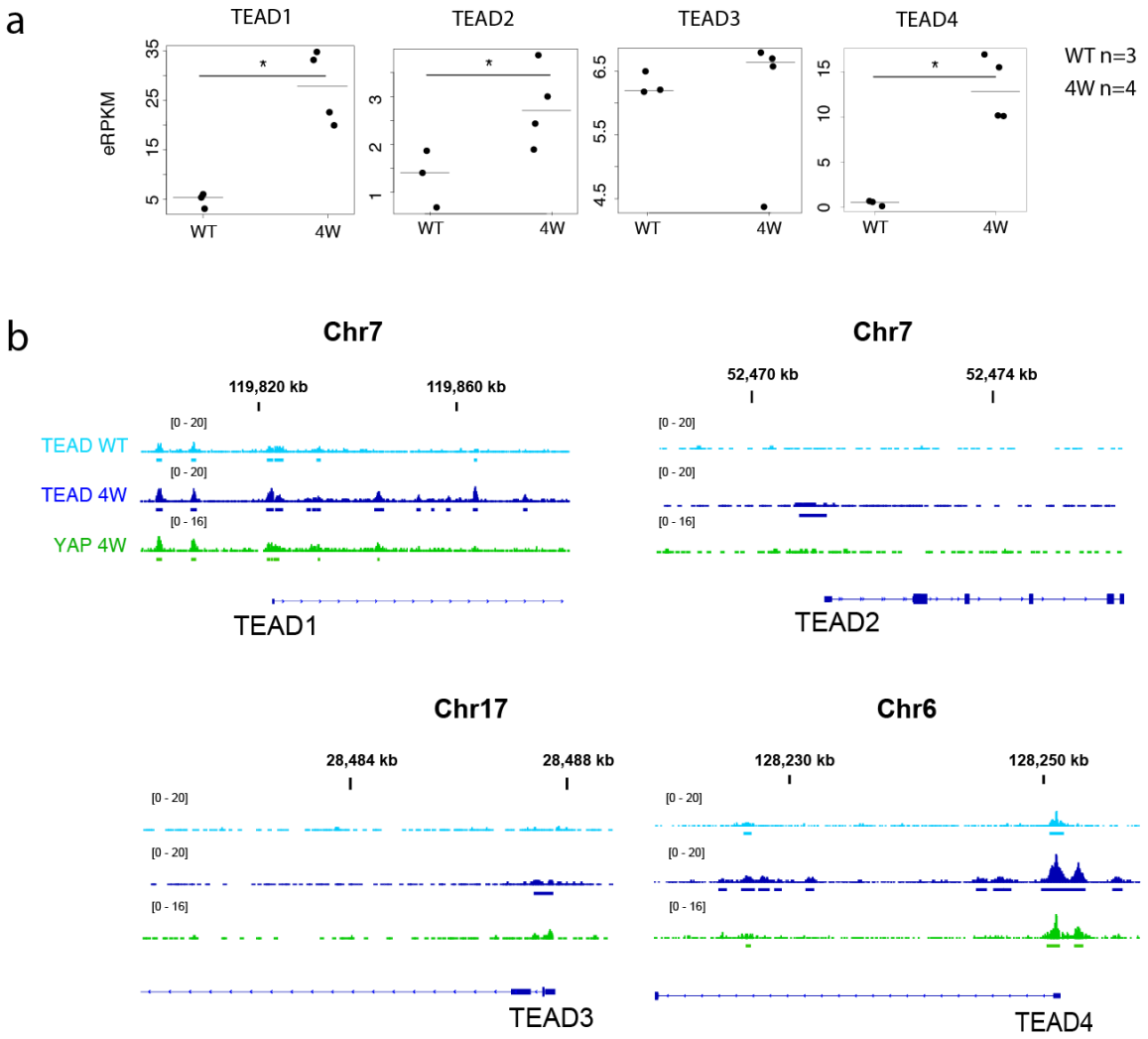

Figure 5: TEAD expression is increased in pre-tumoral liver. a) expression of the TEADs family members (in exonic reads per kilobase per million mapped reads, eRPKM) in three WT livers and four pre-tumoral livers (4W); b) genome browser snapshots showing the enrichment of TEAD in WT liver, and the enrichments of TEAD and YAP in pre-tumoral liver, on all TEADs promoters. (* p<0.01, Student's t-test).

In addition, as will be shown later in more details (see paragraph 1.4, page 35), YAP favors TEAD binding on chromatin (Figure 8a, b; subsets III and II). Therefore, two mechanisms could account for the increase of TEAD genomic interaction observed

upon YAP induction. First, higher TEAD levels could shift the equilibrium between bound/not bound protein on DNA and mediate a global increase of TEAD chromatin association. Second, a YAP-mediated TEAD genomic stabilization could reinforce TEAD binding strength on a specific subset of genomic loci co-bound by both YAP and TEAD (Figure 8, subset II).

1.3 YAP and TEAD co-localize on chromatin

YAP could not be detected by ChIP-Seq in normal liver, possibly owing to its low expression level; however, upon induction, YAP showed an extensive binding genome wide (30768 peaks; Figure 6), albeit lower if compared to TEAD (81682 peaks) (Figure 3). Most of YAP binding occurred at distal sites, with only 18% of its peaks located at promoters in pre-tumoral liver (Figure 6).

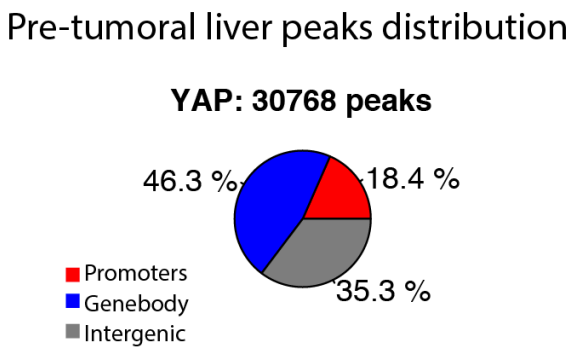

Figure 6: YAP binds chromatin mainly at distal sites in pre-tumoral liver. Piechart representing the YAP peaks localization in pre-tumoral liver; most of the peaks were detected in distal regions.

Almost all YAP binding sites (95% at promoters and 96% at distal sites) overlapped with TEAD peaks (Figure 7, left). Moreover, high correlation of YAP and TEAD enrichments was observed both at promoters (Pearson correlation coefficient=0.89) and distal sites (Pearson correlation coefficient=0.86) (Figure 7, right).

On the contrary, TEAD was able to localize on chromatin independently of YAP, since 66% of its peaks didn't show any overlap with YAP (Figure 7, left). These results

indicate that, *in vivo*, YAP occupies only a subset of TEAD binding sites both at promoters and at distal sites and suggest that TEAD may be required for YAP binding.

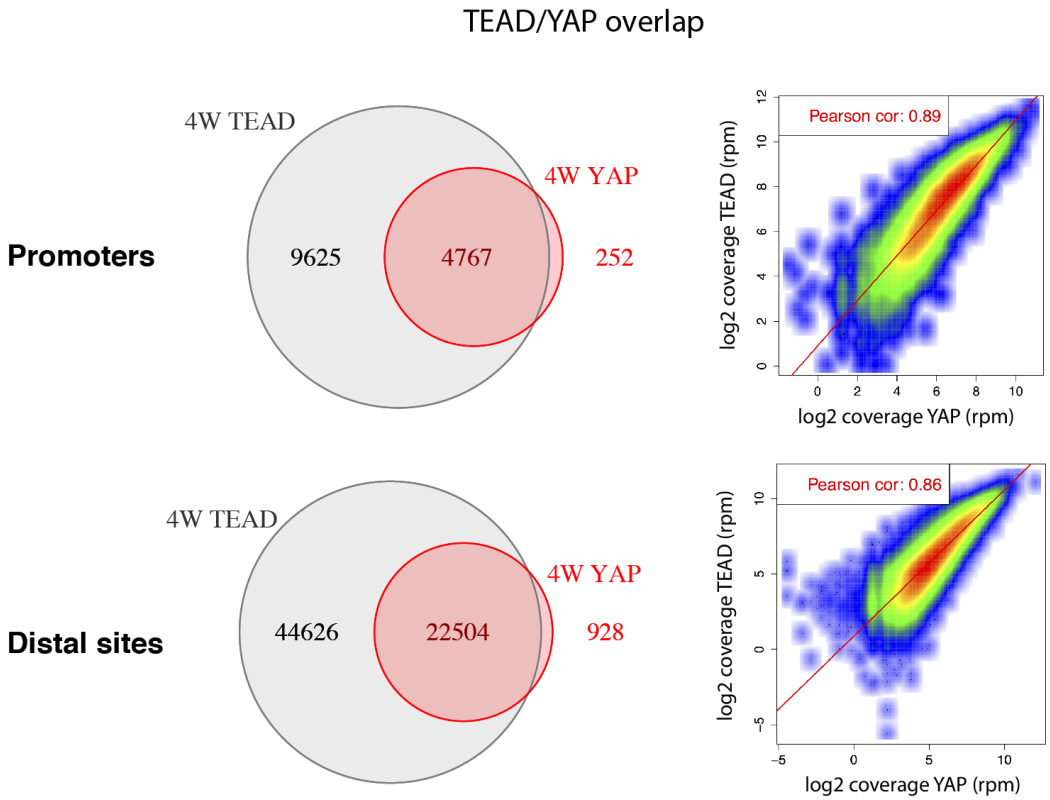

Figure 7: YAP co-localize with TEAD on chromatin. Left: Venn diagrams showing the overlap between YAP and TEAD ChIP-Seq peaks located at promoters (up) and distal sites (down). Right: Scatterplots of the correlation between YAP and TEAD ChIP-Seq enrichments in the union of YAP and TEAD binding sites.

1.4 YAP binding sites are mostly pre-bound by TEAD

We next wondered whether the presence of TEAD on chromatin in WT liver could influence subsequent YAP recruitment. To test this, we calculated the overlap between TEAD peaks detected in WT liver and YAP peaks detected upon its activation. On promoters, the large majority of YAP bound loci were already pre-bound by TEAD in normal liver (76%) (Figure 8a, Venn diagram). This was confirmed at distal sites where half of the sites were already bound by TEAD in WT liver (Figure 8c, Venn diagram).

TEAD peaks detected in WT liver and shared with YAP at 4W (subset II in Figure 8) were more enriched compared to all the other TEAD peaks (Figure 8b, d; subsets II vs I); following YAP activation, TEAD enrichment increased more in the subset of YAP peaks in which TEAD pre-existed in WT liver (Figure 8b, d; subset II).

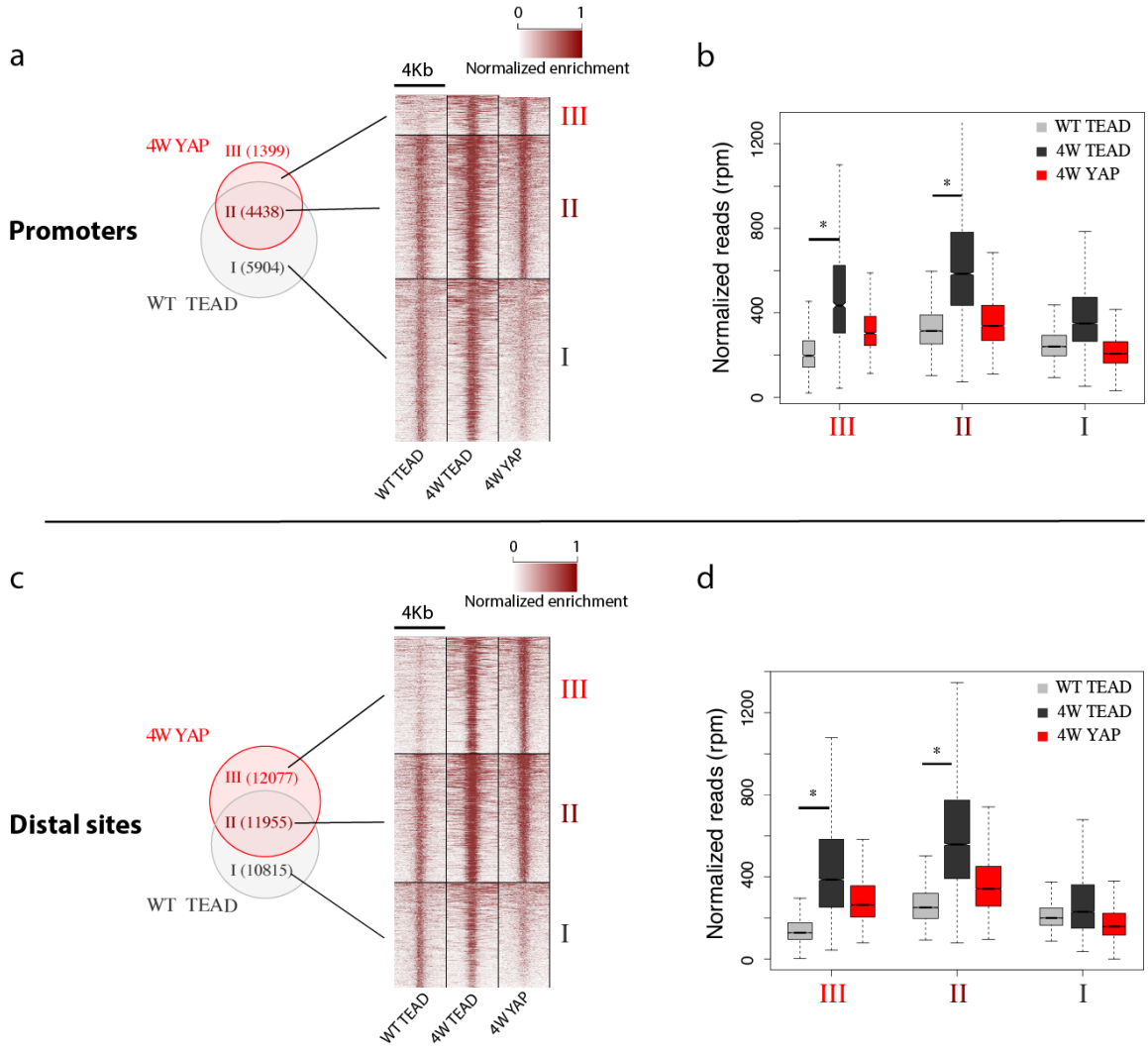

Figure 8: YAP binds genomic sites mostly pre-occupied by TEAD. (a, c) Venn diagrams showing the overlap between TEAD peaks detected in WT liver and YAP peaks detected in pre-tumoral liver at promoters (a) and distal sites (c), the number of peaks is shown in parenthesis; heatmaps represent the enrichment of TEAD (WT, 4W liver) and YAP (4W liver) of the subsets shown in Venn diagrams; (b, d) boxplots representing the enrichments of TEAD and YAP in the three subsets shown in the Venn diagrams, both at promoters (b) and distal sites (d). (* $p<2.2*10^{-16}$, Student's t-test).

Altogether, these data suggest that YAP chromatin binding was favored by pre-existing TEAD binding, with a preference for sites that showed the highest TEAD

enrichment (Figure 8, subset II). This was particularly prominent at promoters (Figure 8a, b). In addition, upon YAP chromatin association, TEAD enrichment was further increased (Figure 8, subset II), thus suggesting a role for YAP in stabilizing the YAP/TEAD complex on chromatin.

1.5 YAP and TEAD bind active chromatin and induce epigenetic changes

We then wanted to explore the chromatin status of YAP and TEAD binding sites. We compared the enrichment of histone modifications in genomic regions co-bound by both YAP and TEAD (YT), to those bound exclusively by TEAD (T) or the remaining regions in active chromatin where neither YAP or TEAD were detected (E).

As expected, YAP was remarkably enriched in YT regions, while in T regions its signal was lower, albeit still detected (Figure 9). Presumably, YAP enrichment in T regions was not sufficiently high to be called by the peak caller.

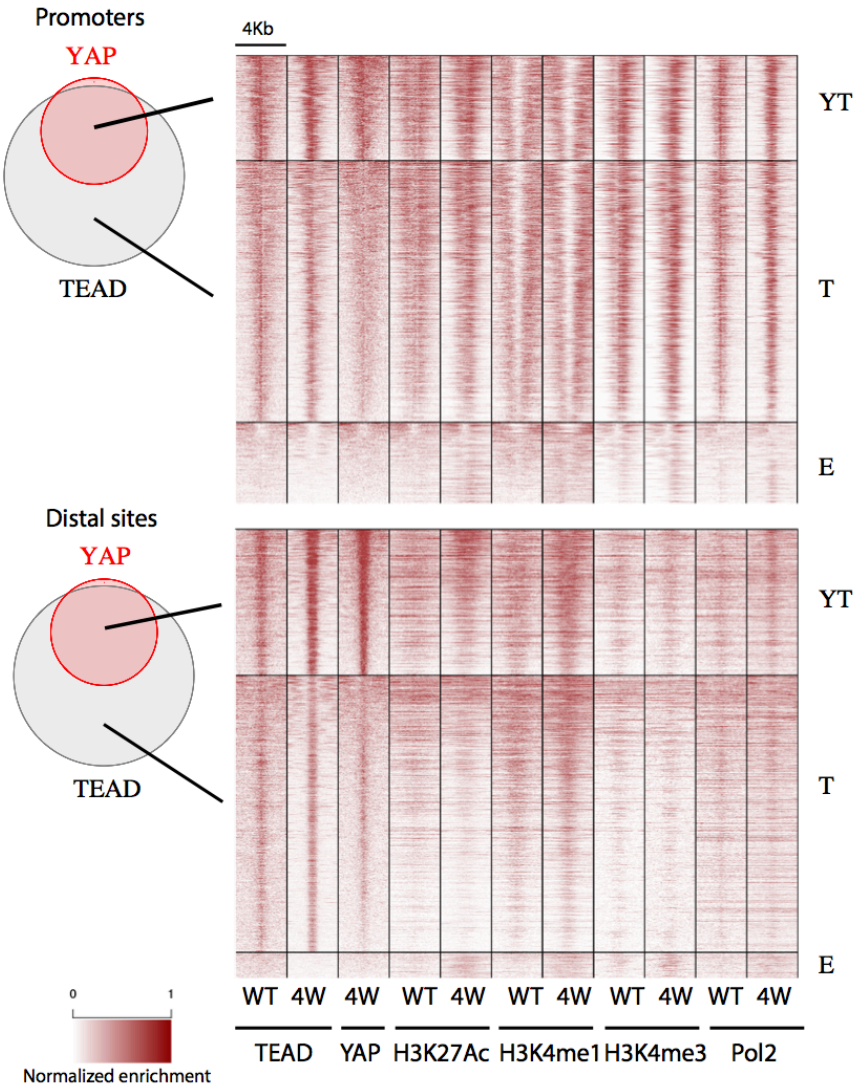

Figure 9: TEAD and YAP bind active chromatin regions (I). Heatmap showing the ChIP-Seq enrichment of YAP, TEAD and histone modifications in YT, T, E subsets, in WT liver and upon YAP induction, both at promoters (up) and distal sites (down) (E= subset of H3K27Ac peaks not overlapping with neither YAP or TEAD peaks).

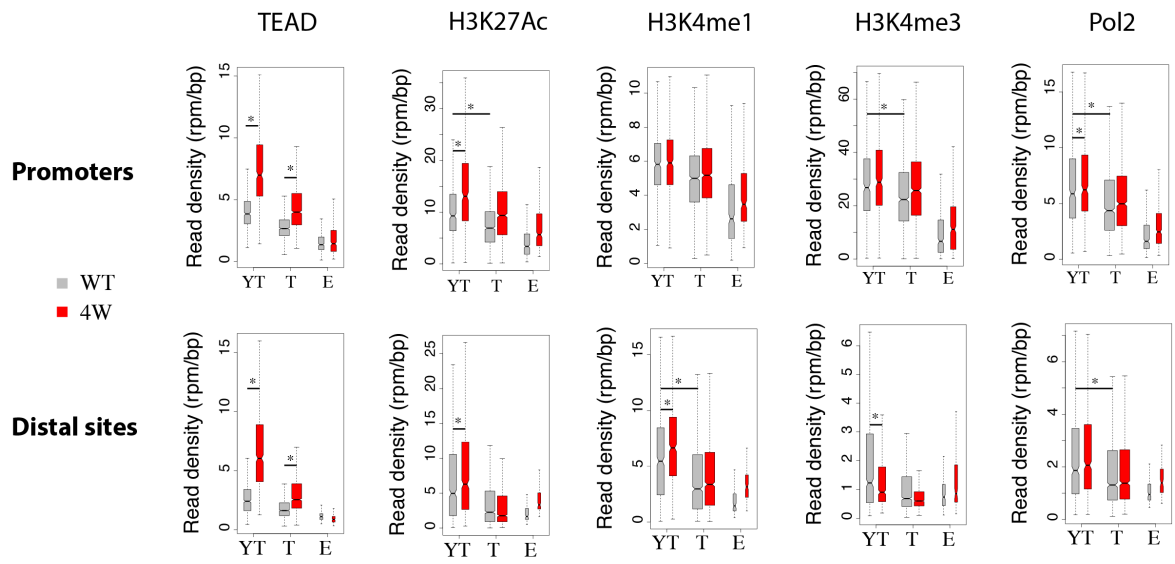

Figure 10: TEAD and YAP bind active chromatin regions (II). Boxplots representing the enrichment of the transcription factors and histone modifications analyzed in the three subsets defined in Figure 9 (YT, T, E) both in normal (WT) and pre-tumoral liver (4W). Globally, YAP and TEAD bind active chromatin regions and YAP further increases activation of chromatin in distal regions. (* p<0.01, Student's t-test).

High levels of H3K27Ac and H3K4me3 modifications were observed at promoters in both T and YT regions compared to sites not bound by either YAP or TEAD (Figure 9, Figure 10), with the YT subset being the most enriched in these histone marks. Higher occupancy of RNA Pol2 (hereafter, Pol2) was also found at promoters of YT sites (Figure 10). These data indicate that YAP recognized a subset of TEAD bound promoters particularly enriched in activating histone modifications (H3K27Ac, H3K4me3) and with high levels of Pol2.

H3K4me1 and H3K27Ac were enriched in YT and T subsets at distal sites, compared to regions not bound (E) (Figure 10); the level of these modifications was higher in the YT subset, suggesting that YAP is able to bind active enhancer elements (Heintzman et al., 2007; Creyghton et al., 2010). Moreover, an increase in Pol2 signal in the distal YT suggests that YAP may be associated with enhancer RNA transcription (Kim et al., 2010).

TEAD enrichment was increased in pre-tumoral liver in both T and YT subsets, at promoters and distal sites; this increase was more prominent where TEAD co-localized with YAP (YT subset; Figure 10), further suggesting that YAP binding promotes stabilization of TEAD chromatin interaction.

We also observed that, upon YAP activation, H3K27Ac and Pol2 increased at the YT subset at promoters (Figure 10); this suggests that YAP may promote the recruitment of acetyl/methyltransferases and further recruitment of Pol2 to activate promoters.

At distal sites, raised H3K4me1 and H3K27Ac levels and decreased H3K4me3 modification were observed at YT subset upon YAP binding (Figure 10). On the contrary, enrichment of these signals was rather consistent in T and E subsets (Figure 10). This suggests that YAP binding contributes to enhancer activation, since high H3K4me1/H3K4me3 signal ratio and H3K27Ac enrichment on distal sites are a characteristic features of active enhancers (Heintzman et al., 2007; Creyghton et al., 2010).

1.6 YAP binds chromatin mainly at distal sites upon its acute activation

We next wanted to investigate YAP chromatin binding upon its short-term activation. We therefore expressed the mutant form YAP^{S127A} in the liver for 2 days (hereafter, 2d liver) and analyzed the chromatin occupancy of YAP and TEAD by ChIP-Seq.

Upon short-term induction, 1328 YAP and 32486 TEAD peaks were detected on chromatin, and their binding occurred mainly at distal sites (Figure 11). The vast majority of YAP peaks overlapped with TEAD at both promoters (88% overlap) and distal sites (83% overlap) (Figure 12, up), confirming that YAP binding may require the presence of TEAD on chromatin; this was consistent with the high correlation of YAP and TEAD enrichments (Pearson correlation coefficient=0.82 at promoters, 0.73 at distal sites; Figure 12, down). Altogether, these data indicate that YAP is able to

bind chromatin upon its short-term overexpression mainly at distal sites and suggest that the presence of TEAD is required on DNA, consistently to what observed in pre-tumoral liver (Figure 7).

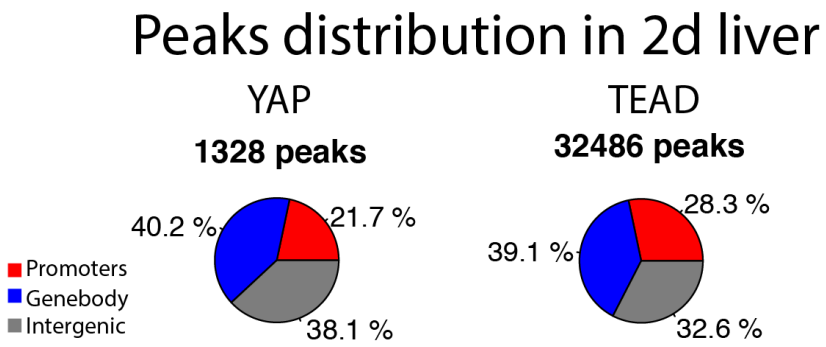

Figure 11: TEAD and YAP bind mainly distal sites upon YAP short-term activation. Piecharts showing the location of YAP peaks (left) and TEAD peaks (right) detected upon its short-term activation. Red: promoters, blue: genebodies, grey: intergenic regions.

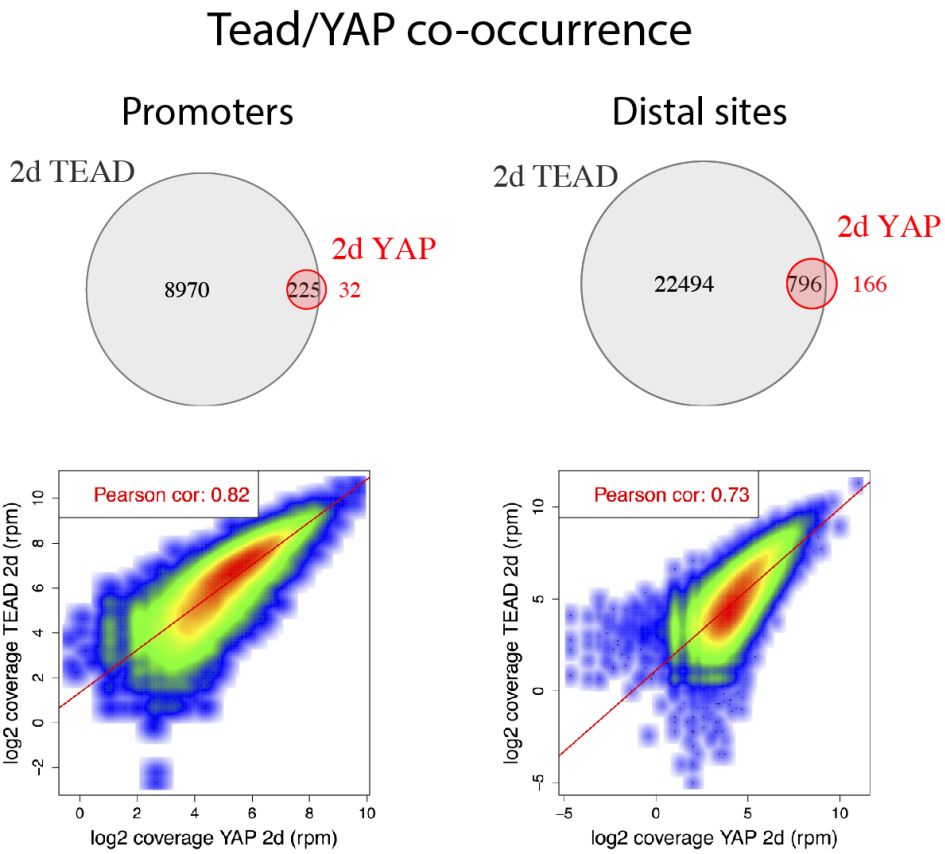

Figure 12: Upon its short-term activation, YAP binding sites co-localize with TEAD. Up: Venn diagrams of YAP/TEAD peaks overlap detected upon 2 days YAP induction, in both promoters (left) and distal sites (right). Down: Scatterplots of the correlation between the enrichments of YAP and TEAD at promoters (left) and distal sites (right).

We then asked if YAP bound genomic sites pre-bound by TEAD also upon short-term activation. We then overlapped YAP binding sites found at 2 days with TEAD binding sites detected in WT liver. Almost all (90%) YAP peaks detected short-term overlapped with TEAD peaks found in WT liver at promoters (Figure 13a); this fraction was lower, yet consistent (80%) at distal sites (Figure 13c). TEAD enrichment in WT liver was higher in sites targeted by YAP, both at promoters and distal sites (Figure 13b, d). These data indicate that YAP recognizes genomic regions pre-marked by TEAD upon short-term activation.

TEAD enrichment wasn't increased upon short-term YAP induction (Figure 13b, d), as opposed to what observed in pre-tumoral liver (Figure 8b, d). Despite the raised TEAD1 and TEAD4 expression after 2 days compared to WT liver (Figure 14), the amount of TEADs transcripts at 2 days was lower compared to pre-tumoral liver and tumors (Figure 20). This may suggest that prolonged YAP activation is required to promote a sufficient TEAD protein production for its subsequent chromatin stabilization.

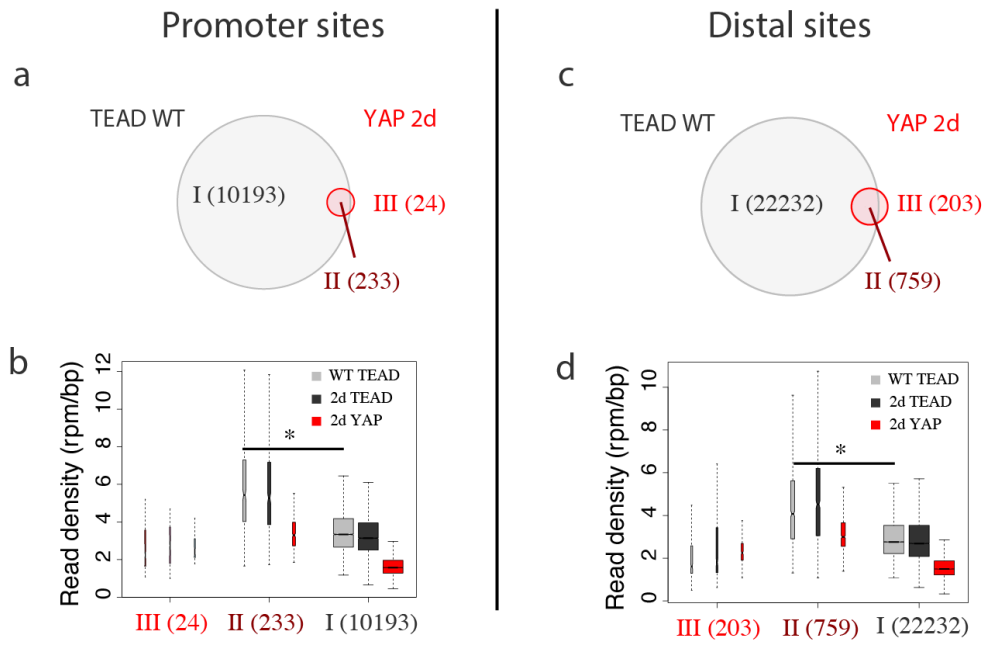

Figure 13: YAP recognizes regions pre-marked by TEAD upon short-term activation. (a, c) Venn diagrams representing the overlap between YAP peaks detected after 2 days of induction and TEAD peaks detected in WT liver, both at promoters (a) and distal sites (c), the number of peaks is shown in parenthesis; (b, d) enrichment of TEAD in WT liver and TEAD and YAP upon short-term induction, both at promoters (b) and distal sites (d) in the subsets shown in a) and c). (* p<0.001, Student's t-test).

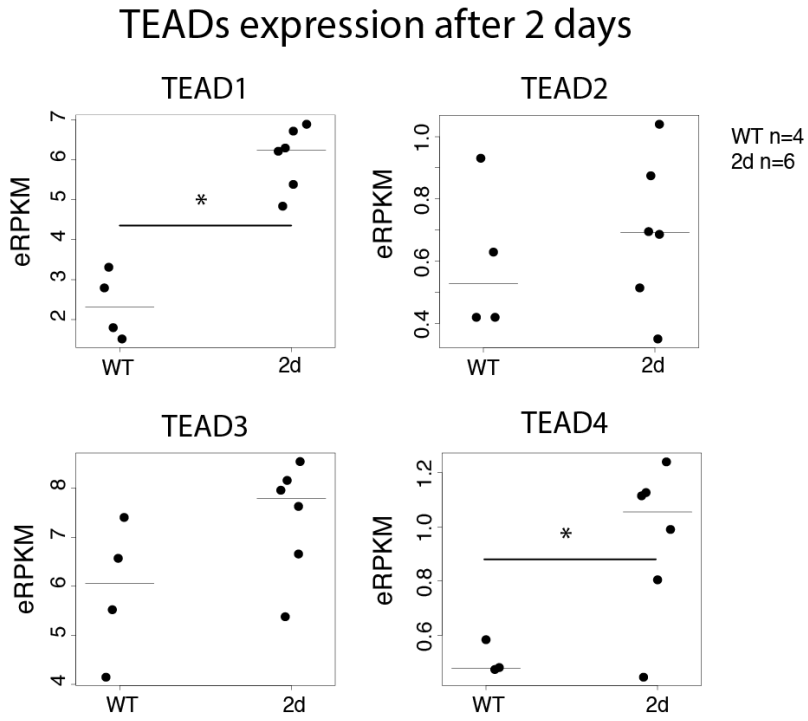

Figure 14: TEAD1 and TEAD4 increase their expression following 2 days YAP activation. Dotplots showing the expression of TEAD genes in eRPKM in the liver of 4 WT mice and 6 mice in which YAP was induced short-term. (* p<0.05, Student's t-test).

1.7 Acute activation of YAP does not lead to global changes in chromatin status

We then wanted to address differences in chromatin status upon short-term YAP induction.

Few changes of TEAD chromatin interactions were detected in 2d liver: at promoters, 77% of TEAD peaks found in normal liver were consistently detected after YAP activation, while 70% were conserved at distal sites (Figure 15). The consistency of TEAD binding sites was also reflected by the fact that its enrichment was unaltered at both promoters and distal sites (Figure 16). H3K27Ac, H3K4me3 and Pol2 peaks detected in WT liver showed almost complete overlap with those detected in 2d liver at promoters; at distal sites, about 80% of H3K27Ac and H3K4me1 binding sites were detected both in WT and 2d liver (Figure 15). Moreover, the enrichment of histone modifications was rather consistent between WT liver and upon short-term YAP activation (Figure 16).

Therefore, chromatin was unaltered at promoters, and only slightly modified at distal sites following short-term YAP induction.

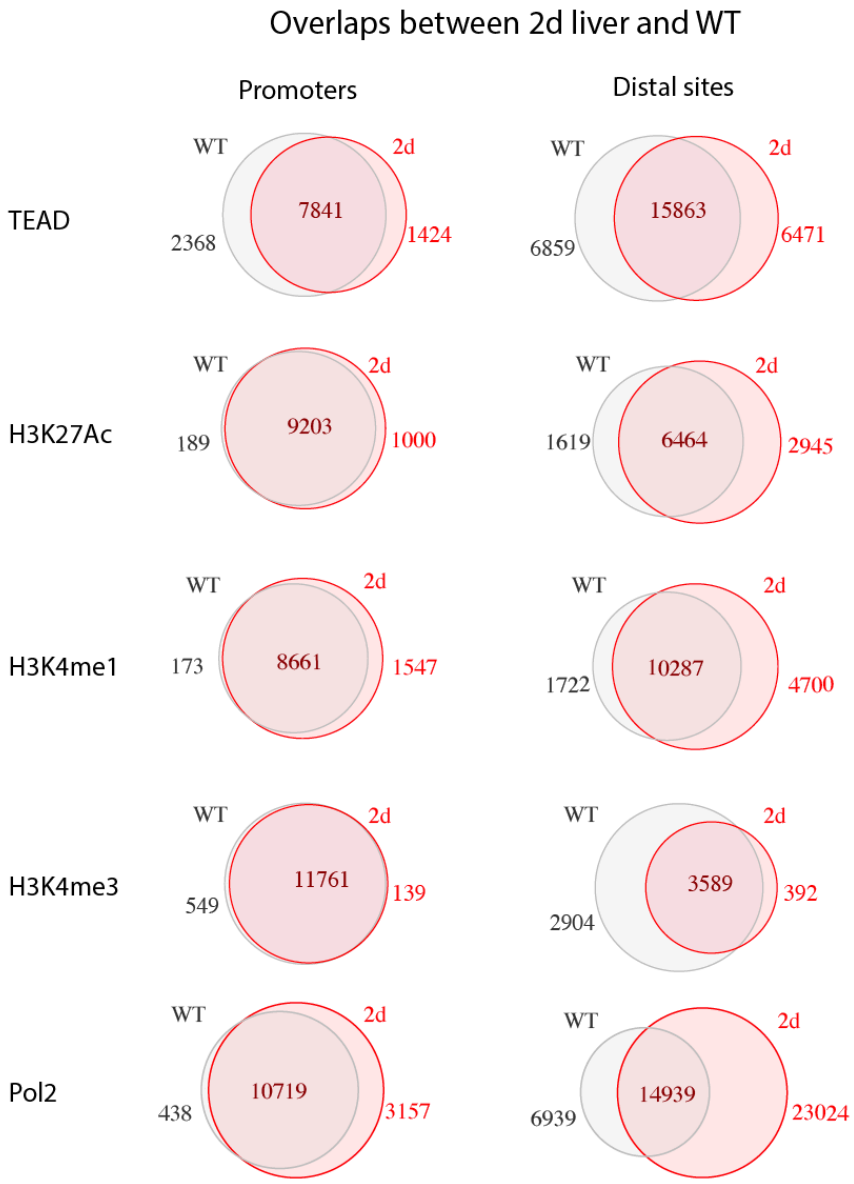

Figure 15: Short-term YAP induction does not lead to global changes in chromatin status (I). Venn diagrams representing the overlap between peaks detected in WT liver and those found upon 2 days YAP induction, both at promoters (left) and distal sites (right).

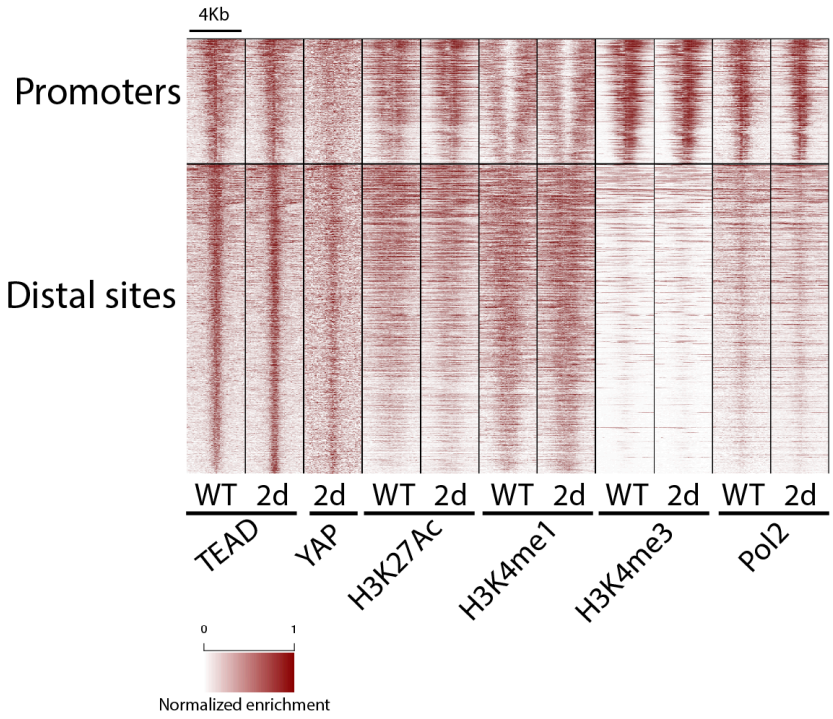

Figure 16: Short-term YAP induction does not lead to global changes in chromatin status (II). Heatmap showing the enrichment of TEAD, YAP, histone modifications and Pol2 in both promoters and distal sites (ROI: union of TEAD and YAP peaks detected at WT and 2d liver).

We next examined genomic sites bound by both YAP and TEAD at 2 days. At distal sites, TEAD enrichment was increased (Figure 17; Figure 18), suggesting that YAP may stabilize TEAD binding on chromatin, as observed before (Figure 8; Figure 10). H3K27 acetylation increased at both promoters and distal sites, while H3K4me1 and H3K4me3 levels were unaffected by YAP (Figure 17; Figure 18). This result strongly suggests that YAP binding could promote changes in histone marks and that H3K27 acetylation may precede further chromatin modifications; additional work will be required to address this point. The acetylation of histones on promoters following YAP binding is linked to an increased Pol2 recruitment and elongation (see Figure 25b in paragraph 1.9, page 53).

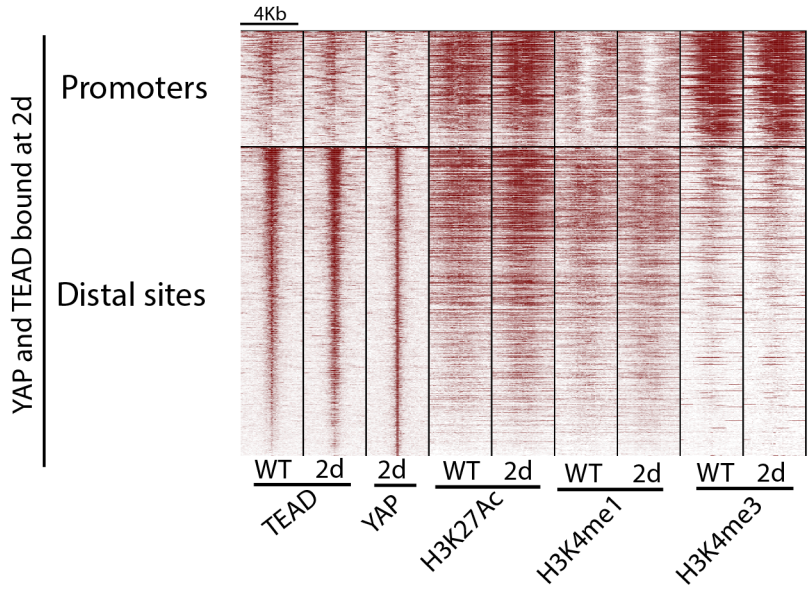

Figure 17: YAP binding promotes H3K27 acetylation upon short-term YAP activation (I). Heatmap representing the promoters and distal sites bound by both YAP and TEAD after short-term YAP activation (2d). The enrichment in H3K27Ac is increased in both promoters and distal sites.

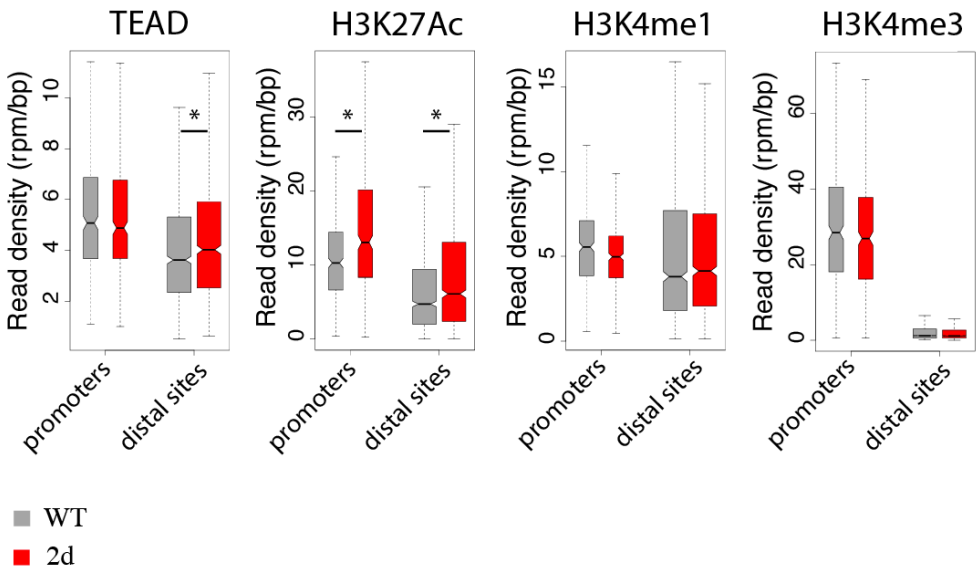

Figure 18: YAP binding promotes H3K27 acetylation upon short-term YAP activation (II). Boxplots representing the enrichment of TEAD and histone modification at promoters and distal sites in genomic regions bound by both YAP and TEAD at 2 days, following short-term YAP activation. H3K27Ac enrichment is increased following acute YAP activation, at both promoters and distal sites. (* $p<0.05$, Student's paired t-test).

1.8 YAP binding and histone modifications differ in distal sites between pre-tumoral liver and tumors

We then collected tumor nodules after 13 weeks YAP activation and asked which major genomic changes may occur at chromatin level during YAP-induced tumorigenesis.

YAP and TEAD showed a global, slight increased occupancy at distal sites between pre-tumoral liver and tumor, both in terms of peaks distribution (Figure 19) and enrichment (Figure 21). This was paralleled by a higher expression of TEAD 2,3,4 in tumors, while TEAD1, which was already highly expressed in pre-tumoral liver, didn't further change its level (Figure 20). Moreover, enrichment of H3K4me1 histone modification was higher in liver tumors at distal sites (Figure 21), consistently with a putative role of YAP in enhancer activation.

Enrichments of H3K27Ac and Pol2 were rather consistent at promoters after 13 weeks of activation (Figure 21), and levels of H3K4me3, that marks active promoters (Mikkelsen et al., 2007) didn't show variations, suggesting that global quantitative changes in modification of chromatin and Pol2 recruitment did not occur in liver tumors.

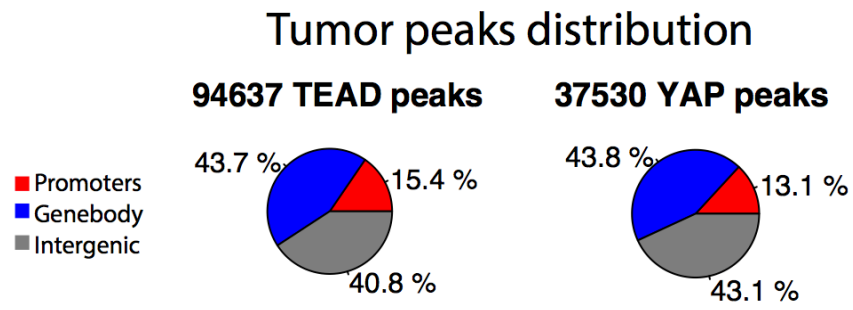

Figure 19: TEAD and YAP bind mainly distal sites in liver tumors. Piecharts representing the TEAD and YAP peaks localization in tumor liver. The fraction of peaks detected at promoters was lower compared to that of pre-tumoral liver (Figure 6).

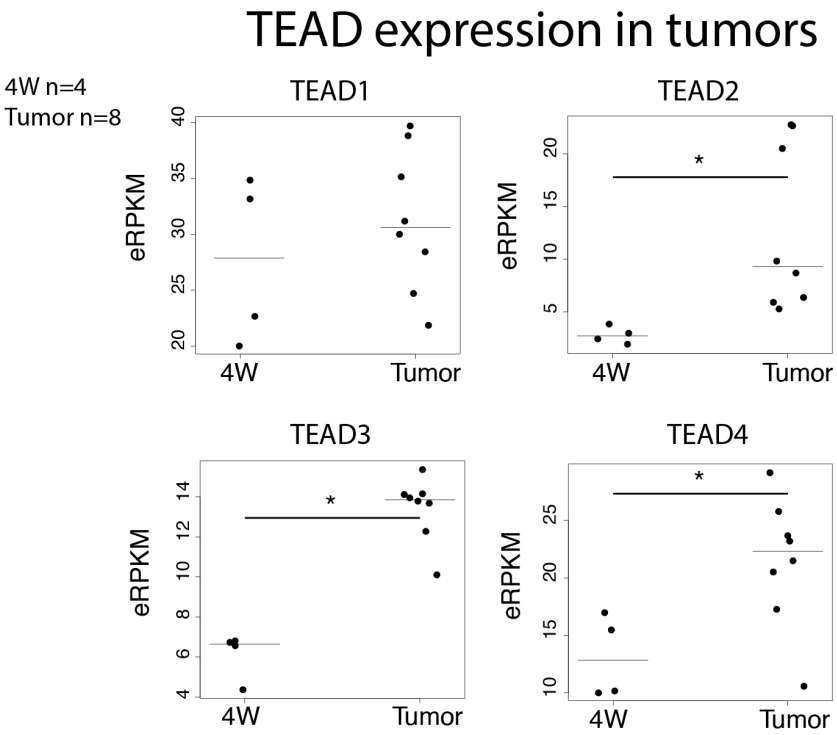

Figure 20: TEADs expression is increased in liver tumors. Dotplots showing the expression of the four TEADs in eRPKMs in 4 pre-tumoral livers (4W) and in 8 tumor nodules. (* $p<0.01$, Student's t-test).

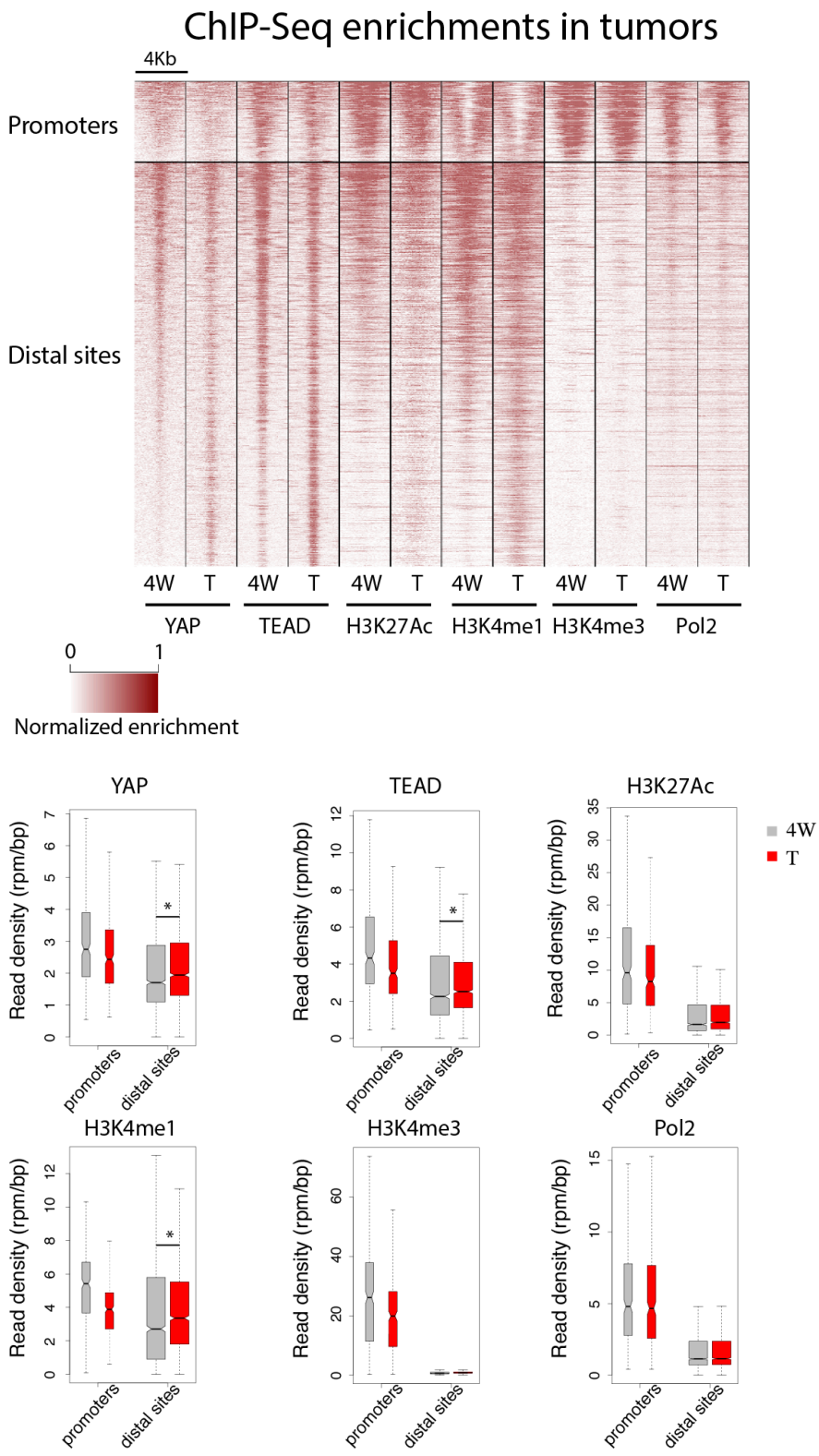

Figure 21: The occupancy of YAP, TEAD and H3K4me1 is increased at distal sites in liver tumors. Up: Heatmap representing the enrichment of YAP, TEAD, histone modifications and Pol2 in promoters and distal sites (ROI=union of YAP and TEAD peaks in pre-tumoral liver and tumors). Down: Boxplots showing the enrichment of TEAD, YAP, histone modifications and Pol2 in pre-tumoral and tumors, both at promoters and distal sites. Globally, chromatin is only slightly modified in liver tumors, except for TEAD, YAP and H3K4me1 levels that increased at distal sites and decreased at promoters. (* $p<0.01$, Wilcoxon test).

We compared ChIP peaks of TEAD, YAP, H3K27Ac, H3K4me1, H3K4me3 and Pol2 detected in pre-tumoral liver and liver tumors to find differences in chromatin occupancies during tumorigenesis.

At promoters, 78% of TEAD peaks and 55% of YAP peaks were conserved also in tumors (Figure 22, left). The shift in YAP binding regions was also reflected by differences in its enrichments (Figure 23). Histone modifications were rather consistent between pre-tumoral liver and tumors; 9962 out of 11523 (86%) H3K27Ac peaks found in 4W liver were consistently detected in tumors; similar results were observed for H3K4me3 (94% peaks conserved) (Figure 22, left). Pol2 binding sites were also unchanged at promoters, since 91% of its peaks were shared between pre-tumoral liver and tumors (Figure 22, left).

At promoters, then, few changes in chromatin occupancy occurred in liver tumors compared to the pre-tumoral stage (Figure 22, left); YAP being the exception, since only half of its binding sites were conserved in tumors (Figure 22, left; Figure 23).

At distal sites, however, we observed a global shift in binding sites of YAP, TEAD and Pol2 and the enrichments of all histone modifications tested (Figure 22, right). In particular, only 62% of TEAD peaks and 57% and YAP peaks were conserved. Only 62% of H3K4me1 peaks were conserved in pre-tumoral liver and tumors and this fraction was lower for H3K27Ac peaks (46%) (Figure 22, right), suggesting that different enhancers were active in pre-tumoral liver compared to tumors.

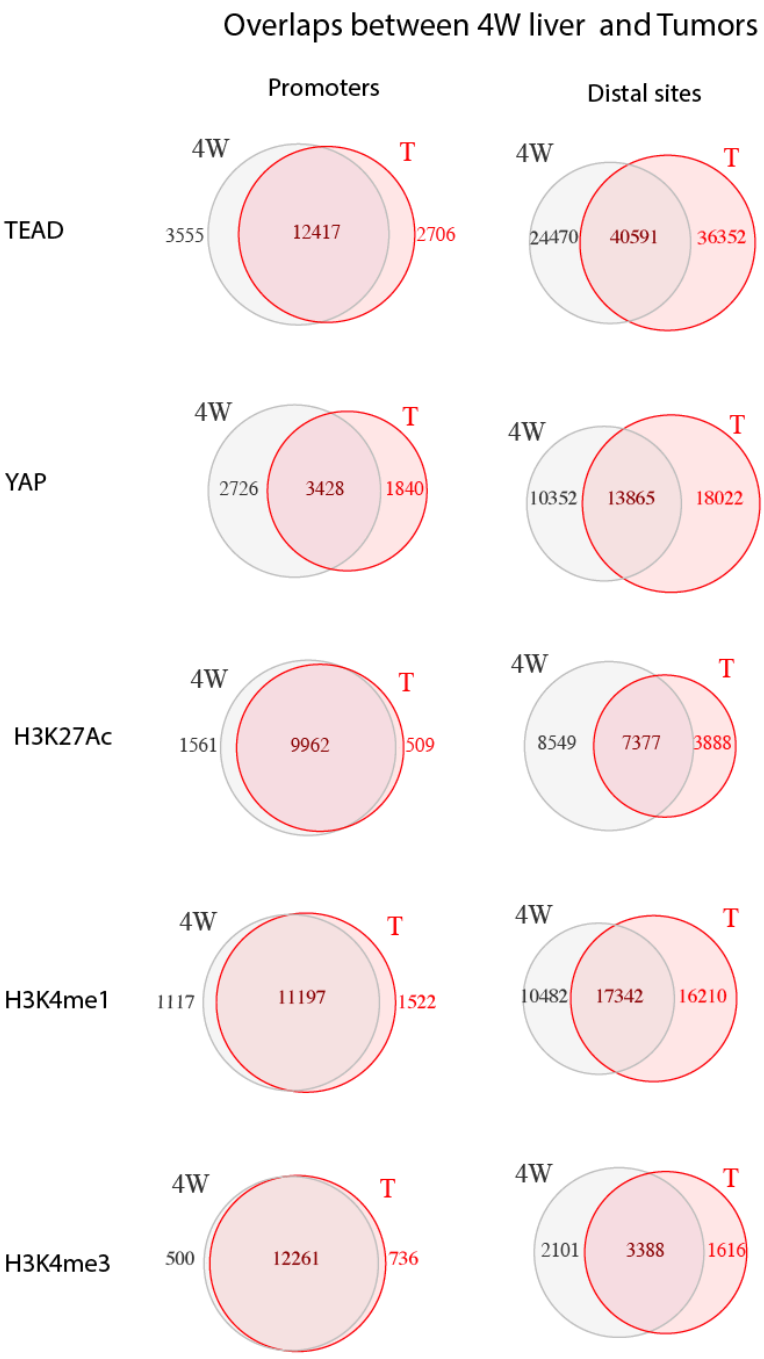

Figure 22: YAP, TEAD, Pol2 binding sites and histone modifications changed their occupancy at distal sites in liver tumors. Venn diagrams showing the overlap between peaks of transcription factors and histone modifications detected in pre-tumoral liver (4W) and those found in tumors (T). TEAD, Pol2, and histone marks are relocalized on the genome at distal sites, while YAP changed its occupancy both at promoters and distal sites.

These data suggest that the phenotypic differences between pre-tumoral liver and tumors may arise from transcriptional programs controlled by distal elements that are selected and activated during tumor development. YAP may play a relevant role in controlling these programs, both at promoters and enhancers.

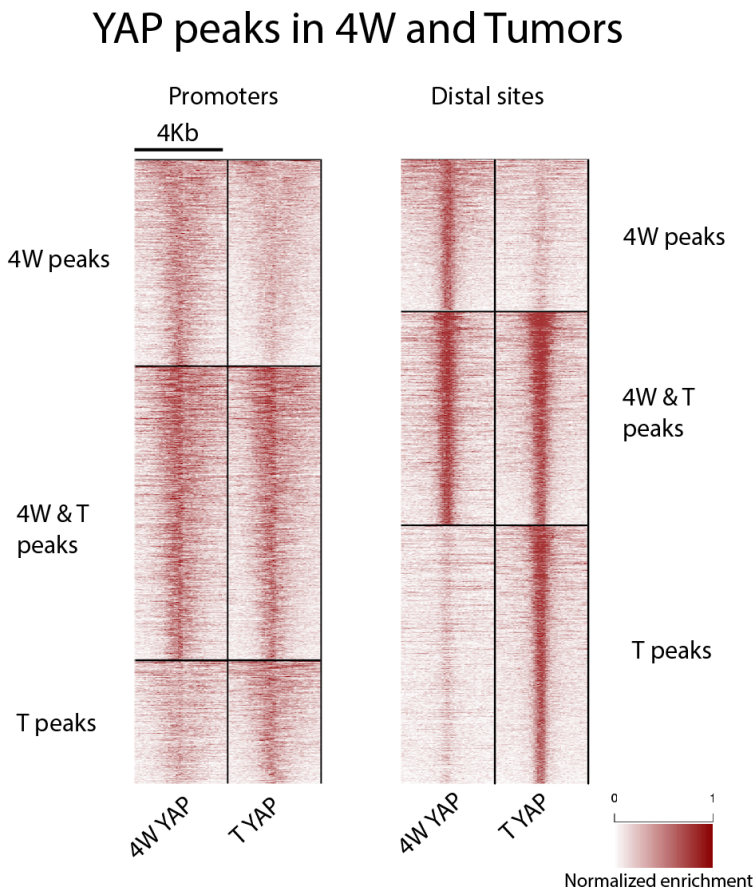

Figure 23: YAP changes its genomic localization in liver tumors. Heatmaps representing the YAP enrichment in pre-tumoral liver (4W) and tumor (T), at promoters and distal sites, in YAP peaks detected in pre-tumoral liver only (4W peaks), tumor liver only (T peaks) or the peaks consistently detected in the two conditions (4W & T peaks). The enrichment of YAP was high only where its peaks were found, indicating that peaks called were reliable.

1.9 Pol2 recruitment and elongation are altered in YAP regulated genes

We then profiled transcriptional responses that followed YAP induction in pre-tumoral liver. Different transcriptional programs were regulated upon YAP activation, as shown by the clustering between RNA-Seq samples (Figure 24).

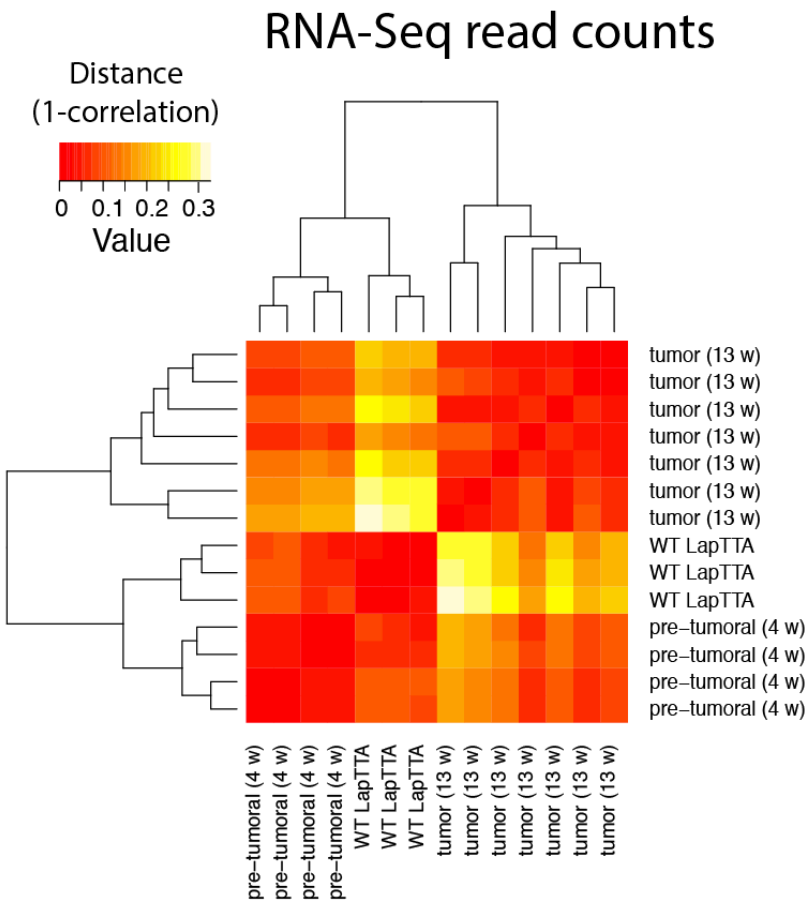

Figure 24: YAP regulates different transcriptional programs in pre-tumoral livers and tumors. Heatmap representing the distance (1-pearson correlation) of RNA-Seq read counts of 3 WT mouse livers (WT LAP-tTA), 4 mouse livers upon YAP induction (4W) and 8 independent tumor nodules detected after 13 weeks of YAP activation. Samples belonging to the same condition clustered well together, and tumors behaved differently compared to pre-tumoral liver, indicating good quality RNA-Seq experiments and consistency between replicates.

Compared to WT liver, 2174 genes (hereafter, DEGs) changed significantly their expression upon 4 weeks of YAP activation. YAP mainly promoted transcriptional activation: 1850 genes were upregulated (DEG up) while only 324 genes were downregulated (DEG down).

To address how YAP induction could modulate gene transcription, we analyzed Pol2 distribution along genes differentially expressed which were also bound by YAP at their promoters in pre-tumoral liver. Upregulated genes, as determined by RNA-Seq analysis, showed marked increase in both pausing and elongating Pol2 (Figure 25a, up), indicating that both Pol2 recruitment and its release from promoters could

account for gene upregulation. Whether pause release was also actively induced or the Pol2 recruitment simply shifted the equilibrium toward the elongating form remains an open question.

In downregulated genes, the signal of both pausing and elongating Pol2 dropped following 4 weeks YAP activation (Figure 25a, center); this suggests that YAP was able to repress genes by inhibiting Pol2 recruitment on promoters and possibly by decreasing elongation.

Similar results were observed upon short-term YAP induction: both Pol2 recruitment and elongation increased in genes upregulated and bound by YAP in 2d liver (Figure 25b). Only 5 genes were bound and repressed by YAP short-term; this was not sufficient to detect with statistical power the changes in stalled or elongating Pol2. This suggests that the effects on transcriptional regulation were mediated directly by YAP and not by secondary effects arising from its long-term activation.

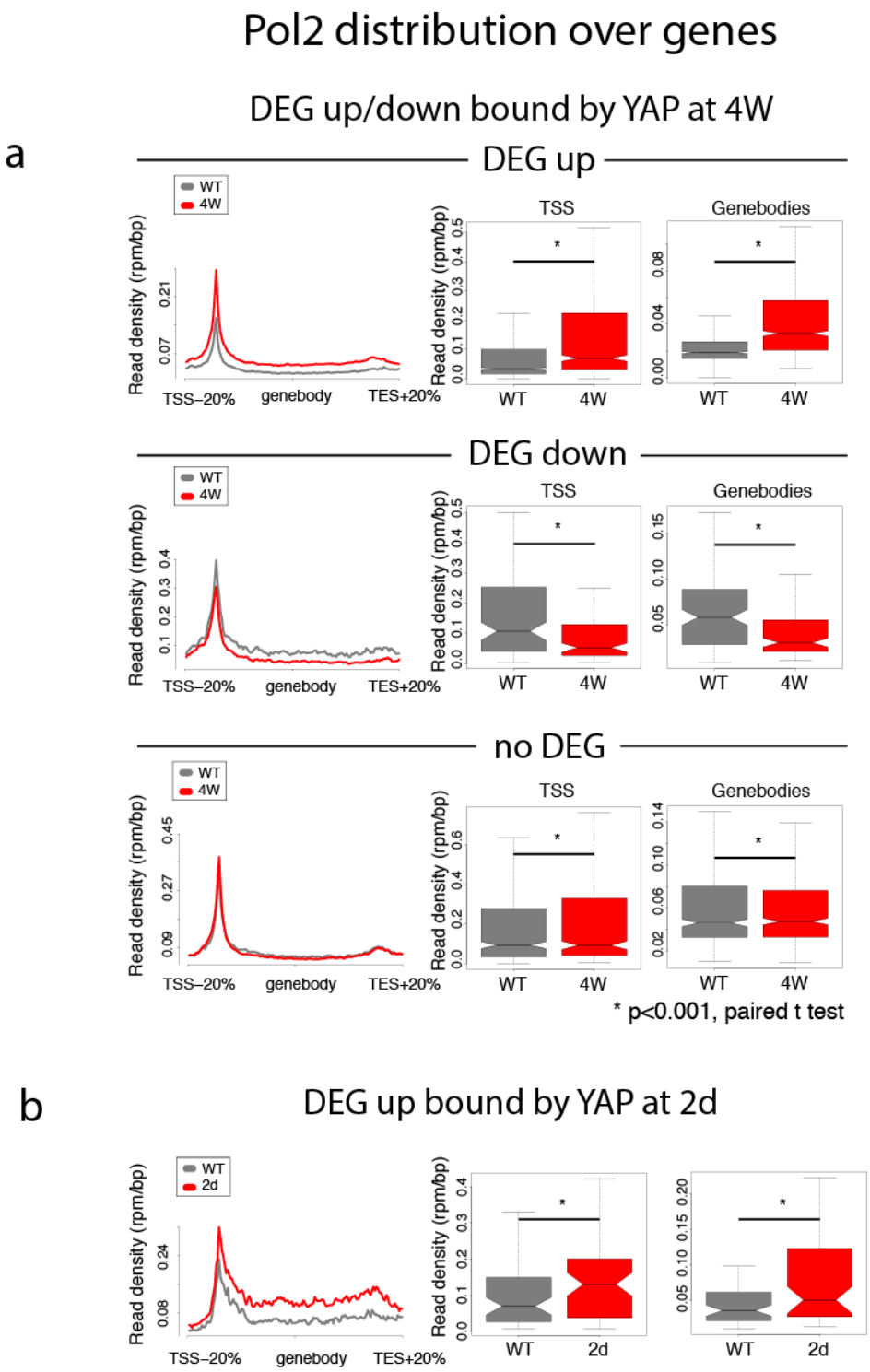

Figure 25: Pol2 recruitment and elongation increases in YAP upregulated genes, while decreases in YAP repressed genes. a) Pol2 enrichments are shown for genes upregulated (Up), downregulated (Center) or not deregulated (Down) upon 4 weeks YAP activation (pre-tumoral liver) bound by YAP on their promoters. Average Pol2 profile is represented on the left for normal liver (WT) or pre-tumoral liver (4W). Read density on transcription start sites (TSS) and genebodies are shown on the right; b) Pol2 enrichments for genes upregulated upon short-term YAP activation and bound by YAP. (* p<0.01, paired Student's t-test).

1.10 YAP induction represses liver-specific programs and activates cell cycle genes

We then carried out a gene set enrichment analysis (GSEA) on DEGs to find which are transcriptional programs regulated by YAP.

The analysis revealed that liver specific genes and cell cycle regulators were altered (Figure 26). In particular, HNF1A and HNF4A targets were inhibited in pre-tumoral tissue. HNF4A (hepatocyte nuclear factor 4 a) is a transcription factor that regulates various biological functions in the liver and pancreas (Babeu and Boudreau, 2014) and belongs to the same family of retinoic acid X receptors (RXR) (Bookout et al., 2006), with which share the DNA binding recognition motif xxxxCAAAGTCCA (Fang et al., 2012). HNF4A promotes lipid metabolism (Martinez-Jimenez et al., 2010), lipid transport through induction of apolipoprotein genes (Leclerc et al., 2001) and bile-acid biosynthesis, since it binds and regulates enzymes involved in bile acid biosynthetic pathway, such as the very long chain acyl-CoA synthase-related gene (VLACSR) (Inoue et al., 2004) and CYP8B1 (Inoue et al., 2006). A relevant role of HNF4A has been demonstrated in gluconeogenesis, because it cooperates with Peroxisome proliferator-activated receptor (PPAR) co-activator 1 (PGC-1) to promote the expression of enzymes involved in this pathway (Rhee et al., 2003). Finally, HNF4A promotes the expression of cytochrome CYP3A4, the enzyme mainly involved in xenobiotic metabolism (Tirona et al., 2003).

HNF1A (hepatocyte nuclear factor 1 a), a homeodomain-containing protein, regulates the expression of genes important for liver development, but is expressed also in pancreas, gut and kidney (Mendel and Crabtree, 1991). In liver, it plays a fundamental role in the metabolism and uptake of bile acid and metabolism of cholesterol (Shih et al., 2001). When bile acid levels rise, both HNF4A expression and binding on DNA are inhibited. Since HNF1A expression depends on HNF4A binding on its promoter, bile acids can inhibit also the HNF1A expression, therefore forming a negative feedback-

loop when their concentration is high (Jung and Kullak-Ublick, 2003).

The pronounced cell proliferation observed in the hepatic tissue upon 4 weeks of YAP activation (De Fazio, personal communication) is consistent with the upregulation of cell cycle programs detected by GSEA, particularly genes involved in G2/M checkpoint progression and E2F targets (Figure 26).

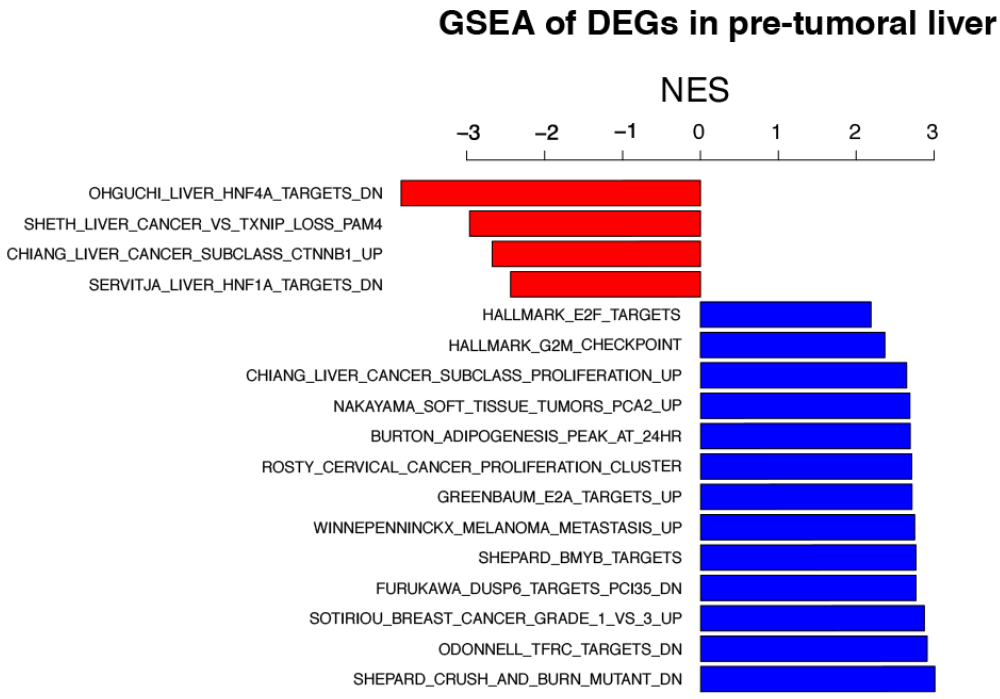

Figure 26: Both liver specific and cell cycle programs are affected upon YAP induction (4 weeks). Barplot showing the normalized enrichment score (NES) of top 10 significant hits of geneset enrichment analysis carried out on DEGs detected in pre-tumoral liver. Among all the signatures detected, HNF4A and HNF1A programs were found downregulated (red bars, up), while cell cycle genes, such as E2F targets and G2M checkpoint genes were found upregulated (blue bars, down).

To find the immediate-early transcriptional response of YAP activation, we carried out a geneset enrichment analysis using DEGs detected upon short-term (2 days) induction.

Interestingly, few specific programs were altered at this stage: HNF1A and SREBP target genes, together with genes involved in the metabolism of cholesterol were downregulated (Figure 27).

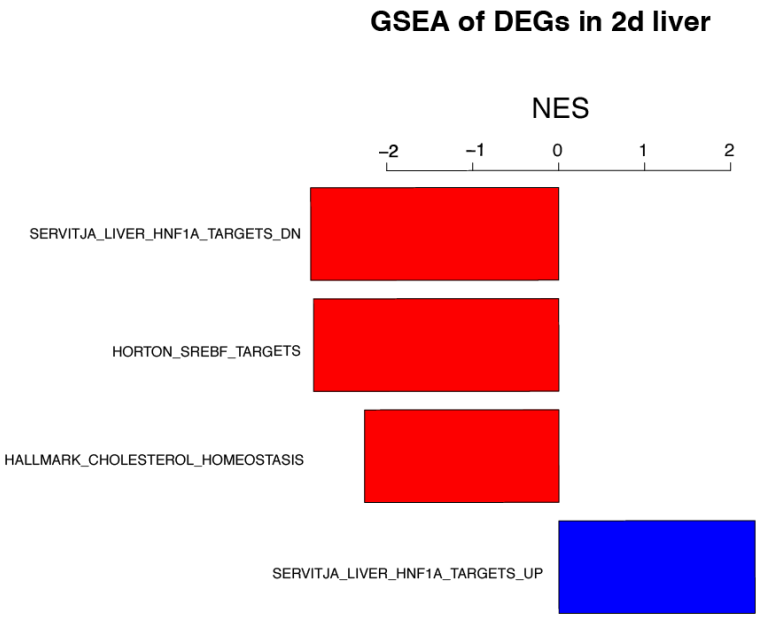

Figure 27: HNF1A and SREBP programs are affected upon short-term YAP induction. Barplot showing the normalized enrichment score (NES) of the geneset enrichment analysis on DEGs upon short-term YAP overexpression. HNF1A and SREBP targets, together with genes involved in cholesterol metabolism, were downregulated (red bars, up). Genes normally repressed by HNF1A were upregulated (blue bar, down).

SREBPs (sterol regulatory element–binding proteins) play an important role in maintaining lipid homeostasis in the liver (Horton et al., 2002). SREBP-1 and SREBP-2, its two isoforms, promote the biosynthesis of fatty acids and cholesterol, respectively (Horton et al., 2002). Regulation of SREBP-1 is achieved by binding of RXR/LXR (liver X receptor) heterodimer on its promoter (Repa et al., 2000).

The expression of genes involved in cell cycle was not altered at this early stage, consistently with the lack of YAP induced proliferation following 2 days of activation (De Fazio, personal communication).

Altogether these data indicate that YAP, when activated, can modulate different transcriptional programs in a time-dependent manner. Targets of HNF1A and SREBP were affected as immediate-early response (Figure 27), while downregulation of HNF4A targets and upregulation of cell cycle genes occurred later, in pre-tumoral stage (Figure 26).

1.11 YAP can directly affect HNF4A liver-specific programs

We then asked if some transcription factors could cooperate or compete *in cis* with YAP to regulate gene expression. We therefore carried out a motif finding analysis on sequences around YAP peak summits associated to DEGs. As expected, TEAD motif was found as the top hit both at promoters and at distal regions (Figure 28), according to the high overlap between YAP and TEAD peaks (Figure 7, left). HNF4A/G motifs were also enriched under YAP peak summits, both at promoters and distal sites (Figure 28), suggesting that the downregulation of HNF4A programs that occurred in pre-tumoral liver was directly mediated by YAP binding on HNF4A binding sites.

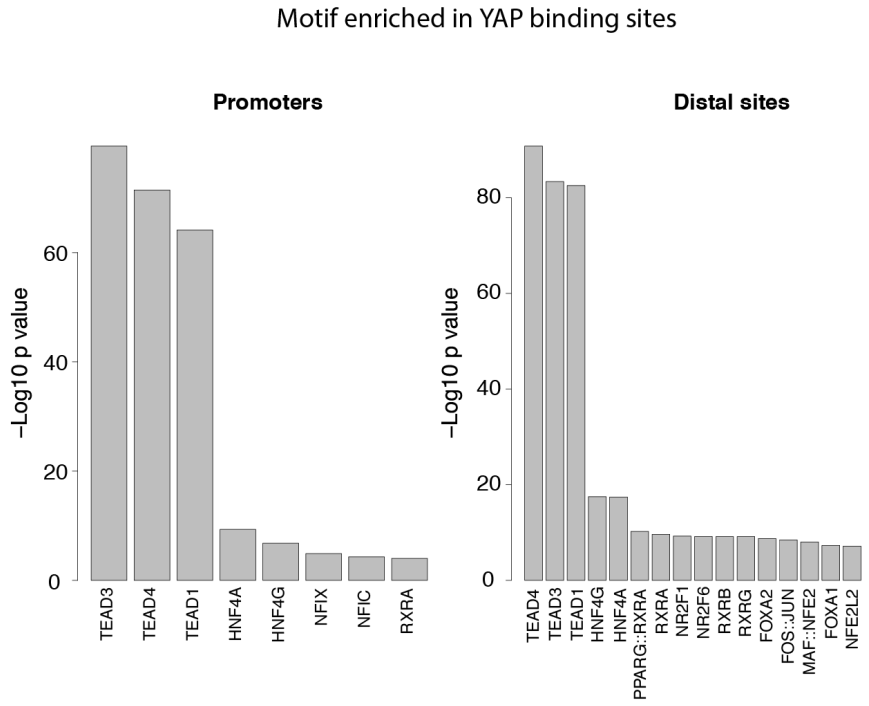

Figure 28: Motif finding analysis in YAP peaks associated to DEGs. Barplots representing the statistical significance (-Log p value) of the result of motif finding analysis carried out using PscanChIP tool (Zambelli et al., 2013) on YAP binding sites associated to DEGs, both at promoters (left) and distal sites (right).

Interestingly, the analysis detected retinoid X receptors (RXR) as another putative transcription factor that can interact with YAP (Figure 28); RXR are nuclear receptors that homodimerize or heterodimerize with other nuclear receptors, bind promoters of target genes and operate as transcription factors (Dawson and Xia, 2012). In the liver, their heterodimerization with liver X receptors (LXR) is able to promote the expression of SREBs, together with other enzymes, involved in the *de novo* fatty acid biosynthesis. Fatty acids produced are then used for cholesterol esterification, and this provides a mechanism to get rid of free cholesterol, which is toxic (Calkin and Tontonoz, 2012).

This suggests that YAP could cooperate with RXR to regulate the expression of SREBs and lipid metabolism. However, RXR and HNF4 transcription factors recognize very similar DNA sequence motifs (Figure 29), raising an issue about the interpretation of this result; therefore, experimental validation will be required to assess the putative YAP/RXR cooperation.

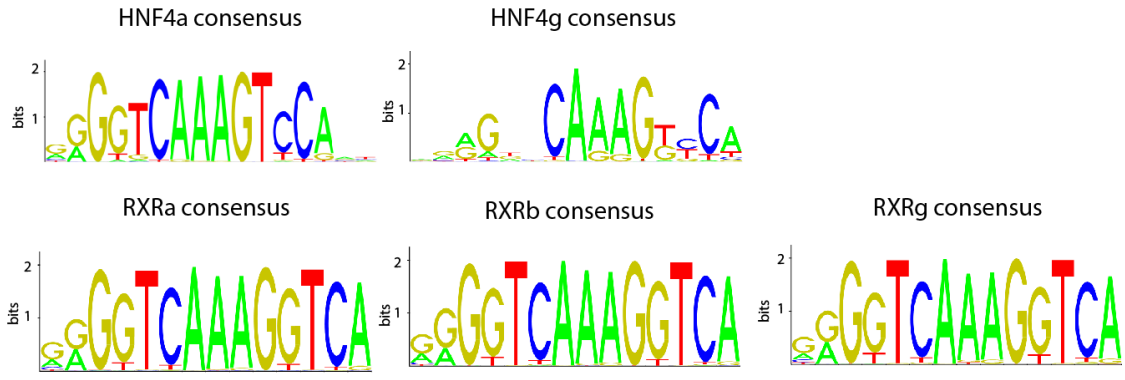

Figure 29: RXR and HNF transcription factors recognize similar DNA sequences. Motifs recognized by HNF4A and HNF4G are very similar to those recognized by RXRa, RXRb and RXRg (Mathelier et al., 2016).

Other motifs were found enriched by this analysis: NR2F1 and NR2F6, FOS/JUN dimer and FOXA2. NR2F1/NR2F6 are two orphan receptors playing a role in immune system (Hermann-Kleiter and Baier, 2014). JUN/FOS, a heterodimer that form the AP1 complex, is known to bind YAP/TEAD complex on chromatin and promote the

expression of genes involved in S-phase progression and mitosis, leading to oncogenic growth in breast cancer cells (Zanconato et al., 2015). FOXA2 transcription factor regulates lipid metabolism in the liver in cooperation with HNF4A (Wolfrum et al., 2004).

1.12 YAP binds HNF4A sites but does not affect their chromatin status

The downregulation of liver-specific genes following YAP activation is consistent with a previous report (Alder et al., 2014). In the adult liver, HNF4A and FOXA2 bind to a set of enhancers to regulate the expression of hepatocyte identity genes (Sekiya and Suzuki, 2011). When YAP is overexpressed, HNF4A and FOXA2 change their chromatin occupancy and activate some enhancers important for embryonic development and silence those active in the adult tissue (Alder et al., 2014).

To better investigate the mechanisms of YAP-mediated suppression of liver-specific programs regulated by HNF4A, we took advantage of published HNF4A and FOXA2 ChIP-Seq data performed in adult and in embryonic liver (Alder et al., 2014). From all 23783 YAP/TEAD co-bound distal sites detected in pre-tumoral liver we defined four subsets: (1) YAP/TEAD regions bound by HNF4A in wild-type adult liver ("Adult"), (2) regions bound by HNF4A in both in the adult and the embryonic liver ("Common") (3) regions bound by HNF4A only in the embryonic liver ("Embryo") and (4) regions not bound by HNF4A in neither the conditions ("Control"). 26% of YAP/TEAD enhancers were bound by HNF4A in normal liver ("Adult" and "Common" subsets; Figure 30, up), indicating that YAP could play a direct role in perturbing HNF4A targets, by interfering with its activity.

We thus compared the enrichment of H3K4me1 and H3K27Ac histone marks in those subsets, both in WT liver and in pre-tumoral liver. Genomic regions bound by HNF4A in WT liver (either in "Adult" or "Common" subsets) were highly enriched in

H3K4me1 and H3K27Ac; upon YAP activation, the enrichment of these two histone modifications remained largely unaffected (Figure 30, down). YAP/TEAD enhancers in the "Control" subset were poorly enriched in H3K4me1 and H3K27Ac, indicating that genomic regions not bound by HNF4A in adult liver were characterized by inactive chromatin context (Figure 30, up). Upon YAP induction, the enrichment of these two histone marks was strongly increased (Figure 30) in this subset, suggesting enhancer activation driven by YAP.

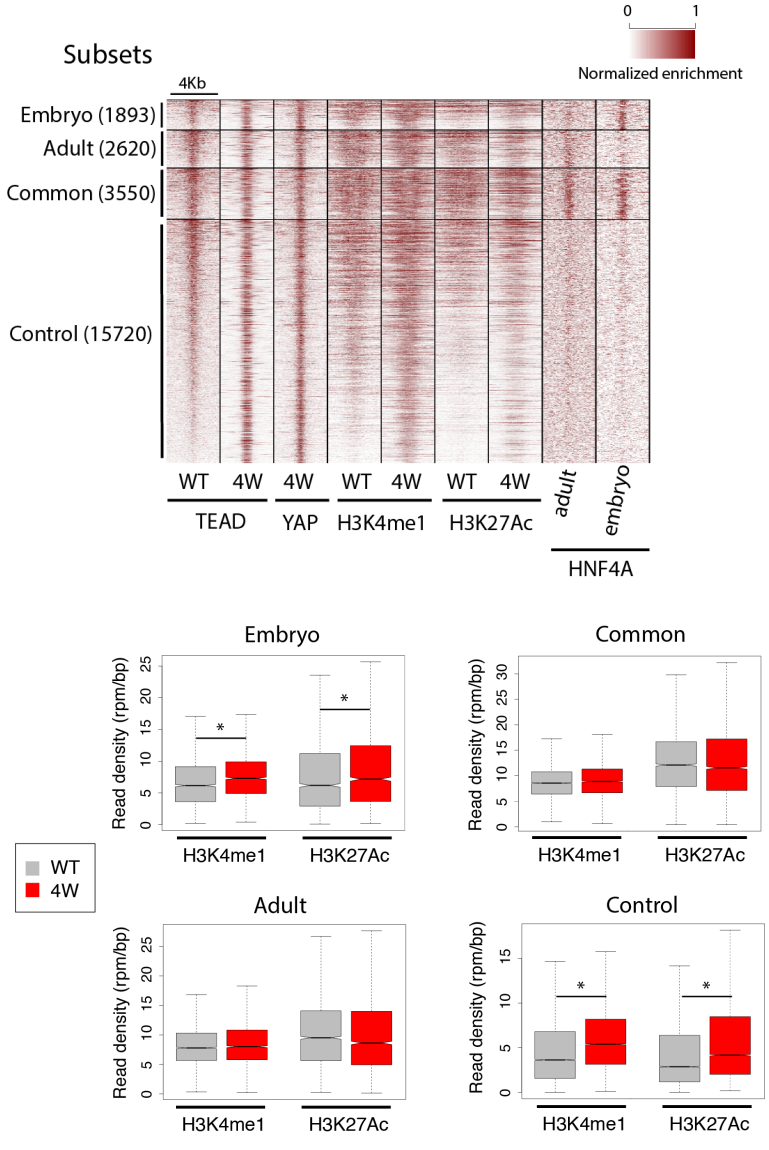

Figure 30: YAP activates chromatin in enhancers not bound by HNF4A in WT liver. Up: heatmap representing the enrichments of YAP, TEAD and histone modifications in the "Embryo", "Adult", "Common" and "Control" subsets (see text). Adult HNF4A ChIP enrichment was retrieved from GEO ID: GSM2055887, while embryonic HNF4A from GEO ID: GSM1318181. Down: Boxplots representing the read density of H3K4me1 and H3K27Ac in WT and pre-tumoral liver in the four subsets. (* p<0.01, paired Student's t-test).

1.13 YAP represses the expression of genes associated to HNF4A bound enhancers

To evaluate the effect of YAP binding on HNF4A bound sites in WT liver ("Common" and "Adult" subsets), we analyzed the transcriptional response of genes regulated by the subsets defined above. For each genomic range, we annotated the nearest gene (if it falls into a distance of 20 kb from its midpoint) and determined the fraction of genes up- or downregulated upon YAP activation.

Genes associated to YAP/TEAD enhancers bound by HNF4A in WT adult liver (either in the "Adult" or "Common" subsets) were mostly downregulated, while genes controlled by enhancers bound by HNF4A in embryonic liver ("Embryo" subset) were prevalently upregulated (Figure 31). Genes regulated by distal YAP/TEAD elements in the "Control" subset were mostly upregulated, as well (Figure 31).

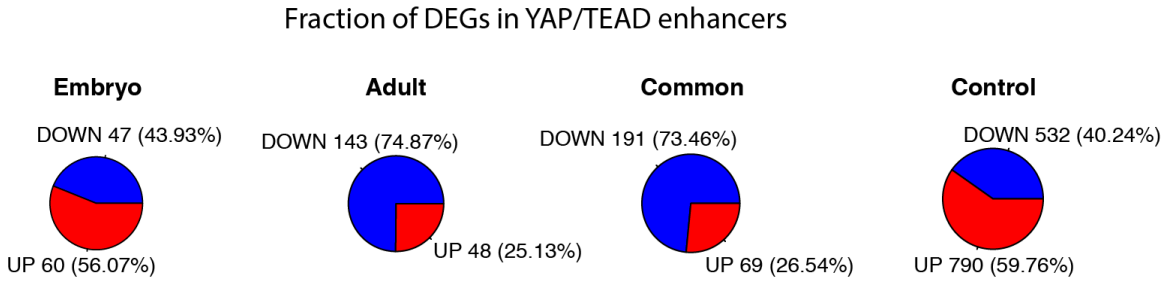

Figure 31: YAP/TEAD enhancers in pre-tumoral liver negatively regulate HNF4A targets. Piecharts representing the fraction of genes up- (red) or downregulated (blue) by YAP/TEAD enhancers bound by HNF4A only in embryonic liver ("Embryo"), in adult liver ("Adult"), in both adult and embryo ("Common"), and not bound by HNF4A in any condition ("Control"). Genes controlled by enhancers bound by HNF4A in adult liver (either "Adult" or "Common") were mostly downregulated, while those regulated by enhancers bound by HNF4A in embryo or not bound by HNF4A at all were mostly upregulated.

A geneset enrichment analysis revealed that downregulated genes controlled by YAP/TEAD enhancers bound by HNF4A in WT liver (subsets "Adult" and "Common") were mainly liver-specific and were also downregulated in samples of hepatocellular carcinoma (Figure 32).

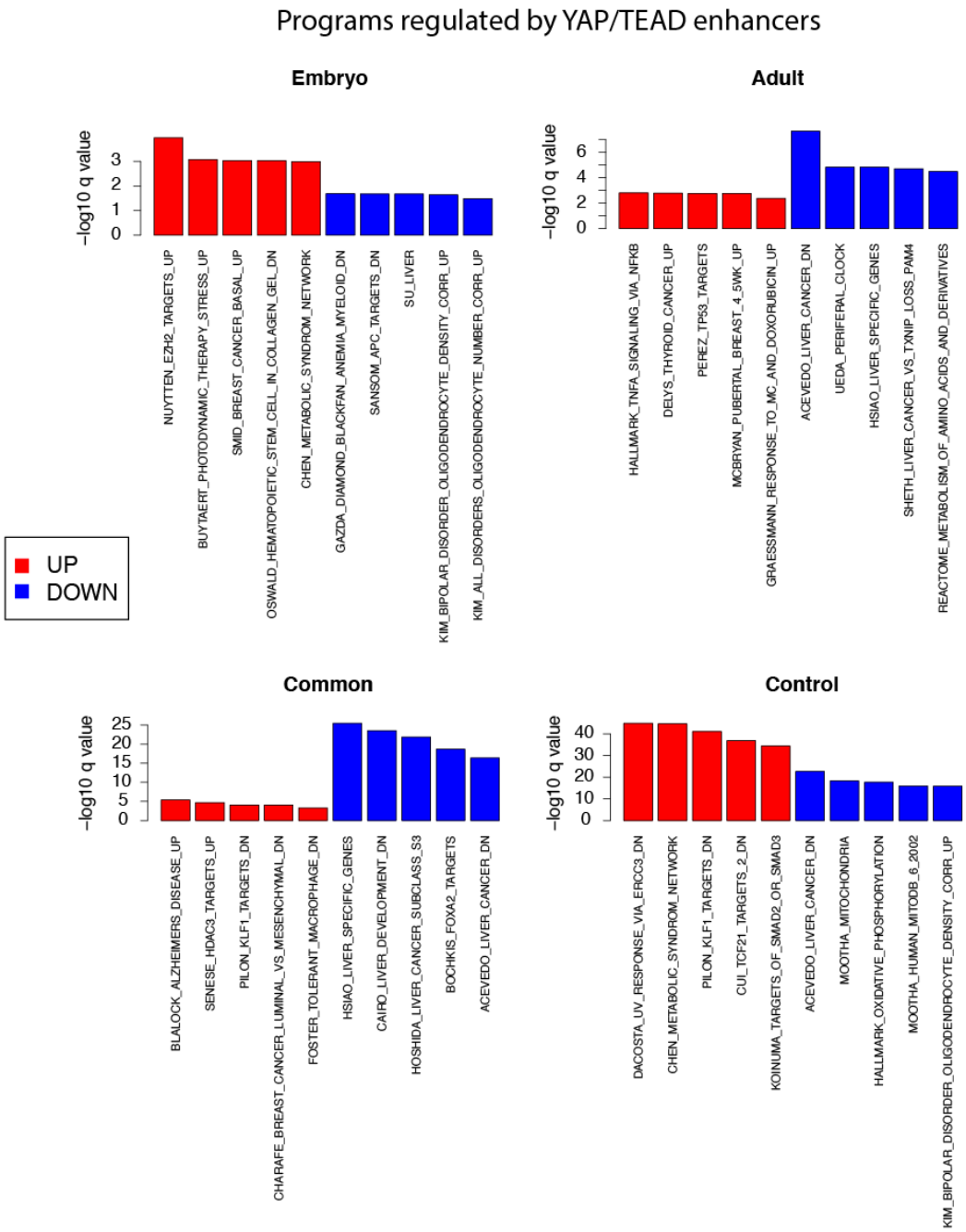

Figure 32: Liver-specific programs controlled by HNF4A are downregulated by YAP. Barplots showing the statistical significance of geneset enrichment analysis (-log10 p value) carried out for genes associated to the four subsets of enhancers ("Adult", "Embryo", "Common", "Control"). Genes downregulated (blue) by YAP/TEAD enhancers bound by HNF4A in WT liver were mostly liver-specific, while no clear signatures can be distinguished for upregulated genes (red).

Upregulated genes controlled by YAP/TEAD in enhancers bound by HNF4A in embryonic liver (subset "Embryo") did not belong to specific categories, the same was found for the subset in which HNF4A is not bound in neither embryonic nor adult liver ("Control") (Figure 32).

These results altogether indicate that when YAP binds to genomic sites pre-marked by HNF4A in normal liver, it then exerts a repressor function on the transcription of liver-specific genes, without affecting the chromatin status (Figure 30, down). In all the other loci, YAP acts as an activator: it probably recruits histone acetyltransferases and/or methyltransferases to increase the level of H3K27Ac and H3K4me1 (Figure 30, down) and promotes the expression of associated genes.

Performing ChIP-Seq experiments and functional studies on HNF4A in pre-tumoral liver could unravel the mechanism behind YAP-mediated repression.

2 Results part 2: YAP cooperates with Myc to promote cell proliferation

2.1 Design and rationale of the study

Myc oncogene is a helix-loop-helix transcription factor, whose activation is fundamental for cell cycle entry and is crucial in determination of organ size (Perna et al., 2012; Trumpp et al., 2001). Myc expression is sufficient to promote cell proliferation both *in vitro* (Perna et al., 2012) and *in vivo* (Pelengaris et al., 1999), but Myc-induced cell cycle entry is impaired in confluent cells (Demeterco et al., 2002) and in adult liver, indicating that Myc expression alone is not sufficient to induce cell proliferation (De Fazio, personal communication). These evidences imply that Myc activation is context dependent. Therefore, we asked whether YAP activation could synergize with Myc to bypass these limitations. Three observations support a putative role of YAP in co-adjuvating Myc response. First, massive cell proliferation was observed in the mouse liver when both YAP and Myc were expressed together (De Fazio, personal communication). Second, their co-expression in confluent fibroblasts was sufficient to induce cell cycle while expression of either factor alone was inconsequential (De Fazio, personal communication). Finally, based on RNA-Seq, Myc was overexpressed in tumors, possibly suggesting that cells with elevated levels of Myc were positively selected during tumor evolution (Figure 33).

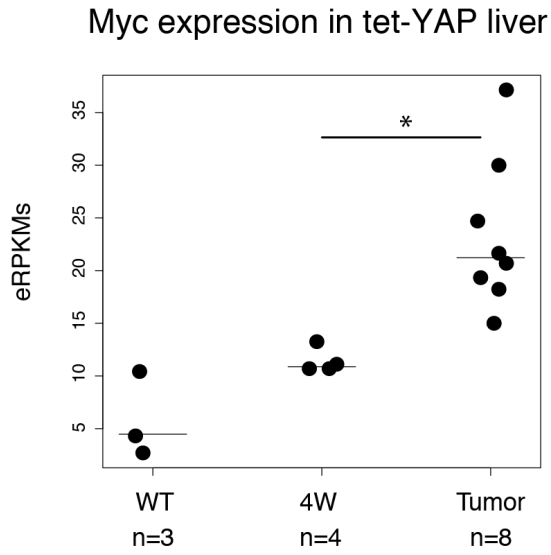

Figure 33: Myc expression is higher in tet-YAP tumor nodules. Myc expression (in eRPKMs) of RNA-Seq replicates in 3 WT mice livers, 4 pre-tumoral livers (4W) and 8 independent tumor nodules. The higher expression in tumor nodules compared to pre-tumoral tissue suggests that cells with high expression of Myc were selected. (* p=0.0018, Student's t-test).

With next generation sequencing data, we carried out genomic and transcriptomic analyses using *in vitro* and *in vivo* models, to better investigate whether and how YAP and Myc can cooperate at genomic level and which are the transcriptional programs they regulate to promote cell proliferation.

2.2 The in vitro approach: 3T9 cell line

As *in vitro* model to study YAP/Myc cooperation we used 3T9 cell line that overexpressed the mutant and active form of YAP (YAP^{S127A}), whose expression was under the control of doxycycline. Myc, fused with estrogen receptor, was constitutively expressed and could be activated upon 4-hydroxytamoxifen (OHT) treatment (Littlewood et al., 1995). Single activation of either Myc or YAP had no effects on confluent cells, while their concomitant activation lead to strong cell proliferation (De Fazio, personal communication). This reflects on the difference in transcriptional regulation observed between experimental conditions, where samples in which both Myc and YAP were active clustered separately (Figure 34).

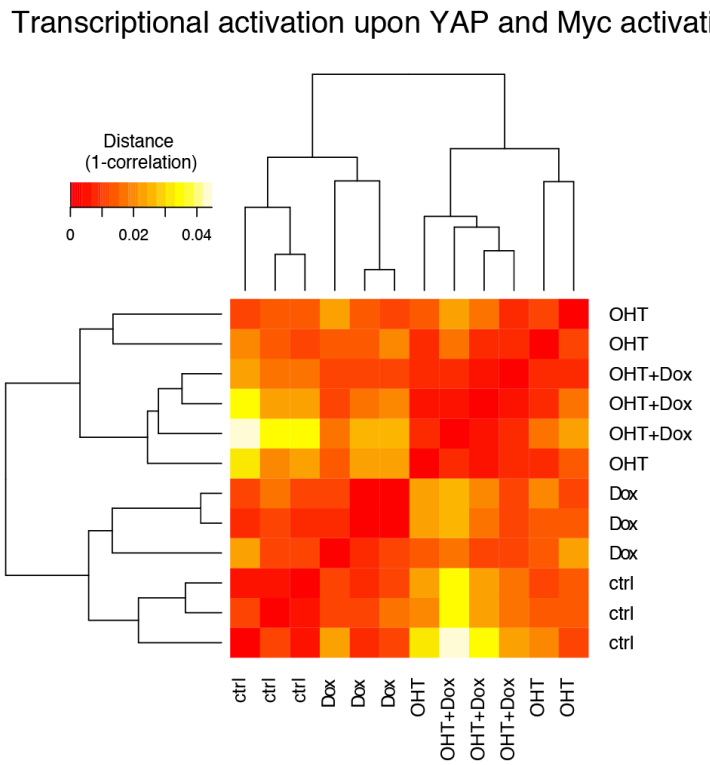

Figure 34: Different transcriptional responses are activated when YAP, Myc or both are induced in 3T9 cells. Heatmap representing the distance (1-correlation) of RNA-Seq read counts in transcripts in different experimental conditions: WT cells (ctrl), YAP and Myc induction alone (Dox and OHT, respectively) on in combination (OHT+Dox). Samples belonging to different experimental conditions clustered almost separately, indicating that different transcriptional programs were active when YAP, Myc, or both were expressed.

Synergistic interaction between YAP and Myc could also be noted by assessing the number of genes de-regulated compared to normal cells; 2377 genes were deregulated (DEGs) when both proteins were co-activated, while the expression of only 300 and 932 genes were altered when only YAP or Myc were induced alone, respectively (Figure 35a). Stronger gene deregulation was observed in YAP/Myc co-activated cells, since the change in gene expression was higher in cells treated with both Doxycycline and OHT (Figure 35b).

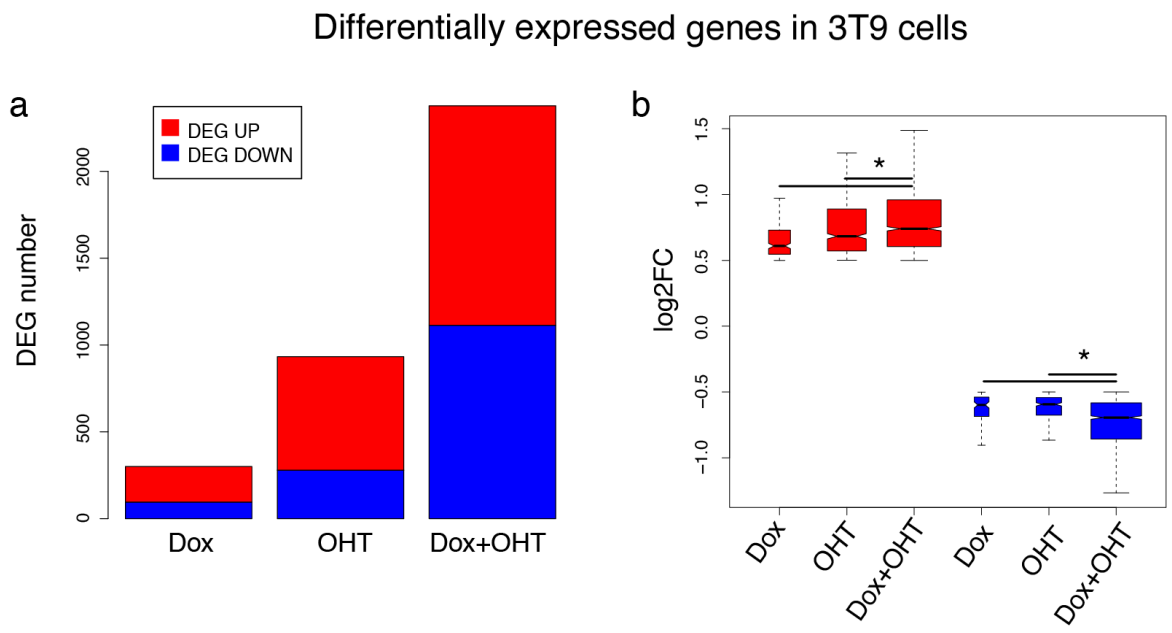

Figure 35: Induction of both YAP and Myc leads to stronger gene de-regulation compared to single Myc or YAP induction alone *in vitro*. a) barplot representing the number of DEG up (red) and DEG down (blue) upon activation of YAP alone (Dox), Myc alone (OHT) or the combination of both (Dox+OHT) in 3T9 cells; b) log2 fold change in gene expression of genes up (red) or downregulated (blue) upon induction of YAP (Dox), Myc (OHT) or YAP+Myc (Dox+OHT). Both number of DEGs and their change in expression were higher when YAP and Myc were overexpressed together. (* $p<0.001$, Student's t-test).

Geneset enrichment analysis on deregulated genes showed that concomitant activation of both Myc and YAP modulated the expression of genes involved in cell cycle (Figure 36).

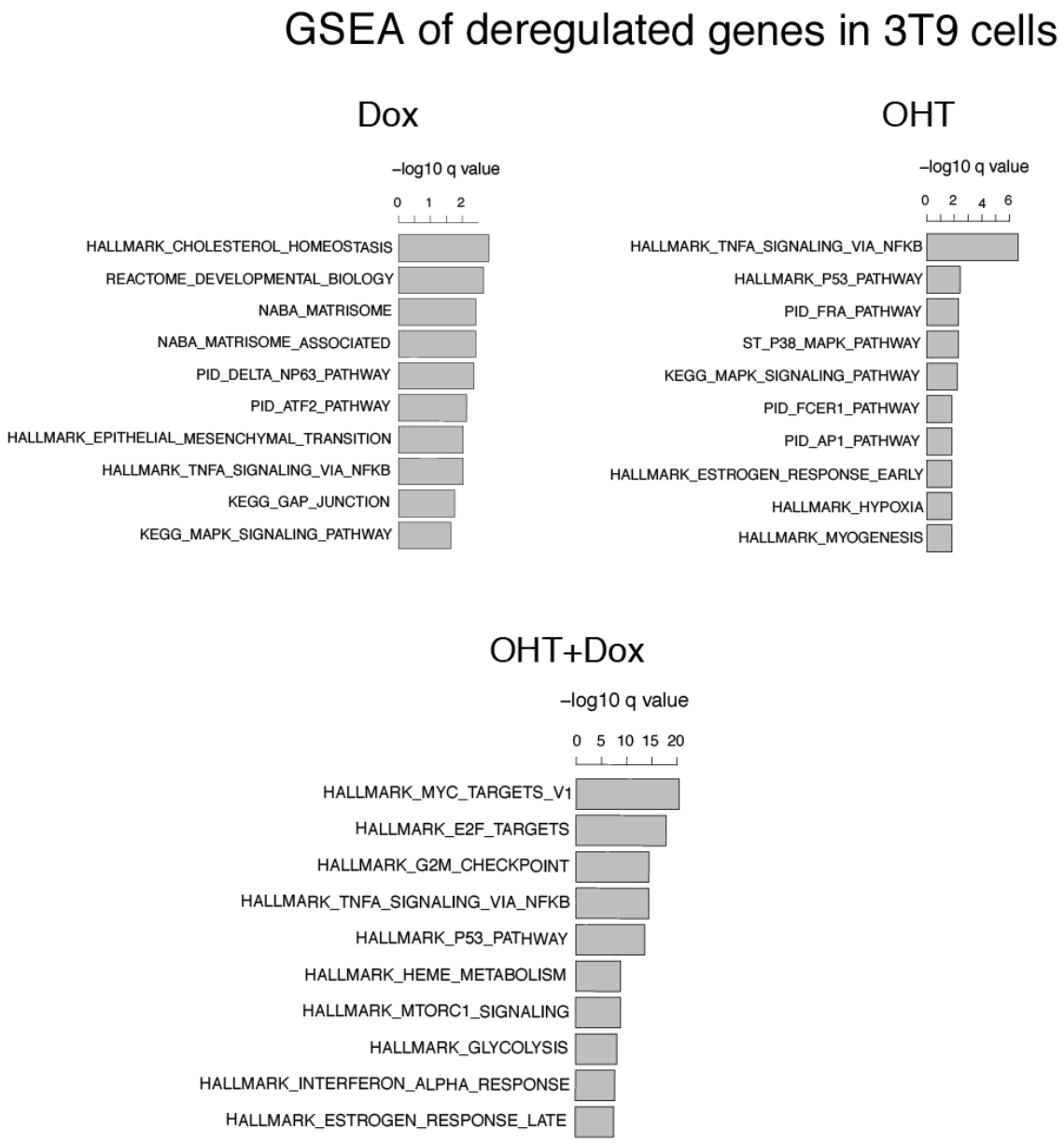

Figure 36: Cell cycle genes are upregulated when both YAP and Myc are activated. Barplots representing p adjusted of GSEA (Subramanian et al., 2005) of the top 10 hits when cells were activated with YAP (Dox), Myc (OHT) or YAP+Myc (OHT+Dox). When both YAP and Myc were activated in 3T9 cells, cell cycle genes were regulated.

These results showed a synergistic effect of Myc and YAP in activating cell cycle gene expression and in promoting cell proliferation.

We then carried out ChIP-Seq analyses of YAP, TEAD and Myc to better understand how YAP and Myc could co-regulate common genes. The majority of Myc chromatin binding involved promoters, while YAP and TEAD bound prevalently distal regions (Figure 37).

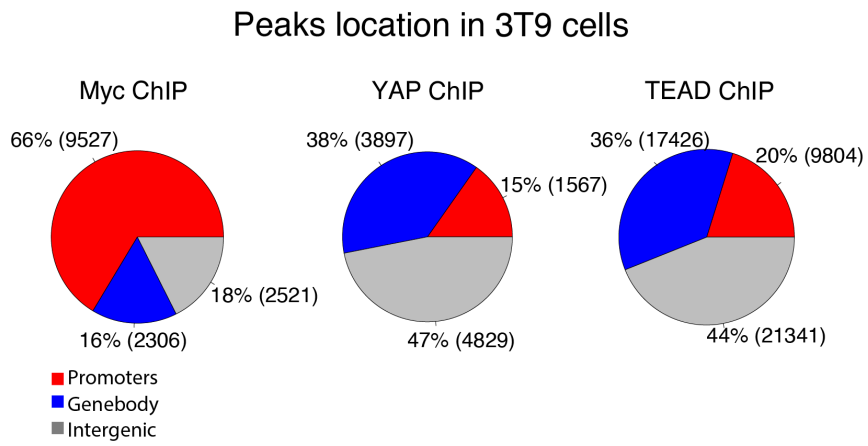

Figure 37: Myc binds mainly promoters, while YAP/TEAD distal sites in 3T9 cells upon YAP and Myc activation. Piecharts representing the fraction of Myc, YAP or TEAD peaks located on promoters (red), genebodies (blue) or intergenic sites (grey).

Almost all promoters that overlapped with YAP were bound also by Myc and TEAD (~90%) (Figure 38a) and the enrichment of these factors, when bound together, was higher compared to their enrichment when they bound chromatin alone (Figure 38b). This suggests that YAP, Myc and TEAD may stabilize each other when they co-localize on chromatin.

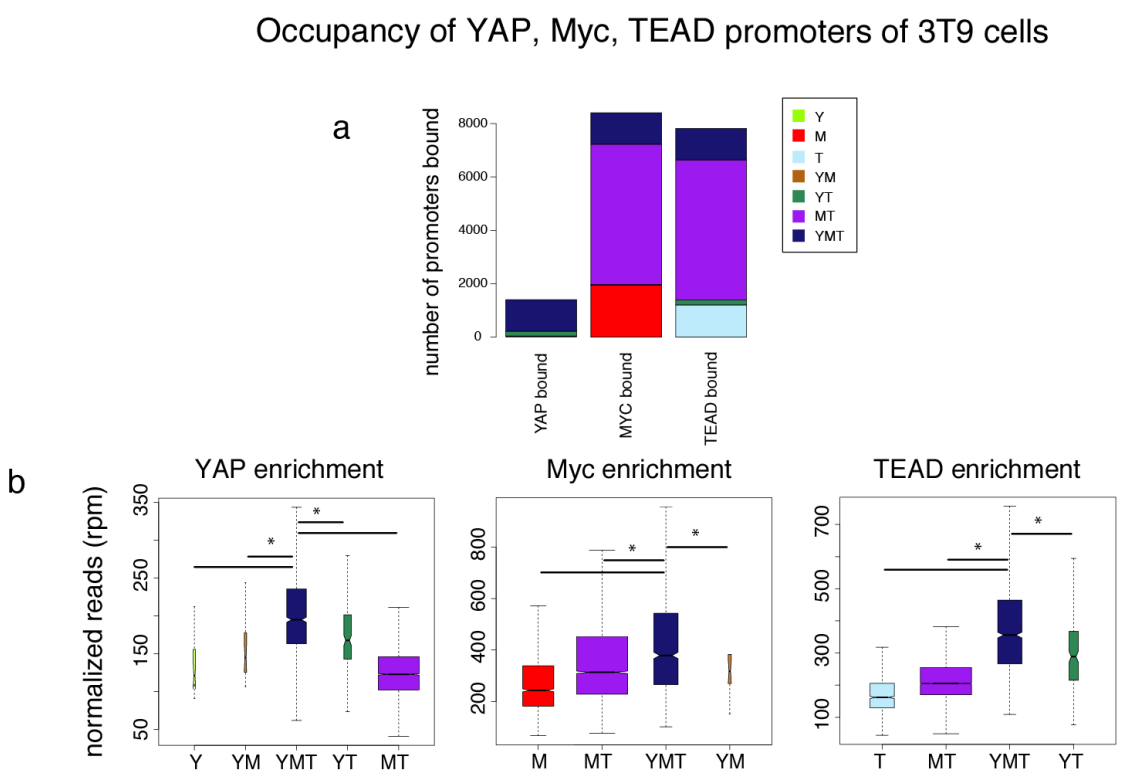

Figure 38: Upon YAP and Myc concomitant activation, YAP and Myc extensively co-localize at promoters in 3T9 cells. a) barplot representing the fraction of promoters bound by YAP, Myc or TEAD that are also co-bound by the other two factors: almost all YAP-bound promoters were also co-bound by Myc and TEAD; b) Enrichment of YAP, Myc or TEAD in promoters bound by Myc alone (M), TEAD alone (T), Myc+TEAD (MT), Myc+TEAD+YAP (YMT) or YAP+Myc (YM); the enrichment in YMT promoters was higher for all the three transcription factors, suggesting that Myc, TEAD and YAP were stabilized when bound together. (* $p<0.001$, Student's t-test).

Figure adapted from "Transcriptional integration of mitogenic and mechanical signals by Myc and YAP" (Croci et al., 2017) Copyright © 2017 Croci et al.; Published by Cold Spring Harbor Laboratory Press.

To identify genes bound and regulated by YAP, Myc and TEAD, we examined the change in expression of genes whose promoters were bound by YAP, Myc and TEAD together. These genes changed more their expression when Myc and YAP were overexpressed together, compared to when these transcription factors were overexpressed alone (Figure 39), indicating that their simultaneous binding to promoters associated with stronger genes deregulation.

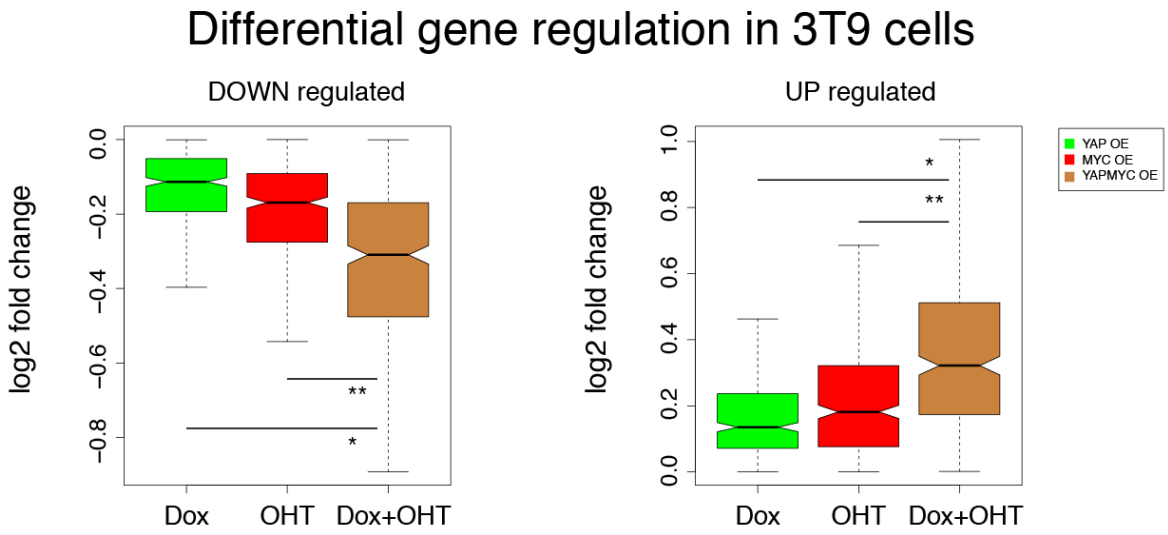

Figure 39: Genes bound by both YAP, TEAD, Myc undergo greater changes in gene expression when both YAP and Myc are expressed. Boxplots representing the log2 fold change of expression of genes whose promoters were bound by both YAP and Myc in YAP+Myc activated cells. Genes downregulated upon concomitant YAP and Myc expression (left) were only mildly downregulated when either YAP or Myc were overexpressed alone (Dox / OHT), but strongly downregulated when both were expressed (Dox+OHT). The same was true for upregulation (right). (*, ** $p<0.05$, Student's t-test.

Figure adapted from "Transcriptional integration of mitogenic and mechanical signals by Myc and YAP" (Croci et al., 2017) Copyright © 2017 Croci et al.; Published by Cold Spring Harbor Laboratory Press.

These data indicate that YAP and Myc cooperate *in cis* on the DNA, stabilize each other's binding and strongly enhance the expression of genes involved in the cell cycle.

2.3 The in vivo approach: mouse liver

To verify if the cooperation between YAP and Myc observed in 3T9 cells occurred also *in vivo*, we carried out experiments in the adult liver of mouse models where the expression of Myc, YAP (YAP^{S127A}) or the combination of both could be switched on using doxycycline (tet-Myc, tet-YAP, tet-YAP/Myc liver, respectively). We examined the hepatic tissue after 2 days of doxycycline treatment. Robust cell proliferation occurred only when both YAP and Myc were expressed (tet-YAP/Myc liver), while

only weak cell proliferation was observed when either Myc or YAP were induced alone (De Fazio personal communication), in accordance to the different transcriptional programs activated in these mice (Figure 40).

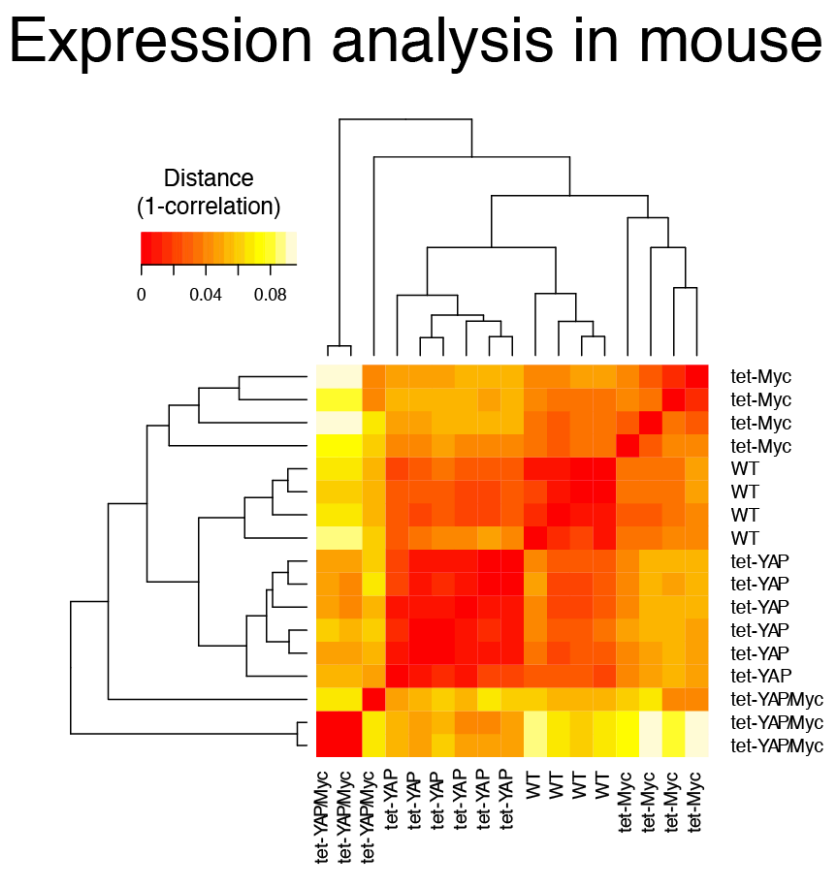

Figure 40: Different transcriptional programs are active when both Myc and YAP were induced *in vivo*. Heatmap representing the distance (1-correlation) of RNA-Seq read counts of 4 WT livers or livers in which Myc alone (tet-Myc), YAP alone (tet-YAP) or both (tet-YAP/Myc) were overexpressed for 2 days. YAP/Myc concomitant overexpression lead to the activation of different transcriptional programs compared to when single factors were expressed alone.

Consistent with this, many genes (3586) were found significantly de-regulated only when both YAP and Myc were overexpressed together (Figure 41a) and their change in expression was higher compared to DEGs resulting from single expression of Myc or YAP alone (Figure 41b).

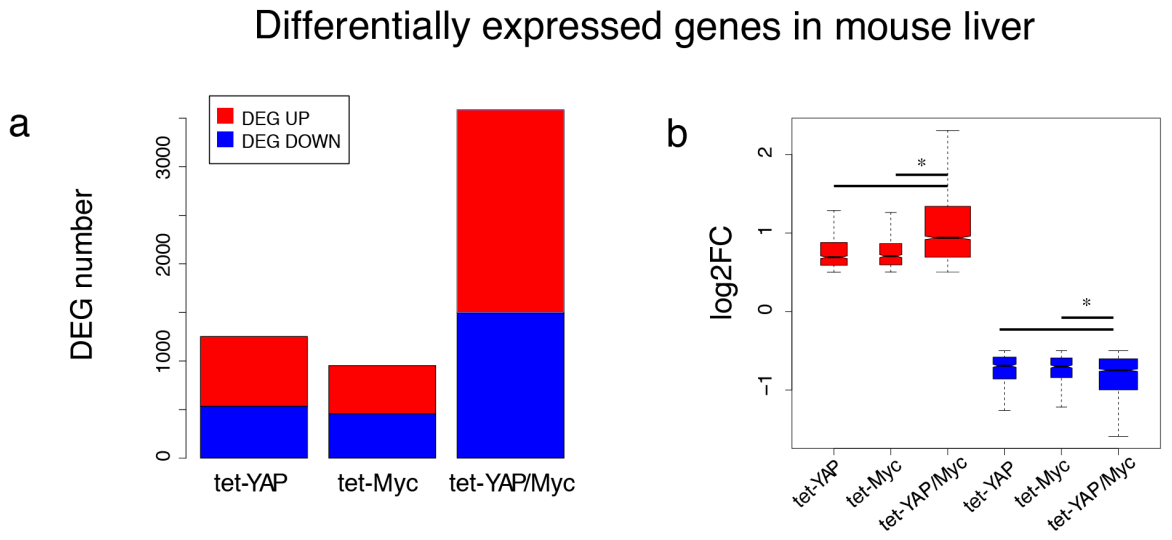

Figure 41: Induction of both YAP and Myc *in vivo* leads to stronger gene de-regulation compared to single Myc or YAP induction. a) barplot representing the number of DEG up (red) and DEG down (blue) upon activation of YAP alone (tet-YAP), Myc alone (tet-Myc) or the combination of both (tet-YAP/Myc); b) boxplot representing log2 fold change in gene expression of genes up (red) or down (blue) regulated upon induction of YAP (tet-YAP), Myc (tet-Myc), YAP+Myc (tet-YAP/Myc). Both number of DEGs and their change in expression was higher when both YAP and Myc were overexpressed. (* $p<0.01$, Student's t-test).

Figure adapted from "Transcriptional integration of mitogenic and mechanical signals by Myc and YAP" (Croci et al., 2017) Copyright © 2017 Croci et al.; Published by Cold Spring Harbor Laboratory Press.

Moreover, genes differentially regulated when both Myc and YAP were overexpressed were enriched in ontological terms linked to cell growth and cell cycle control (Figure 42).

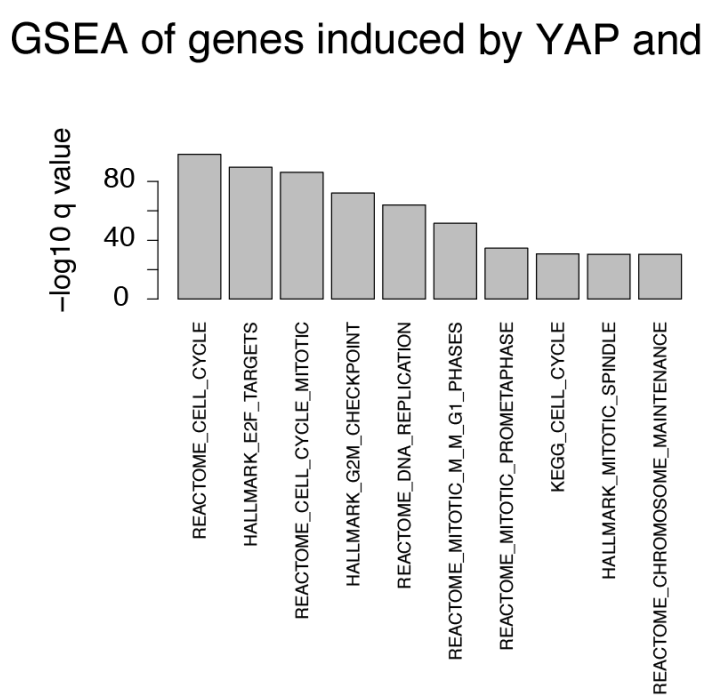

Figure 42: Concomitant induction of Myc and YAP upregulates cell cycle genes in mouse liver. Barplot representing p adjusted of top 10 hits of GSEA (Subramanian et al., 2005) of genes upregulated when both Myc and YAP were induced in tet-YAP/Myc liver.

To understand if YAP/Myc cooperation involved co-occurrence of these factors on chromatin, we analyzed genomic occupancy of Myc, TEAD and YAP in WT, tet-YAP, tet-Myc and tet-YAP/Myc livers by performing ChIP-Seq experiments.

In normal (WT) liver, Myc was weakly bound to DNA (only about 5000 peaks), but upon its overexpression, its association with chromatin was strongly enhanced (32000 and 30000 peaks detected in tet-Myc and tet-YAP/Myc liver, respectively) (Figure 43, left); YAP induction alone was able to increase the number of Myc binding sites, but only mildly (13000 Myc peaks in tet-YAP) (Figure 43, left). This indicates that Myc chromatin binding scales with its own overexpression levels and is not further increased by YAP expression.

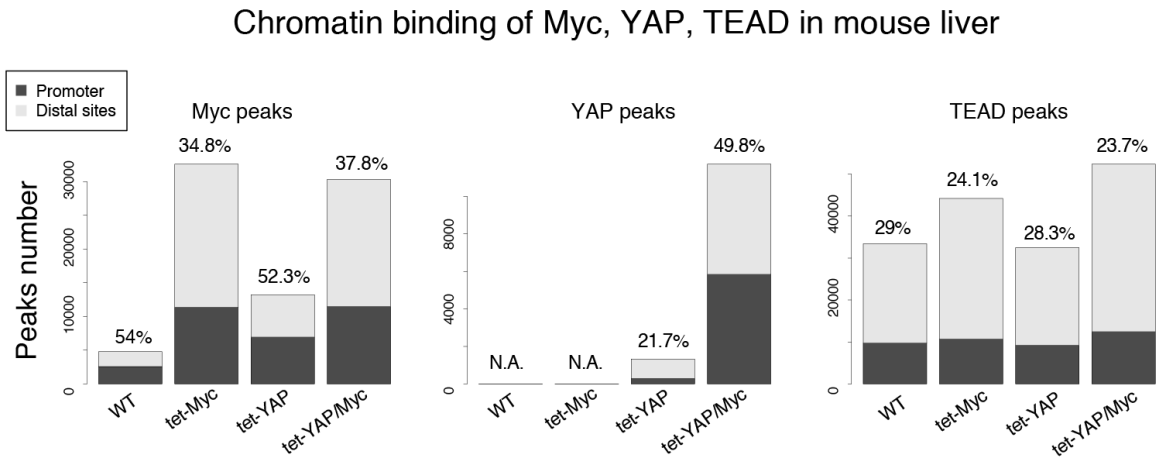

Figure 43: ChIP peaks of Myc, YAP and TEAD detected in mouse liver. Barplots representing the number of peaks of Myc (left), YAP (center), TEAD (right) at promoters (dark grey) and distal sites (light grey) in mouse liver, in all the conditions tested (WT liver, tet-Myc, tet-YAP, tet-YAP/Myc). The percentage represents the fraction of peaks located at promoters.

Figure adapted from "Transcriptional integration of mitogenic and mechanical signals by Myc and YAP" (Croci et al., 2017) Copyright © 2017 Croci et al.; Published by Cold Spring Harbor Laboratory Press.

YAP chromatin binding in WT liver and tet-Myc liver was negligible, while upon its induction about 1300 binding sites were found in tet-YAP liver (Figure 43, center). When YAP and Myc were induced together (tet-YAP/Myc liver), YAP chromatin interaction was strongly increased (about 12000 peaks detected) (Figure 43, center), suggesting that Myc promotes the binding of YAP to chromatin.

Finally, TEAD chromatin occupancy was extensive and rather consistent in all the condition tested, with a slight increase in conditions when Myc was expressed (Figure 43, right).

To verify if TEAD, Myc and YAP co-localized on chromatin as observed in 3T9 cells, we overlapped YAP/Myc/TEAD peaks in all the conditions tested. On average, 70% of Myc peaks co-localized with TEAD (Figure 44). While only a negligible fraction (23%) of YAP binding sites were shared with Myc in tet-YAP liver, almost all (91%) of them co-localized with Myc in tet-YAP/Myc liver (Figure 44).

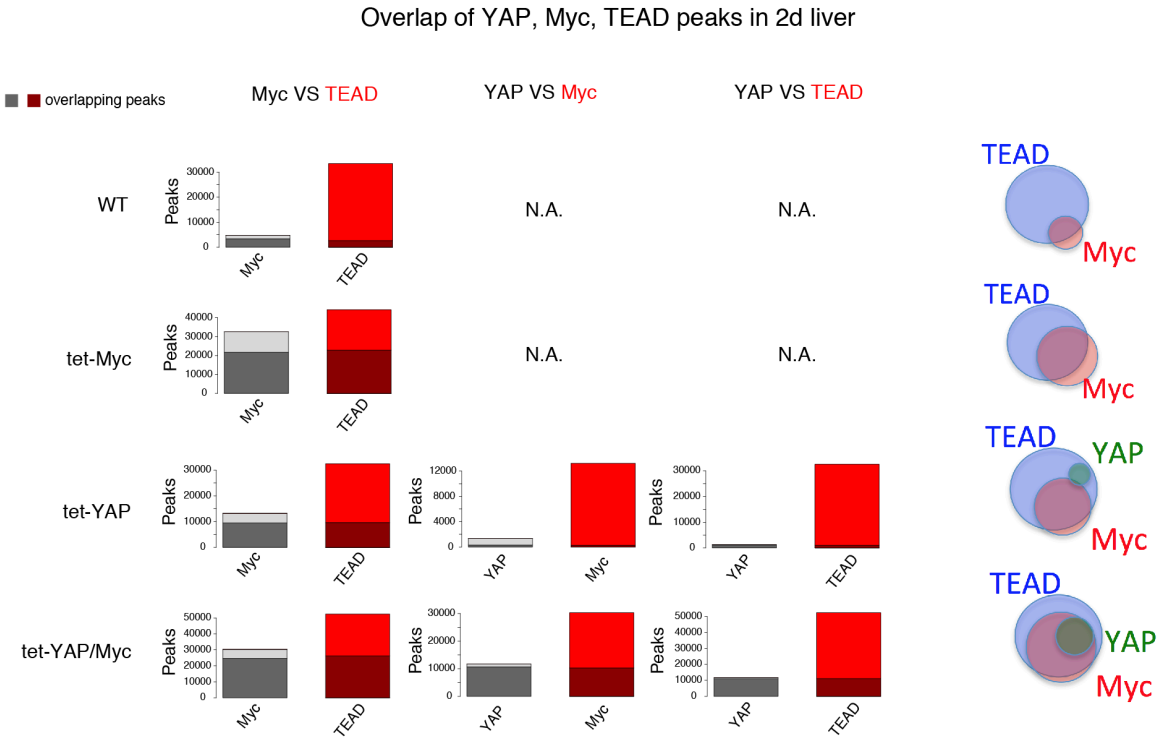

Figure 44: YAP and Myc co-localize when expressed together in tet-YAP/Myc liver. Left: Barplot representing the fraction of overlapping peaks in different comparisons of ChIP-Seq experiments. In WT liver or tet-Myc liver, Myc and TEAD peaks showed high overlap. When YAP was expressed alone (tet-YAP), both YAP and Myc co-localized with TEAD, but weak overlap was present between Myc and YAP. In tet-YAP/Myc liver, YAP and Myc co-localized together, and the vast majority of YAP binding sites were shared with Myc. Right: Venn diagram representation of these overlaps.
Figure adapted from "Transcriptional integration of mitogenic and mechanical signals by Myc and YAP" (Croci et al., 2017) Copyright © 2017 Croci et al.; Published by Cold Spring Harbor Laboratory Press.

YAP localization to Myc binding sites reflected also on the change in the distribution of YAP ChIP-Seq peaks: while the majority of YAP peaks were located at distal sites in tet-YAP liver (Figure 45, left), 50% were found at promoters when YAP was overexpressed together with Myc (Figure 45, right).

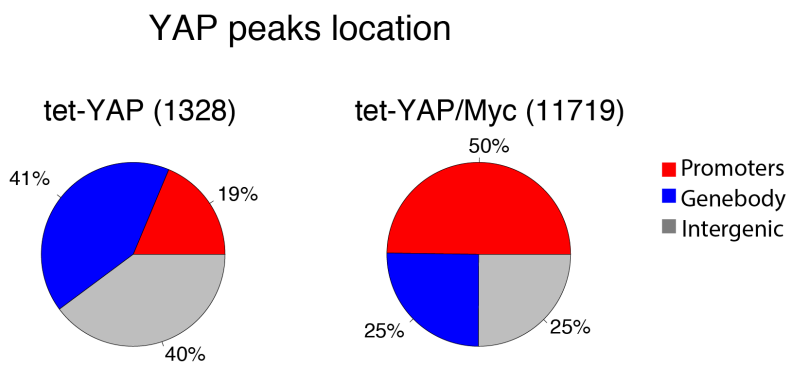

Figure 45: YAP is recruited on promoters when co-expressed with Myc in tet-YAP/Myc liver. Piecharts showing the YAP peaks distribution in tet-YAP liver (left) and tet-YAP/Myc liver (right). The majority (81%) of YAP peaks were located in distal sites in tet-YAP liver (left); when Myc was overexpressed with YAP (tet-YAP/Myc liver, right), YAP was recruited on Myc bound sites, and 50% of them occupied promoters.

Figure adapted from "Transcriptional integration of mitogenic and mechanical signals by Myc and YAP" (Croci et al., 2017) Copyright © 2017 Croci et al.; Published by Cold Spring Harbor Laboratory Press.

Co-localization of YAP and Myc correlated with gene regulation: a consistent fraction of genes deregulated upon Myc/YAP activation was bound by both YAP and Myc (Figure 46).

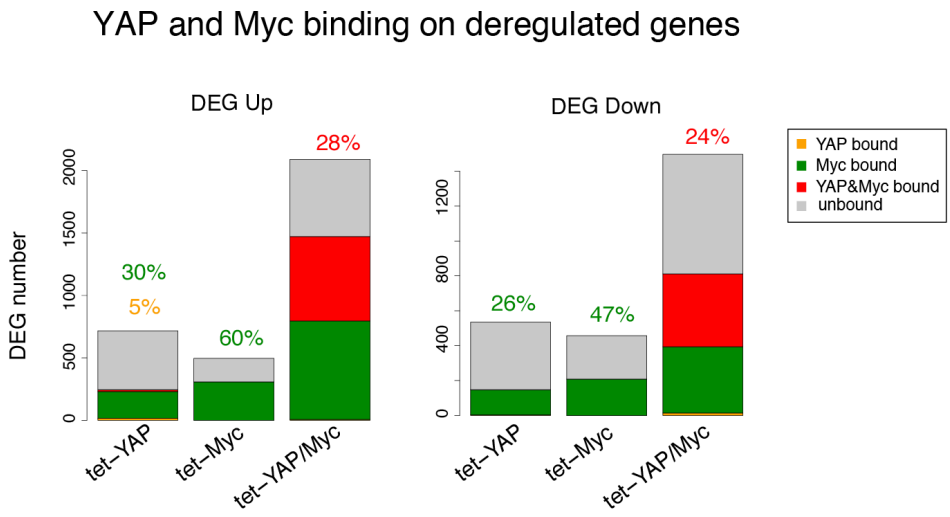

Figure 46: Co-occurrence of YAP and Myc on promoters is associated with gene deregulation. Barplot representing the fraction of genes upregulated (left) or downregulated (right) bound by YAP, Myc or both at their promoter, in tet-YAP, tet-Myc or tet-YAP/Myc liver. The fraction of DEGs bound by both YAP and Myc was higher in tet-YAP/Myc liver, compared to the other conditions tested.

Figure adapted from "Transcriptional integration of mitogenic and mechanical signals by Myc and YAP" (Croci et al., 2017) Copyright © 2017 Croci et al.; Published by Cold Spring Harbor Laboratory Press.

Moreover, promoters of up- and downregulated genes in tet-YAP/Myc liver were pre-bound by H3K27Ac and H3K4me3 (Figure 47); this was expected, since Myc requires open, pre-activated chromatin to bind DNA (Sabò et al., 2014). Upon Myc overexpression, the enrichment of H3K4me3 was further increased (Figure 47, down), suggesting the possible recruitment of methyltransferases on these sites.

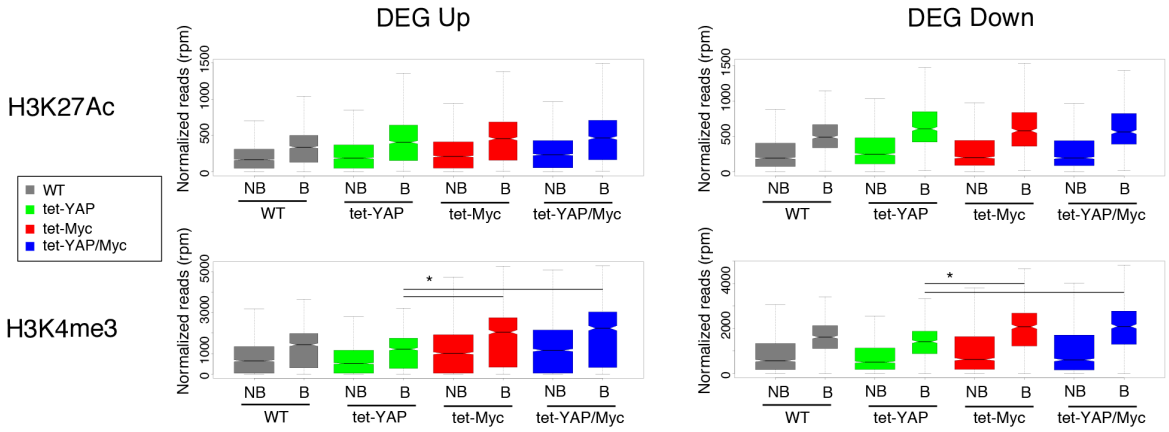

Figure 47: Myc binding is associated with pre-activated chromatin and an increase in H3K4 trimethylation. Boxplots representing the enrichment of and H3K27Ac (up) and H3K4me3 (down) on promoters of up (left) and downregulated genes (right) in tet-YAP/Myc liver. Promoters bound (B) by Myc had higher enrichments compared to those not bound (NB) and enrichment of H3K4me3 was increased upon Myc overexpression (tet-Myc and tet-YAP/Myc). (* p<0.001, Student's t-test).
Figure adapted from "Transcriptional integration of mitogenic and mechanical signals by Myc and YAP" (Croci et al., 2017) Copyright © 2017 Croci et al.; Published by Cold Spring Harbor Laboratory Press.

Genes upregulated by concomitant Myc/YAP activation and bound by both these factors showed increased Pol2 recruitment and elongation (Figure 48), according to the mechanism of Myc and YAP in promoting transcriptional activation (Rahl et al., 2010; Sabò et al., 2014; Galli et al., 2015; Kress et al., 2016).

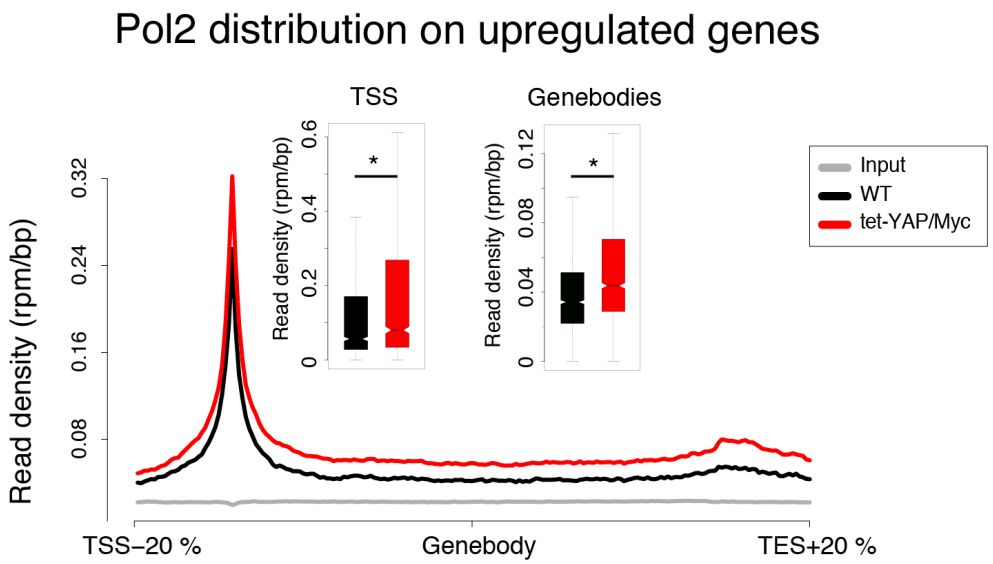

Figure 48: Genes upregulated upon concomitant YAP and Myc expression have increased Pol2 recruitment and elongation. Average profile of Pol2 enrichment on genebodies of upregulated genes bound by YAP, Myc and TEAD, both in WT and tet-YAP/Myc liver. Boxplots represent the read density of Pol2 at TSS and genebodies. Pol2 levels increased both at TSS (recruitment) and genebodies (elongation). (* $p < 0.05$, paired Student's t-test).

Figure adapted from "Transcriptional integration of mitogenic and mechanical signals by Myc and YAP" (Croci et al., 2017) Copyright © 2017 Croci et al.; Published by Cold Spring Harbor Laboratory Press.

These data together suggest that, when Myc is overexpressed with YAP, it binds chromatin in promoters pre-marked by TEAD (Figure 44) and pre-activated by H3K27Ac and H3K4me3 (Figure 47), and hijack YAP binding to those sites. Then, through recruiting more Pol2 and promoting its elongation (Figure 48), is able to induce the expression of cell cycle genes and cell proliferation (Figure 42).

2.4 YAP cooperates with Myc upon their long-term induction

We then wanted to address the long-term effects of YAP/Myc cooperation in the liver. We overexpressed Myc, YAP or both in mouse liver for 4 weeks, using the LAP-tTA system. While YAP expression alone (tet-YAP) lead to hepatomegaly as reported (Camargo et al., 2007) and Myc expression alone (tet-Myc) did not alter significantly

liver phenotype, concomitant expression of both (tet-YAP/Myc) resulted in severe hepatomegaly and the survival of these mice was impaired compared to those in which Myc alone or YAP alone were overexpressed (De Fazio, personal communication). This phenotype was consistent with gene expression: clustering of RNA-Seq read counts indicated that tet-YAP/Myc livers exhibit a high similarity to tumor transcriptional profiles compared to livers in which only Myc (tet-Myc) or only YAP (tet-YAP) were overexpressed (Figure 49).

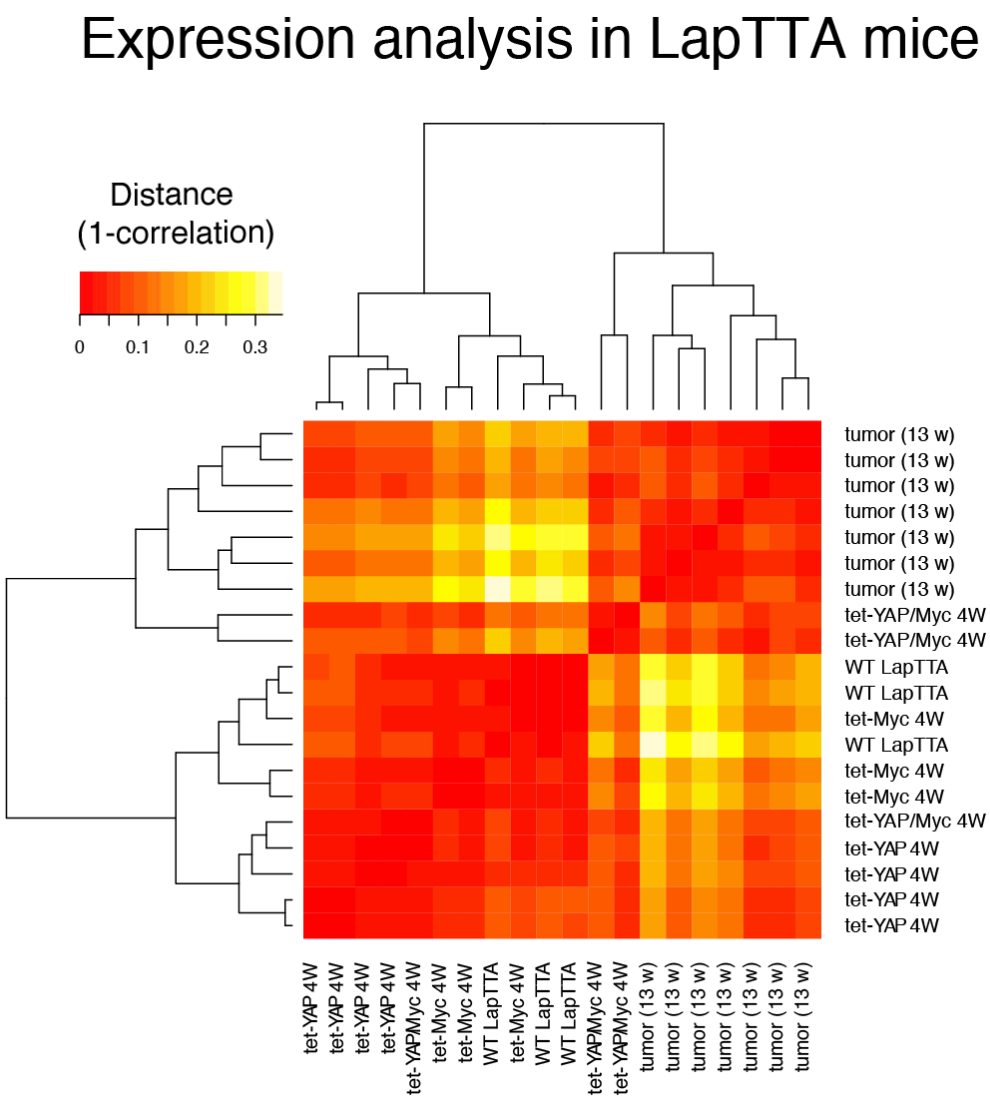

Figure 49: Transcriptional profile of liver after 4 weeks of concomitant Myc and YAP activation is similar to tet-YAP tumors. Heatmap representing the distance (1-correlation) of RNA-Seq reads count on 3 WT livers, 4 tet-YAP livers, 3 tet-Myc livers, 3 tet-YAP/Myc livers activated for 4 weeks and tet-YAP tumors derived from 13 weeks YAP activation. Transcriptional programs of the tet-YAP/Myc replicates resemble those of tumors.

To address whether YAP and Myc co-localization on chromatin persisted also upon their combined long-term activation, we profiled YAP and Myc chromatin binding by ChIP-Seq.

Myc binding was highly increased if both YAP and Myc were induced long-term, since more than 50000 peaks were detected in tet-YAP/Myc liver, while lower numbers were found in WT or tet-YAP liver (Figure 50).

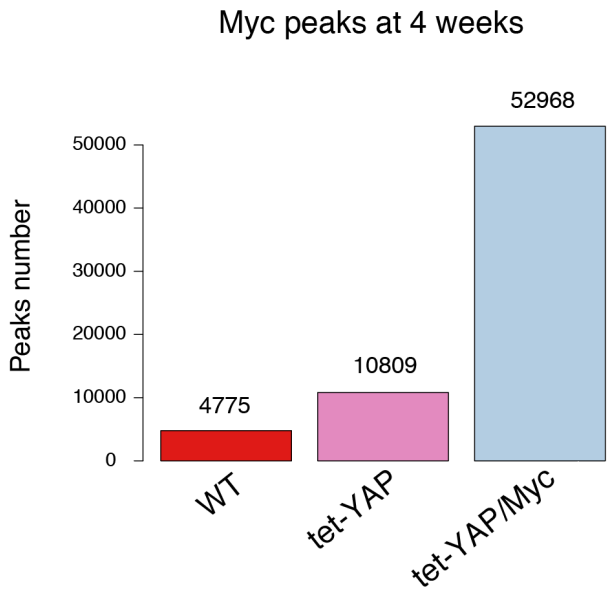

Figure 50: Myc chromatin association is increased in long-term YAP/Myc co-activation. Barplot representing the number of Myc peaks detected in WT, tet-YAP and tet-YAP/Myc liver; when Myc was overexpressed with YAP, its chromatin binding increased compared to WT liver.

Only part (11%) of YAP binding sites co-localized with Myc in tet-YAP liver (Figure 51, left), while the vast majority of them (87%) were located in Myc bound regions in tet-YAP/Myc mice (Figure 51, right), confirming the relocalization seen in short-term experiments. Moreover, their binding was stronger in co-bound sites compared to regions bound by YAP or Myc alone (Figure 52).

All these data together indicate that cooperation between YAP and Myc persists long-term and leads to hepatomegaly, resembling tumor nodules, both genotipically and phenotypically.

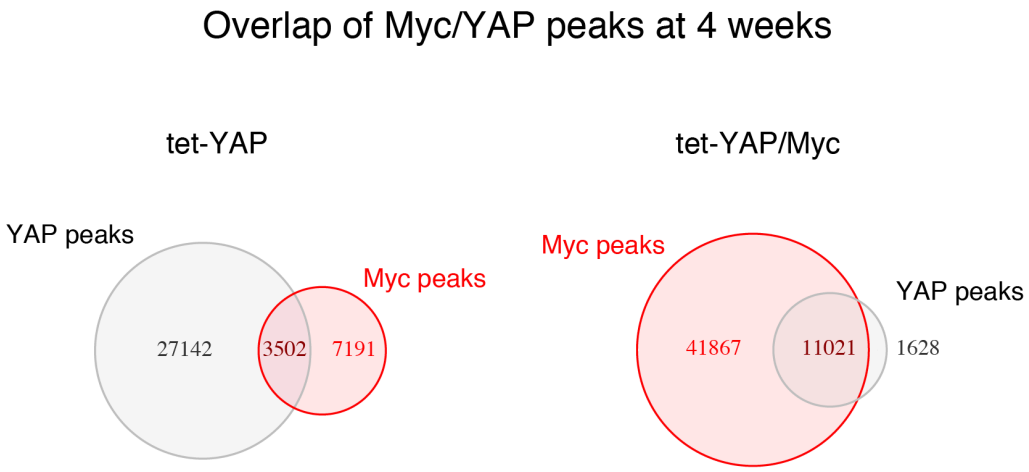

Figure 51: Concomitant of YAP and Myc leads to co-localization of their binding sites upon their long-term overexpression in liver. Venn diagrams showing the overlap between YAP and Myc peaks detected in tet-YAP liver (left) and tet-YAP/Myc liver (right) after 4 weeks. In tet-YAP liver, only 11% of YAP binding sites overlapped with Myc (left), but in tet-YAP/Myc liver, this overlap was highly improved (87%, right).

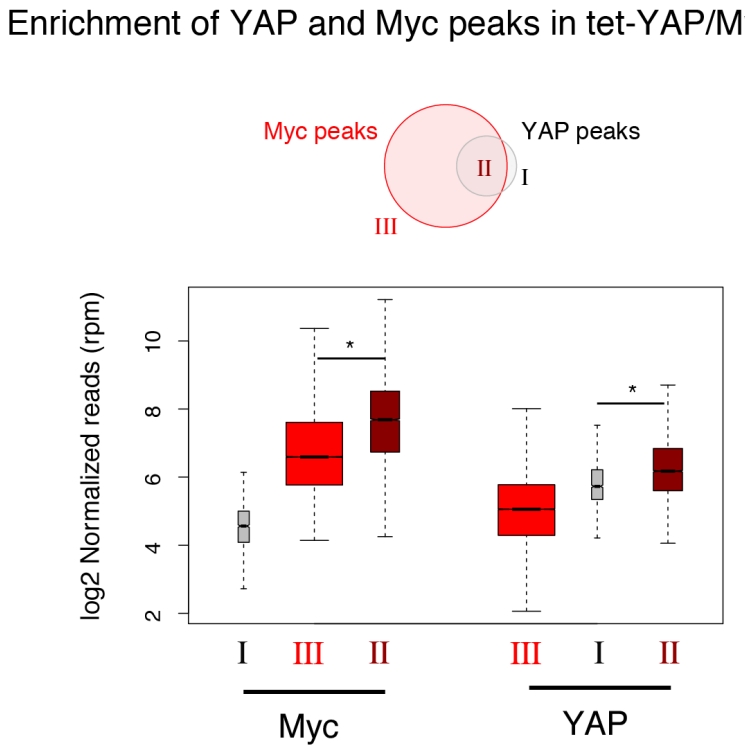

Figure 52: YAP and Myc chromatin binding is stronger when they are bound together. Boxplot representing the enrichment of Myc and YAP in peaks detected in tet-YAP/Myc liver. Co-bound sites (subset II) were more enriched in YAP and Myc compared to the sites bound by only one of the factors (subsets I and III), suggesting that YAP and Myc could stabilize each other. (* $p<0.01$, Student's t-test).

V Discussion

YAP and TEAD play a crucial role in liver, promoting cell de-differentiation, proliferation and tumor formation (Camargo et al., 2007; Zanconato et al., 2016). Here, by using genomic analyses based on next-generation sequencing, we were able to investigate the transcriptional regulation mediated by YAP and TEAD in mouse liver.

In the liver of WT animals, YAP binding wasn't detected on chromatin, probably because of its low expression level. When ectopically activated, its chromatin binding involved mainly distal sites (Figure 6) and always co-localized with TEAD (Figure 7; Figure 12), suggesting that TEAD is required for YAP binding *in vivo*. This is consistent with recent experiments in which YAP and TEAD strongly co-localize *in vitro* (Stein et al., 2015; Zanconato et al., 2015); moreover, suppression of TEAD expression by either knockdown or siRNA impaired YAP chromatin binding (Stein et al., 2015; Zanconato et al., 2015).

A subset of YAP peaks in pre-tumoral liver weren't pre-bound by TEAD in normal liver; upon induction, TEAD enrichment strongly increased in those sites (Figure 8, subset III), indicating the formation of new YAP and TEAD binding sites. We can hypothesize two different mechanisms for this observation: (1) YAP activation, through a positive feedback loop, could induce TEAD expression (Figure 5), therefore increasing TEAD binding to chromatin (Figure 3, left) by acting on the equilibrium between bound/not bound protein on DNA; (2) on the other hand, YAP could bind TEAD and this can further stabilize TEAD on chromatin. Further experiments will be needed to confirm whether YAP promotes TEAD chromatin stabilization, for instance, TEAD occupancy could be evaluated upon acute repression of YAP (if TEAD binding is lost, then YAP would play a role in stabilizing TEAD genomic interaction).

When overexpressed, YAP was able to bind a set of distal elements enriched in H3K27Ac and H3K4me1 (Figure 9; Figure 10), two histone modifications that are present on active enhancers. In those sites, the enrichment of H3K27Ac and H3K4me1 histone marks further increased by YAP expression (Figure 9; Figure 10); thus suggesting that YAP could recruit acetyltransferases or methyltransferases to promote enhancer activation. This is in line with previous experiments in *Drosophila*, where Yorkie was shown to bind and recruit NcoA6, a subunit of the *Trithorax*-mediated (Trr) methyltransferase complex (Oh et al., 2014). Similarly, YAP can recruit NcoA6 in mammals to promote H3K4 methylation (Oh et al., 2014). *In vitro*, CBP/p300, a histone acetyltransferase complex, is able to bind YAP in H3K27Ac marked sites, thus linking H3K27 acetylation to YAP activity (Stein et al., 2015; Zanconato et al., 2015). These experimental evidences suggest that YAP could recruit both methyltransferases and acetyltransferases also *in vivo*.

De-differentiation of the adult hepatocytes observed upon prolonged YAP activation (4 weeks) was consistent with the repression of the transcriptional programs controlled by HNF1A and HNF4A (Figure 26), two transcription factors that regulate liver specific functions, such as bile acid biosynthesis and gluconeogenesis (see paragraph IV1.10, page 57). The motif finding analysis revealed that HNF4A consensus binding motif was enriched under YAP peaks summits (Figure 28), suggesting that YAP could antagonize HNF4A target gene expression *in cis.*

By exploiting published HNF4A ChIP-Seq data from WT and embryonic liver (Alder et al., 2014), we created a subset of enhancers regulated by HNF4A and YAP/TEAD during embryonic development and in adult liver. Genes associated to distal sites bound by HNF4A in embryonic liver and YAP/TEAD ("Embryo" subset,

Figure 3030) were strongly upregulated (Figure 31). Moreover, H3K4me1 and H3K27Ac marks in those sites were increased (Figure 30, subset "Embryo"), strongly suggesting that YAP may recruit acetyl/methyltransferases to promote enhancer activation and induce the expression of the related genes (Figure 31). This is consistent with previous data showing that YAP expression induces HNF4A localization to embryonic enhancers and promote their activation (Alder et al., 2014).

Upon its induction, YAP was also able to bind sites that were previously pre-bound by HNF4A in normal liver ("Adult" and "Common" subsets,

Figure 3030); in those sites, the levels of H3K27Ac and H3K4me1 remained unaltered in pre-tumoral liver (Figure 30, down) while the expression of the associated liver-specific genes was inhibited (Figure 32). YAP could therefore act as a transcriptional repressor on a specific subset of HNF4A targets active in normal liver, to promote de-differentiation.

How the repression of these targets would be achieved needs to be addressed. Polycomb repressive complexes (PRC1 and PRC2) inhibit transcription by modifying histones. While PRC1 is able to catalyze H2A ubiquitination, PRC2 promotes the trimethylation of H3K27; these two chromatin modifications exert inhibitory effects on gene expression (Margueron and Reinberg, 2011). Transcription could also be modulated by acting on chromatin remodeling; in particular, protein complexes such as SWI/SNF can be recruited on target promoters by transcription factors and regulate the position of nucleosomes (Becker and Workman, 2013). Nucleosome depletion on promoters facilitates transcription, while an increased nucleosome density determines a closed chromatin conformation, thus reducing the accessibility to transcriptional machinery and decreasing gene expression.

ChIP-Seq experiments on PRC components (such as Suz12) or the profiling of nucleosome positioning could reveal whether HNF4A target genes repression in pre-

tumoral liver was achieved by chromatin modifications, chromatin remodeling or a combination of both.

The pronounced cell proliferation resulting from YAP activation was consistent with the upregulation of genes involved in cell cycle, such as E2F1 targets and those promoting G2/M progression (Figure 26). In our work we found that YAP can cooperate *in cis* with Myc to promote transcription of cell cycle genes.

Prolonged activation of the Myc transcription factor by mitogenic stimuli induces cell proliferation and tumor formation (Dang, 2013), but specific circumstances need to be present for Myc targets activation (Xiao et al., 2001; Murphy et al., 2008). When both YAP and Myc were activated, YAP recognized genomic regions pre-bound by TEAD and Myc (Figure 44), leading to the stabilization of their binding on chromatin (Figure 38; Figure 43) and the increase in transcription of the target mitogenic programs (Figure 36; Figure 42), both *in vitro* and *in vivo*. Therefore, YAP is able to co-adjuvate Myc transcriptional response.

Mitogenic signals promote Myc activation (Bernard and Eilers, 2006); however, in confluent cells, Myc induced cell division is inhibited (Demeterco et al., 2002). To fully exert its transcriptional effects on cell cycle genes, Myc requires the activation of YAP, which is induced by high cytoskeletal tension, a situation commonly found in sub-confluent cells (Yu et al., 2012). Therefore, in our work we reveal a mechanism of integration between mitogenic and mechanical stimuli that translates into cooperation *in cis* between YAP and Myc to promote cell proliferation.

Our data suggest a model in which YAP is able to potentiate Myc transcriptional response. Myc bind promoters pre-bound by TEAD (Figure 44) and inside active chromatin context (Figure 47); this binding further activates chromatin by increasing H3K4me3 and H3K27Ac levels (Figure 47), and promotes YAP recruitment. YAP could

be targeted in those regions either by recognizing a suitable chromatin environment for its binding or through a direct interaction with Myc, as suggested by a co-IP experiment in which YAP protein can be pulled down by immunoprecipitating Myc (Xiao et al., 2013).

Similar to Myc, the AP1 complex plays an important role in regulating cell proliferation (Eferl and Wagner, 2003); FOS and JUN, two of its components, are known to bind and co-localize with YAP/TEAD dimer on enhancers and promote the expression of cell cycle genes (Zanconato et al., 2015). Consistently with this, we were able to detect JUN/FOS consensus DNA binding motif under YAP peaks associated to deregulated genes (Figure 28), suggesting that AP1 complex may cooperate with YAP/TEAD dimer to promote cell division also in mouse liver.

Therefore, the expression of genes involved in cell proliferation observed following YAP activation (Figure 26; Figure 36; Figure 42) can be strongly enhanced either by a cooperation *in cis* between YAP and Myc in regulating Myc target genes and a direct interaction between YAP/TEAD and AP1 complex (Figure 28) (Zanconato et al., 2015).

SREBP targets and genes involved in the metabolism of cholesterol were downregulated upon short-term YAP induction (Figure 27). SREB proteins play a role in the biosynthesis of cholesterol in cooperation with HNF4A (Misawa et al., 2003).

YAP activation could therefore interfere with the production of enzymes involved in cholesterol biosynthesis by perturbing SREBPs and HNF4A target gene expression.

Most of YAP and TEAD chromatin binding occurred at distal sites (Figure 3; Figure 6; Figure 11; Figure 19). Therefore, the identification of transcriptional programs controlled by YAP/TEAD may have been limited by our ability to link enhancers to

the corresponding genes. To improve the association between enhancers and target promoters, experiments on the structure of chromosomes need to be performed. Recently, a technique called Capture Hi-C (CHi-C) was developed (Mifsud et al., 2015); this strategy is similar to a regular Hi-C experiment, but it allows to select particular regions of interest (in this case promoters) and potentially detect enhancer-promoter pairs.

VI Appendix 1. Compensatory effects of RNA Pol2 determine BET inhibition specificity

1 Introduction

1.1 The c-Myc transcription factor

c-Myc (henceforth Myc) is a transcription factor belonging to the basic helix-loop-helix leucine zipper family (Dang et al., 1999); it is able to control transcriptional programs that promote cell proliferation (Grandori et al., 2000) and inhibit cell differentiation (Demeterco et al., 2002), both *in vitro* (Zhang et al., 2009b) and *in vivo* (Mauleon et al., 2004). Myc promotes cell proliferation by modulating the expression of cell cycle genes; it can both repress the production of cell cycle inhibitors, such as p21 (Gartel et al., 2001) and induce the expression of cyclins, such as cyclin E (Pérez-Roger et al., 1997), cyclin D (Mateyak et al., 1999) and cyclin B1 (Yin et al., 2001). Other than cell cycle genes, Myc is responsible for the activation of metabolic genes: T cells lacking Myc expression have a reduced glucose and glutamine catabolism (Wang et al., 2011) and in neural stem cells, loss of Myc impairs the expression of genes involved in metabolism of nucleotides (Wey and Knoepfler, 2010). Cell differentiation is also controlled by Myc: together with Oct3/4, Sox2 and Klf4, Myc is one of the transcription factors that, when expressed in adult fibroblasts, are able to induce re-programming into pluripotent stem cells (Takahashi and Yamanaka, 2006) and when Myc is deleted in those cells, their self-renewal capacity is lost (Smith et al., 2010). Therefore, Myc plays a fundamental role in maintaining the pluripotency of stem cells.

Other roles of Myc involve the production of energy (through glycolysis and mitochondrial development), the synthesis of amino acids, nucleotides and lipids and the DNA replication (Kress et al., 2015); moreover, it is able to promote the transcription of ribosomal RNA and ribosome biogenesis (Arabi et al., 2005).

1.2 MYC forms heterodimers with MAX and binds specific DNA sequences

Myc, as a transcription factor, binds chromatin to exert its functions. Following its dimerization with Max, it binds DNA, with a strong preference for an exanucleotidic sequence (i.e. CACGTG), called "E-box" (Walhout et al., 1997). Albeit with lower affinity, The Myc/Max heterodimer can also bind "non-canonical E-boxes" (CANNTG), which differs from canonical E-box in the two central nucleotides (Blackwell et al., 1993). Max, in turn, besides forming heterodimers with Myc, is also able to either homodimerize or to heterodimerize with Mad proteins (Luscher, 2001). While association with Myc translates into cell cycle progression, the Max-Mad dimer inhibits cell proliferation (Luscher, 2001).

In quiescent cells, Myc prevalently binds promoters in its high affinity binding sites, the E-box sequences. When overexpressed in cancer, Myc increase s its occupancy on DNA particularly at enhancers, even without the presence of the E-box. This increase in binding stabilization occurs on genomic sites characterized by open chromatin (DNase hypersensitive sites), indicating that Myc is not a pioneer factor, but its binding requires pre-activated chromatin (Sabò et al., 2014).

1.3 Myc is frequently altered in tumors

Myc is known to have a role in tumor initiation and maintenance. Years ago, studies on chickens highlighted the oncogenic properties of the Myc protein: v-Myc, the homologous of the human gene present in some oncogenic retroviruses, is able to

transform cells and trigger tumor formation (Lee and Reddy, 1999). Moreover, when Myc is inactivated in tumor cells, proliferative phenotype is reversed, and cells undergo senescence or apoptosis (Gabay et al., 2014), indicating that Myc is required for tumor maintenance. The role of Myc as an oncogene is supported also by the fact that its expression is altered in a variety of cancers, such as acute myeloid leukemias (Salvatori et al., 2011), chronic myeloid leukemias (Albajar et al., 2011), gastric tumors (de Souza et al., 2013), pancreas tumors (Hessmann et al., 2016), breast cancers (Xu et al., 2010), prostate cancers (Koh et al., 2010), colorectal cancers (Sikora et al., 1987)(Annibali et al., 2014), gliomas (Annibali et al., 2014).

Common causes of the alterations in Myc levels in cancer are the amplifications or translocations of the myc locus. Amplifications have been observed in many tumor types, such as prostate carcinomas (Jenkins et al., 1997), neuroblastomas (Slavc et al., 1990) and breast carcinomas (Escot et al., 1986). Myc was also found to be amplified in metastases from primary tumors of breast cancer, suggesting that its overexpression may give survival advantage to disseminated cells (Singhi et al., 2012).

One of the most studied translocations involves the IgH enhancer with Myc locus: this allows the control of Myc expression in B-cell, and gives rise to Burkitt's lymphomas and multiple myelomas (Bergsagel and Kuehl, 2001). The increase in Myc expression due to the translocation occurs during B lymphocytes development, when cells start to express immunoglobulins on the plasma membrane and exit the bone marrow (Yan et al., 2007). Although point mutations of Myc are much less common in tumors, few have been reported in Burkitt's lymphomas (Bahram et al., 2000) that may increase tumor potential (Schmitz et al., 2012). In particular, Ser-62 and Thr-58 sites, when phosphorylated, can be recognized by ubiquitin ligases; their mutation can thus confer stronger stability to the Myc protein because its proteasome degradation is

reduced (Welcker et al., 2004). Transforming activity of mutant Myc is stronger compared to wild-type Myc: point mutations confer to Myc the ability to bypass the p53 tumor suppressor activity and to induce lymphomagenesis earlier (Hemann et al., 2005).

1.4 Regulation of transcription by Myc

In higher eukaryotes, RNA Pol2 is the enzyme responsible for the transcription of the protein-coding genes. The first step of transcription, called "initiation", involves Pol2 recruitment and binding on the TSS. Here it is phosphorylated by cyclin H-CDK7 (Komarnitsky et al., 2000) in the Ser-5 residue of its C-terminal domain (CTD): this yet inactive form of the enzyme is called "paused" Pol2. Transcription of many genes bound by paused Pol2 at their promoter is blocked by negative elongation complexes, such as NELF and DSIF (Rahl et al., 2010), which prevent the full mRNa synthesis. In order to confer Pol2 processivity and mRNA production, Ser-2 residue must be phosphorylated by CDK9, a subunit of P-TEFB complex (Price, 2000); this step, known as "elongation", induces Pol2 release into the genebody to allow RNA transcription until reaching the transcription end site (TES) (Bowman and Kelly, 2014). Only 30% of human genes which bear initiating Pol2 on their TSS are actively transcribed to produce full-length RNA; this because the two steps of transcription are tightly controlled and promoter-pause release is a limiting step in gene expression in higher eukaryotes (Guenther et al., 2007).

Experiments in embryonic stem cells showed that Myc is able to recruit P-TEFB to its target genes to phosphorylate negative elongation factors NELF and DSIF and induce RNA Pol2 elongation (Rahl et al., 2010), as well as promoting RNA Pol2 recruitment itself (Walz et al., 2014; Sabò et al., 2014). Importantly, even on instances when Myc over-expression leads to its wide spread chromatin interaction, Myc does not

generally amplify the expression of every bound gene, but still regulates specific targets, which, in turn, can lead to global RNA amplification (Sabò et al., 2014).

1.5 Therapeutic strategies to target Myc-driven cancers

Since Myc is essential for tumor cell proliferation and survival, the inhibition of its activity should be promising for cancer therapy (Soucek and Evan, 2010; Felsher, 2010). An approach to evaluate the efficacy of therapeutic approaches based on Myc inhibition is to use Omomyc (Soucek et al., 1998), which is obtained modifying 4 residues in Myc sequence; this new protein can homodymerise with WT Myc and can therefore sequester it from its binding with MAX, provoking the proliferation arrest of NIH3T3 cells (Soucek et al., 1998).

Unfortunately, the "undruggability" of this molecule impedes the development of small molecules that could impair its activity as a transcription factor; this is mainly due to the lack of a druggable pocket in its protein structure (Koh et al., 2016). Therefore, alternative approaches are being explored, such as targeting Myc stability, reducing its mRNA levels or performing screens to find synthetic lethal genes (Koh et al., 2016).

A compound that inhibits the Myc IRES (internal ribosomal entry site) activity has been recently developed; this compound synergized with ER stress to induce apoptosis in multiple myeloma cells (Shi et al., 2016). Despite the challenge, some small molecules have been developed as Myc inhibitors: some compounds were found to reduce Myc/MAX heterodimers formation, while others stabilize MAX/MAX homodimers; in this latter case, MAX is sequester and is not available for dimerization with Myc, thus reducing Myc oncogenic potential (Berg, 2010).

Myc expression can be inhibited also by using a 15-bp antisense oligonucleotide targeting Myc mRNA; this treatment was able to induce cell death in prostate cancer

cells (Balaji et al., 1997). High throughput screening using siRNAs identified genes that are synthetic lethal with Myc: these belong to DNA repair system, mitosis, metabolism, apoptosis, transcription and ribosomal RNA biogenesis (Toyoshima et al., 2012). This screen also identified CDK12 and BRD4 as vulnerable in Myc overexpressing cancers, two genes implicated in transcriptional elongation. BRD4 was independently found by another group (Kessler et al., 2012) to be synthetic lethal with Myc.

1.6 BRD4 is a therapeutic target for cancer treatment

BRD4 (Bromodomain containing protein 4) is a chromatin reader and is part of the bromodomain and extraterminal domain (BET) family proteins. The members of this family share two bromodomains (BRD), which recognize acetylated chromatin (Filippakopoulos et al., 2012), and an extraterminal domain (ET), that is required for BET proteins interaction with other proteins (Rahman et al., 2011).

Several evidences linked BRD4 to the control of gene expression, by means of different mechanisms.

Recently it has been demonstrated that BRD4 not only is a chromatin reader, but can induce chromatin decompaction and nucleosome eviction driven its intrinsic histone acetyltransferase activity (Devaiah et al., 2016). BRD4 can also promote transcriptional elongation by recruiting P-TEFB to promoters (Yang et al., 2005), by acting as an atypical protein kinase to catalyze phosphorylation of Ser-2 in the C-terminal domain of Polymerase II (Devaiah et al., 2012) and by promoting anti-pause enhancer activation (Liu et al., 2013a).

Different studies showed that BRD4 protein is an important cell cycle regulator. During mitosis, the mechanisms by which transcription is inherited by daughter cells are poorly known. BRD4 binds genes of the M/G1 phase that need to be expressed

after mitosis, thus instructing the daughter cells on which transcripts will have to be produce (Dey et al., 2009). Then, by promoting G1-phase genes expression, it is required for S-phase progression (Mochizuki et al., 2008). SPA-1, a GTP-ase activating protein negatively regulates the G2/M progression because it can bind BRD4 and induce its cytoplasmic retention; therefore, BRD4 and SPA-1 levels need to be balanced for correct cell cycle progression (Farina et al., 2004).

BRD4 aberrant activity is correlated to tumor growth. Its expression is high in hepatocellular carcinoma and when it was knocked down using RNA interference, reduced tumor proliferation was observed (Zhang et al., 2015b). Translocation of BRD4 next to NUT gene can produce a fusion protein that leads to an aggressive form of squamous cell carcinomas (French, 2012); when the interaction between acetylated chromatin and BRD4 is blocked by inhibitors, tumor cells differentiate and stop to proliferate. Overall, these data provide a rationale for targeting BRD4 in cancer therapy.

Among BRD4 inhibitors that have been developed, I-BET (Nicodeme et al., 2010) and JQ1 (Filippakopoulos et al., 2010) are the most widely used in research. Both these small molecules mimic and compete with the acetylated histones: they can bind BRD domains with high affinity and can displace BRD4 from chromatin, reducing its ability to regulate transcription.

1.7 Treatment of Myc-driven tumors through BRD4 inhibition

Several experiments indicated that BRD4 inhibition blocks cell growth in Myc-driven tumors.

One of the first studies that achieved this was conducted on Multiple Myelomas (MM), in which the immunoglobulin heavy chain (IgH) enhancer is translocated upstream of the Myc locus, and modulates its expression. Experiments on MM1.S, a cell line

derived from a MM patient (Greenstein et al., 2003) showed that BRD4 is bound to the IgH enhancer and plays a key role in promoting Myc expression; if BRD4 is inhibited by JQ1 treatment, Myc levels are reduced, together with Myc target genes (Delmore et al., 2011) thus leading to a block in cell proliferation and induction of senescence.

MM are not the only tumors in which BRD4 inhibition leads to cell cycle arrest dependent on Myc downregulation. Some forms of leukemia derive from the fusion between Mixed lineage leukemia (MLL) and AF9 proteins; these can form complexes with BRD4 to promote gene transcription (Dawson et al., 2011). A BET inhibitor that detaches BRD4 from chromatin can reduce the abnormal Myc expression driven by MLL/AF9 chimera (Dawson et al., 2011). Burkitt's lymphoma and Acute myeloid leukemia (AML) are also vulnerable to BET inhibition: nanomolar concentrations of JQ1 can downregulate Myc expression and its target genes, thus reducing the proliferation of these tumors in mouse models (Mertz et al., 2011). Other evidence of AML sensitivity to BET inhibition came from an shRNA screen in which knock-down of BRD4 reduced Myc and Myc target genes *in vivo*, inducing myeloid differentiation and reducing leukemia stem cells (Zuber et al., 2011).

The BRD4 inhibition potential in reducing growth of malignant cells is not limited to the tumors mentioned above: treatment of acute lymphoblastic leukemia (ALL) cell lines with JQ1 was able to decrease BRD4 binding on Myc promoter thus leading to strong downregulation of Myc expression (Ott et al., 2012). As a result cell proliferation and survival were greatly affected. Similarly, Myc expression can be inhibited by nanomolar concentrations of JQ1 to induce apoptosis of Myc-amplified medulloblastoma (Bandopadhayay et al., 2014) and Bladder cancer cells (Wu et al., 2016). Here, BRD4 can bind to and cooperate with Myc to promote Ezh2 expression, a

gene important for bladder cancer cell proliferation; JQ1 treatment evicts BRD4-associated Myc from EZH2 promoter, thus reducing its levels and inducing apoptosis.

The selectivity of BRD4 inhibition for tumor genes has been investigated through ChIP-sequencing approach using MM1.S cell lines (Lovén et al., 2013). Super-enhancers, a subset of particularly large enhancers, drive the expression of genes important for MM identity, one of which is Myc. Super-enhancers are highly enriched in BRD4; thus accounting for their high vulnerability to JQ1 treatment (Lovén et al., 2013).

1.8 Background and Rationale

In our lab, we investigated the mechanisms of BET inhibition in Myc induced tumors, testing different cell lines derived from human or murine B-cell lymphomas. In particular, we used RAJI, DAUDI, BL-28, P3H1R, RAMOS, BL-2 as different Burkitt's lymphomas (BL) and murine B-cell lymphomas derived from Eμ-Myc transgenic mice (Adams et al., 1985).

As BET inhibitor, we used JQ1; this compound mimics acetylated histones, binds the bromodomain of BRD4 and prevents its interaction with acetylated chromatin (Filippakopoulos et al., 2010).

Following JQ1 treatment, both BL and Eμ-Myc underwent cell cycle arrest, that was time and dose-dependent. Both RAJI and Eμ-Myc lymphomas showed sensitivity to BET inhibition, evidenced by growth arrest visible from 48h onward, even at the lowest concentration tested (Figure 53a, b).

Profiling the level of Myc expression we noticed that while low JQ1 concentrations were sufficient to decrease Myc protein levels in DAUDI, BL-2 and RAMOS cell lines, RAJI, BL-28 cells and Eμ-Myc lymphomas required higher concentrations of the inhibitor (500nM JQ1) (Figure 53c).

Yet, the cytostatic effect observed in RAJI, BL-28 and DAUDI cell lines was observed in the absence of change in Myc protein levels (Figure 53c); suggesting that BET inhibition was cytostatic independently of the downregulation of Myc.

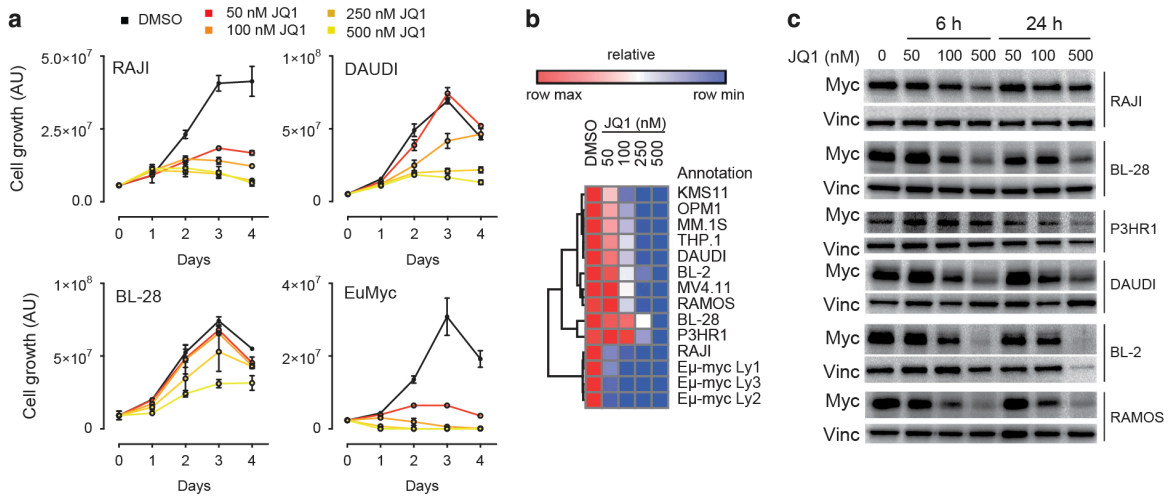

Figure 53: BRD4 inhibition blocks cell cycle of B-cell lymphomas, without affecting Myc levels. a) Growth curve of RAJI, DAUDI and BL-28 Burkitt's Lymphoma cell lines and Eμ-Myc lymphoma, grown in different JQ1 concentrations. b) Heatmap representing the relative growth of different cell lines tested in different JQ1 concentrations. c) Western blot experiments showing Myc protein levels in different cell lines tested at different JQ1 concentrations, after 6h or 24h. Myc level decreased in RAJI, BL-28 and DAUDI cells at high (500nM) JQ1 concentration.

Figure adapted from "Compensatory RNA polymerase 2 loading determines the efficacy and transcriptional selectivity of JQ1 in Myc-driven tumors" (Donato et al., 2016) Copyright © 2016 Macmillan Publishers Limited, part of Springer Nature. All rights reserved.

We therefore focused our attention on RAJI cell lines and profiled the transcriptional response following JQ1 treatment with microarrays: expression of genes involved in cell cycle, DNA replication and E2F1 targets were reduced upon BET inhibition (Figure 54a, b). Moreover, two signatures of genes deregulated in MM1.S cells upon JQ1 treatment were also found enriched in downregulated genes (Delmore et al., 2011) (Figure 54c), indicating that BET inhibition can perturb specific transcriptional programs in common between MM1.S and RAJI cells.

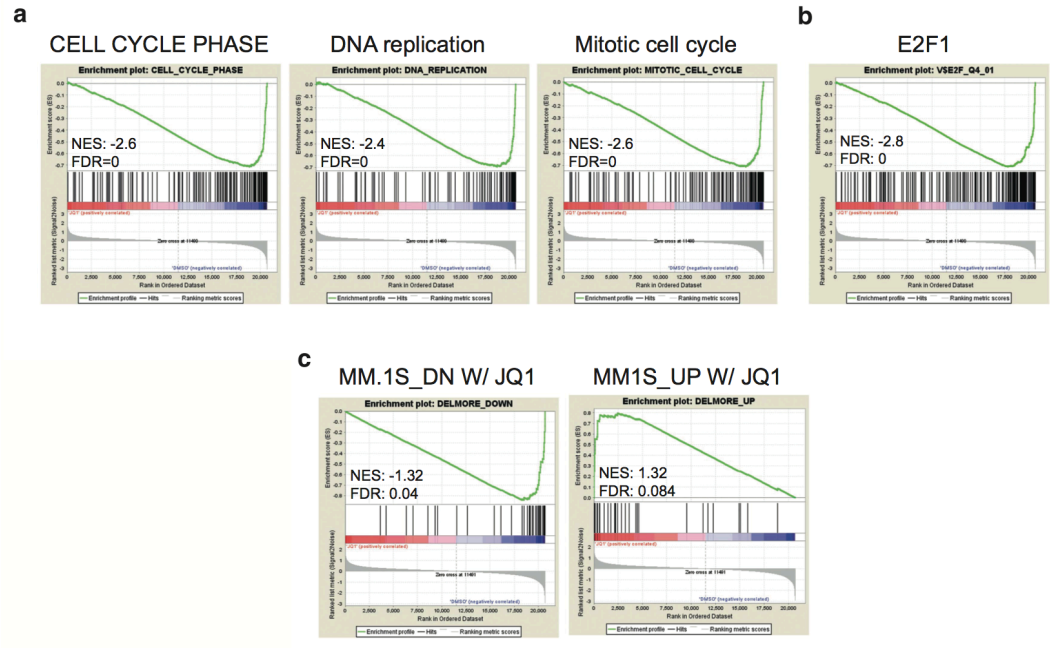

Figure 54: Myc targets are affected in RAJI cells upon JQ1 treatment. GSEA analysis showing transcriptional programs downregulated in RAJI cells following 100nM JQ1 treatment for 24h. (a, b) Cell cycle and E2F1 transcriptional programs were affected by BET inhibition; c) similar transcriptional programs were deregulated also in MM1.S cells when treated with JQ1.
Figure adapted from "Compensatory RNA polymerase 2 loading determines the efficacy and transcriptional selectivity of JQ1 in Myc-driven tumors" (Donato et al., 2016)

Overall these data suggested an alternative mechanism of action of BET inhibitors and raised the question of how inhibition of BRD4 can result in selective inhibition of Myc activity.

2 Materials and methods

2.1 Biological experiments

All the protocols used for Burkitt's lymphoma (BL-2, BL-28, DAUDI, P3HR1, RAJI and RAMOS), acute myeloid leukemia cell lines and EuMyc lymphoma, including cell growth conditions, western blot experiments, cell growth assays, plasmids used, 4SU labelling and analysis, chromatin extraction and immunoprecipitation, RNA-

extraction and quantification, antibodies and primers were published (Donato et al., 2016).

2.2 Data analyses

All the data analyses were performed as before (see materials and methods, paragraph III2, page 22). Reads were aligned on hg19 assembly as reference genome (Meyer et al., 2013). As the annotation package to determine promoters and genebodies we used TxDb.Hsapiens.UCS*C*.hg19.knownGene for OCI-Ly1 and RAJI cells, while TxDb.Hsapiens.UCSC.hg18.knownGene (Meyer et al., 2013) for MM1.S cells.

Super enhancers were defined as in Lovén *et al* (Lovén et al., 2013); BRD4 peaks were merged together (known as "stitching") if their distance to each other was less than 12.5 Kb. Then, merged peaks were ranked in ascending order according to the total number of BRD4 library-normalized reads (r.p.m.), giving rise to a distribution (Figure 58); enhancers above the inflection point were considered as "super enhancers", while the others were considered "regular enhancers".

We applied the random forest algorithm using the functions implemented in "randomForest" R library. A random forest model is a non-linear classifier based on a set of decision trees; in each tree a random sample of the features is selected, and, based on them, a classification is given as output. The outputs of all the trees in the model are joined together to produce a p value for the classification of each observation. In our model, we used 4000 trees for the classification.

2.3 Public datasets

External data were retrieved from GEO (Edgar, 2002). MM.1S cell line: GSE31365 (expression data), GSE42355 (ChIP-Seq data relative to BRD4 and Pol2), GSE42161

(Myc ChIP-Seq), GSE43743 (Pol2 ChIP-Seq in CDK9i treated cells). OCI-Ly1 cell line: GSE45630 (expression data) and GSE46663 (ChIP-Seq). ChIP-Seq data for RAJI cell line were deposited in GEO database, under the accession ID GSE76192.

3 Results

3.1 BRD4 is globally evicted from chromatin upon JQ1 treatment

To verify whether JQ1 specificity depends on selective BRD4 binding to a subset of genes or selective BRD4 eviction from chromatin in specific loci, we profiled genomic occupancy of BRD4 through ChIP-Seq. In normal conditions (i.e. cells treated with DMSO) 11915 BRD4 binding sites were detected, which decreased to 3084 upon JQ1 treatment (Figure 55).

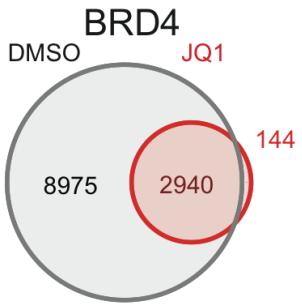

Figure 55: BRD4 is evicted from chromatin following JQ1 treatment. Venn diagram representing the overlap of BRD4 peaks in RAJI cells treated with DMSO (control) or JQ1 100nM for 24 h. Only part of BRD4 peaks were consistently detected upon BET inhibition.
Figure adapted from "Compensatory RNA polymerase 2 loading determines the efficacy and transcriptional selectivity of JQ1 in Myc-driven tumors" (Donato et al., 2016)

The decrease in peaks number was observed both at promoters, genebodies and distal sites (Figure 56a); this was accompanied by a reduction in chromatin occupancy in the residual peaks, as determined by the reduction in BRD4 enrichment

(Figure 56b). This indicates that BRD4 detachment from chromatin occurred genome-wide.

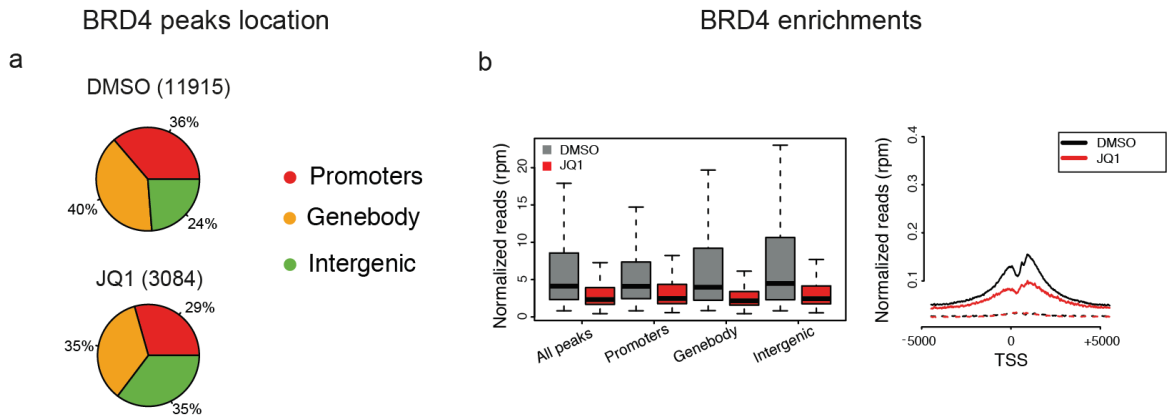

Figure 56: BRD4 eviction occurs in all genomic sites. a) piecharts representing BRD4 peak location. Eviction of BRD4 upon JQ1 treatment occurred equally at promoters, genebodies and intergenic sites. b) Boxplot and average profile on TSS representing BRD4 enrichment in promoters, genebodies and distal sites, both in DMSO and JQ1 treated cells. The chromatin occupancy was decreased both at promoters, genebodies and distal sites.

Figure adapted from "Compensatory RNA polymerase 2 loading determines the efficacy and transcriptional selectivity of JQ1 in Myc-driven tumors" (Donato et al., 2016)

The specificity of JQ1 on selected transcriptional programs (i.e. Myc target genes) is therefore not mediated by a selective loss of BRD4 binding to particular genomic regions. We then profiled BRD4 binding on promoters of genes upregulated (DEG up), downregulated (DEG down) or not deregulated (no DEG) by the treatment. While only 18% (6416) of promoters of no DEGs were bound by BRD4, 59% (821) and 26% (321) of down or up regulated genes were bound, respectively (Figure 57), indicating a correlation between BRD4 occupancy and gene regulation, particularly transcriptional activation.

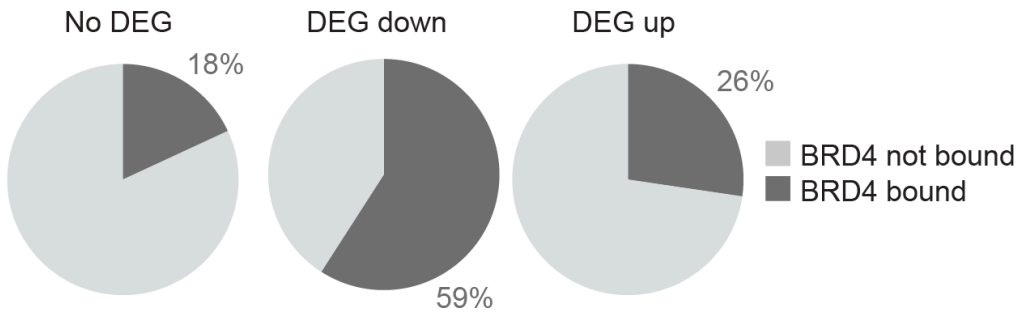

Figure 57: BRD4 binding is associated with gene deregulation. Piecharts representing the fraction of no DEG, DEG down and DEG up upon JQ1 treatment, bound by BRD4 at promoters. The fraction of bound deregulated genes was higher compared to the fraction bound on no DEGs, especially that of downregulated genes. BRD4 binding is therefore correlated to gene regulation, in particular downregulation.

Figure adapted from "Compensatory RNA polymerase 2 loading determines the efficacy and transcriptional selectivity of JQ1 in Myc-driven tumors" (Donato et al., 2016)

3.2 Super enhancer-associated genes are sensitive to BET inhibition

The expression of cell identity genes (Whyte et al., 2013) and genes important for the oncogenic activity of MM cells is under the control of super enhancers, a subset of very large enhancers with high load of BRD4, H3K27Ac and Med1 (Lovén et al., 2013) (Figure 58).

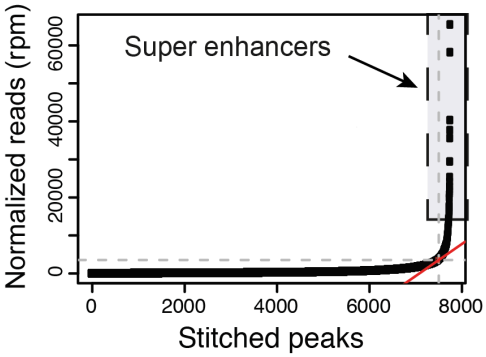

Figure 58: Super enhancers calling. Distal BRD4 peaks were joined together if they were close to each other and ranked according to their BRD4 enrichment. Enhancers above the inflection point of the plot were defined as "super enhancers", while the other being normal enhancers.

Figure adapted from "Compensatory RNA polymerase 2 loading determines the efficacy and transcriptional selectivity of JQ1 in Myc-driven tumors" (Donato et al., 2016)

Previous work showed that MM1.S cells, when treated with JQ1, underwent preferential detachment of BRD4 associated to super enhancers and downregulation of its target genes, leading to cell cycle arrest (Lovén et al., 2013). We then asked if, in RAJI cells, super enhancers-associated genes were particularly susceptible to JQ1 administration as observed for MM cell lines. We computationally identified 269 super enhancers that were highly enriched in BRD4 in untreated cells (DMSO treatment). Of these super enhancers, only 77 were preserved following JQ1 treatment (Figure 59).

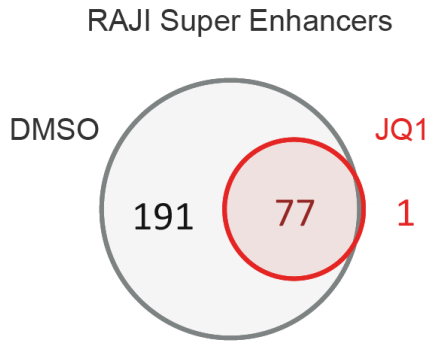

Figure 59: Most super enhancers are lost upon JQ1 treatment. Venn diagram showing the overlap between super enhancers detected in cells treated with DMSO and JQ1. Many super enhancers were lost upon BET inhibition.
Figure adapted from "Compensatory RNA polymerase 2 loading determines the efficacy and transcriptional selectivity of JQ1 in Myc-driven tumors" (Donato et al., 2016)

As expected, the loss in BRD4 occupancy was more pronounced on super enhancers compared to regular enhancers (Figure 60).

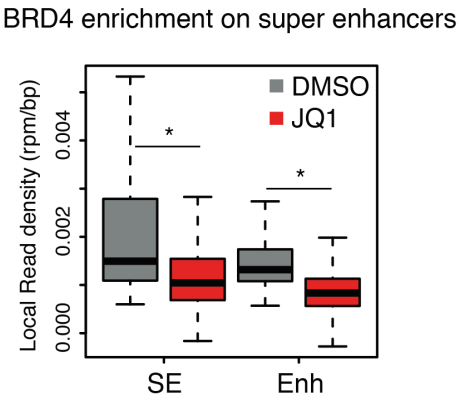

Figure 60: BRD4 eviction occurs preferentially in super enhancers. Boxplot representing the read density of BRD4 peaks inside super enhancers (SE) and regular enhancers (Enh) in cells treated with DMSO or JQ1. Even if BRD4 eviction was widespread, super enhancers were particularly vulnerable to BET inhibition, compared to regular enhancers. (* $p<0.05$, Student's t-test).

Figure adapted from "Compensatory RNA polymerase 2 loading determines the efficacy and transcriptional selectivity of JQ1 in Myc-driven tumors" (Donato et al., 2016) Copyright © 2016 Macmillan Publishers Limited, part of Springer Nature. All rights reserved.

As expected, super enhancers were characterized by stronger enrichment of H3K27Ac compared to normal enhancers (Figure 61, left), and higher H3K4me1/H3K4me3 abundance ratio compared to promoters (Figure 61, right), which are features of active enhancers (Heintzman et al., 2007).

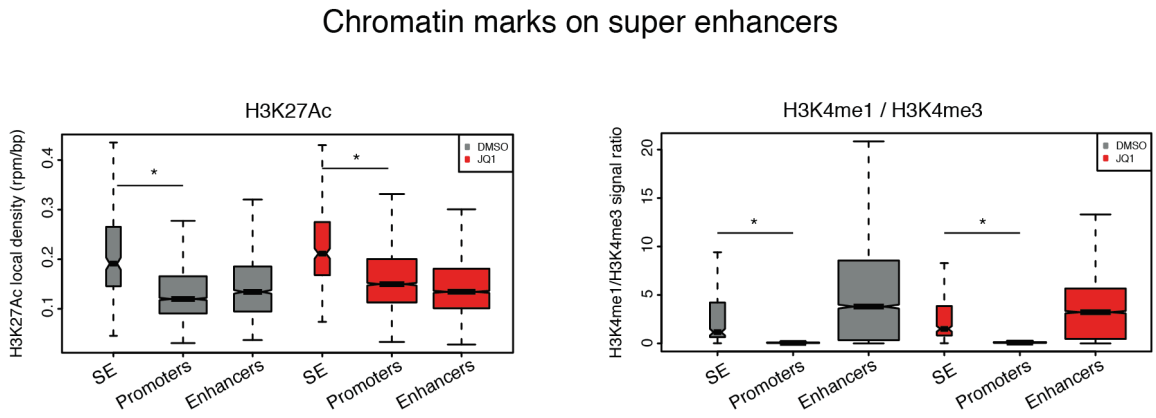

Figure 61: Super enhancers bear features of active enhancers. Left: boxplot representing the read density of H3K27Ac inside BRD4 peaks that constitute super enhancers (SE), promoters and normal enhancers. Super enhancers were particularly acetylated, thus active. Right: H3K4me1/H3K4me3 signal ratio inside super enhancers, promoters, regular enhancers. The value in super enhancers was comparable to those of normal enhancers, which was higher compared to promoters. (* $p<0.001$, Student's t-test).

Figure adapted from "Compensatory RNA polymerase 2 loading determines the efficacy and transcriptional selectivity of JQ1 in Myc-driven tumors" (Donato et al., 2016) Copyright © 2016 Macmillan Publishers Limited, part of Springer Nature. All rights reserved.

The fraction of JQ1 sensitive genes controlled by super enhancers was slightly higher compared to those controlled by regular enhancers (Figure 62, 16% vs 6%), possibly reflecting an intrinsic higher vulnerability of SEs to BET inhibition.

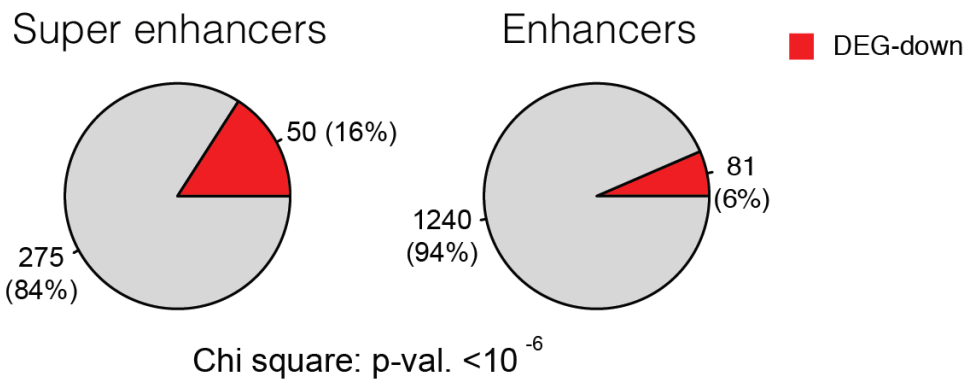

Figure 62: Super enhancer controlled genes are particularly susceptible to JQ1. Piecharts representing the fraction of genes associated to super enhancers and regular enhancers that were downregulated following JQ1 treatment. Genes associated to super enhancers were more downreguated compared to those associated to normal enhancers.
Figure adapted from "Compensatory RNA polymerase 2 loading determines the efficacy and transcriptional selectivity of JQ1 in Myc-driven tumors" (Donato et al., 2016) Copyright © 2016 Macmillan Publishers Limited, part of Springer Nature. All rights reserved.

3.3 Myc and E2F1 genomic occupancy is not affected by JQ1 treatment

We then carried out ChIP-Seq experiments to address if JQ1 treatment affected also Myc and E2F1 occupancy on chromatin. These factors promote the expression of cell cycle genes and cell proliferation (Leung et al., 2008); moreover, the geneset enrichment analysis showed that E2F1 may regulate JQ1 sensitive genes (Figure 54b) and E2F targets were inhibited by JQ1 treatment in diffuse large B cell lymphomas (Chapuy et al., 2013).

As expected, both Myc and E2F1 binding showed a marked preference for promoters (Figure 63).

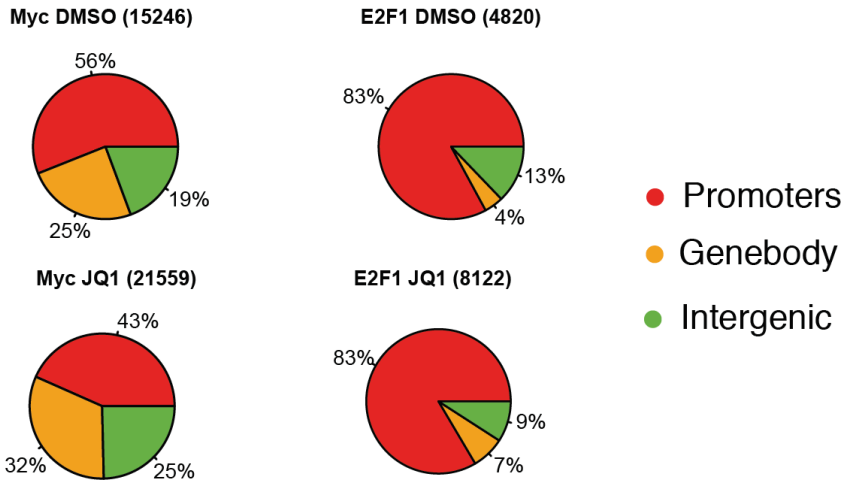

Figure 63: Myc and E2F1 bind mainly promoters. Piecharts representing the location of the Myc and E2F1 peaks detected in cells treated with DMSO and JQ1. About 50% of Myc peaks and 83% of E2F1 peaks were located in promoters of annotated genes, both in DMSO and JQ1 treated cells.
Figure adapted from "Compensatory RNA polymerase 2 loading determines the efficacy and transcriptional selectivity of JQ1 in Myc-driven tumors" (Donato et al., 2016)

Surprisingly, both their number of peaks and their enrichments were slightly increased upon BET inhibition (Figure 64), indicating that JQ1 vulnerability does not associate with eviction of either Myc or E2F1 from their target genes.

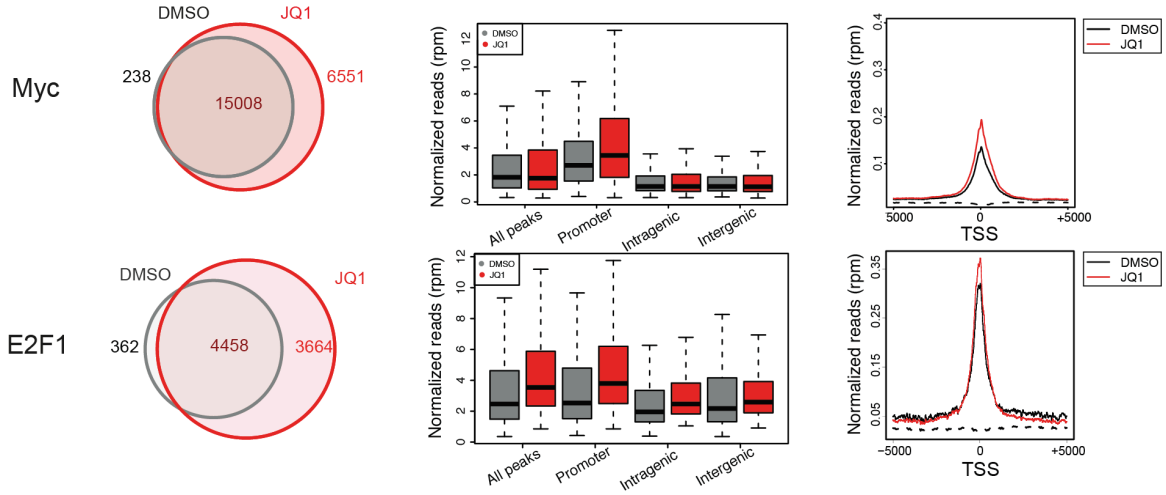

Figure 64: Myc and E2F1 occupancy is slightly increased genome-wide following JQ1. Left: Venn diagrams representing the overlap of Myc and E2F1 peaks detected in cells treated with DMSO or JQ1. Upon treatment, the number of binding sites of both transcription factors is increased. Middle: Boxplot of the enrichment of Myc and E2F1 in promoters, genebodies and intergenic regions, upon JQ1 inhibition. The enrichment of both transcription factors was increased in all the subsets, particularly at promoters. Right: Average profile of Myc and E2F1 occupancy at TSSs. Upon JQ1, peaks were higher and sharper compared to DMSO treated cells.

Figure adapted from "Compensatory RNA polymerase 2 loading determines the efficacy and transcriptional selectivity of JQ1 in Myc-driven tumors" (Donato et al., 2016) Copyright © 2016 Macmillan Publishers Limited, part of Springer Nature. All rights reserved.

3.4 Pol2 occupancy is not altered by JQ1 treatment

Next we analyzed Pol2 ChIP-Seq to understand whether JQ1 treatment influenced Pol2 genomic occupancy. Most of Pol2 was found associated to genebodies, as expected, which represents the amount of transcribing enzyme (Figure 65).

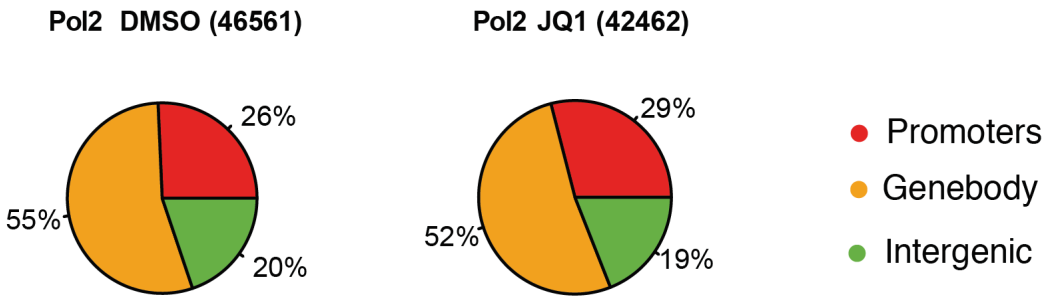

Figure 65: Pol2 is mainly located at genebodies. Piecharts showing the location of the peaks of Pol2 detected in DMSO and JQ1 treated cells. Most of Pol2 was located in genebodies. Following JQ1 inhibition, both the number of peaks and location were unaffected.

Figure adapted from "Compensatory RNA polymerase 2 loading determines the efficacy and transcriptional selectivity of JQ1 in Myc-driven tumors" (Donato et al., 2016) Copyright © 2016 Macmillan Publishers Limited, part of Springer Nature. All rights reserved.

Even though the number of Pol2 binding sites was slightly decreased by JQ1 administration, its promoter occupancy was strengthen (Figure 66).

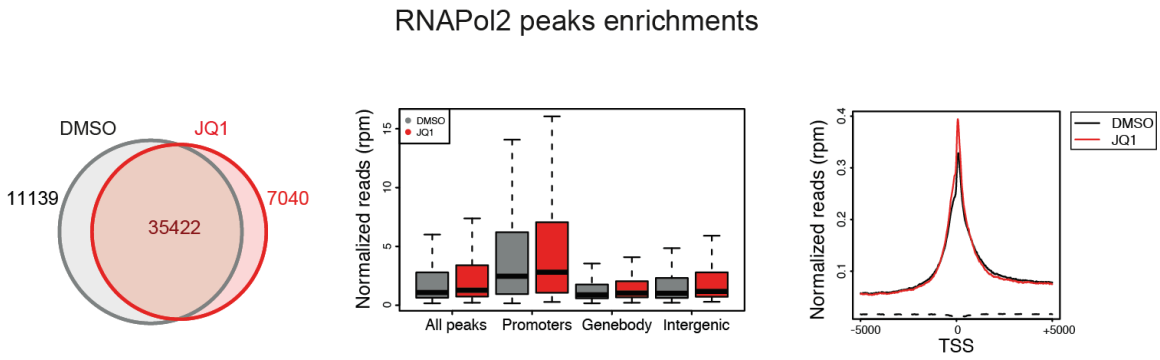

Figure 66: Pol2 chromatin occupancy is weakly affected by JQ1 treatment. Left: Venn diagram representing the overlap of Pol2 peaks detected in cells treated with DMSO or JQ1. Middle: boxplot of the enrichment of Pol2 in different locations, treated with DMSO or JQ1. Right: average profile of Pol2 on TSSs. Globally, Pol2 enrichment was slightly increased by JQ1.

Figure adapted from "Compensatory RNA polymerase 2 loading determines the efficacy and transcriptional selectivity of JQ1 in Myc-driven tumors" (Donato et al., 2016) Copyright © 2016 Macmillan Publishers Limited, part of Springer Nature. All rights reserved.

This indicates that JQ1 specificity for a subset of genes is not accounted by reduced Pol2 promoter recruitment.

3.5 Genes highly expressed and enriched in transcription factors and activating histone marks are downregulated upon JQ1 treatment

We next wanted to identify properties able to distinguish genes downregulated (vulnerable to BET inhibition) from those that did not change expression. We compared the occupancy of transcription factors and histone marks on promoters of these two subsets of genes; DEG down were characterized by high levels of BRD4, Myc, E2F1, H3K4me3 and H3K27Ac, two activating histone marks (Calo and Wysocka, 2013), while genes not deregulated showed lower enrichments (Figure 67).

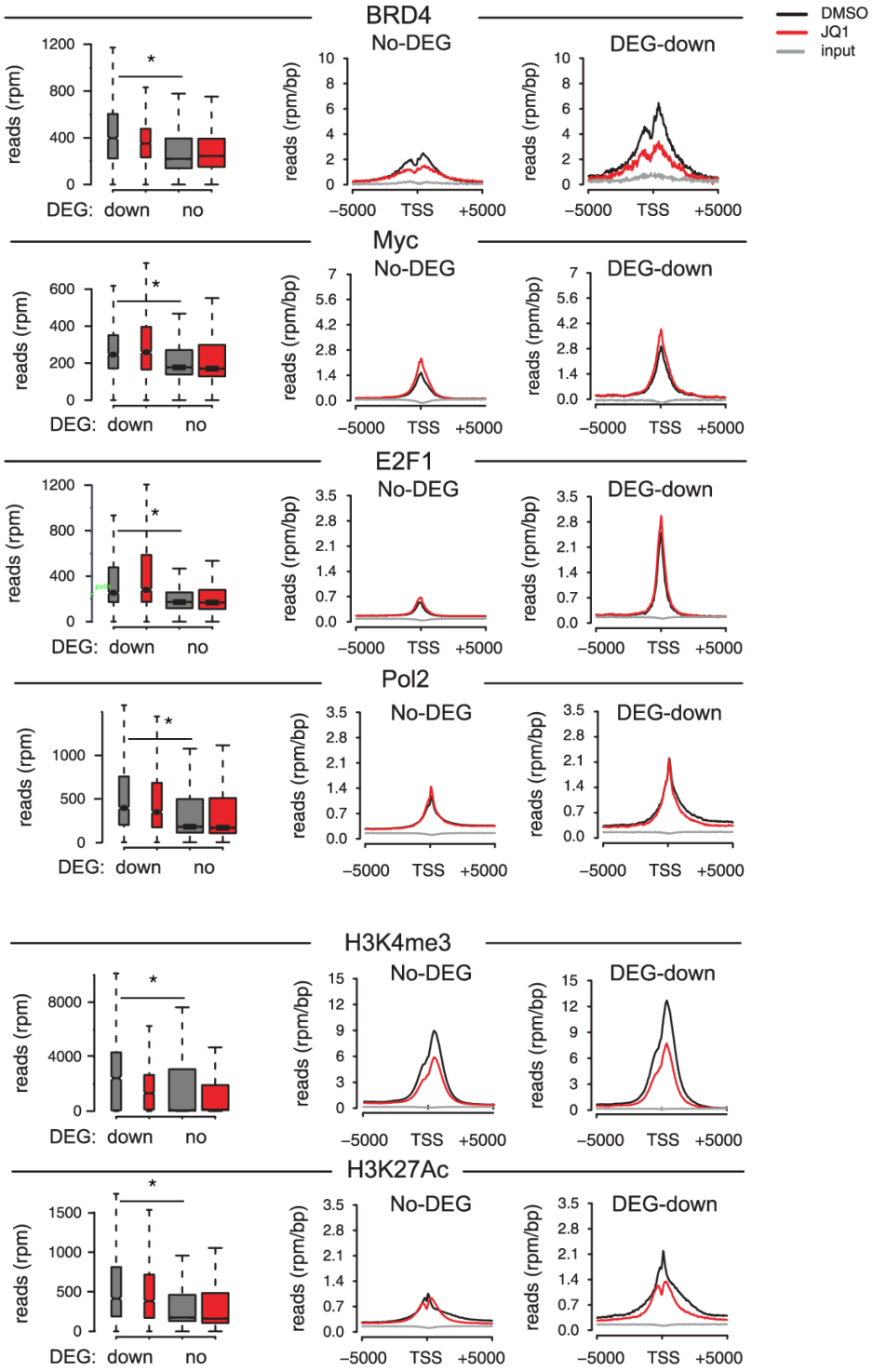

Figure 67: JQ1 sensitive genes are highly enriched in transcription factors, Pol2 and activating histone marks at their promoters. Left: Boxplot representing the ChIP-Seq enrichments of transcription factors or histone marks in promoters of genes downregulated or not deregulated in cells treated with DMSO or JQ1. Right: average profiles of transcription factors and histone marks around TSS of DEG down or no DEG following JQ1 treatment. Genes vulnerable to JQ1 treatment were enriched in transcription factors, Pol2 and activating histone marks. Only BRD4 was lost upon treatment. (* $p<2.2*10^{-16}$, Student's t-test).

Figure adapted from "Compensatory RNA polymerase 2 loading determines the efficacy and transcriptional selectivity of JQ1 in Myc-driven tumors" (Donato et al., 2016)

Then, to extend our findings to other tumors, we took advantage of publicly available ChIP-Seq datasets of OCI-Ly1 and MM1.S cells, treated or not with JQ1. OCI-Ly1 cell line derives from a non Hodgkin lymphoma (Mehra et al., 2002) which upon treatment with JQ1 shows Myc and Myc targets downregulation and proliferation arrest (Chapuy et al., 2013). Similarly, when MM1.S were treated with JQ1, repression of Myc expression and its targets was observed, thus leading to a cytostatic effect (Delmore et al., 2011) (see paragraph 1.7, page 98). In line with what observed in RAJI cells, both OCI-Ly1 and MM1.S cells showed strong enrichment of transcription factors, Pol2 and activating histone marks (H3K4me3, H3K27Ac) at promoters of JQ1 sensitive genes (Figure 68; Figure 69).

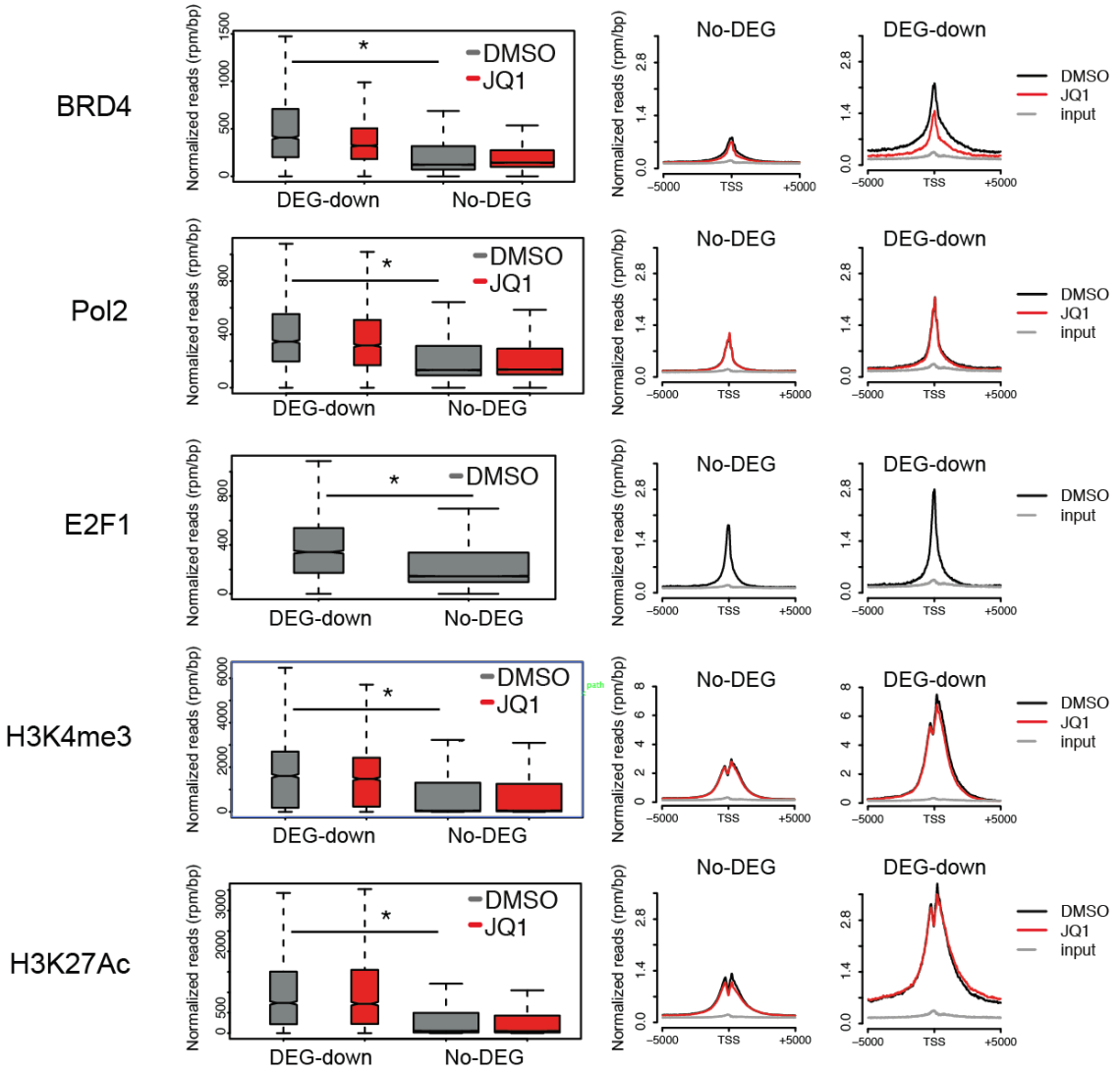

Figure 68: Genes downregulated upon JQ1 inhibition are more enriched in transcription factors and histone marks in OCI-Ly1 cells. Boxplots and profiles representing the enrichment of transcription factors and histone marks in TSSs of genes no DEG and DEG down following JQ1 inhibition, for OCI-Ly1 cells. (* $p<2.2*10^{-16}$, Student's t-test).

Figure adapted from "Compensatory RNA polymerase 2 loading determines the efficacy and transcriptional selectivity of JQ1 in Myc-driven tumors" (Donato et al., 2016)

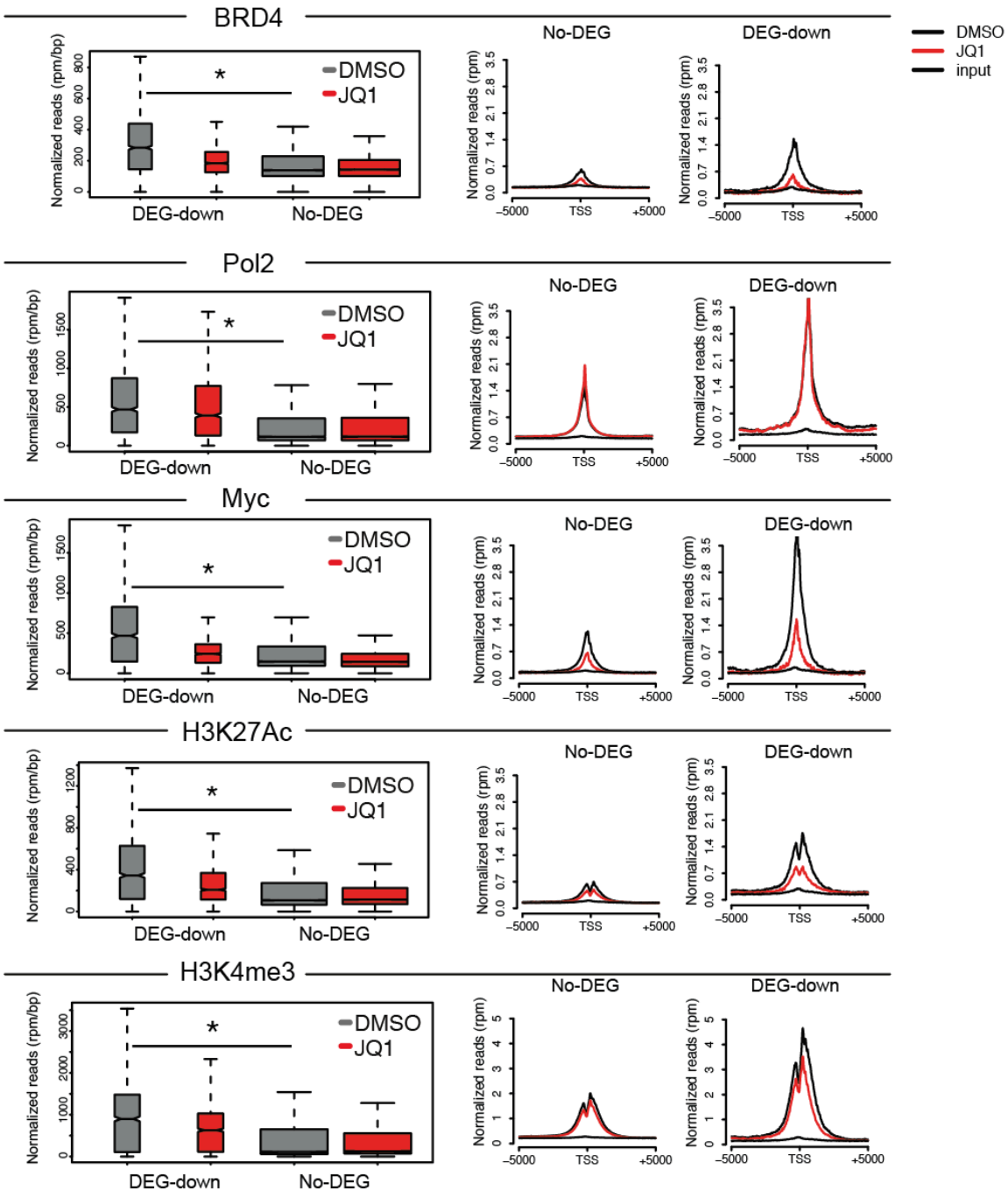

Figure 69: Genes downregulated upon JQ1 inhibition are more enriched in transcription factors and histone marks in MM1.S cells. Boxplots and profiles representing the enrichment of transcription factors and histone marks in TSSs of genes no DEG and DEG down following JQ1 inhibition, for MM1.S cells. (* $p<2.2*10^{-16}$, Student's t-test).

Figure adapted from "Compensatory RNA polymerase 2 loading determines the efficacy and transcriptional selectivity of JQ1 in Myc-driven tumors" (Donato et al., 2016) Copyright © 2016 Macmillan Publishers Limited, part of Springer Nature. All rights reserved.

According to our microarray experiments, downregulated genes were generally more abundant compared to no DEGs (Figure 70, left). To evaluate whether gene

downregulation may also depend on RNA instability, we calculated half life of mRNAs of no DEG and DEG down using a published dataset (Schwanhausser et al., 2011); this analysis showed that there was no significant difference between the two groups (Figure 70, right).

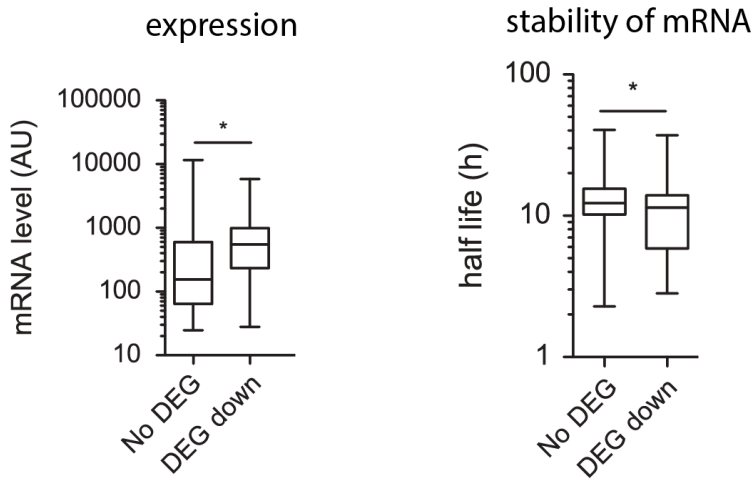

Figure 70: Downregulation of genes is not caused by mRNA instability. Left: boxplot representing the abundance of RNA of no DEGs and DEG down; downregulated genes were the more expressed. Right: Boxplot representing the half life of mRNAs of no DEG and DEG down genes; stability of mRNA was similar between no DEG and DEG down. (* $p<0.05$, Student's t-test).

Moreover, nascent RNA analysis by 4sU confirmed that the level of JQ1 sensitive genes was reduced due to inhibition of transcription (Figure 71).

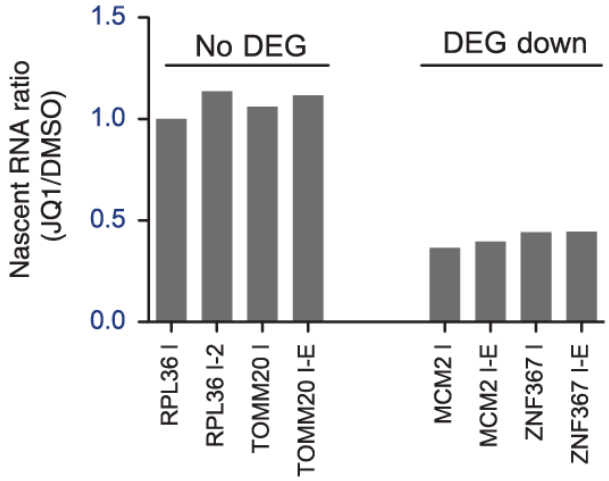

Figure 71: Downregulation of JQ1 sensitive genes is mediated by transcriptional inhibition. Barplot representing the rate of nascent RNA from the 4SU experiment. Reduction in transcription was observed in DEG down.

Figure adapted from "Compensatory RNA polymerase 2 loading determines the efficacy and transcriptional selectivity of JQ1 in Myc-driven tumors" (Donato et al., 2016)

To find whether JQ1 sensitivity could be predicted from specific genomic features, we built a random forest-based machine learning model trained with features of each single gene (mRNA abundance and ChIP-Seq enrichments of Myc, E2F1, BRD4 and histone modifications) aimed at classifying no DEGs from DEG down. The model was able to perform the prediction with high accuracy (AUC=0.83) (Figure 72, left), and indicated mRNA level, E2F1 and Pol2 ChIP enrichments as the most discriminative elements (Figure 72, right).

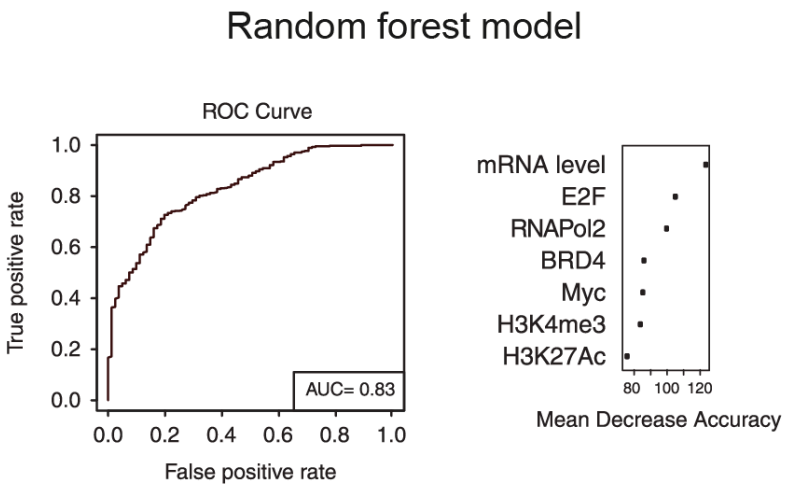

Figure 72: Random forest model predicts JQ1 sensitivity with high accuracy. Left: receiver operating characteristic (ROC) curve of the random forest model to predict if genes were sensitive to JQ1 treatment. Right: importance of the features for the classification of random forest model.
Figure adapted from "Compensatory RNA polymerase 2 loading determines the efficacy and transcriptional selectivity of JQ1 in Myc-driven tumors" (Donato et al., 2016)

Therefore, genes highly expressed and with high enrichment of Myc, E2F1 and histone marks at their promoters are more sensitive to JQ1, and this sensitivity can be predicted with high accuracy based on such features.

3.6 Selective Pol2 compensation at promoters determines JQ1 selectivity

We then characterized the mechanisms of BRD4 selective inhibition on transcription by profiling Pol2 enrichment on JQ1 sensitive genes. Following 24h of JQ1 treatment, Pol2 stalling index (i.e. the stalling Pol2/elongating Pol2 ratio, known also as "traveling ratio") increased in both no DEG and DEG down. This genome-wide effect was in accordance with a general role of BRD4 in promoting Pol2 elongation (see paragraph 1.6, page 97). However, while downregulated genes showed a reduction in elongating Pol2 (Figure 73, up), which was coherent with their reduced expression,

no DEGs had no alteration in elongation but displayed enhanced Pol2 pausing on promoters (Figure 73, down).

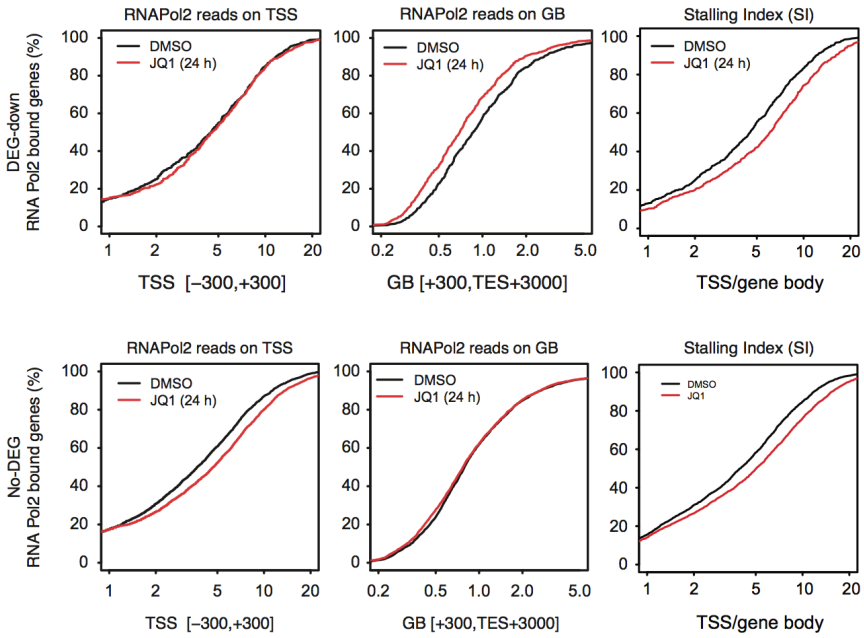

Figure 73: Pol2 stalling index decreases in both DEG down and no DEGs. Cumulative distribution of the enrichments of Pol2 in TSS (left), genebodies (middle) and of stalling indexes (right) of DEG down (up) and no DEG (down). While in DEG down the elongating Pol2 was decreased, in no DEG the Pol2 recruitment at promoters was increased. This lead to a raised stalling index for both subsets.
Figure adapted from "Compensatory RNA polymerase 2 loading determines the efficacy and transcriptional selectivity of JQ1 in Myc-driven tumors" (Donato et al., 2016) Copyright © 2016 Macmillan Publishers Limited, part of Springer Nature. All rights reserved.

The enrichment of Pol2 phosphorylated on Ser-5 (i.e. pausing Pol2) and Ser-2 (i.e. processive Pol2) (see paragraph 1.4, page 95) on DEG down showed that, following JQ1, the pausing Pol2 on promoters was not affected, while the elongating form was severely impaired (Figure 74).

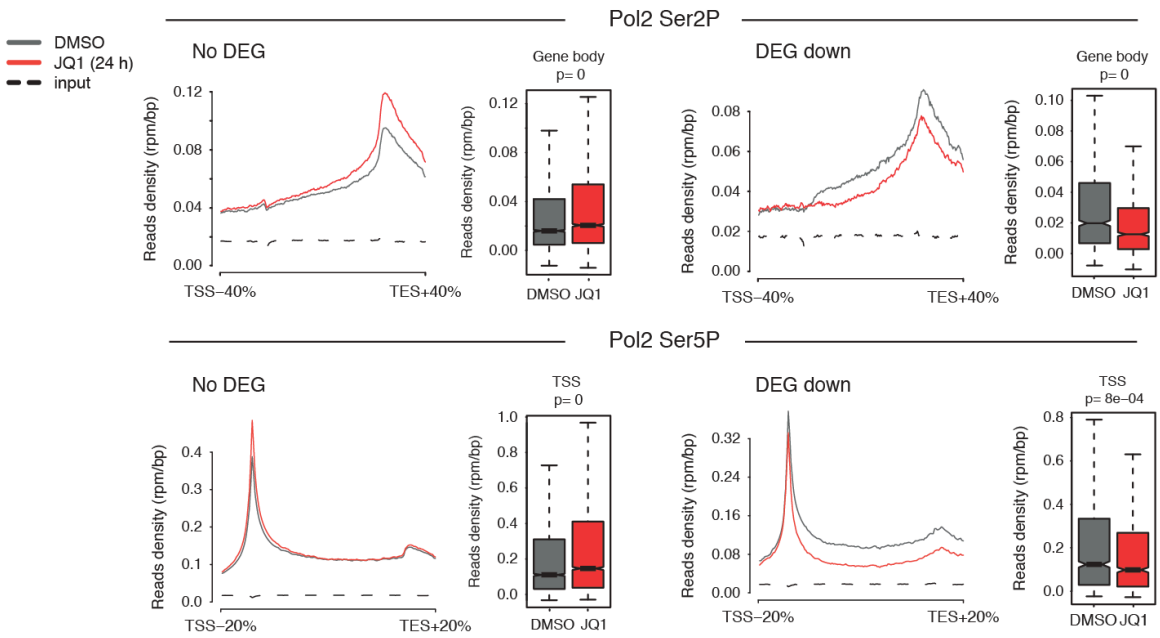

Figure 74: The amount of elongating form of Pol2 is impaired in DEG down. Up: Pol2 Ser-2P average profile on no DEGs and DEG down; drop in elongating Pol2 occurred only in DEG down. Down: Average profile of Pol2 Ser-5P (pausing Pol2) on no DEGs and DEG down; Promoter occupancy of paused Pol2 was unaffected upon JQ1 treatment in DEG down, while was increased in no DEG.
Figure adapted from "Compensatory RNA polymerase 2 loading determines the efficacy and transcriptional selectivity of JQ1 in Myc-driven tumors" (Donato et al., 2016)

In no DEGs, processive Pol2 was not impaired as shown by Pol2 Ser-2P profile (Figure 74, up), while a slight increase in Pol2 Ser-5P (paused Pol2) suggested recruitment of the enzyme on promoters (Figure 74, down), possibly reflecting compensatory recruitment of Pol2 (see below). Similar results were obtained in MM1.S cells treated with JQ1. While a drop in elongating Pol2 was observed for downregulated genes, no DEGs maintained a constant level of Pol2 on genebodies and increased the amount of pausing Pol2 on their promoters (Figure 75).

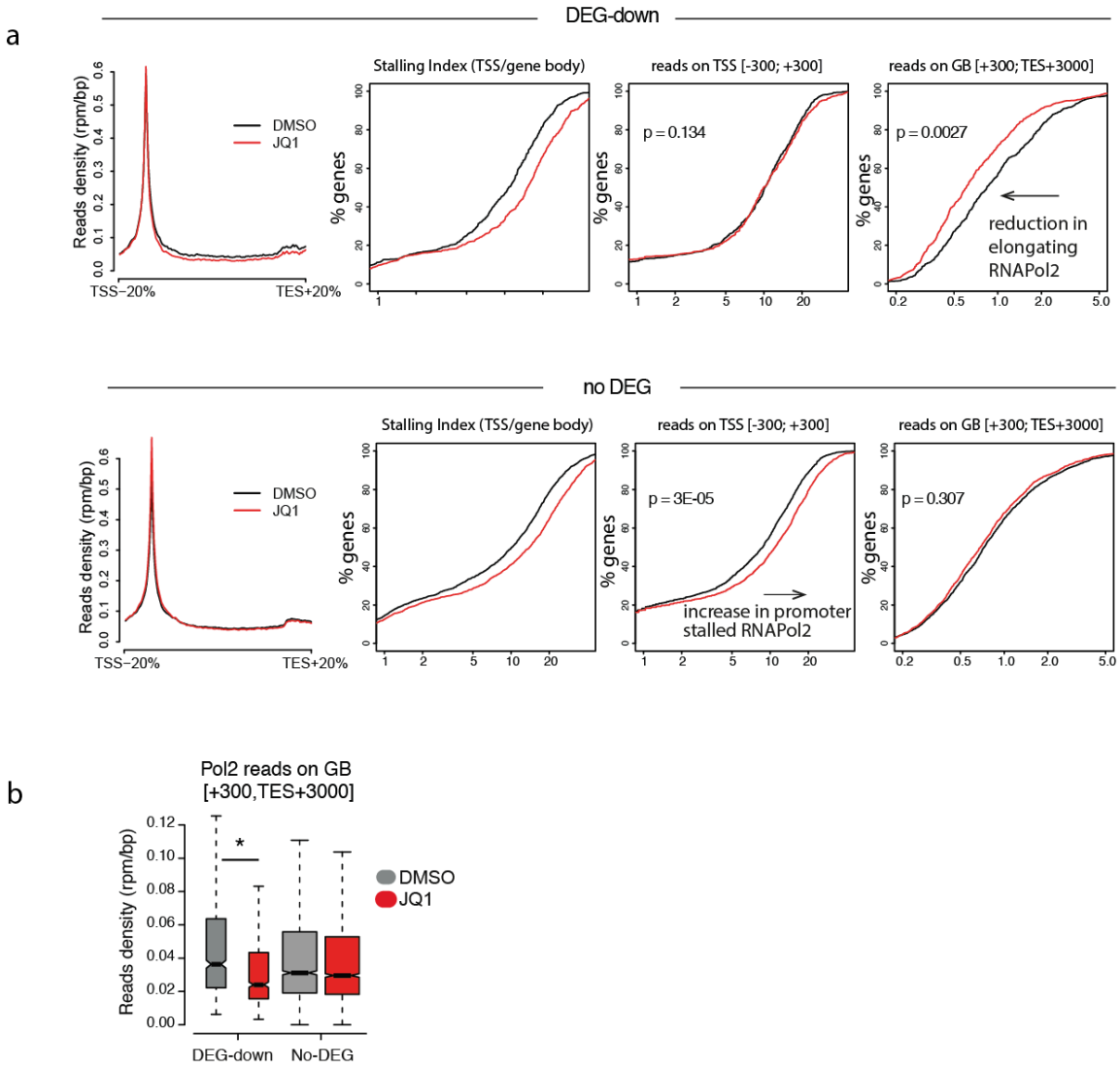

Figure 75: Increase in Pol2 recruitment cannot compensate the drop in elongation in DEG down of MM1.S cells following JQ1 treatment. Distribution of Pol2 in genes downregulated or not deregulated following JQ1 treatment, based on published datasets (Pol2 ChIP-Seq: GSE42355, expression: GSE31365) a) Pol2 enrichments of downregulated and not deregulated genes in MM1.S cells following JQ1 treatment; b) Boxplot representing read density of Pol2 in genebodies of DEG down and no DEG. A decrease in elongating Pol2 was observed only in downregulated genes. (* p=0.00019, Student's t-test).

Figure adapted from "Compensatory RNA polymerase 2 loading determines the efficacy and transcriptional selectivity of JQ1 in Myc-driven tumors" (Donato et al., 2016) Copyright © 2016 Macmillan Publishers Limited, part of Springer Nature. All rights reserved.

The effects that JQ1 exerted on transcription and Pol2 enrichments lead us to postulate that, while BET inhibition could reduce the elongation rate genome-wide,

genes insensitive to JQ1 (no DEGs) could compensate this reduction by increasing Pol2 recruitment on their promoters.

To verify this, we profiled Pol2 occupancy in cells treated with JQ1 short-term (6h) and long-term (24h), to test whether reduction of elongating Pol2 occurring short-term is restored after 24h only in genes refractory to JQ1. Both DEG down and no DEGs showed decreased Pol2 elongation after 6h (Figure 76). While this loss was persistent at longer time points (24h) for DEG down (Figure 76, up), no DEGs were able to compensate the reduction of elongating Pol2 at 24 h (Figure 76, down), to reach levels comparable to control cells treated with DMSO.

All these data indicate that BRD4 inhibition led to a global decrease in elongating Pol2 short-term, independently on the gene (DEG down or no DEG), consistently with the fact that BRD4 promotes elongation (Moon et al., 2005). While after prolonged inhibition (24h) no DEGs can compensate the loss of processive Pol2 (the amount of Pol2 Ser-2P) by further recruiting polymerase on their promoters, JQ1 sensitive genes cannot, because are already "saturated" of transcription factors and Pol2 on their promoters (Pol2 recruitment at promoters is already maximized). Therefore, upon JQ1 treatment, while no DEGs are able to maintain a proficient mRNA production, vulnerable genes (DEG down) undergo transcriptional inhibition.

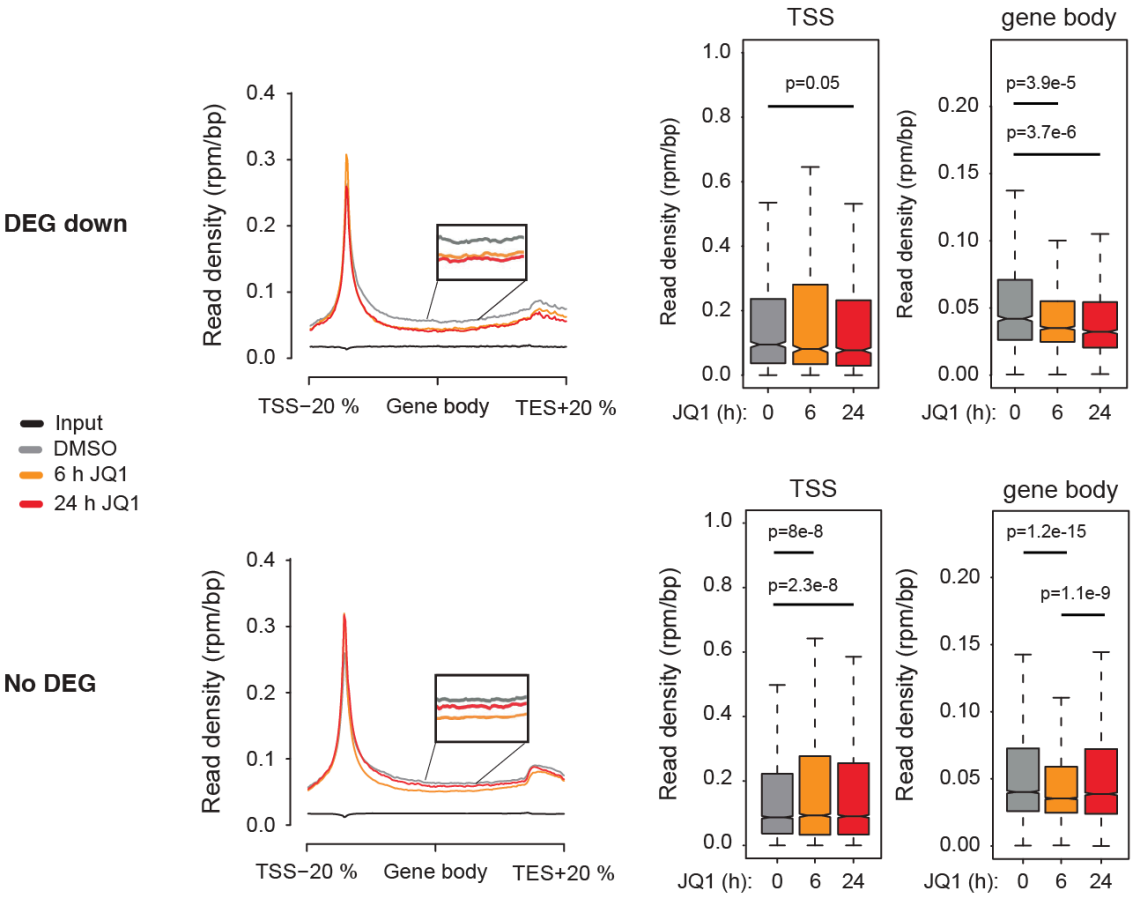

Figure 76: Drop in elongating Pol2 in DEG down is not compensated by further Pol2 recruitment on their promoters. Left: average Pol2 profiles on DEG down and no DEG, after short-term (6h) or long-term (24h) JQ1 treatment. Right: Boxplots representing the enrichment of Pol2 in TSS and genebodies of the two subsets of genes. The drop in elongating Pol2 that occurred short-term in both categories was not compensated by further recruitment on promoters in DEG down.

3.7 Inhibition of elongation selectively represses JQ1 sensitive genes

BRD4 inhibition leads to a reduction in Pol2 elongation; this translates into dowregulation of genes highly expressed and with high enrichment of Pol2 and transcription factors on their promoters. Since they cannot compensate the loss in elongating Pol2 with further recruitment of this enzyme to keep a constant mRNA levels, they are particularly vulnerable to JQ1 treatment.

If this mechanism were true, any inhibitor of elongation would selectively affect the expression of genes sensitive to BET inhibition, thus phenocopying JQ1 treatment. To test this, we took advantage of a published dataset and we analyzed Pol2 distribution in MM1.S cells treated with a CDK9 inhibitor (Anders et al., 2013).

The enrichment of Pol2 on genebodies of downregulated genes was reduced, while pausing form of Pol2 remained largely unaffected. In genes not deregulated, instead, the decrease in elongating Pol2 was less pronounced compared to DEG down, and an average increase in Pol2 recruitment was observed at their promoters (Figure 77).

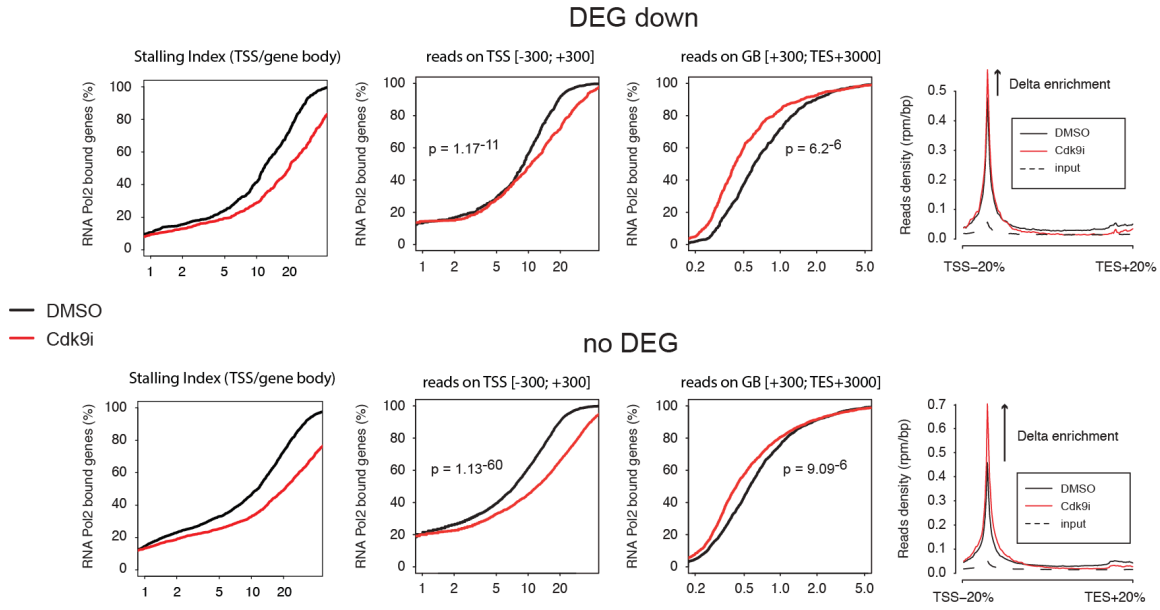

Figure 77: Elongation inhibition recapitulates JQ1 treatment. Pol2 enrichments of DEG down and no DEG in MM1.S treated with a CDK9 inhibitor (CDK9i). The treatment was able to perturb Pol2 equilibrium similarly to what observed for BET inhibition.

Figure adapted from "Compensatory RNA polymerase 2 loading determines the efficacy and transcriptional selectivity of JQ1 in Myc-driven tumors" (Donato et al., 2016)

Thus, independently of how elongation was inhibited, genes with higher levels of Pol2 on promoters showed a lower capacity to compensate the drop in Pol2 present on genebodies with further promoter recruitment and consequently their expression was reduced. On the contrary, genes that didn't change significantly their expression

could maintain a constant mRNA level because they recruited more Pol2 on their promoters. Altogether, these results show how a general perturbation of elongation could translate into regulation of specific transcriptional programs.

4 Discussion

BRD4 inhibition is a strategy to inhibit the proliferation of Myc driven tumors (Delmore et al., 2011; Dawson et al., 2011; Zuber et al., 2011; Lovén et al., 2013). While in some systems JQ1 treatment causes a reduction in Myc mRNA and protein levels, we noticed that some cell lines, such as Burkitt's and Eμ-Myc lymphomas were vulnerable to BET inhibition independently on Myc downregulation (Figure 53). Therefore, JQ1 treatment can block tumor cell proliferation either by reducing Myc oncogene expression or by interfering with Myc activity, independently on its levels.

We found that JQ1 treatment impairs transcription genome-wide, as evidenced by the global eviction of BRD4 from chromatin (Figure 55) and the global reduction of Pol2 elongation observed upon acute BRD4 inhibition (Figure 76). However, only a specific subset of genes was affected by BET inhibition (DEG down), where the expression of the other genes (no DEGs) was unaltered, despite the global effect of this drug on transcriptional elongation, thus suggesting potential adaptive transcriptional responses on this latter group of genes.

Indeed, while no DEGs could compensate the drop in elongating Pol2 by recruiting more RNA polymerase on their promoters, DEG down could not, since they had already reached their maximal Pol2 loading and thus were unable to maintain a proficient mRNA synthesis (Figure 73-77).

This may suggest that high transcriptional rate of genes important for cancer cell proliferation, such as cell cycle and metabolic genes, will make tumor cells vulnerable to BET inhibition because their expression is rate-limited by their Pol2 pause release.

Any perturbation affecting Pol2 elongation (i.e. JQ1 treatment) would therefore impair gene expression.

These effects of JQ1 treatment could be recapitulated by a general inhibitor of elongation (Figure 77); again, genes sensitive to the treatment were highly enriched in Pol2 and couldn't restore elongation with further recruitment of Pol2 on promoters to maintain transcriptional rate, further indicating that elongation is the limiting step for the expression of JQ1 sensitive genes.

Our work provides a rationale to how a treatment that impairs elongation can lead to specific repression of a particular subset of genes.

VII Appendix 2. Chrokit: a user-friendly multiplatform web application to interactively explore genomic data

1 Introduction

In the last years, Next-generation sequencing (NGS) has become fundamental for genome-wide scale studies. Based on this technology a number of techniques have been devised to interrogate the genome and gain insight on how genetic information is interpreted by cells. In particular, transcription factor binding on the DNA can be addressed using chromatin immunoprecipitation coupled with sequencing (ChIP-Seq) (Nakato and Shirahige, 2017), expression of genes can be quantified with RNA-Sequencing (Wang et al., 2009), and accessibility of DNA with DNase-Seq (Song and Crawford, 2010). While different algorithms can be applied for these computational analyses, some of the steps are conserved among different kind of experiments.

In general, each of these experiments produces millions of short DNA reads; these reads are filtered for their quality and aligned to the reference genome, leading to the production of an alignment file, usually in BAM format. This file contains information about the position in the genome for each read. Usually, secondary analyses are carried out after the alignment. For example, peak-calling is performed in ChIP-Seq experiments to find where a transcription factor binds to the genome; in DNase-Seq, instead, chromatin-accessible regions are found from the sequencing of DNase I hypersensitive sites (Song and Crawford, 2010). Secondary analyses, then, usually take as input the alignment files and output genomic regions of particular interest.

From this point, higher-level analyses are usually performed to gain information about genome regulation; these involves a number of computational operations, such as the annotation of genomic regions, the determination of their overlap and

quantification and correlation of the signals (i.e. read enrichments) determined within such regions.

While programs that perform alignments and secondary analyses have been extensively developed and optimized in the last few years (Trapnell et al., 2009; Li and Durbin, 2009; Love et al., 2014; Zhang et al., 2008), user friendly applications built for higher-level NGS data analyses are still in their initial stage of development and fail to fully meet the need of the genomics community. Examples of these applications are seqMINER (Ye et al., 2011) and EpiMINE (Jammula and Pasini, 2016): these programs can calculate and plot, using heatmaps and profiles, the read enrichment on a specific set of genomic coordinates using a graphical user interface (GUI). Another tool recently published is EaSeq (Lerdrup et al., 2016), which performs multiple analyses on genomic data using a GUI in an interactive way. Finally, compEpiTools (Kishore et al., 2015) is a versatile R library that allows all these analyses to be integrated in R scripts. All these programs, despite their usefulness, suffer from limitations which restrict their usage, that are described below.

An important problem that is shared among the tools mentioned above is that none of them is able to be run as a web application: this implies that they must be used on local machines, thus preventing the user from performing computationally intensive tasks (such as those performed on dedicated clusters) and precluding their use by different users simultaneously.

In particular, seqMINER and EpiMINE are not able to separate computationally intensive tasks from the faster plot generation; this makes the analysis quite inefficient and cumbersome. These programs are also limited in the number of analyses they can perform; moreover, even if these two applications offer a user-friendly GUI, the plots generated lack interactivity and the filtering or modification of

genomic region of interest (ROI) is not implemented. On the other hand, EaSeq can produce interactive plots, but it runs only on windows operating systems, which is rarely used in bioinformatic community; moreover, it is written in Microsoft Visual Studio and .NET framework, which makes the implementation of new functions less user friendly.

We created Chrokit, a web application that overcomes many of the above mentioned limitations: it performs most of the genomic analyses with an interactive and easy-to-use GUI, designed for intuitive use to minimize dedicated training of perspective users. The application, written completely in R (R Development Core Team, 2016), can be installed on a remote server and run on any platform (Windows, Linux, MacOS) through a web interface. This guarantees increased computational power, accessibility to different users at the same time and the possibility to run the application remotely from different kind of devices (laptops, tablets, smartphones).

2 Materials and methods

2.1 Implementation

The application was developed in R programming language (R Development Core Team, 2016). Web interface was build using shiny, shinyFiles, shinydashboard libraries (Winston Chang, Joe Cheng, JJ Allaire and McPherson, 2017; Pedersen, 2016; Chang, 2016). The main engine of the program uses the following libraries: fastcluster (Müllner, 2013), Vennerable (Swinton, 2013), VennDiagram (Chen, 2016), GenomicRanges (Lawrence et al., 2013), data.table (Srinivasan, 2017), RColorBrewer (Neuwirth, 2014), Rsamtools (Hayden, 2016), ppcor (Kim, 2015), parallel.

The enrichment calculation for each base pair on DNA (the “primitive” function from which other operations are carried out) was implemented using a modified version of the “baseCoverage” function of “compEpiTools” R package (Kishore et al., 2015).

The method for calculating the stalling index of a particular transcription factor (usually polymerase) of a specific set of genes was inspired by "stallingIndex" function in "compEpiTools" R package (Kishore et al., 2015).

2.2 Description of the method

Central in the implementation of the program is the class "RegionOfInterest" (ROI). This class contains attributes and functions useful for the management of genomic regions. It is composed by the following attributes:

- genomic ranges: a GRanges class object, that represents the coordinates in the genome each ROI refers to, the strand of the DNA (if available, represent the orientation) and eventually the annotation
- a name: the name of the ROI
- a fixed point: useful when coordinates have to be resized or center on a specific point, that is not simply the midpoint of the GRange (i.e. the summit)
- a flag: is the kind of genomic regions a ROI belongs to (it could be a promoter, a transcript or a generic range). This is useful because for specific operations, different kind of ROIs should be treated differently
- a BAMlist: each ROI can be associated to a set of BAM files (i.e. files of aligned reads) that represent the enrichments of genomic features (for example, ChIPped transcription factors or histone marks) for each position of a specific genomic region
- a source: during the analysis, new ROIs can be produced; the more the analysis goes on, the more complex the steps to create a ROI can be. For this reason, each ROI brings a message that represent how the ROI has been constructed (i.e. a log message)

To determine the enrichment of a feature in a specific genomic region, the program calculates the number of reads of pileup for each base of the DNA that belongs to a specific set of genomic coordinates and stores them in memory, as a "primitive" operation. Once the object ("BAMlist" of the class "RegionOfInterest") has been stored in the RAM, every operation that will require the determination of the enrichment either in the entire region or in a variable number of bins chosen by the user is done quickly by performing the sum of the enrichments already pre-calculated for each base pair. The Figure 78 summarizes this structure.

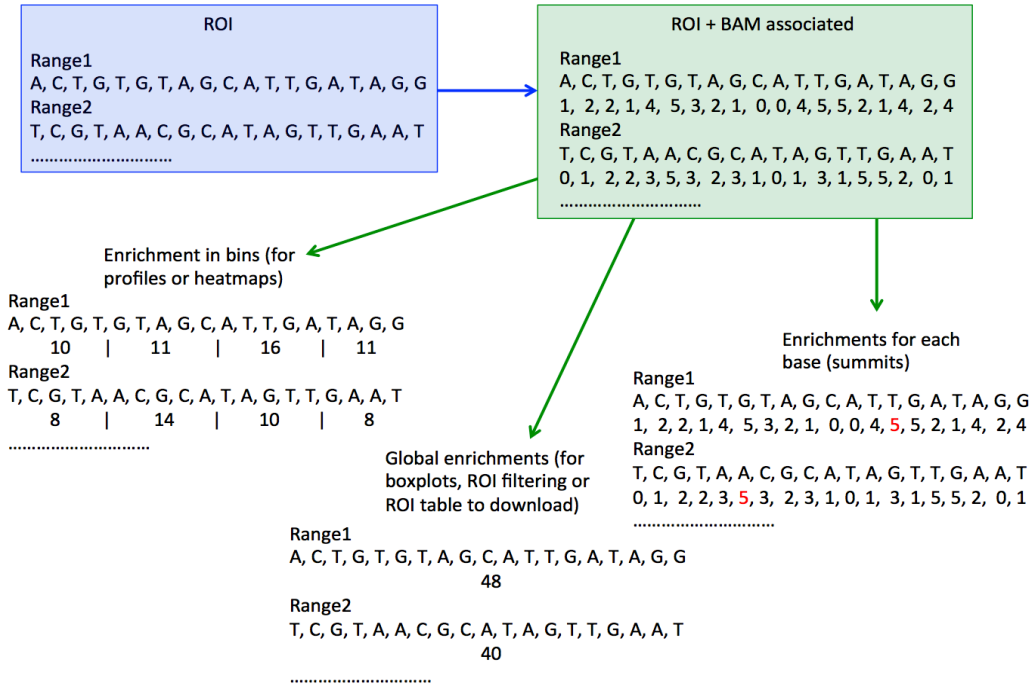

Figure 78: Enrichment at base-pair level is pre-computed by Chrokit application. During BAM association step (from blue to green square), the number of reads aligned to each base pair of the genomic range is calculated; this computationally intensive operation is carried out only once. Then, each task that involves enrichments (binning, sum of the enrichments, summit detection) will be fast.

Figures 3(left),5, 8-10, 13, 15-18, 21-23, 30, 50-52 of this thesis were built using Chrokit application.

3 Results

3.1 Overview of Chrokit implementation

Either BED files or gene lists derived from upstream NGS analyses can be used as input by Chrokit application (Figure 79, left) to create the genomic regions of interest (ROI, see materials and methods, paragraph 2.2, page 132); briefly, a ROI is an R object representing a set of genomic regions associated to their genomic coordinates (chromosome number, start position and end position). Other ROIs can then be created starting from these primary ROIs or modified in multiple ways. From this point, a user can find the fraction of genomic regions of a ROI inside annotated promoters or genes and evaluate the co-localization of two or multiple ROIs; finally, he can download the region of interest object as a table (Figure 79, right).

If alignment files (i.e. BAM files) are available, they can be associated to ROIs (Figure 79, center); from this point, it is possible to evaluate the enrichments of genomic features by using different graphical representations, such as quantitative heatmaps, profiles, boxplots or calculate the correlations/partial correlations between enrichments in specific regions and representing them through heatmaps or scatterplots; finally, a meta-gene representations of reads enrichment is available (Figure 79, right).

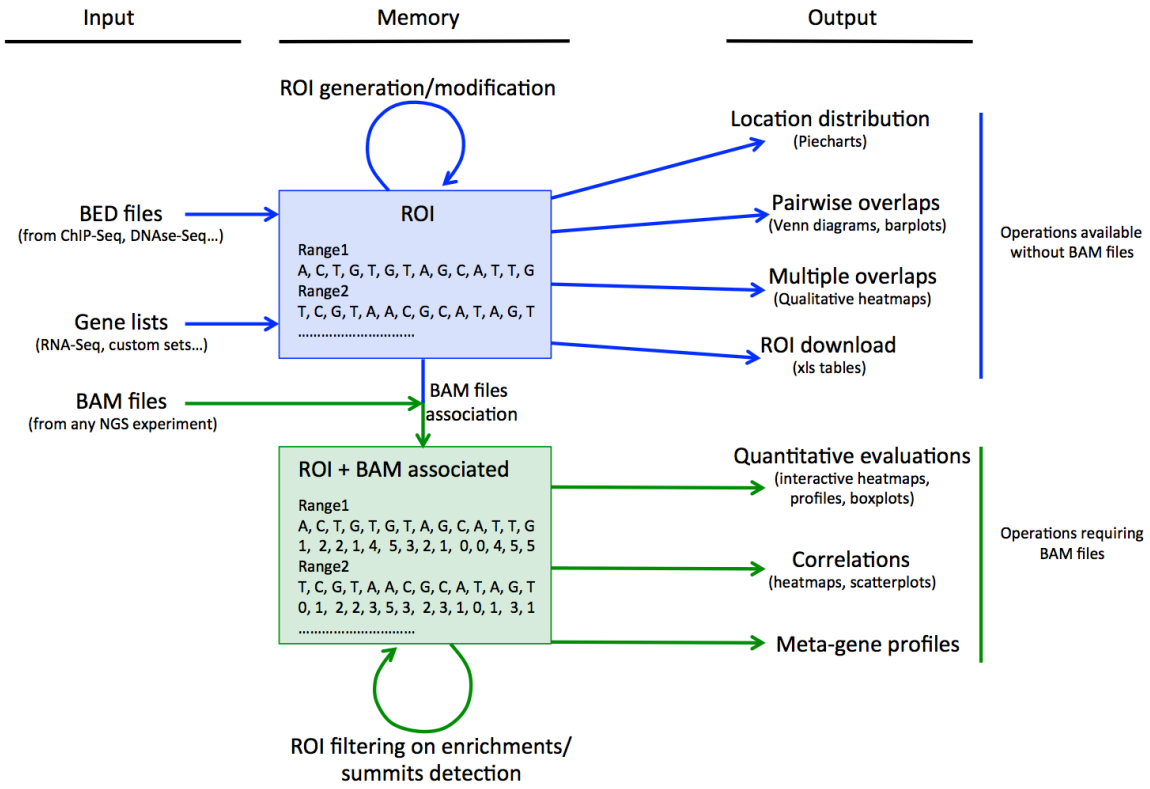

Figure 79: Overview of Chrokit application. Left: Chrokit accepts BED files and gene lists as input, and save them in memory as regions of interest (ROI). BED files can derive from NGS experiments, such as ChIP-Seq or DNase-Seq; gene lists can be a group of up/downregulated genes from RNA-Seq analyses or custom gene sets. BAM files can be used to calculate the enrichment at base-pair level in a specific region of interest (see materials and methods). Center: ROIs are R object that are stored in the system memory. ROIs can be created or modified in multiple ways and, if BAM files were associated, it is possible to filter ROIs according to their enrichments or detect summits. Right: Chrokit can return different kind of outputs. If BAM files were not associated to ROIs (up, blue), it is possible to determine the distribution of genomic regions in promoters of annotated genes, perform overlaps between ROIs and download them as xls file. If BAM files were associated to ROIs (down, green), the program allows to evaluate quantitative information of reads enrichment with interactive heatmaps, profiles or boxplots; it can calculate correlations between enrichments (showing them as heatmaps or scatterplots) and display reads distribution along genes.

3.2 Inputs for the program: data type and format(s)

Chrokit uses the output from first-level analyses of NGS experiments to obtain "region of interest" (ROI), which are the objects at the basis of the Chrokit application.

The user can import coordinates files in BED format either by searching in the filesystem or by providing the path of the file; then, a preview of the file is displayed on a dedicated window as a table, showing the genomic coordinates (chromosome position, start, end) and eventually the file can be imported as ROI.

Coordinates of promoters or genebodies can be imported by providing a list of ENTREZ gene IDs, either by uploading a text file containing the IDs or by pasting them into a dedicated window. This is useful, for example, to investigate genomic features of a list of genes found upregulated in an RNA-Seq experiment. In this case, a transcript database based on UCSC annotation (Meyer et al., 2013) can be imported in the program, to convert each ID to the coordinate of the corresponding promoters and transcripts and producing the ROIs; promoters can be further refined by the user by choosing a genomic window around annotated transcription start sites (TSS). All the isoforms of genes are considered during this conversion, and the user can set a threshold on the maximum allowed transcript length; this is useful in some situations in which big transcripts (usually >100 Kb) may cause memory problems.

Gene Symbols can be provided instead of IDs, but a genome-wide annotation database (such as org.Mm.eg.db for mouse (Carlson, 2016)) is required for symbol-to-ID conversion, which is performed by Chrokit.

Both transcript database and genome annotation database are chosen depending on the organism of interest and, if the corresponding libraries are not installed in the system, the user can download them from Bioconductor (Huber et al., 2015) within Chrokit.

In many NGS experiments BAM files are used to calculate the enrichments of reads in defined regions of interest; for example, in ChIP-Seq, the enrichment represents the binding intensity of a specific transcription factor, while in DNase-Seq the chromatin accessibility.

Path to BAM files can be imported in Chrokit: a user can browse the entire filesystem or manually provide the path of the file. When the file is selected, the program checks whether the BAM index is present; if so, the path to the BAM file is imported.

3.3 Regions of interest can be created and modified by Chrokit

Once necessary files have been imported, it is possible to create and modify ROIs starting from genomic regions loaded in memory. As example, to merge ChIP-Seq replicates together, a user can select multiple regions of interest corresponding to peaks of a transcription factor and calculate their union, to find regions present in at least one ROI or the intersection, to find only regions in common (Figure 80a). It is also possible to subset existing ROIs to keep ranges that overlap with other ROIs. For example, to retrieve the binding sites of a transcription factor on promoters of annotated genes, the user can select the ROI corresponding to ChIP-Seq peaks in the panel shown in Figure 80a and then ask for the overlap with the ROI corresponding to promoters, in the panel shown in Figure 80b; alternatively, to find the binding events at distal sites, the ROI corresponding to promoters must not overlap with ChIP-Seq peaks (Figure 80c).

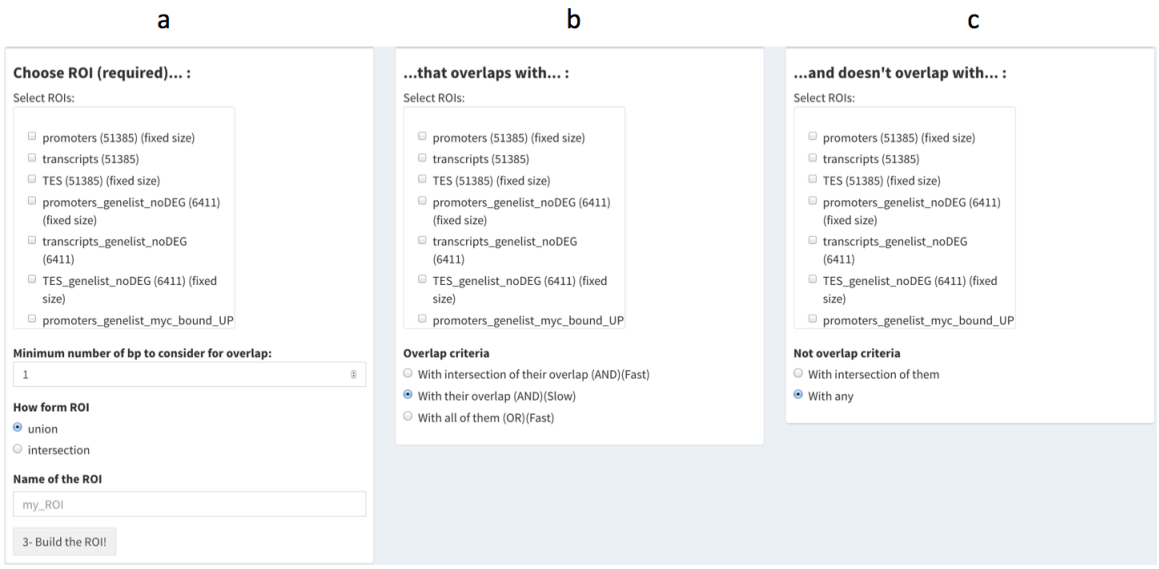

Figure 80: ROIs can be created from pre-existing regions of interest. Panel for the creation of a new ROI from pre-existing ROIs. A selected ROI or the union/intersection of multiple ROIs (a) can be filtered to keep only those overlapping (b) or not overlapping (c) with other ROIs.

Once a ROI has been created, it is possible to perform different operations to modify it. Genomic coordinates can be resized from the center of the ROI (Figure 81a); this is particularly useful for further representation of data, in which a fixed width for all ranges of a ROI is recommended (see below, Figure 85). Usually, a motif finding analysis is carried out using the summit of peaks of a transcription factor in a ChIP-Seq experiment. For this reason, a user can retrieve the summits of a ROI by selecting the BAM file for which the maximum pileup of reads is desired (Figure 81b). Sometimes ChIP-Seq peaks must be filtered according to the width of the peaks or the enrichments of some chromatin features; this can be easily accomplished through the interface (Figure 81c, e). Finally, the management of ROIs characterized by a high number of genomic regions can be a computationally intensive, or even unfeasible on some platforms lacking powerful hardware. Therefore, a representative random sample of a ROI can be selected for use in further analyses (Figure 81d).

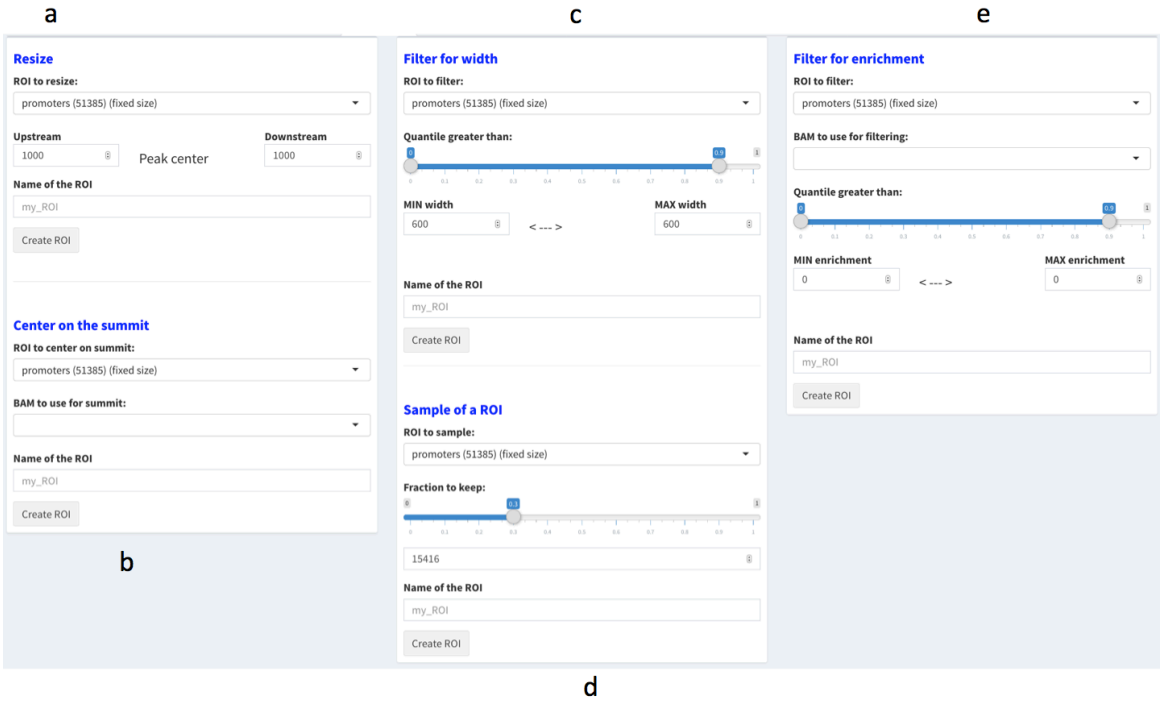

Figure 81: ROIs can be modified in multiple ways. Multiple operations can be performed on ROIs: a) change the genomic boundaries of its ranges; b) center on the summits, using a particular associated BAM file as a reference; c) filtering on width, d) subsampling; e) filtering on enrichments.

Annotation of ROIs becomes particularly useful when a gene ontology analysis has to be carried out on genes associated to a specific subset of ChIP-Seq peaks. For this, a suitable annotation database must be imported (see paragraph 3.2, page 135), and the program finds the closest gene from the midpoint (or from the boundaries) of each genomic range inside a ROI; alternatively, Chrokit can find all the genes inside a fixed genomic window from the midpoint of genomic ranges.

To perform the analyses on enrichments, BAM files can be associated to ROIs; this is the most computationally intensive task and usually require 1 minute.

Finally, ROIs can be downloaded as *.xls file, a tab delimited text file which contains the ranges, the nearest gene ID or symbol (if annotated) and (potentially) the enrichments of specific chromatin features associated to the ROI, such as transcription factors binding, histone modifications, RNA abundance or DNA accessibility.

3.4 Genomic analyses

Upon ROI construction and (potentially) BAM association, a user can perform higher-level analyses, whose output usually consists of publication-quality plots that can be downloaded as *.pdf files.

Single evaluation of a ROI

Detailed evaluation of a selected ROI can be performed using gene annotation information and BAM files associated to the ROI. For example, a user needs to examine the binding of a transcription factor in a ChIP-Seq experiment; he then selects a ROI corresponding to the peaks of the ChIP-ed transcription factor and the BAM file associated to it. Chrokit outputs a piechart representing the peaks location of the transcription factor inside promoters, genebodies and intergenic regions (Figure 82a; in this example only a minority of peaks were located at promoters). Then, the program plots the distribution of the peak width in these three subsets (in this example, peaks at promoter were wider on average compared to the other subsets, Figure 82b). Finally, the enrichments of the transcription factor inside the three subsets are shown in a lower panel, both as boxplots (Figure 82c) and average peak profile (Figure 82d).

This kind of analysis is then commonly used to obtain basic information of a ChIP-Seq analysis.

The user can set different parameters for this analysis, such as the colors, the log2 transformation of read enrichments or the choice between total read coverage (rpm, reads per million) or read density (rpm/bp, rpm normalized by width of the genomic range).

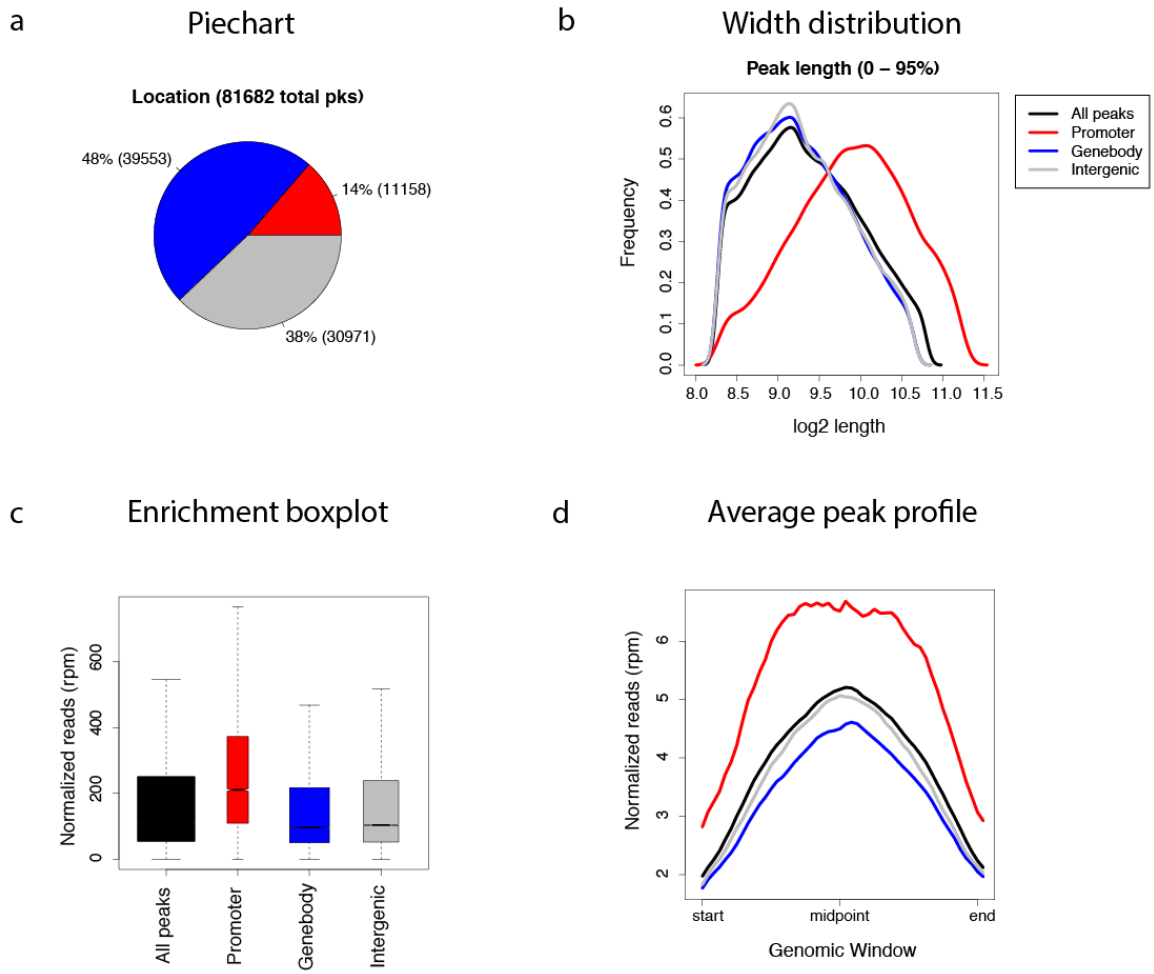

Figure 82: Chrokit evaluates features of single ROIs. a) piechart showing the fraction of genomic regions of the ROI at promoters (red), genebodies (blue) or intergenic regions (grey); b) Distribution of the width of genomic range of the ROI; c) Boxplot showing the enrichments at promoters, genebodies or intergenic regions; d) Average read profile at promoters, genebodies, intergenic regions.

Pairwise comparison of ROIs

Chrokit can compare two different ROIs to evaluate their overlap and the enrichment of chromatin features in the common sites or in sites present exclusively in one of the two ROIs. For example, this function can be used to evaluate the consistency of replicates in a ChIP-Seq experiments, the co-localization of two different transcription factors or the co-occurrence of a transcription factor with open chromatin sites detected by a DNase-Seq experiment.

A Venn diagram is used to show such kind of overlaps (Figure 83a). Then, a boxplot or a scatterplot show the enrichment of a genomic feature inside regions in common or specific for each ROIs (Figure 83b).

The user can select different parameters in a dedicated panel, including the log2 transformation of read enrichments, the choice between total read coverage (rpm) or read density (rpm/bp) or the minimum number of base pair to consider for the overlaps.

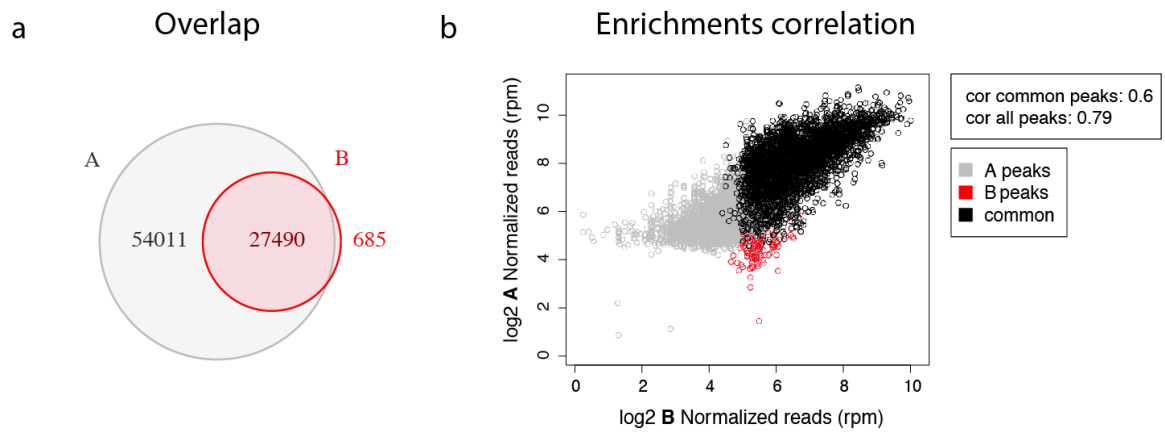

Figure 83: Chrokit evaluates overlaps between ROIs. a) Venn diagram showing the overlap between two ROIs (A and B); b) scatterplot showing the read enrichments in genomic regions common for both ROIs (black) or present in only one of the two ROIs (grey or red). This example shows the overlap of peaks of a ChIP-Seq experiment.

Multiple ROIs analyses

When multiple (>2) ROIs are compared together, the program provides a heatmap representation of the overlaps of chosen ROIs (Figure 84a) compared to a defined ROI or multiple ROIs of reference (the "master" ROI). For example, a user can investigate if a transcription factor whose binding was detected by ChIP-Seq co-localize with other transcription factors, histone modifications or regions of open chromatin found by DNase-Seq. The output is a heatmap in which overlapping regions are represented by a color, while regions not overlapping are shown in white (Figure 84a).

Then, the program outputs a matrix with the Jaccard index of all the pairwise comparisons of the selected ROIs. Jaccard index is a measure of the amount of the overlap between two genomic ranges, and is defined as the fraction between the intersection and the union of the two genomic ranges.

Figures can be downloaded as *.pdf files and variables, such as the colors, the number of bins in which the heatmap is divided and the clustering parameters of the heatmap can be set by the user in a dedicated panel.

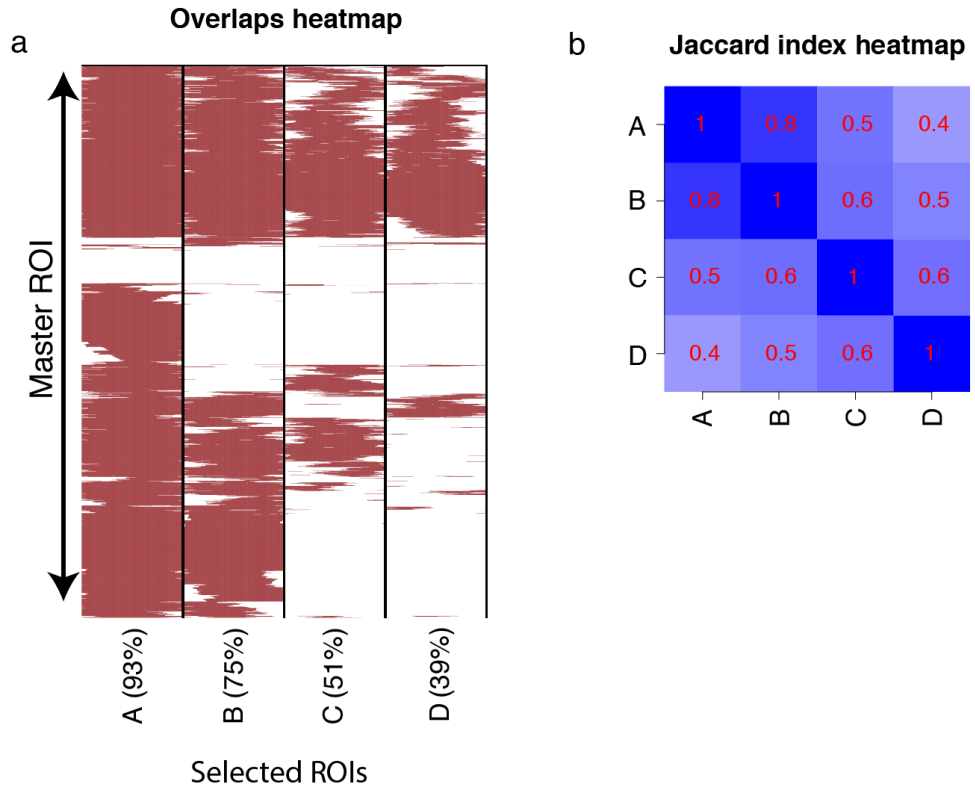

Figure 84: Multiple ROI overlap is represented by a heatmap. a) Heatmap representing multiple overlaps inside a reference ROI (the "Master" ROI) of other selected ROIs (A,B,C and D). Overlapping ranges are depicted in red; b) heatmap showing the Jaccard index for each pair of selected ROIs inside the master ROI.

Enrichments of features inside ROIs (I)

If signal intensities of specific chromatin features need to be evaluated, BAM files must be associated to ROIs. Chrokit provides a heatmap representation of these enrichments (i.e. a "quantitative" heatmap). When a ROI or multiple ROIs are selected, Chrokit returns a heatmap representing the enrichments of the BAM files associated

(Figure 85a) using a color scale to display signal intensity. For example, if a user needs to determine histone modifications, binding intensities of transcription factors or accessible chromatin regions inside promoters, he can associate BAM files of those chromatin features to the ROI corresponding to promoters and then obtain the heatmap shown in Figure 85.

The heatmap is interactive: when variables are modified, such as the color saturation, the number of bins or the clustering method, the heatmap is modified with the new parameters. If a portion of the heatmap is selected by dragging the mouse cursor (Figure 85a, blue area), different visualizations of enrichments are shown instantly in a different panel, including profiles (Figure 85b, up) and boxplots (Figure 85b, down). When the selected area is changed, all these plots are updated interactively.

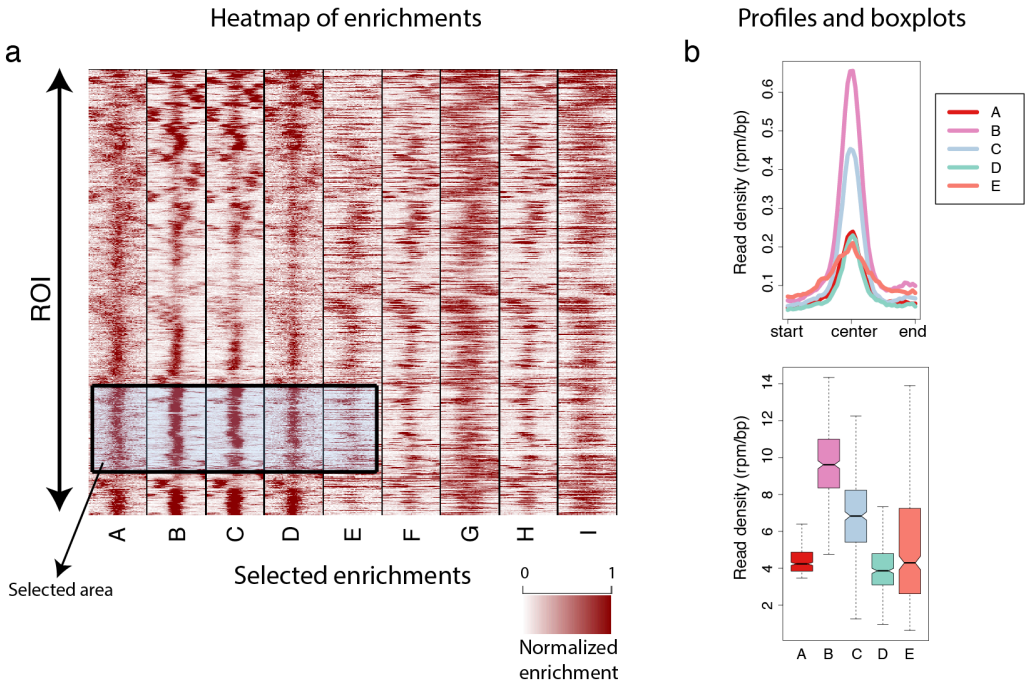

Figure 85: Quantitative heatmap shows read enrichments on specific region of interest. a) Quantitative heatmap: given a reference ROI, the enrichments of associated BAM files (A-I) are shown in red scale. When part of the heatmap is selected (blue area), the corresponding enrichments are plotted as profiles (b, up), boxplots (b, down) or with other graphical representations.

By default, only 2000 random genomic ranges out of the total are considered for the heatmap representation to avoid memory overloads; this number is sufficient to correctly represent the entire ROI; however, a user can change this parameter to show all the genomic ranges available inside the ROI.

Enrichments of features inside ROIs (II)

The program has a dedicated section to carry out more accurate analyses on the enrichments in ROIs. In this section, profiles and boxplot representation of the enrichments are available (Figure 86a, b) as before (Figure 85b). Moreover, a heatmap representing the pairwise correlations or partial correlations between enrichments is produced in a lower panel (Figure 86c); when a user clicks a square in the correlation matrix corresponding to a combination of two enrichments, the scatterplot of the pairwise correlation of these enrichments is drawn at the same time (Figure 86d).

The user can set different parameters, including the log2 transformation of the enrichments, the correlation method ("Pearson" or "Spearman") and the number of bins. Moreover, data table originating the boxplots can be downloaded for downstream analyses.

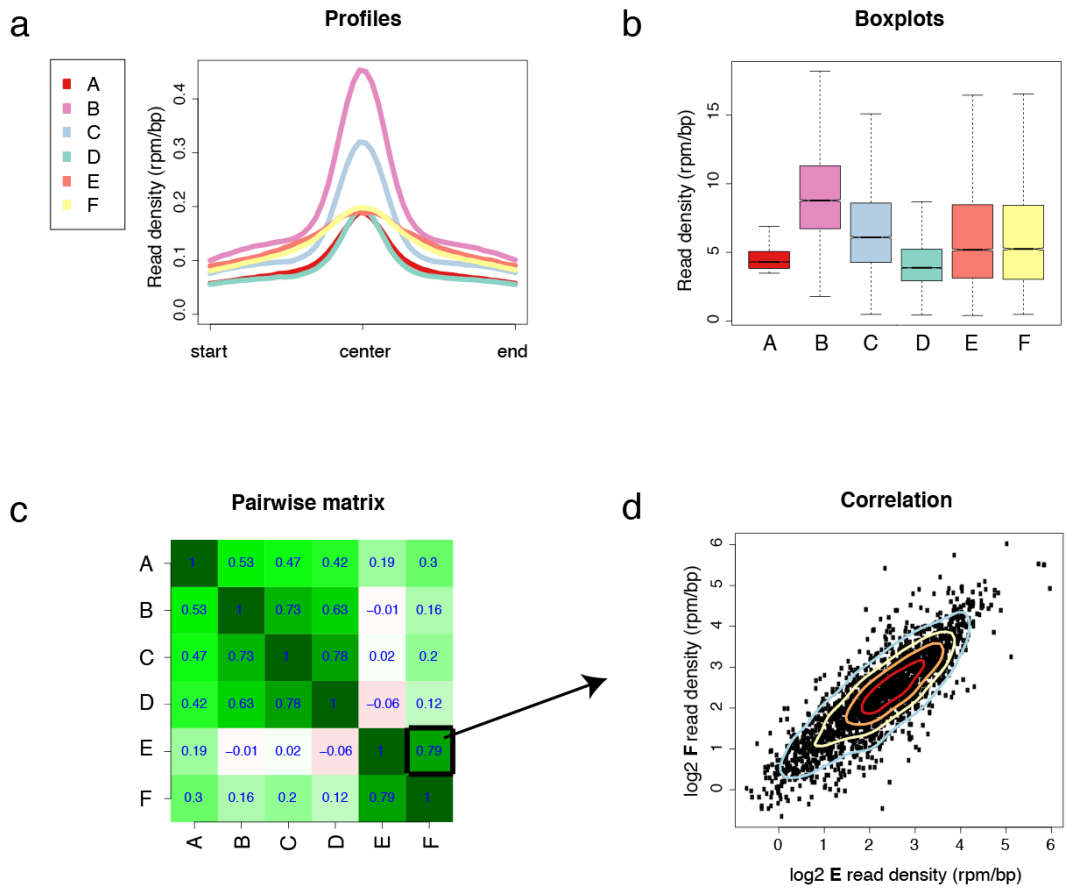

Figure 86: Chrokit provides multiple representations of enrichments inside ROIs. a) Profile of the read enrichments of BAM files (A,B,C,D and E) associated to a specific ROI; b) boxplot of the enrichments of BAM files associated to the ROI; c) matrix of the pairwise correlations of the enrichments inside the ROI; d) Scatterplot of the pairwise correlations of two enrichments selected in c). When a user clicks on one element of the correlation/partial correlation matrix, the corresponding scatterplot of the pairwise correlation is drawn at the same time.

Analyses of enrichments within genes

Chrokit can compute the enrichment of chromatin features inside a specific subset of genes; this can be useful for example when a user has to profile the Pol2 distribution along up or downregulated genes determined by previous RNA-Seq experiments. In this case, the user imports the gene lists as mentioned before (see paragraph 3.2, page 135), and retrieves the promoters, transcripts and transcription end sites (TES) related to each gene as ROIs. Then, he associates the BAM files of interest to the subsets of promoters, transcripts and TES created before (for example, the BAM files

of Pol2 ChIP-Seq in two or more different conditions). Then, Chrokit outputs three different results. In the first, a meta-gene representation of the average profile of read enrichment (Pol2 as example) is shown (Figure 87a); then, boxplots representing the read density of the on promoters, along genebodies and on TES are shown in a lower panel (Figure 87b). Finally, the cumulative reads on TSS, genebodies and the stalling index are represented (Figure 87c). The stalling index is defined as the ratio between the number of reads inside promoters and the number of reads in the genebodies.

This function can be also used to represent other features along genes, such as chromatin accessibility found by DNase-Seq or specific histone modifications.

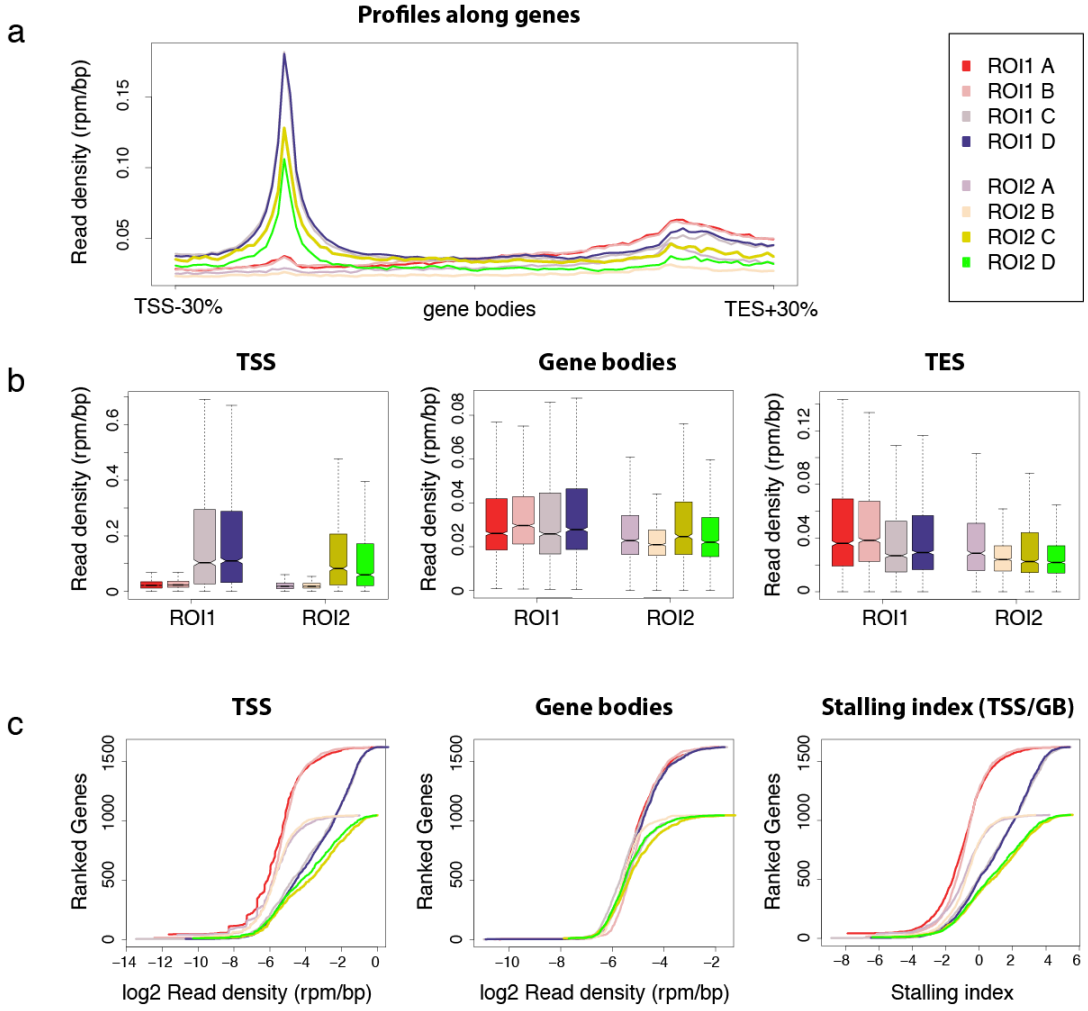

Figure 87: Chrokit provides a "meta-gene" visualization of the enrichment of aligned reads. a) average profile of read enrichments of A,B,C and D along genebodies (in this example, RNA Pol2) of two ROIs (ROI1 and ROI2); b) Boxplots representing the enrichments calculated with the same BAM file(s) on TSS, genebodies and TES of ROI1 and ROI2; c) cumulative reads on TSS, genebodies and stalling index of A,B,C and D enrichments on ROI1 and ROI2.

3.5 Efficiency and flexibility

Once Chrokit associates a BAM file to a ROI, it can calculate the enrichments in a variable number of bins inside selected genomic regions very fast (see materials and methods, paragraph 2.2, page 132), thus making it an efficient program: only few seconds are needed for most of the operations. The only two critical points are session saving/loading and the association of BAM files to ROIs.

Usually, saving/loading a session requires 3/4 minutes with 10/20 ROIs each with 20000 ranges and 2/3 BAM files associated. The speed also depends on the storage in which session files were saved: network storages are slower compared to local hard drives, which, in turn, are slower compared to solid state drives (SSD).

The time needed for BAM association depends on the size of the ROI (both width and number of genomic ranges), the size of the BAM file and the storage in which BAM files were saved, but generally is less than 1 minute. If sufficient RAM is available (about 4 Gb RAM/core) and multiple CPUs are present, multiple BAM files can be associated in parallel to improve the speed.

The possibility to run the Chrokit web application on a remote machine, on any operating system and to be accessed by different users simultaneously gives it an extreme flexibility. The use of clusters in computational biology is now widespread through research centers (Ocana and de Oliveira, 2015); they can concentrate the most computationally-intensive tasks in dedicated, powerful machines. This program can be run as a server inside a cluster and can be accessed and used through a web browser by multiple users. Running this application in a cluster allows the session files produced by the application to be shared between researchers, improving the reproducibility and speed of the analyses. Given its web interface, when running on a remote machine, the application can be accessed using different devices, such as laptops, smartphones or tablets, thus providing high accessibility.

3.6 The graphical user interface

When the Chrokit application is executed, the server opens a socket on the machine on a specific IP:PORT combination, that could be reached by any web browser. The interface provides different tabs, according to the kind of analysis a user needs to carry out.

The web page shows three main sections on the left. The first, "Input files" (Figure 88a), is dedicated to the import of input files: BED files, BAM files, databases and gene lists. The second section ("Work with data", Figure 88b) is dedicated to the analyses; in particular, a user can create or modify ROIs or plot the results. Finally, the working sessions can be saved or loaded using the last section (Figure 88c).

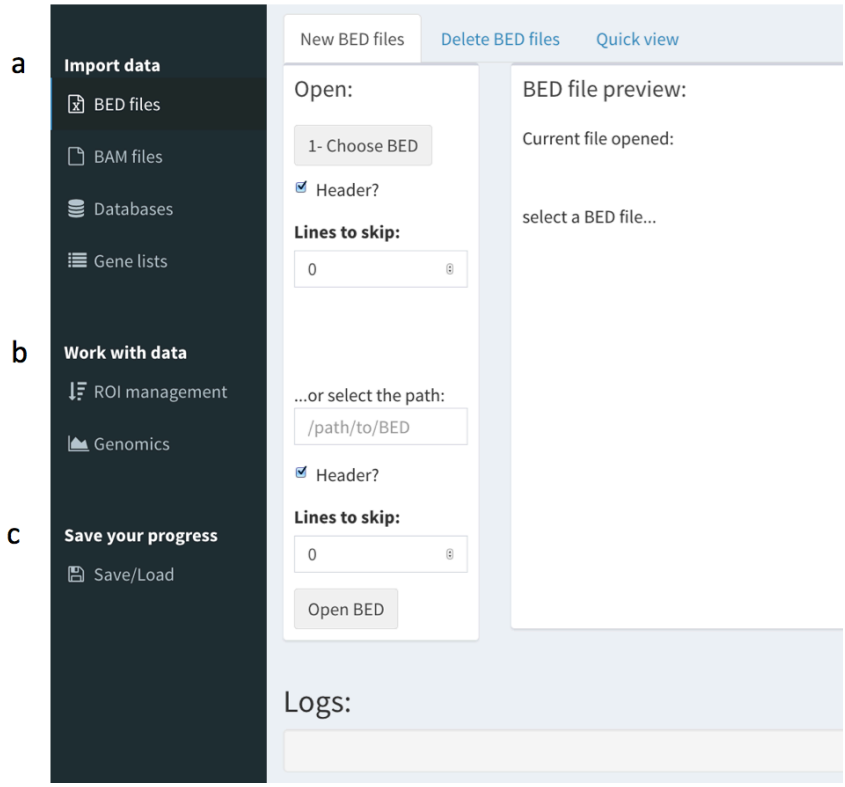

Figure 88: Sections of Chrokit graphical user interface. a) Section to import files in BED and BAM format, databases and list of genes; b) Section to create, modify ROIs and perform genomic analyses; c) Section to save/load working sessions.

Two subsections are available inside "Work with data" section: "ROI management" and "Genomics" (Figure 88b). In "ROI management" it is possible to create, delete, or

rename and reorder ROIs (Figure 89a, b and c, respectively), annotate ROIs using different criteria (Figure 89d), modify the genomic range of the ROIs (Figure 89e), view ROI features (Figure 89f) or download them (Figure 89g) and associate, rename or reorder BAM files associated to ROIs (Figure 89h, i).

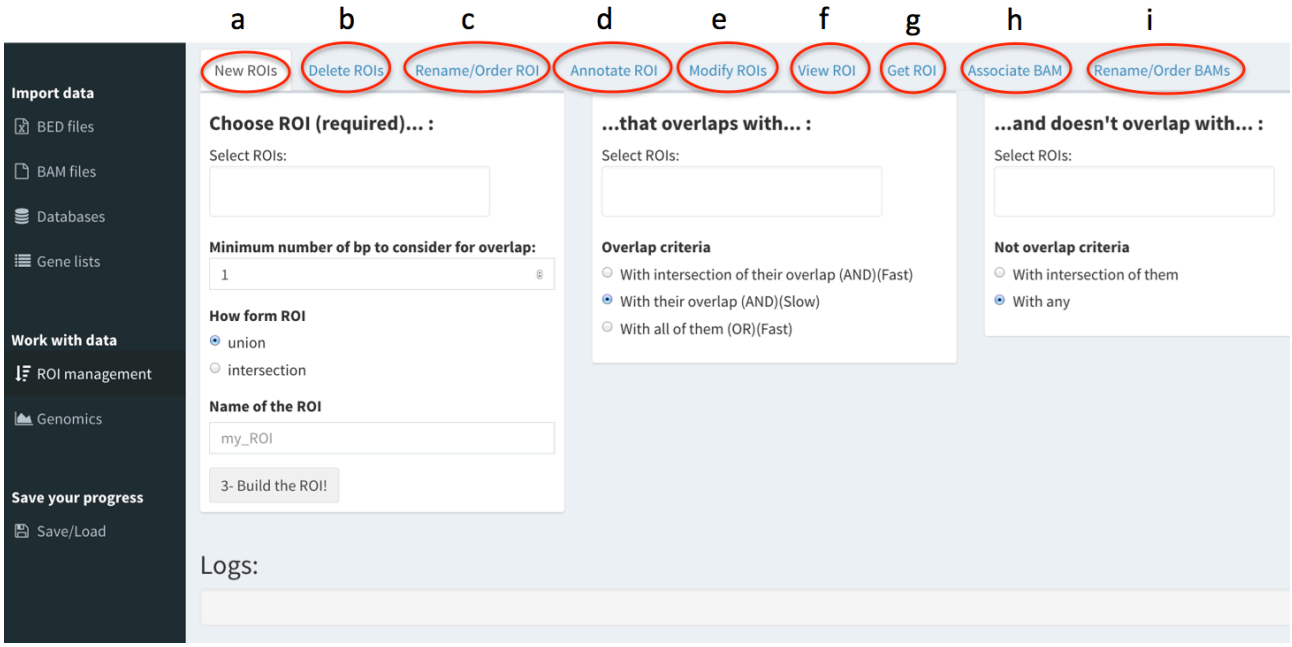

Figure 89: Tabs in "ROI management" subsection. Chrokit can manage ROIs: a) create new ROIs (see Figure 80); b) delete existing ROIs; c) rename or change the order of the ROIs; d) annotate ROIs to the corresponding genes; e) modify ROIs (see Figure 81); f) view the number or width of genomic ranges of a ROI; g) download ROIs as tables; h) associate or remove BAM files; i) rename or reorder BAM files associated to a ROI.

The output plots can be obtained using the tabs inside "Genomics" subsection (Figure 88b). In particular, single (Figure 90a) or pairwise (Figure 90b) ROI evaluation can be performed, together with the heatmap representation of multiple overlaps (Figure 90c) and quantitative heatmaps of the enrichments (Figure 90d). Finally, pairwise matrix correlation of the enrichments and read profiles on genes can be visualized using the last two tabs (Figure 90e, f)

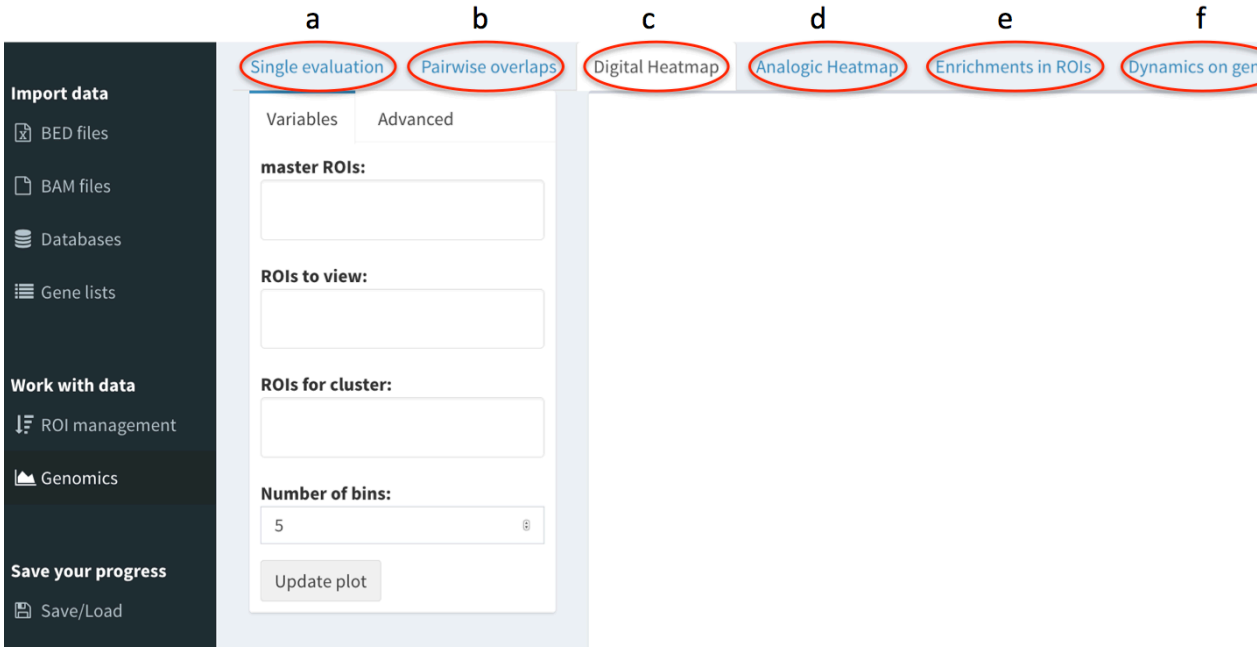

Figure 90: The "Genomics" subsection. This screenshot shows the tabs contained in "Genomics" subsection. a) single ROI evaluation (see Figure 82); b) comparison between two ROIs (see Figure 83; c) overlaps between multiple ROIs (see Figure 84); d) quantitative heatmaps (see Figure 85); e) correlation matrix and pairwise correlation between enrichments (see Figure 86); f) met a-gene profiles inside ROIs (see Figure 87).

4 Discussion

The analysis of genomic data is a challenging task in bioinformatics field and requires the development of specific tools to handle next-generation sequencing data. For this purpose, we developed Chrokit, an open source, multiplatform web application that allows working with genomic regions and visualizing data in an intuitive and interactive way with its graphical user interface. Chrokit could be executed on local machines, given its low hardware requirements. However, when run on powerful machines, many users can access the application simultaneously with any kind of device, thus providing high flexibility. Requiring only an R interpreter and few R libraries make the installation of this program straightforward and multiplatform, since the interpreter is available for all commonly used operating systems (Windows, Linux, MacOS).

Novel features have to be implemented to improve Chrokit functionality, such as the integration with RNA-Seq data and geneset enrichment analyses.

VIII References

Adams, J.M., A.W. Harris, C.A. Pinkert, L.M. Corcoran, W.S. Alexander, S. Cory, R.D. Palmiter, and R.L. Brinster. 1985. The c-myc oncogene driven by immunoglobulin enhancers induces lymphoid malignancy in transgenic mice. *Nature*. 318:533–538. doi:10.1038/318533a0.

Di Agostino, S., G. Sorrentino, E. Ingallina, F. Valenti, M. Ferraiuolo, S. Bicciato, S. Piazza, S. Strano, G. Del Sal, and G. Blandino. 2015. YAP enhances the pro-proliferative transcriptional activity of mutant p53 proteins. *EMBO Rep.* 1–14. doi:10.15252/embr.201540488.

Albajar, M., M.T. Gómez-Casares, J. Llorca, I. Mauleon, J.P. Vaqué, J.C. Acosta, A. Bermúdez, N. Donato, M.D. Delgado, and J. León. 2011. MYC in chronic myeloid leukemia: induction of aberrant DNA synthesis and association with poor response to imatinib. *Mol. Cancer Res.* 9:564–576. doi:10.1158/1541-7786.MCR-10-0356.

Alder, O., R. Cullum, S. Lee, A.C. Kan, W. Wei, Y. Yi, V.C. Garside, M. Bilenky, M. Griffith, A.S. Morrissy, G.A. Robertson, N. Thiessen, Y. Zhao, Q. Chen, D. Pan, S.J.M. Jones, M.A. Marra, and P.A. Hoodless. 2014. Hippo signaling influences HNF4A and FOXA2 enhancer switching during hepatocyte differentiation. *Cell Rep.* 9:261–271. doi:10.1016/j.celrep.2014.08.046.

Anders, L., M.G. Guenther, J. Qi, Z.P. Fan, J.J. Marineau, P.B. Rahl, J. Lovén, A.A. Sigova, W.B. Smith, T.I. Lee, J.E. Bradner, and R.A. Young. 2013. Genome-wide localization of small molecules. *Nat. Biotechnol.* 32:92–96. doi:10.1038/nbt.2776.

Andrews, S. 2010. FastQC: A quality control tool for high throughput sequence data. *Http://Www.Bioinformatics.Babraham.Ac.Uk/Projects/Fastqc/*. http://www.bioinformatics.babraham.ac.uk/projects/. doi:citeulike-article-id:11583827.

Annibali, D., J.R. Whitfield, E. Favuzzi, T. Jauset, E. Serrano, I. Cuartas, S. Redondo-Campos, G. Folch, A. Gonzàlez-Juncà, N.M. Sodir, D. Massó-Vallés, M.-E. Beaulieu, L.B. Swigart, M.M. Mc Gee, M.P. Somma, S. Nasi, J. Seoane, G.I. Evan, and L. Soucek. 2014. Myc inhibition is effective against glioma and reveals a role for Myc in proficient mitosis. *Nat. Commun.* 5. doi:10.1038/ncomms5632.

Arabi, A., S. Wu, K. Ridderstråle, H. Bierhoff, C. Shiue, K. Fatyol, S. Fahlén, P. Hydbring, O. Söderberg, I. Grummt, L.-G. Larsson, and A.P.H. Wright. 2005. c-Myc associates with ribosomal DNA and activates RNA polymerase I transcription. *Nat. Cell Biol.* 7:303–310. doi:10.1038/ncb1225.

Aragona, M., T. Panciera, A. Manfrin, S. Giulitti, F. Michielin, N. Elvassore, S. Dupont, and S. Piccolo. 2013. A mechanical checkpoint controls multicellular growth through YAP/TAZ regulation by actin-processing factors. *Cell*. 154:1047–1059. doi:10.1016/j.cell.2013.07.042.

Babeu, J.P., and F. Boudreau. 2014. Hepatocyte nuclear factor 4-alpha involvement in liver and intestinal inflammatory networks. *World J. Gastroenterol.* 20:22–30. doi:10.3748/wjg.v20.i1.22.

Bahram, F., N. von der Lehr, C. Cetinkaya, and L.G. Larsson. 2000. c-Myc hot spot mutations in lymphomas result in inefficient ubiquitination and decreased proteasome-mediated turnover. *Blood*. 95:2104–2110.

Baia, G.S., O.L. Caballero, B.A. Orr, A. Lal, J.S.Y. Ho, C. Cowdrey, T. Tihan, C. Mawrin, and

G.J. Riggins. 2012. Yes-Associated Protein 1 Is Activated and Functions as an Oncogene in Meningiomas. *Mol. Cancer Res.* 10:904–913. doi:10.1158/1541-7786.MCR-12-0116.

Balaji, K.C., H. Koul, S. Mitra, C. Maramag, P. Reddy, M. Menon, R.K. Malhotra, and S. Laxmanan. 1997. Antiproliferative effects of c-myc antisense oligonucleotide in prostate cancer cells: a novel therapy in prostate cancer. *Urology*. 50:1007–1015. doi:S0090429597003907 [pii].

Bandopadhayay, P., G. Bergthold, B. Nguyen, S. Schubert, S. Gholamin, Y. Tang, S. Bolin, S.E. Schumacher, R. Zeid, S. Masoud, F. Yu, N. Vue, W.J. Gibson, B.R. Paolella, S.S. Mitra, S.H. Cheshier, J. Qi, K.W. Liu, R. Wechsler-Reya, W.A. Weiss, F.J. Swartling, M.W. Kieran, J.E. Bradner, R. Beroukhim, and Y.J. Cho. 2014. BET bromodomain inhibition of MYC-amplified medulloblastoma. *Clin. Cancer Res.* 20:912–925. doi:10.1158/1078-0432.CCR-13-2281.

Basu, S., N.F. Totty, M.S. Irwin, M. Sudol, and J. Downward. 2003. Akt phosphorylates the Yes-associated protein, YAP, to induce interaction with 14-3-3 and attenuation of p73-mediated apoptosis. *Mol. Cell*. 11:11–23. doi:10.1016/S1097-2765(02)00776-1.

Becker, P.B., and J.L. Workman. 2013. Nucleosome remodeling and epigenetics. *Cold Spring Harb. Perspect. Biol.* 5. doi:10.1101/cshperspect.a017905.

Berg, T. 2010. Small-molecule modulators of c-Myc/Max and Max/Max interactions. *Curr. Top. Microbiol. Immunol.* 348:139–149. doi:10.1007/82-2010-90.

Bergsagel, P.L., and W.M. Kuehl. 2001. Chromosome translocations in multiple myeloma. *Oncogene*. 20:5611–5622. doi:10.1038/sj.onc.1204641.

Bernard, S., and M. Eilers. 2006. Control of cell proliferation and growth by Myc proteins. *Results Probl. Cell Differ.* 42:329–342. doi:10.1007/400_004.

Bianchi, V., A. Ceol, A.G.E. Ogier, S. de Pretis, E. Galeota, K. Kishore, P. Bora, O. Croci, S. Campaner, B. Amati, M.J. Morelli, and M. Pelizzola. 2016. Integrated Systems for NGS Data Management and Analysis: Open Issues and Available Solutions. *Front. Genet.* 7. doi:10.3389/fgene.2016.00075.

Blackwell, T.K., J. Huang, a Ma, L. Kretzner, F.W. Alt, R.N. Eisenman, and H. Weintraub. 1993. Binding of myc proteins to canonical and noncanonical DNA sequences. *Mol. Cell. Biol.* 13:5216–24. doi:10.1128/MCB.13.9.5216.Updated.

Bochkis, I.M., N.E. Rubins, P. White, E.E. Furth, J.R. Friedman, and K.H. Kaestner. 2008. Hepatocyte-specific ablation of Foxa2 alters bile acid homeostasis and results in endoplasmic reticulum stress. *Nat. Med.* 14:828–836. doi:10.1038/nm.1853.

Boin, A., A. Couvelard, C. Couderc, I. Brito, D. Filipescu, M. Kalamarides, P. Bedossa, L. De Koning, C. Danelsky, T. Dubois, P. Hupé, D. Louvard, and D. Lallemand. 2014. Proteomic screening identifies a YAP-driven signaling network linked to tumor cell proliferation in human schwannomas. *Neuro. Oncol.* 16:1196–1209. doi:10.1093/neuonc/nou020.

Bonzo, J. a., C.H. Ferry, T. Matsubara, J.-H. Kim, and F.J. Gonzalez. 2012. Suppression of Hepatocyte Proliferation by Hepatocyte Nuclear Factor 4 in Adult Mice. *J. Biol. Chem.* 287:7345–7356. doi:10.1074/jbc.M111.334599.

Bookout, A.L., Y. Jeong, M. Downes, R.T. Yu, R.M. Evans, and D.J. Mangelsdorf. 2006. Anatomical Profiling of Nuclear Receptor Expression Reveals a Hierarchical Transcriptional Network. *Cell*. 126:789–799. doi:10.1016/j.cell.2006.06.049.

Bowman, E. a, and W. Kelly. 2014. RNA Polymerase II transcription elongation and Pol II CTD Ser2 phosphorylation: A tail of two kinases. *Nucleus*. 5:1–13. doi:10.4161/nucl.29347.

Burrows, M., and D. Wheeler. 1994. A block-sorting lossless data compression algorithm. *Algorithm, Data Compression*. 18. doi:10.1.1.37.6774.

Cacemiro, M. da C., M.G. Berzoti-Coelho, J.G. Cominal, S.M. Burin, and F.A. de Castro. 2017. Hippo pathway deregulation: implications in the pathogenesis of haematological malignancies. *J. Clin. Pathol.* 70:9–14. doi:10.1136/jclinpath-2016-204055.

Calkin, A.C., and P. Tontonoz. 2012. Transcriptional integration of metabolism by the nuclear sterol-activated receptors LXR and FXR. *Nat. Rev. Mol. Cell Biol.* doi:10.1038/nrm3312.

Calo, E., and J. Wysocka. 2013. Modification of Enhancer Chromatin: What, How, and Why? *Mol. Cell*. 49:825–837. doi:10.1016/j.molcel.2013.01.038.

Camargo, F.D., S. Gokhale, J.B. Johnnidis, D. Fu, G.W. Bell, R. Jaenisch, and T.R. Brummelkamp. 2007. YAP1 Increases Organ Size and Expands Undifferentiated Progenitor Cells. *Curr. Biol.* 17:2054–2060. doi:10.1016/j.cub.2007.10.039.

Carlson, M. 2016. org.Mm.eg.db: Genome wide annotation for Mouse.

Cebola, I., S.A. Rodríguez-Seguí, C.H.-H. Cho, J. Bessa, M. Rovira, M. Luengo, M. Chhatriwala, A. Berry, J. Ponsa-Cobas, M.A. Maestro, R.E. Jennings, L. Pasquali, I. Morán, N. Castro, N.A. Hanley, J.L. Gomez-Skarmeta, L. Vallier, and J. Ferrer. 2015. TEAD and YAP regulate the enhancer network of human embryonic pancreatic progenitors. *Nat. Cell Biol.* 17:615–626. doi:10.1038/ncb3160.

Chan, L.H., W. Wang, W. Yeung, Y. Deng, P. Yuan, and K.K. Mak. 2014. Hedgehog signaling induces osteosarcoma development through Yap1 and H19 overexpression. *Oncogene*. 33:4857–4866. doi:10.1038/onc.2013.433.

Chang, W. 2016. shinydashboard: Create Dashboards with "Shiny."

Chapuy, B., M.R. McKeown, C.Y. Lin, S. Monti, M.G.M. Roemer, J. Qi, P.B. Rahl, H.H. Sun, K.T. Yeda, J.G. Doench, E. Reichert, A.L. Kung, S.J. Rodig, R.A. Young, M.A. Shipp, and J.E. Bradner. 2013. Discovery and Characterization of Super-Enhancer-Associated Dependencies in Diffuse Large B Cell Lymphoma. *Cancer Cell*. 24:777–790. doi:10.1016/j.ccr.2013.11.003.

Chen, H. 2016. VennDiagram: Generate High-Resolution Venn and Euler Plots.

Chen, Q., N. Zhang, R.S. Gray, H. Li, A.J. Ewald, C.A. Zahnow, and D. Pan. 2014. A temporal requirement for Hippo signaling in mammary gland differentiation, growth, and tumorigenesis. *Genes Dev.* 28:432–437. doi:10.1101/gad.233676.113.

Cordenonsi, M., F. Zanconato, L. Azzolin, M. Forcato, A. Rosato, C. Frasson, M. Inui, M. Montagner, A.R. Parenti, A. Poletti, M.G. Daidone, S. Dupont, G. Basso, S. Bicciato, and S. Piccolo. 2011. The hippo transducer TAZ confers cancer stem cell-related traits on breast cancer cells. *Cell*. 147:759–772. doi:10.1016/j.cell.2011.09.048.

Cottini, F., T. Hideshima, C. Xu, M. Sattler, M. Dori, L. Agnelli, E. ten Hacken, M.T. Bertilaccio, E. Antonini, A. Neri, M. Ponzoni, M. Marcatti, P.G. Richardson, R. Carrasco, A.C. Kimmelman, K.-K. Wong, F. Caligaris-Cappio, G. Blandino, W.M. Kuehl, K.C. Anderson, and G. Tonon. 2014. Rescue of Hippo coactivator YAP1 triggers DNA damage–induced apoptosis in hematological cancers. *Nat. Med.*

20:599–606. doi:10.1038/nm.3562.

Creyghton, M.P., A.W. Cheng, G.G. Welstead, T. Kooistra, B.W. Carey, E.J. Steine, J. Hanna, M.A. Lodato, G.M. Frampton, P.A. Sharp, L.A. Boyer, R.A. Young, and R. Jaenisch. 2010. Histone H3K27ac separates active from poised enhancers and predicts developmental state. *Proc. Natl. Acad. Sci.* 107:21931–21936. doi:10.1073/pnas.1016071107.

Croci, O., S. De Fazio, F. Biagioni, E. Donato, M. Caganova, L. Curti, M. Doni, S. Sberna, D. Aldeghi, C. Biancotto, A. Verrecchia, D. Olivero, B. Amati, and S. Campaner. 2017. Transcriptional integration of mitogenic and mechanical signals by Myc and YAP. *Genes Dev.* doi:10.1101/gad.301184.117.

Dang, C. V. 2013. MYC, metabolism, cell growth, and tumorigenesis. *Cold Spring Harb. Perspect. Biol.* 5. doi:10.1101/cshperspect.a014217.

Dang, C. V., L.M.S. Resar, E. Emison, S. Kim, Q. Li, J.E. Prescott, D. Wonsey, and K. Zeller. 1999. Function of the c-Myc Oncogenic Transcription Factor. *Exp. Cell Res.* 253:63–77. doi:10.1006/excr.1999.4686.

Dawson, M. a., R.K. Prinjha, A. Dittman, G. Giotopoulos, M. Bantscheff, W.-I. Chan, S.C. Robson, C. Chung, C. Hopf, M.M. Savitski, C. Huthmacher, E. Gudgin, D. Lugo, S. Beinke, T.D. Chapman, E.J. Roberts, P.E. Soden, K.R. Auger, O. Mirguet, K. Doehner, R. Delwel, A.K. Burnett, P. Jeffrey, G. Drewes, K. Lee, B.J.P. Huntly, T. Kouzarides, and A. Dittmann. 2011. Inhibition of BET recruitment to chromatin as an effective treatment for MLL-fusion leukaemia. Supp data. *Nature*. 478:529–33. doi:10.1038/nature10509.

Dawson, M.I., and Z. Xia. 2012. The retinoid X receptors and their ligands. *Biochim. Biophys. Acta*. 1821:21–56. doi:10.1016/j.bbalip.2011.09.014.

Delmore, J.E., G.C. Issa, M.E. Lemieux, P.B. Rahl, J. Shi, H.M. Jacobs, E. Kastritis, T. Gilpatrick, R.M. Paranal, J. Qi, M. Chesi, A.C. Schinzel, M.R. McKeown, T.P. Heffernan, C.R. Vakoc, P.L. Bergsagel, I.M. Ghobrial, P.G. Richardson, R.A. Young, W.C. Hahn, K.C. Anderson, A.L. Kung, J.E. Bradner, and C.S. Mitsiades. 2011. BET bromodomain inhibition as a therapeutic strategy to target c-Myc. *Cell*. 146:904–917. doi:10.1016/j.cell.2011.08.017.

Demeterco, C., P. Itkin-Ansari, B. Tyrberg, L.P. Ford, R.A. Jarvis, and F. Levine. 2002. c-Myc controls proliferation Versus differentiation in human pancreatic endocrine cells. *J. Clin. Endocrinol. Metab.* 87:3475–3485. doi:10.1210/jc.87.7.3475.

deRan, M., J. Yang, C.H. Shen, E.C. Peters, J. Fitamant, P. Chan, M. Hsieh, S. Zhu, J.M. Asara, B. Zheng, N. Bardeesy, J. Liu, and X. Wu. 2014. Energy stress regulates Hippo-YAP signaling involving AMPK-mediated regulation of angiomotin-like 1 protein. *Cell Rep.* 9:495–503. doi:10.1016/j.celrep.2014.09.036.

Descombes, P., M. Chojkier, S. Lichtsteiner, E. Falvey, and U. Schibler. 1990. LAP, a novel member of the C/EBP gene family, encodes a liver-enriched transcriptional activator protein. *Genes Dev.* 4:1541–1551. doi:10.1101/gad.4.9.1541.

Devaiah, B.N., C. Case-Borden, A. Gegonne, C.H. Hsu, Q. Chen, D. Meerzaman, A. Dey, K. Ozato, and D.S. Singer. 2016. BRD4 is a histone acetyltransferase that evicts nucleosomes from chromatin. *Nat. Struct. Mol. Biol.* 23:540–548. doi:10.1038/nsmb.3228.

Devaiah, B.N., B.A. Lewis, N. Cherman, M.C. Hewitt, B.K. Albrecht, P.G. Robey, K. Ozato, R.J. Sims, and D.S. Singer. 2012. BRD4 is an atypical kinase that phosphorylates Serine2 of the RNA Polymerase II carboxy-terminal domain. *Proc. Natl. Acad. Sci.*

109:6927–6932. doi:10.1073/pnas.1120422109.

Dey, A., A. Nishiyama, T. Karpova, J. McNally, and K. Ozato. 2009. Brd4 Marks Select Genes on Mitotic Chromatin and Directs Postmitotic Transcription. *Mol. Biol. Cell*. 20:4899–4909. doi:10.1091/mbc.E09-05-0380.

Donato, E., O. Croci, A. Sabò, H. Muller, M.J. Morelli, M. Pelizzola, and S. Campaner. 2017. Compensatory RNA polymerase 2 loading determines the efficacy and transcriptional selectivity of JQ1 in Myc-driven tumors. *Leukemia*. 31:479–490. doi:10.1038/leu.2016.182.

Dong, J., G. Feldmann, J. Huang, S. Wu, N. Zhang, S.A. Comerford, M.F. Gayyed, R.A. Anders, A. Maitra, and D. Pan. 2007. Elucidation of a Universal Size-Control Mechanism in Drosophila and Mammals. *Cell*. 130:1120–1133. doi:10.1016/j.cell.2007.07.019.

Dupont, S. 2016. Role of YAP/TAZ in cell-matrix adhesion-mediated signalling and mechanotransduction. *Exp. Cell Res.* 343:42–53. doi:10.1016/j.yexcr.2015.10.034.

Dupont, S., L. Morsut, M. Aragona, E. Enzo, S. Giulitti, M. Cordenonsi, F. Zanconato, J. Le Digabel, M. Forcato, S. Bicciato, N. Elvassore, and S. Piccolo. 2011. Role of YAP/TAZ in mechanotransduction. *Nature*. 474:179–183. doi:10.1038/nature10137.

Edgar, R. 2002. Gene Expression Omnibus: NCBI gene expression and hybridization array data repository. *Nucleic Acids Res.* 30:207–210. doi:10.1093/nar/30.1.207.

Eferl, R., and E.F. Wagner. 2003. AP-1: a double-edged sword in tumorigenesis. *Nat. Rev. Cancer*. 3:859–868. doi:10.1038/nrc1209.

Enzo, E., G. Santinon, A. Pocaterra, M. Aragona, S. Bresolin, M. Forcato, D. Grifoni, A. Pession, F. Zanconato, G. Guzzo, S. Bicciato, and S. Dupont. 2015. Aerobic glycolysis tunes YAP/TAZ transcriptional activity. *EMBO J.* 34:e201490379. doi:10.15252/embj.201490379.

Escot, C., C. Theillet, R. Lidereau, F. Spyratos, M.H. Champeme, J. Gest, and R. Callahan. 1986. Genetic alteration of the c-myc protooncogene (MYC) in human primary breast carcinomas. *Proc. Natl. Acad. Sci. U. S. A.* 83:4834–4838. doi:10.1073/pnas.83.13.4834.

Ewing, B., L. Hillier, M.C. Wendl, and P. Green. 1998. Base-Calling of Automated Sequencer Traces UsingPhred. I. Accuracy Assessment. *Genome Res.* 8:175–185. doi:10.1101/gr.8.3.175.

Fang, B., D. Mane-Padros, E. Bolotin, T. Jiang, and F.M. Sladek. 2012. Identification of a binding motif specific to HNF4 by comparative analysis of multiple nuclear receptors. *Nucleic Acids Res.* 40:5343–5356. doi:10.1093/nar/gks190.

Farina, A., M. Hattori, J. Qin, Y. Nakatani, N. Minato, and K. Ozato. 2004. Bromodomain protein Brd4 binds to GTPase-activating SPA-1, modulating its activity and subcellular localization. *Mol. Cell. Biol.* 24:9059–69. doi:10.1128/MCB.24.20.9059-9069.2004.

Felsher, D.W. 2010. MYC Inactivation Elicits Oncogene Addiction through Both Tumor Cell-Intrinsic and Host-Dependent Mechanisms. *Genes Cancer*. 1:597–604. doi:10.1177/1947601910377798.

Feng, X., M. Degese, R. Iglesias-Bartolome, J.P. Vaque, A.A. Molinolo, M. Rodrigues, M.R. Zaidi, B.R. Ksander, G. Merlino, A. Sodhi, Q. Chen, and J.S. Gutkind. 2014. Hippo-

independent activation of YAP by the GNAQ uveal melanoma oncogene through a Trio-regulated Rho GTPase Signaling Circuitry. *Cancer Cell*. 25:831–845. doi:10.1016/j.ccr.2014.04.016.

Ferragina, P., and G. Manzini. 2000. Opportunistic data structures with applications. *Proceeding FOCS '00 Proc. 41st Annu. Symp. Found. Comput. Sci. FOCS '00 Proc. 41st Annu. Symp. Found. Comput. Sci.* 390–398. doi:10.1109/SFCS.2000.892127.

Filippakopoulos, P., S. Picaud, M. Mangos, T. Keates, J.P. Lambert, D. Barsyte-Lovejoy, I. Felletar, R. Volkmer, S. Müller, T. Pawson, A.C. Gingras, C.H. Arrowsmith, and S. Knapp. 2012. Histone recognition and large-scale structural analysis of the human bromodomain family. *Cell*. 149:214–231. doi:10.1016/j.cell.2012.02.013.

Filippakopoulos, P., J. Qi, S. Picaud, Y. Shen, W.B. Smith, O. Fedorov, E.M. Morse, T. Keates, T.T. Hickman, I. Felletar, M. Philpott, S. Munro, M.R. McKeown, Y. Wang, A.L. Christie, N. West, M.J. Cameron, B. Schwartz, T.D. Heightman, N. La Thangue, C.A. French, O. Wiest, A.L. Kung, S. Knapp, and J.E. Bradner. 2010. Selective inhibition of BET bromodomains. *Nature*. 468:1067–1073. doi:10.1038/nature09504.

Fitamant, J., F. Kottakis, S. Benhamouche, H.S. Tian, N. Chuvin, C.A. Parachoniak, J.M. Nagle, R.M. Perera, M. Lapouge, V. Deshpande, A.X. Zhu, A. Lai, B. Min, Y. Hoshida, J. Avruch, D. Sia, G. Campreciós, A.I. McClatchey, J.M. Llovet, D. Morrissey, L. Raj, and N. Bardeesy. 2015. YAP Inhibition Restores Hepatocyte Differentiation in Advanced HCC, Leading to Tumor Regression. *Cell Rep.* 10:1692–1707. doi:10.1016/j.celrep.2015.02.027.

French, C.A. 2012. Pathogenesis of NUT midline carcinoma. *Annu Rev Pathol*. 7:247–265. doi:10.1146/annurev-pathol-011811-132438.

Fuller, C.W., L.R. Middendorf, S.A. Benner, G.M. Church, T. Harris, X. Huang, S.B. Jovanovich, J.R. Nelson, J.A. Schloss, D.C. Schwartz, and D. V Vezenov. 2009. The challenges of sequencing by synthesis. *Nat. Biotechnol.* 27:1013–1023. doi:10.1038/nbt.1585.

Gabay, M., Y. Li, and D.W. Felsher. 2014. MYC activation is a hallmark of cancer initiation and maintenance. *Cold Spring Harb. Perspect. Med.* 4. doi:10.1101/cshperspect.a014241.

Galli, G.G., M. Carrara, W.C. Yuan, C. Valdes-Quezada, B. Gurung, B. Pepe-Mooney, T. Zhang, G. Geeven, N.S. Gray, W. de Laat, R.A. Calogero, and F.D. Camargo. 2015. YAP Drives Growth by Controlling Transcriptional Pause Release from Dynamic Enhancers. *Mol. Cell*. 60:328–337. doi:10.1016/j.molcel.2015.09.001.

Gartel, A.L., X. Ye, E. Goufman, P. Shianov, N. Hay, F. Najmabadi, and A.L. Tyner. 2001. Myc represses the p21(WAF1/CIP1) promoter and interacts with Sp1/Sp3. *Proc. Natl. Acad. Sci.* 98:4510–4515. doi:10.1073/pnas.081074898.

George, N.M., C.E. Day, B.P. Boerner, R.L. Johnson, and N.E. Sarvetnick. 2012. Hippo Signaling Regulates Pancreas Development through Inactivation of Yap. *Mol. Cell. Biol.* 32:5116–5128. doi:10.1128/MCB.01034-12.

Grandori, C., S.M. Cowley, L.P. James, and R.N. Eisenman. 2000. The Myc/Max/Mad network and the transcriptional control of cell behavior. *Annu. Rev. Cell Dev. Biol.* 16:653–699. doi:10.1146/annurev.cellbio.16.1.653.

Greenstein, S., N.L. Krett, Y. Kurosawa, C. Ma, D. Chauhan, T. Hideshima, K.C. Anderson, and S.T. Rosen. 2003. Characterization of the MM.1 human multiple myeloma (MM) cell lines: A model system to elucidate the characteristics, behavior, and

signaling of steroid-sensitive and -resistant MM cells. *Exp. Hematol.* 31:271–282. doi:10.1016/S0301-472X(03)00023-7.

Gregorieff, A., Y. Liu, M.R. Inanlou, Y. Khomchuk, and J.L. Wrana. 2015. Yap-dependent reprogramming of Lgr5+ stem cells drives intestinal regeneration and cancer. *Nature*. 526:715–718. doi:10.1038/nature15382.

Grijalva, J.L., M. Huizenga, K. Mueller, S. Rodriguez, J. Brazzo, F. Camargo, G. Sadri-Vakili, and K. Vakili. 2014. Dynamic alterations in Hippo signaling pathway and YAP activation during liver regeneration. *AJP Gastrointest. Liver Physiol.* 307:G196–G204. doi:10.1152/ajpgi.00077.2014.

Guenther, M.G., S.S. Levine, L.A. Boyer, R. Jaenisch, and R.A. Young. 2007. A Chromatin Landmark and Transcription Initiation at Most Promoters in Human Cells. *Cell*. 130:77–88. doi:10.1016/j.cell.2007.05.042.

Hansen, C.G., T. Moroishi, and K.L. Guan. 2015. YAP and TAZ: A nexus for Hippo signaling and beyond. *Trends Cell Biol.* 25:499–513. doi:10.1016/j.tcb.2015.05.002.

Hao, Y., A. Chun, K. Cheung, B. Rashidi, and X. Yang. 2008. Tumor suppressor LATS1 is a negative regulator of oncogene YAP. *J. Biol. Chem.* 283:5496–5509. doi:10.1074/jbc.M709037200.

Harvey, K.F., C.M. Pfleger, and I.K. Hariharan. 2003. The Drosophila Mst ortholog, hippo, restricts growth and cell proliferation and promotes apoptosis. *Cell*. 114:457–467. doi:10.1016/S0092-8674(03)00557-9.

Haskins, J.W., D.X. Nguyen, and D.F. Stern. 2014. Neuregulin 1-activated ERBB4 interacts with YAP to induce Hippo pathway target genes and promote cell migration. *Sci. Signal.* 7:ra116-ra116. doi:10.1126/scisignal.2005770.

Hata, S., J. Hirayama, H. Kajiho, K. Nakagawa, Y. Hata, T. Katada, M. Furutani-Seiki, and H. Nishina. 2012. A novel acetylation cycle of transcription co-activator yes-associated protein that is downstream of hippo pathway is triggered in response to S N2 alkylating agents. *J. Biol. Chem.* 287:22089–22098. doi:10.1074/jbc.M111.334714.

Hayden, M.M. and H.P. and V.O. and N. 2016. Rsamtools: Binary alignment (BAM), FASTA, variant call (BCF), and tabix file import.

He, C., D. Mao, G. Hua, X. Lv, X. Chen, P.C. Angeletti, J. Dong, S.W. Remmenga, K.J. Rodabaugh, J. Zhou, P.F. Lambert, P. Yang, J.S. Davis, and C. Wang. 2015. The Hippo/YAP pathway interacts with EGFR signaling and HPV oncoproteins to regulate cervical cancer progression. *EMBO Mol. Med.* 7:1426–49. doi:10.15252/emmm.201404976.

He, M., Z. Zhou, A.A. Shah, Y. Hong, Q. Chen, and Y. Wan. 2016. New insights into posttranslational modifications of Hippo pathway in carcinogenesis and therapeutics. *Cell Div.* 11:4. doi:10.1186/s13008-016-0013-6.

Heallen, T., M. Zhang, J. Wang, M. Bonilla-Claudio, E. Klysik, R.L. Johnson, and J.F. Martin. 2011. Hippo Pathway Inhibits Wnt Signaling to Restrain Cardiomyocyte Proliferation and Heart Size. *Science (80-.).* 332:458–461. doi:10.1126/science.1199010.

Heintzman, N.D., R.K. Stuart, G. Hon, Y. Fu, C.W. Ching, R.D. Hawkins, L.O. Barrera, S. Van Calcar, C. Qu, K.A. Ching, W. Wang, Z. Weng, R.D. Green, G.E. Crawford, and B. Ren. 2007. Distinct and predictive chromatin signatures of transcriptional promoters and enhancers in the human genome. *Nat. Genet.* 39:311–318.

doi:10.1038/ng1966.

Hemann, M.T., A. Bric, J. Teruya-Feldstein, A. Herbst, J.A. Nilsson, C. Cordon-Cardo, J.L. Cleveland, W.P. Tansey, and S.W. Lowe. 2005. Evasion of the p53 tumour surveillance network by tumour-derived MYC mutants. *Nature*. 436:807–811. doi:10.1038/nature03845.

Hermann-Kleiter, N., and G. Baier. 2014. Orphan nuclear receptor NR2F6 acts as an essential gatekeeper of Th17 CD4+ T cell effector functions. *Cell Commun. Signal.* 12:38. doi:10.1186/1478-811X-12-38.

Hessmann, E., G. Schneider, V. Ellenrieder, and J.T. Siveke. 2016. MYC in pancreatic cancer: novel mechanistic insights and their translation into therapeutic strategies. *Oncogene*. 35:1609–1618. doi:10.1038/onc.2015.216.

Hiemer, S.E., A.D. Szymaniak, and X. Varelas. 2014. The transcriptional regulators TAZ and YAP direct transforming growth factor ??-induced tumorigenic phenotypes in breast cancer cells. *J. Biol. Chem.* 289:13461–13474. doi:10.1074/jbc.M113.529115.

Hong, L., Y. Cai, M. Jiang, D. Zhou, and L. Chen. 2015. The Hippo signaling pathway in liver regeneration and tumorigenesis. *Acta Biochim. Biophys. Sin. (Shanghai).* 47:46–52. doi:10.1093/abbs/gmu106.

Horton, J.D., J.L. Goldstein, and M.S. Brown. 2002. SREBPs: Activators of the complete program of cholesterol and fatty acid synthesis in the liver. *J. Clin. Invest.* 109:1125–1131. doi:10.1172/JCI200215593.

Huang, J., S. Wu, J. Barrera, K. Matthews, and D. Pan. 2005. The Hippo signaling pathway coordinately regulates cell proliferation and apoptosis by inactivating Yorkie, the Drosophila homolog of YAP. *Cell*. 122:421–434. doi:10.1016/j.cell.2005.06.007.

Huang, W., X. Lv, C. Liu, Z. Zha, H. Zhang, Y. Jiang, Y. Xiong, Q.Y. Lei, and K.L. Guan. 2012. The N-terminal phosphodegron targets TAZ/WWTR1 protein for SCF β-TrCP-dependent degradation in response to phosphatidylinositol 3-kinase inhibition. *J. Biol. Chem.* 287:26245–26253. doi:10.1074/jbc.M112.382036.

Huber, W., V.J. Carey, R. Gentleman, S. Anders, M. Carlson, B.S. Carvalho, H.C. Bravo, S. Davis, L. Gatto, T. Girke, R. Gottardo, F. Hahne, K.D. Hansen, R.A. Irizarry, M. Lawrence, M.I. Love, J. MacDonald, V. Obenchain, A.K. Oleś, H. Pagès, A. Reyes, P. Shannon, G.K. Smyth, D. Tenenbaum, L. Waldron, and M. Morgan. 2015. Orchestrating high-throughput genomic analysis with Bioconductor. *Nat. Methods*. 12:115–121. doi:10.1038/nmeth.3252.

Imajo, M., M. Ebisuya, and E. Nishida. 2014. Dual role of YAP and TAZ in renewal of the intestinal epithelium. *Nat. Cell Biol.* 17:7–19. doi:10.1038/ncb3084.

Inoue, Y., A.-M. Yu, S.H. Yim, X. Ma, K.W. Krausz, J. Inoue, C.C. Xiang, M.J. Brownstein, G. Eggertsen, I. Björkhem, and F.J. Gonzalez. 2006. Regulation of bile acid biosynthesis by hepatocyte nuclear factor 4alpha. *J. Lipid Res.* 47:215–27. doi:10.1194/jlr.M500430-JLR200.

Inoue, Y., A.M. Yu, J. Inoue, and F.J. Gonzalez. 2004. Hepatocyte Nuclear Factor 4α Is a Central Regulator of Bile Acid Conjugation. *J. Biol. Chem.* 279:2480–2489. doi:10.1074/jbc.M311015200.

Jammula, S., and D. Pasini. 2016. EpiMINE, a computational program for mining epigenomic data. *Epigenetics Chromatin*. 9:42. doi:10.1186/s13072-016-0095-z.

Jang, E.J., H. Jeong, K.H. Han, H.M. Kwon, J.-H. Hong, and E.S. Hwang. 2012. TAZ Suppresses NFAT5 Activity through Tyrosine Phosphorylation. *Mol. Cell. Biol.* 32:4925–4932. doi:10.1128/MCB.00392-12.

Jenkins, R.B., J. Qian, M.M. Lieber, and D.G. Bostwick. 1997. Detection of c-myc oncogene amplification and chromosomal anomalies in metastatic prostatic carcinoma by fluorescence in Situ hybridization. *Cancer Res.* 57:524–531.

Jiang, Q., D. Liu, Y. Gong, Y. Wang, S. Sun, Y. Gui, and H. Song. 2009. yap is required for the development of brain, eyes, and neural crest in zebrafish. *Biochem. Biophys. Res. Commun.* 384:114–119. doi:10.1016/j.bbrc.2009.04.070.

Joshi, S., G. Davidson, S. Le Gras, S. Watanabe, T. Braun, G. Mengus, and I. Davidson. 2017. TEAD transcription factors are required for normal primary myoblast differentiation in vitro and muscle regeneration in vivo. *PLoS Genet.* 13. doi:10.1371/journal.pgen.1006600.

Jung, D., and G. a Kullak-Ublick. 2003. Hepatocyte nuclear factor 1 alpha: a key mediator of the effect of bile acids on gene expression. *Hepatology*. 37:622–31. doi:10.1053/jhep.2003.50100.

Justice, R.W., O. Zilian, D.F. Woods, M. Noll, and P.J. Bryant. 1995. The Drosophila tumor suppressor gene warts encodes a homolog of human myotonic dystrophy kinase and is required for the control of cell shape and proliferation. *Genes Dev.* 9:534–546. doi:10.1101/GAD.9.5.534.

Kanai, F., P.A. Marignani, D. Sarbassova, R. Yagi, R.A. Hall, M. Donowitz, A. Hisaminato, T. Fujiwara, Y. Ito, L.C. Cantley, and M.B. Yaffe. 2000. TAZ: A novel transcriptional co-activator regulated by interactions with 14-3-3 and PDZ domain proteins. *EMBO J.* 19:6778–6791. doi:10.1093/emboj/19.24.6778.

Keshet, R., J. Adler, I. Ricardo Lax, M. Shanzer, Z. Porat, N. Reuven, and Y. Shaul. 2015. c-Abl antagonizes the YAP oncogenic function. *Cell Death Differ.* 22:935–945. doi:10.1038/cdd.2014.182.

Kessler, J.D., K.T. Kahle, T. Sun, K.L. Meerbrey, M.R. Schlabach, E.M. Schmitt, S.O. Skinner, Q. Xu, M.Z. Li, Z.C. Hartman, M. Rao, P. Yu, R. Dominguez-Vidana, A.C. Liang, N.L. Solimini, R.J. Bernardi, B. Yu, T. Hsu, I. Golding, J. Luo, C.K. Osborne, C.J. Creighton, S.G. Hilsenbeck, R. Schiff, C.A. Shaw, S.J. Elledge, and T.F. Westbrook. 2012. A SUMOylation-Dependent Transcriptional Subprogram Is Required for Myc-Driven Tumorigenesis. *Science (80-.).* 335:348–353. doi:10.1126/science.1212728.

Kim, N.G., and B.M. Gumbiner. 2015. Adhesion to fibronectin regulates Hippo signaling via the FAK-Src-PI3K pathway. *J. Cell Biol.* 210:503–515. doi:10.1083/jcb.201501025.

Kim, S. 2015. ppcor: Partial and Semi-Partial (Part) Correlation.

Kim, T.-K., M. Hemberg, J.M. Gray, A.M. Costa, D.M. Bear, J. Wu, D.A. Harmin, M. Laptewicz, K. Barbara-Haley, S. Kuersten, E. Markenscoff-Papadimitriou, D. Kuhl, H. Bito, P.F. Worley, G. Kreiman, and M.E. Greenberg. 2010. Widespread transcription at neuronal activity-regulated enhancers. *Nature*. 465:182–187. doi:10.1038/nature09033.

Kishore, K., S. de Pretis, R. Lister, M.J. Morelli, V. Bianchi, B. Amati, J.R. Ecker, and M. Pelizzola. 2015. methylPipe and compEpiTools: a suite of R packages for the integrative analysis of epigenomics data. *BMC Bioinformatics*. 16:313. doi:10.1186/s12859-015-0742-6.

Kisseberth, W.C., N.T. Brettingen, J.K. Lohse, and E.P. Sandgren. 1999. Ubiquitous expression of marker transgenes in mice and rats. *Dev. Biol.* 214:128–38. doi:10.1006/dbio.1999.9417.

Koh, C.M., C.J. Bieberich, C. V. Dang, W.G. Nelson, S. Yegnasubramanian, and A.M. De Marzo. 2010. MYC and Prostate Cancer. *Genes Cancer*. 1:617–628. doi:10.1177/1947601910379132.

Koh, C.M., A. Sabò, and E. Guccione. 2016. Targeting MYC in cancer therapy: RNA processing offers new opportunities. *BioEssays*. 38:266–275. doi:10.1002/bies.201500134.

Komarnitsky, P., E.J. Cho, and S. Buratowski. 2000. Different phosphorylated forms of RNA polymerase II and associated mRNA processing factors during transcription. *Genes Dev.* 14:2452–2460. doi:10.1101/gad.824700.

Komuro, A., M. Nagai, N.E. Navin, and M. Sudol. 2003. WW domain-containing protein YAP associates with ErbB-4 and acts as a co-transcriptional activator for the carboxyl-terminal fragment of ErbB-4 that translocates to the nucleus. *J. Biol. Chem.* 278:33334–33341. doi:10.1074/jbc.M305597200.

Kress, T.R., P. Pellanda, L. Pellegrinet, V. Bianchi, P. Nicoli, M. Doni, C. Recordati, S. Bianchi, L. Rotta, T. Capra, M. Rava, A. Verrecchia, E. Radaelli, T.D. Littlewood, G.I. Evan, and B. Amati. 2016. Identification of MYC-dependent transcriptional programs in oncogene-addicted liver tumors. *Cancer Res.* 76:3463–3472. doi:10.1158/0008-5472.CAN-16-0316.

Kress, T.R., A. Sabò, and B. Amati. 2015. MYC: connecting selective transcriptional control to global RNA production. *Nat. Rev. Cancer*. 15:593–607. doi:10.1038/nrc3984.

Lai, Z.C., X. Wei, T. Shimizu, E. Ramos, M. Rohrbaugh, N. Nikolaidis, L.L. Ho, and Y. Li. 2005. Control of cell proliferation and apoptosis by mob as tumor suppressor, mats. *Cell*. 120:675–685. doi:10.1016/j.cell.2004.12.036.

Lange, A.W., A. Sridharan, Y. Xu, B.R. Stripp, A.K. Perl, and J.A. Whitsett. 2015. Hippo/Yap signaling controls epithelial progenitor cell proliferation and differentiation in the embryonic and adult lung. *J. Mol. Cell Biol.* 7:35–47. doi:10.1093/jmcb/mju046.

Lapi, E., S. Di Agostino, S. Donzelli, H. Gal, E. Domany, G. Rechavi, P.P. Pandolfi, D. Givol, S. Strano, X. Lu, and G. Blandino. 2008. PML, YAP, and p73 Are Components of a Proapoptotic Autoregulatory Feedback Loop. *Mol. Cell*. 32:803–814. doi:10.1016/j.molcel.2008.11.019.

Lau, A.N., S.J. Curtis, C.M. Fillmore, S.P. Rowbotham, M. Mohseni, D.E. Wagner, A.M. Beede, D.T. Montoro, K.W. Sinkevicius, Z.E. Walton, J. Barrios, D.J. Weiss, F.D. Camargo, K.K. Wong, and C.F. Kim. 2014. Tumor-propagating cells and Yap/Taz activity contribute to lung tumor progression and metastasis. *EMBO J.* 33:468–481. doi:10.1002/embj.201386082.

Lawrence, M., W. Huber, H. Pagès, P. Aboyoun, M. Carlson, R. Gentleman, M.T. Morgan, and V.J. Carey. 2013. Software for Computing and Annotating Genomic Ranges. *PLoS Comput. Biol.* 9. doi:10.1371/journal.pcbi.1003118.

Leclerc, I., C. Lenzner, L. Gourdon, S. Vaulont, A. Kahn, and B. Viollet. 2001. Hepatocyte nuclear factor-4alpha involved in type 1 maturity-onset diabetes of the young is a novel target of AMP-activated protein kinase. *Diabetes*. 50:1515–1521. doi:10.2337/diabetes.50.7.1515.

Lee, C.M., and E.P. Reddy. 1999. The v-myc oncogene. *Oncogene*. 18:2997–3003. doi:10.1038/sj.onc.1202786.

Lee, K.-P., J. Lee, T.-S. Kim, T.-H. Kim, H. Park, J. Byun, M. Kim, W.-I. Jeong, D.F. Calvisi, J.-M. Kim, and D.-S. Lim. 2010. The Hippo-Salvador pathway restrains hepatic oval cell proliferation, liver size, and liver tumorigenesis. *Proc. Natl. Acad. Sci. U. S. A.* 107:8248–8253. doi:10.1073/pnas.0912203107.

Lerdrup, M., J.V. Johansen, S. Agrawal-Singh, and K. Hansen. 2016. An interactive environment for agile analysis and visualization of ChIP-sequencing data. *Nat. Struct. Mol. Biol.* 23:349–357. doi:10.1038/nsmb.3180.

Leung, J.Y., G.L. Ehmann, P.H. Giangrande, and J.R. Nevins. 2008. A role for Myc in facilitating transcription activation by E2F1. *Oncogene*. 27:4172–4179. doi:10.1038/onc.2008.55.

Levy, D., Y. Adamovich, N. Reuven, and Y. Shaul. 2008a. Yap1 Phosphorylation by c-Abl Is a Critical Step in Selective Activation of Proapoptotic Genes in Response to DNA Damage. *Mol. Cell*. 29:350–361. doi:10.1016/j.molcel.2007.12.022.

Levy, D., N. Reuven, and Y. Shaul. 2008b. A regulatory circuit controlling itch-mediated p73 degradation by Runx. *J. Biol. Chem.* 283:27462–27468. doi:10.1074/jbc.M803941200.

Li, H., and R. Durbin. 2009. Fast and accurate short read alignment with Burrows-Wheeler transform. *Bioinformatics*. 25:1754–1760. doi:10.1093/bioinformatics/btp324.

Li, H., and B.M. Gumbiner. 2016. Deregulation of the Hippo pathway in mouse mammary stem cells promotes mammary tumorigenesis. *Mamm. Genome*. 27:556–564. doi:10.1007/s00335-016-9662-7.

Li, Z., Y. Wang, Y. Zhu, C. Yuan, D. Wang, W. Zhang, B. Qi, J. Qiu, X. Song, J. Ye, H. Wu, H. Jiang, L. Liu, Y. Zhang, L.N. Song, J. Yang, and J. Cheng. 2015. The Hippo transducer TAZ promotes epithelial to mesenchymal transition and cancer stem cell maintenance in oral cancer. *Mol. Oncol.* 9:1091–1105. doi:10.1016/j.molonc.2015.01.007.

Lian, I., J. Kim, H. Okazawa, J. Zhao, B. Zhao, J. Yu, A. Chinnaiyan, M.A. Israel, L.S.B. Goldstein, R. Abujarour, S. Ding, and K.L. Guan. 2010. The role of YAP transcription coactivator in regulating stem cell self-renewal and differentiation. *Genes Dev.* 24:1106–1118. doi:10.1101/gad.1903310.

Liao, Y., G.K. Smyth, and W. Shi. 2014. FeatureCounts: An efficient general purpose program for assigning sequence reads to genomic features. *Bioinformatics*. 30:923–930. doi:10.1093/bioinformatics/btt656.

Lin, C., E. Yao, and P.T. Chuang. 2015. A conserved MST1/2-YAP axis mediates Hippo signaling during lung growth. *Dev. Biol.* 403:101–113. doi:10.1016/j.ydbio.2015.04.014.

Littlewood, T.D., D.C. Hancock, P.S. Danielian, M.G. Parker, and G.I. Evan. 1995. A modified oestrogen receptor ligand-binding domain as an improved switch for the regulation of heterologous proteins. *Nucleic Acids Res.* 23:1686–1690. doi:10.1093/nar/23.10.1686.

Liu-Chittenden, Y., B. Huang, J.S. Shim, Q. Chen, S.J. Lee, R.A. Anders, J.O. Liu, and D. Pan. 2012. Genetic and pharmacological disruption of the TEAD-YAP complex suppresses the oncogenic activity of YAP. *Genes Dev.* 26:1300–1305. doi:10.1101/gad.192856.112.

Liu, C.Y., X. Lv, T. Li, Y. Xu, X. Zhou, S. Zhao, Y. Xiong, Q.Y. Lei, and K.L. Guan. 2011. PP1 cooperates with ASPP2 to dephosphorylate and activate TAZ. *J. Biol. Chem.* 286:5558–5566. doi:10.1074/jbc.M110.194019.

Liu, C.Y., Z.Y. Zha, X. Zhou, H. Zhang, W. Huang, D. Zhao, T. Li, S.W. Chan, C.J. Lim, W. Hong, S. Zhao, Y. Xiong, Q.Y. Lei, and K.L. Guan. 2010. The hippo tumor pathway promotes TAZ degradation by phosphorylating a phosphodegron and recruiting the SCFβ-TrCP E3 ligase. *J. Biol. Chem.* 285:37159–37169. doi:10.1074/jbc.M110.152942.

Liu, W., Q. Ma, K. Wong, W. Li, K. Ohgi, J. Zhang, A.K. Aggarwal, and M.G. Rosenfeld. 2013a. Brd4 and JMJD6-associated anti-pause enhancers in regulation of transcriptional pause release. *Cell*. 155:1581–1595. doi:10.1016/j.cell.2013.10.056.

Liu, X., N. Yang, S.A. Figel, K.E. Wilson, C.D. Morrison, I.H. Gelman, and J. Zhang. 2013b. PTPN14 interacts with and negatively regulates the oncogenic function of YAP. *Oncogene*. 32:1266–1273. doi:10.1038/onc.2012.147.

Llado, V., Y. Nakanishi, A. Duran, M. Reina-Campos, P.M. Shelton, J.F. Linares, T. Yajima, A. Campos, P. Aza-Blanc, M. Leitges, M.T. Diaz-Meco, and J. Moscat. 2015. Repression of intestinal stem cell function and tumorigenesis through direct phosphorylation of ?-catenin and yap by PKC? *Cell Rep.* 10:740–754. doi:10.1016/j.celrep.2015.01.007.

Love, M.I., W. Huber, and S. Anders. 2014. Moderated estimation of fold change and dispersion for RNA-seq data with DESeq2. *Genome Biol.* 15:550. doi:10.1186/s13059-014-0550-8.

Lovén, J., H.A. Hoke, C.Y. Lin, A. Lau, D.A. Orlando, C.R. Vakoc, J.E. Bradner, T.I. Lee, and R.A. Young. 2013. Selective inhibition of tumor oncogenes by disruption of super-enhancers. *Cell*. 153:320–334. doi:10.1016/j.cell.2013.03.036.

Lu, L., Y. Li, S.M. Kim, W. Bossuyt, P. Liu, Q. Qiu, Y. Wang, G. Halder, M.J. Finegold, J.-S. Lee, and R.L. Johnson. 2010. Hippo signaling is a potent in vivo growth and tumor suppressor pathway in the mammalian liver. *Proc. Natl. Acad. Sci. U. S. A.* 107:1437–42. doi:10.1073/pnas.0911427107.

Luscher, B. 2001. Function and regulation of the transcription factors of the Myc/Max/Mad network. *Gene*. 277:1–14. doi:S0378111901006977 [pii].

Ma, B., Y. Chen, L. Chen, H. Cheng, C. Mu, J. Li, R. Gao, C. Zhou, L. Cao, J. Liu, Y. Zhu, Q. Chen, and S. Wu. 2014. Hypoxia regulates Hippo signalling through the SIAH2 ubiquitin E3 ligase. *Nat. Cell Biol.* 17:95–103. doi:10.1038/ncb3073.

Mahoney, J.E., M. Mori, A.D. Szymaniak, X. Varelas, and W. V. Cardoso. 2014. The Hippo Pathway Effector Yap Controls Patterning and Differentiation of Airway Epithelial Progenitors. *Dev. Cell*. 30:137–150. doi:10.1016/j.devcel.2014.06.003.

Manderfield, L.J., K.A. Engleka, H. Aghajanian, M. Gupta, S. Yang, L. Li, J.E. Baggs, J.B. Hogenesch, E.N. Olson, and J.A. Epstein. 2014. Pax3 and Hippo Signaling Coordinate Melanocyte Gene Expression in Neural Crest. *Cell Rep.* 9:1885–1896. doi:10.1016/j.celrep.2014.10.061.

Margueron, R., and D. Reinberg. 2011. The Polycomb complex PRC2 and its mark in life. *Nature*. 469:343–349. doi:10.1038/nature09784.

Martinez-Jimenez, C.P., I. Kyrmizi, P. Cardot, F.J. Gonzalez, and I. Talianidis. 2010. Hepatocyte nuclear factor 4alpha coordinates a transcription factor network regulating hepatic fatty acid metabolism. *Mol. Cell. Biol.* 30:565–77.

doi:10.1128/MCB.00927-09.

Mateyak, M.K., A.J. Obaya, and J.M. Sedivy. 1999. c-Myc Regulates Cyclin D-Cdk4 and -Cdk6 Activity but Affects Cell Cycle Progression at Multiple Independent Points. *Mol. Cell. Biol.* 19:4672–4683. doi:10.1128/MCB.19.7.4672.

Mathelier, A., O. Fornes, D.J. Arenillas, C.Y. Chen, G. Denay, J. Lee, W. Shi, C. Shyr, G. Tan, R. Worsley-Hunt, A.W. Zhang, F. Parcy, B. Lenhard, A. Sandelin, and W.W. Wasserman. 2016. JASPAR 2016: A major expansion and update of the open-access database of transcription factor binding profiles. *Nucleic Acids Res.* 44:D110–D115. doi:10.1093/nar/gkv1176.

Mauleon, I., M.N. Lombard, M.J. Muñoz-Alonso, M. Cañelles, and J. Leon. 2004. Kinetics of myc-max-mad Gene Expression during Hepatocyte Proliferation In Vivo: Differential Regulation of mad Family and Stress-Mediated Induction of c-myc. *Mol. Carcinog.* 39:85–90. doi:10.1002/mc.20000.

Mehra, S., H. Messner, M. Minden, and R.S.K. Chaganti. 2002. Molecular cytogenetic characterization of non-Hodgkin lymphoma cell lines. *Genes. Chromosomes Cancer*. 33:225–234. doi:10.1002/gcc.10025.

Mendel, D.B., and G.R. Crabtree. 1991. HNF-1, a member of a novel class of dimerizing homeodomain proteins. *J. Biol. Chem.* 266:677–680.

Meng, Z., T. Moroishi, and K. Guan. 2016. Mechanisms of Hippo pathway regulation. *Genes Dev.* 30:1–17. doi:10.1101/gad.274027.115.1/2.

Mertz, J.A., A.R. Conery, B.M. Bryant, P. Sandy, S. Balasubramanian, D.A. Mele, L. Bergeron, and R.J. Sims. 2011. Targeting MYC dependence in cancer by inhibiting BET bromodomains. *Proc. Natl. Acad. Sci.* 108:16669–16674. doi:10.1073/pnas.1108190108.

Meyer, L.R., A.S. Zweig, A.S. Hinrichs, D. Karolchik, R.M. Kuhn, M. Wong, C.A. Sloan, K.R. Rosenbloom, G. Roe, B. Rhead, B.J. Raney, A. Pohl, V.S. Malladi, C.H. Li, B.T. Lee, K. Learned, V. Kirkup, F. Hsu, S. Heitner, R.A. Harte, M. Haeussler, L. Guruvadoo, M. Goldman, B.M. Giardine, P.A. Fujita, T.R. Dreszer, M. Diekhans, M.S. Cline, H. Clawson, G.P. Barber, D. Haussler, and W.J. Kent. 2013. The UCSC Genome Browser database: Extensions and updates 2013. *Nucleic Acids Res.* 41. doi:10.1093/nar/gks1048.

Mifsud, B., F. Tavares-Cadete, A.N. Young, R. Sugar, S. Schoenfelder, L. Ferreira, S.W. Wingett, S. Andrews, W. Grey, P.A. Ewels, B. Herman, S. Happe, A. Higgs, E. LeProust, G.A. Follows, P. Fraser, N.M. Luscombe, and C.S. Osborne. 2015. Mapping long-range promoter contacts in human cells with high-resolution capture Hi-C. *Nat. Genet.* 47:598–606. doi:10.1038/ng.3286.

Mikkelsen, T.S., M. Ku, D.B. Jaffe, B. Issac, E. Lieberman, G. Giannoukos, P. Alvarez, W. Brockman, T.-K. Kim, R.P. Koche, W. Lee, E. Mendenhall, A. O'Donovan, A. Presser, C. Russ, X. Xie, A. Meissner, M. Wernig, R. Jaenisch, C. Nusbaum, E.S. Lander, and B.E. Bernstein. 2007. Genome-wide maps of chromatin state in pluripotent and lineage-committed cells. *Nature*. 448:553–560. doi:10.1038/nature06008.

Miller, E., J. Yang, M. Deran, C. Wu, A.I. Su, G.M.C. Bonamy, J. Liu, E.C. Peters, and X. Wu. 2012. Identification of serum-derived sphingosine-1-phosphate as a small molecule regulator of YAP. *Chem. Biol.* 19:955–962. doi:10.1016/j.chembiol.2012.07.005.

Misawa, K., T. Horiba, N. Arimura, Y. Hirano, J. Inoue, N. Emoto, H. Shimano, M. Shimizu, and R. Sato. 2003. Sterol regulatory element-binding protein-2 interacts

with hepatocyte nuclear factor-4 to enhance sterol isomerase gene expression in hepatocytes. *J. Biol. Chem.* 278:36176–36182. doi:10.1074/jbc.M302387200.

Mo, J.S., F.X. Yu, R. Gong, J.H. Brown, and K.L. Guan. 2012. Regulation of the Hippo-YAP pathway by protease-activated receptors (PARs). *Genes Dev.* 26:2138–2143. doi:10.1101/gad.197582.112.

Mochizuki, K., A. Nishiyama, K.J. Moon, A. Dey, A. Ghosh, T. Tamura, H. Natsume, H. Yao, and K. Ozato. 2008. The bromodomain protein Brd4 stimulates g1 gene transcription and promotes progression to S phase. *J. Biol. Chem.* 283:9040–9048. doi:10.1074/jbc.M707603200.

Moon, K.J., K. Mochizuki, M. Zhou, H.S. Jeong, J.N. Brady, and K. Ozato. 2005. The bromodomain protein Brd4 is a positive regulatory component of P-TEFb and stimulates RNA polymerase II-dependent transcription. *Mol. Cell*. 19:523–534. doi:10.1016/j.molcel.2005.06.027.

Moustakas, a, S. Souchelnytskyi, and C.H. Heldin. 2001. Smad regulation in TGF-beta signal transduction. *J. Cell Sci.* 114:4359–4369. doi:10.1152/ajpgi.00208.2007.

Müllner, D. 2013. **fastcluster** : Fast Hierarchical, Agglomerative Clustering Routines for *R* and *Python*. *J. Stat. Softw.* 53:1–18. doi:10.18637/jss.v053.i09.

Murphy, D.J., M.R. Junttila, L. Pouyet, A. Karnezis, K. Shchors, D.A. Bui, L. Brown-Swigart, L. Johnson, and G.I. Evan. 2008. Distinct Thresholds Govern Myc's Biological Output In Vivo. *Cancer Cell*. 14:447–457. doi:10.1016/j.ccr.2008.10.018.

Nakato, R., and K. Shirahige. 2017. Recent advances in ChIP-seq analysis: From quality management to whole-genome annotation. *Brief. Bioinform.* 18:279–290. doi:10.1093/bib/bbw023.

Neuwirth, E. 2014. RColorBrewer: ColorBrewer Palettes.

Nguyen, L.T., M.S. Tretiakova, M.R. Silvis, J. Lucas, O. Klezovitch, I. Coleman, H. Bolouri, V.I. Kutyavin, C. Morrissey, L.D. True, P.S. Nelson, and V. Vasioukhin. 2015. ERG Activates the YAP1 Transcriptional Program and Induces the Development of Age-Related Prostate Tumors. *Cancer Cell*. 27:797–808. doi:10.1016/j.ccell.2015.05.005.

Ni, C.-Y. 2001. gamma -Secretase Cleavage and Nuclear Localization of ErbB-4 Receptor Tyrosine Kinase. *Science (80-.).* 294:2179–2181. doi:10.1126/science.1065412.

Nicodeme, E., K.L. Jeffrey, U. Schaefer, S. Beinke, S. Dewell, C. Chung, R. Chandwani, I. Marazzi, P. Wilson, H. Coste, J. White, J. Kirilovsky, C.M. Rice, J.M. Lora, R.K. Prinjha, K. Lee, and A. Tarakhovsky. 2010. Suppression of inflammation by a synthetic histone mimic. *Nature*. 468:1119–1123. doi:10.1038/nature09589.

Niessen, C.M., D. Leckband, and A.S. Yap. 2011. Tissue Organization by Cadherin Adhesion Molecules: Dynamic Molecular and Cellular Mechanisms of Morphogenetic Regulation. *Physiol. Rev.* 91:691–731. doi:10.1152/physrev.00004.2010.

Ocana, K., and D. de Oliveira. 2015. Parallel computing in genomic research: advances and applications. *Adv Appl Bioinform Chem*. 8:23–35. doi:10.2147/AABC.S64482.

Oh, H., and K.D. Irvine. 2008. In vivo regulation of Yorkie phosphorylation and localization. *Development*. 135:1081–1088. doi:10.1242/dev.015255.

Oh, H., M. Slattery, L. Ma, K.P. White, R.S. Mann, and K.D. Irvine. 2014. Yorkie Promotes

Transcription by Recruiting a Histone Methyltransferase Complex. *Cell Rep.* 8:449–459. doi:10.1016/j.celrep.2014.06.017.

Ota, M., and H. Sasaki. 2008. Mammalian Tead proteins regulate cell proliferation and contact inhibition as transcriptional mediators of Hippo signaling. *Development*. 135:4059–4069. doi:10.1242/dev.027151.

Ott, C.J., N. Kopp, L. Bird, R.M. Paranal, J. Qi, T. Bowman, S.J. Rodig, A.L. Kung, J.E. Bradner, and D.M. Weinstock. 2012. BET bromodomain inhibition targets both c-Myc and IL7R in high-risk acute lymphoblastic leukemia. *Blood*. 120:2843–2852. doi:10.1182/blood-2012-02-413021.

Oudhoff, M.J., S.A. Freeman, A.L. Couzens, F. Antignano, E. Kuznetsova, P.H. Min, J.P. Northrop, B. Lehnertz, D. Barsyte-Lovejoy, M. Vedadi, C.H. Arrowsmith, H. Nishina, M.R. Gold, F.M. V Rossi, A.C. Gingras, and C. Zaph. 2013. Control of the Hippo Pathway by Set7-Dependent Methylation of Yap. *Dev. Cell*. 26:188–194. doi:10.1016/j.devcel.2013.05.025.

Pedersen, T.L. 2016. shinyFiles: A Server-Side File System Viewer for Shiny.

Pelengaris, S., T. Littlewood, M. Khan, G. Elia, and G. Evan. 1999. Reversible activation of c-Myc in skin: Induction of a complex neoplastic phenotype by a single oncogenic lesion. *Mol. Cell*. 3:565–577. doi:10.1016/S1097-2765(00)80350-0.

Pérez-Roger, I., D.L. Solomon, a Sewing, and H. Land. 1997. Myc activation of cyclin E/Cdk2 kinase involves induction of cyclin E gene transcription and inhibition of p27(Kip1) binding to newly formed complexes. *Oncogene*. 14:2373–81. doi:10.1038/sj.onc.1201197.

Perna, D., G. Fagà, A. Verrecchia, M.M. Gorski, I. Barozzi, V. Narang, J. Khng, K.C. Lim, W.-K. Sung, R. Sanges, E. Stupka, T. Oskarsson, A. Trumpp, C.-L. Wei, H. Müller, and B. Amati. 2012. Genome-wide mapping of Myc binding and gene regulation in serum-stimulated fibroblasts. *Oncogene*. 31:1695–1709. doi:10.1038/onc.2011.359.

Price, D.H. 2000. P-TEFb, a cyclin-dependent kinase controlling elongation by RNA polymerase II. *Mol. Cell. Biol.* 20:2629–2634. doi:10.1128/MCB.20.8.2629-2634.2000.

R Development Core Team. 2016. R: A Language and Environment for Statistical Computing. *R Found. Stat. Comput. Vienna Austria*. 0:{ISBN} 3-900051-07-0. doi:10.1038/sj.hdy.6800737.

Rahl, P.B., C.Y. Lin, A.C. Seila, R.A. Flynn, S. McCuine, C.B. Burge, P.A. Sharp, and R.A. Young. 2010. C-Myc regulates transcriptional pause release. *Cell*. 141:432–445. doi:10.1016/j.cell.2010.03.030.

Rahman, S., M.E. Sowa, M. Ottinger, J.A. Smith, Y. Shi, J.W. Harper, and P.M. Howley. 2011. The Brd4 Extraterminal Domain Confers Transcription Activation Independent of pTEFb by Recruiting Multiple Proteins, Including NSD3. *Mol. Cell. Biol.* 31:2641–2652. doi:10.1128/MCB.01341-10.

Reginensi, A., R.P. Scott, A. Gregorieff, M. Bagherie-Lachidan, C. Chung, D.S. Lim, T. Pawson, J. Wrana, and H. McNeill. 2013. Yap- and Cdc42-Dependent Nephrogenesis and Morphogenesis during Mouse Kidney Development. *PLoS Genet.* 9. doi:10.1371/journal.pgen.1003380.

Repa, J.J., G. Liang, J. Ou, Y. Bashmakov, J.M.A. Lobaccaro, I. Shimomura, B. Shan, M.S. Brown, J.L. Goldstein, and D.J. Mangelsdorf. 2000. Regulation of mouse sterol regulatory element-binding protein-1c gene (SREBP-1c) by oxysterol receptors,

LXRα and LXRβ. *Genes Dev.* 14:2819–2830. doi:10.1101/gad.844900.

Rhee, J., Y. Inoue, J.C. Yoon, P. Puigserver, M. Fan, F.J. Gonzalez, and B.M. Spiegelman. 2003. Regulation of hepatic fasting response by PPARgamma coactivator-1alpha (PGC-1): Requirement for hepatocyte nuclear factor 4alpha in gluconeogenesis. *Pnas*. 100:4012–4017. doi:10.1073/pnas.0730870100.

Van Riggelen, J., J. Müller, T. Otto, V. Beuger, A. Yetil, P.S. Choi, C. Kosan, T. Möröy, D.W. Felsher, and M. Eilers. 2010. The interaction between Myc and Miz1 is required to antagonize TGFβ-dependent autocrine signaling during lymphoma formation and maintenance. *Genes Dev.* 24:1281–1294. doi:10.1101/gad.585710.

Rodriguez-Boulan, E., and I.G. Macara. 2014. Organization and execution of the epithelial polarity programme. *Nat. Rev. Mol. Cell Biol.* 15:225–242. doi:10.1038/nrm3775.

Romero-Pérez, L., P. Garcia-Sanz, A. Mota, S. Leskelä, M. Hergueta-Redondo, J. Díaz-Martín, M.A. López-García, M.A. Castilla, A. Martínez-Ramírez, R.A. Soslow, X. Matias-Guiu, G. Moreno-Bueno, and J. Palacios. 2015. A role for the transducer of the Hippo pathway, TAZ, in the development of aggressive types of endometrial cancer. *Mod. Pathol.* 28:1492–503. doi:10.1038/modpathol.2015.102.

Rosenbluh, J., D. Nijhawan, A.G. Cox, X. Li, J.T. Neal, E.J. Schafer, T.I. Zack, X. Wang, A. Tsherniak, A.C. Schinzel, D.D. Shao, S.E. Schumacher, B.A. Weir, F. Vazquez, G.S. Cowley, D.E. Root, J.P. Mesirov, R. Beroukhim, C.J. Kuo, W. Goessling, and W.C. Hahn. 2012. β-Catenin-driven cancers require a YAP1 transcriptional complex for survival and tumorigenesis. *Cell*. 151:1457–1473. doi:10.1016/j.cell.2012.11.026.

Sabò, A., T.R. Kress, M. Pelizzola, S. de Pretis, M.M. Gorski, A. Tesi, M.J. Morelli, P. Bora, M. Doni, A. Verrecchia, C. Tonelli, G. Fagà, V. Bianchi, A. Ronchi, D. Low, H. Müller, E. Guccione, S. Campaner, and B. Amati. 2014. Selective transcriptional regulation by Myc in cellular growth control and lymphomagenesis. *Nature*. 511:488–492. doi:10.1038/nature13537.

Salvatori, B., I. Iosue, N. Djodji Damas, A. Mangiavacchi, S. Chiaretti, M. Messina, F. Padula, A. Guarini, I. Bozzoni, F. Fazi, and A. Fatica. 2011. Critical Role of c-Myc in Acute Myeloid Leukemia Involving Direct Regulation of miR-26a and Histone Methyltransferase EZH2. *Genes Cancer*. 2:585–592. doi:10.1177/1947601911416357.

Schlegelmilch, K., M. Mohseni, O. Kirak, J. Pruszak, J.R. Rodriguez, D. Zhou, B.T. Kreger, V. Vasioukhin, J. Avruch, T.R. Brummelkamp, and F.D. Camargo. 2011. Yap1 acts downstream of ??-catenin to control epidermal proliferation. *Cell*. 144:782–795. doi:10.1016/j.cell.2011.02.031.

Schmitz, R., R.M. Young, M. Ceribelli, S. Jhavar, W. Xiao, M. Zhang, G. Wright, A.L. Shaffer, D.J. Hodson, E. Buras, X. Liu, J. Powell, Y. Yang, W. Xu, H. Zhao, H. Kohlhammer, A. Rosenwald, P. Kluin, H.K. Müller-Hermelink, G. Ott, R.D. Gascoyne, J.M. Connors, L.M. Rimsza, E. Campo, E.S. Jaffe, J. Delabie, E.B. Smeland, M.D. Ogwang, S.J. Reynolds, R.I. Fisher, R.M. Braziel, R.R. Tubbs, J.R. Cook, D.D. Weisenburger, W.C. Chan, S. Pittaluga, W. Wilson, T.A. Waldmann, M. Rowe, S.M. Mbulaiteye, A.B. Rickinson, and L.M. Staudt. 2012. Burkitt lymphoma pathogenesis and therapeutic targets from structural and functional genomics. *Nature*. 490:116–120. doi:10.1038/nature11378.

Schwanhausser, B., D. Busse, N. Li, G. Dittmar, J. Schuchhardt, J. Wolf, W. Chen, and M. Selbach. 2011. Global quantification of mammalian gene expression control.

Nature. 473:337–342. doi:10.1038/nature10098.

Sekiya, S., and A. Suzuki. 2011. Direct conversion of mouse fibroblasts to hepatocyte-like cells by defined factors. *Nature*. 475:390–393. doi:10.1038/nature10263.

Semenza, G.L. 2001. Hypoxia-inducible factor 1: Oxygen homeostasis and disease pathophysiology. *Trends Mol. Med.* 7:345–350. doi:10.1016/S1471-4914(01)02090-1.

Shi, Y., Y. Yang, B. Hoang, C. Bardeleben, B. Holmes, J. Gera, and A. Lichtenstein. 2016. Therapeutic potential of targeting IRES-dependent c-myc translation in multiple myeloma cells during ER stress. *Oncogene*. 35:1015–1024. doi:10.1038/onc.2015.156.

Shih, D.Q., M. Bussen, E. Sehayek, M. Ananthanarayanan, B.L. Shneider, F.J. Suchy, S. Shefer, J.S. Bollileni, F.J. Gonzalez, J.L. Breslow, and M. Stoffel. 2001. Hepatocyte nuclear factor-1alpha is an essential regulator of bile acid and plasma cholesterol metabolism. *Nat. Genet.* 27:375–382. doi:10.1038/86871.

Sikora, K., S. Chan, G. Evan, H. Gabra, N. Markham, J. Stewart, and J. Watson. 1987. c-myc oncogene expression in colorectal cancer. *Cancer*. 59:1289–95. doi:10.1002/1097-0142(19870401)59:7<1289::AID-CNCR2820590710>3.0.CO;2-O.

Singhi, A.D., A. Cimino-Mathews, R.B. Jenkins, F. Lan, S.R. Fink, H. Nassar, R. Vang, J.H. Fetting, J. Hicks, S. Sukumar, A.M. De Marzo, and P. Argani. 2012. MYC gene amplification is often acquired in lethal distant breast cancer metastases of unamplified primary tumors. *Mod. Pathol.* 25:378–387. doi:10.1038/modpathol.2011.171.

Slavc, I., R. Ellenbogen, W.H. Jung, G.F. Vawter, C. Kretschmar, H. Grier, and B.R. Korf. 1990. myc gene amplification and expression in primary human neuroblastoma. *Cancer Res*. 50:1459–1463.

Smith, K.N., A.M. Singh, and S. Dalton. 2010. Myc represses primitive endoderm differentiation in pluripotent stem cells. *Cell Stem Cell*. 7:343–354. doi:10.1016/j.stem.2010.06.023.

Song, H., K.K. Mak, L. Topol, K. Yun, J. Hu, L. Garrett, Y. Chen, O. Park, J. Chang, R.M. Simpson, C.-Y. Wang, B. Gao, J. Jiang, and Y. Yang. 2010. Mammalian Mst1 and Mst2 kinases play essential roles in organ size control and tumor suppression. *Proc. Natl. Acad. Sci.* 107:1431–1436. doi:10.1073/pnas.0911409107.

Song, L., and G.E. Crawford. 2010. DNase-seq: A high-resolution technique for mapping active gene regulatory elements across the genome from mammalian cells. *Cold Spring Harb. Protoc.* 5. doi:10.1101/pdb.prot5384.

Sorrentino, G., N. Ruggeri, V. Specchia, M. Cordenonsi, M. Mano, S. Dupont, A. Manfrin, E. Ingallina, R. Sommaggio, S. Piazza, A. Rosato, S. Piccolo, and G. Del Sal. 2014. Metabolic control of YAP and TAZ by the mevalonate pathway. *Nat. Cell Biol.* 16:357–366. doi:10.1038/ncb2936.

Soucek, L., and G.I. Evan. 2010. The ups and downs of Myc biology. *Curr. Opin. Genet. Dev.* 20:91–95. doi:10.1016/j.gde.2009.11.001.

Soucek, L., M. Helmer-Citterich, A. Sacco, R. Jucker, G. Cesareni, and S. Nasi. 1998. Design and properties of a Myc derivative that efficiently homodimerizes. *Oncogene*. 17:2463–2472. doi:10.1038/sj.onc.1202199.

de Souza, C.R.T., M.F. Leal, D.Q. Calcagno, E.K. Costa Sozinho, B. do N. Borges, R.C.

Montenegro, Â.K.C.R. dos Santos, S.E.B. dos Santos, H.F. Ribeiro, P.P. Assumpção, M. de Arruda Cardoso Smith, and R.R. Burbano. 2013. MYC Deregulation in Gastric Cancer and Its Clinicopathological Implications. *PLoS One*. 8. doi:10.1371/journal.pone.0064420.

Srinivasan, M.D. and A. 2017. data.table: Extension of `data.frame`.

Stein, C., A.F. Bardet, G. Roma, S. Bergling, I. Clay, A. Ruchti, C. Agarinis, T. Schmelzle, T. Bouwmeester, D. Schübeler, and A. Bauer. 2015. YAP1 Exerts Its Transcriptional Control via TEAD-Mediated Activation of Enhancers. *PLoS Genet.* 11. doi:10.1371/journal.pgen.1005465.

Subramanian, A., P. Tamayo, V.K. Mootha, S. Mukherjee, B.L. Ebert, M.A. Gillette, A. Paulovich, S.L. Pomeroy, T.R. Golub, E.S. Lander, and J.P. Mesirov. 2005. Gene set enrichment analysis: A knowledge-based approach for interpreting genome-wide expression profiles. *Proc. Natl. Acad. Sci.* 102:15545–15550. doi:10.1073/pnas.0506580102.

Swinton, J. 2013. Vennerable: Venn and Euler area-proportional diagrams.

Takahashi, K., and S. Yamanaka. 2006. Induction of Pluripotent Stem Cells from Mouse Embryonic and Adult Fibroblast Cultures by Defined Factors. *Cell*. 126:663–676. doi:10.1016/j.cell.2006.07.024.

Tapon, N., K.F. Harvey, D.W. Bell, D.C.R. Wahrer, T.A. Schiripo, D.A. Haber, and I.K. Hariharan. 2002. salvador promotes both cell cycle exit and apoptosis in Drosophila and is mutated in human cancer cell lines. *Cell*. 110:467–478. doi:10.1016/S0092-8674(02)00824-3.

Tirona, R.G., W. Lee, B.F. Leake, L.B. Lan, C.B. Cline, V. Lamba, F. Parviz, S.A. Duncan, Y. Inoue, F.J. Gonzalez, E.G. Schuetz, and R.B. Kim. 2003. The orphan nuclear receptor HNF4alpha determines PXR and CAR mediated xenobiotic induction of CYP3A4. *Nat. Med.* 9:220–224.

Toyoshima, M., H.L. Howie, M. Imakura, R.M. Walsh, J.E. Annis, A.N. Chang, J. Frazier, B.N. Chau, A. Loboda, P.S. Linsley, M.A. Cleary, J.R. Park, and C. Grandori. 2012. Functional genomics identifies therapeutic targets for MYC-driven cancer. *Proc. Natl. Acad. Sci.* 109:9545–9550. doi:10.1073/pnas.1121119109.

Trapnell, C., L. Pachter, and S.L. Salzberg. 2009. TopHat: Discovering splice junctions with RNA-Seq. *Bioinformatics*. 25:1105–1111. doi:10.1093/bioinformatics/btp120.

Tremblay, A.M., E. Missiaglia, G.G. Galli, S. Hettmer, R. Urcia, M. Carrara, R.N. Judson, K. Thway, G. Nadal, J.L. Selfe, G. Murray, R.A. Calogero, C. DeBari, P.S. Zammit, M. Delorenzi, A.J. Wagers, J. Shipley, H. Wackerhage, and F.D. Camargo. 2014. The Hippo transducer YAP1 transforms activated satellite cells and is a potent effector of embryonal rhabdomyosarcoma formation. *Cancer Cell*. 26:273–287. doi:10.1016/j.ccr.2014.05.029.

Trumpp, A., Y. Refaeli, T. Oskarsson, S. Gasser, M. Murphy, G.R. Martin, and J.M. Bishop. 2001. c-Myc regulates mammalian body size by controlling cell number but not cell size. *Nature*. 414:768–773. doi:10.1038/414768a.

Varelas, X. 2014. The Hippo pathway effectors TAZ and YAP in development, homeostasis and disease. *Development*. 141:1614–1626. doi:10.1242/dev.102376.

Varelas, X., R. Sakuma, P. Samavarchi-Tehrani, R. Peerani, B.M. Rao, J. Dembowy, M.B. Yaffe, P.W. Zandstra, and J.L. Wrana. 2008. TAZ controls Smad nucleocytoplasmic

shuttling and regulates human embryonic stem-cell self-renewal. *Nat. Cell Biol.* 10:837–848. doi:10.1038/ncb1748.

Varelas, X., P. Samavarchi-Tehrani, M. Narimatsu, A. Weiss, K. Cockburn, B.G. Larsen, J. Rossant, and J.L. Wrana. 2010. The Crumbs Complex Couples Cell Density Sensing to Hippo-Dependent Control of the TGF-β-SMAD Pathway. *Dev. Cell*. 19:831–844. doi:10.1016/j.devcel.2010.11.012.

Walhout, A.J.M., J.M. Gubbels, R. Bernards, P.C. Van Der Vliet, and H.T.M. Timmers. 1997. C-Myc/Max heterodimers bind cooperatively to the E-box sequences located in the first intron of the rat ornithine decarboxylase (ODC) gene. *Nucleic Acids Res.* 25:1493–1501. doi:10.1093/nar/25.8.1493.

Walz, S., F. Lorenzin, J. Morton, K.E. Wiese, B. von Eyss, S. Herold, L. Rycak, H. Dumay-Odelot, S. Karim, M. Bartkuhn, F. Roels, T. Wüstefeld, M. Fischer, M. Teichmann, L. Zender, C.-L. Wei, O. Sansom, E. Wolf, and M. Eilers. 2014. Activation and repression by oncogenic MYC shape tumour-specific gene expression profiles. *Nature*. 511:483–487. doi:10.1038/nature13473.

Wang, J., Y. Xiao, C.-W. Hsu, I.M. Martinez-Traverso, M. Zhang, Y. Bai, M. Ishii, R.E. Maxson, E.N. Olson, M.E. Dickinson, J.D. Wythe, and J.F. Martin. 2016. Yap and Taz play a crucial role in neural crest-derived craniofacial development. *Development*. 143:504–515. doi:10.1242/dev.126920.

Wang, R., C.P. Dillon, L.Z. Shi, S. Milasta, R. Carter, D. Finkelstein, L.L. McCormick, P. Fitzgerald, H. Chi, J. Munger, and D.R. Green. 2011. The Transcription Factor Myc Controls Metabolic Reprogramming upon T Lymphocyte Activation. *Immunity*. 35:871–882. doi:10.1016/j.immuni.2011.09.021.

Wang, W., Z.-D. Xiao, X. Li, K.E. Aziz, B. Gan, R.L. Johnson, and J. Chen. 2015. AMPK modulates Hippo pathway activity to regulate energy homeostasis. *Nat. Cell Biol.* 17:490–499. doi:10.1038/ncb3113.

Wang, Z., M. Gerstein, and M. Snyder. 2009. RNA-Seq: a revolutionary tool for transcriptomics. *Nat. Rev. Genet.* 10:57–63. doi:10.1038/nrg2484.

Welcker, M., A. Orian, J. Jin, J.E. Grim, J.A. Grim, J.W. Harper, R.N. Eisenman, and B.E. Clurman. 2004. The Fbw7 tumor suppressor regulates glycogen synthase kinase 3 phosphorylation-dependent c-Myc protein degradation. *Proc. Natl. Acad. Sci. U. S. A.* 101:9085–90. doi:10.1073/pnas.0402770101.

Wells, C.D., J.P. Fawcett, A. Traweger, Y. Yamanaka, M. Goudreault, K. Elder, S. Kulkarni, G. Gish, C. Virag, C. Lim, K. Colwill, A. Starostine, P. Metalnikov, and T. Pawson. 2006. A Rich1/Amot Complex Regulates the Cdc42 GTPase and Apical-Polarity Proteins in Epithelial Cells. *Cell*. 125:535–548. doi:10.1016/j.cell.2006.02.045.

Wennmann, D.O., B. Vollenbröker, A.K. Eckart, J. Bonse, F. Erdmann, D.A. Wolters, L.K. Schenk, U. Schulze, J. Kremerskothen, T. Weide, and H. Pavenstädt. 2014. The Hippo pathway is controlled by Angiotensin II signaling and its reactivation induces apoptosis in podocytes. *Cell Death Dis.* 5:e1519. doi:10.1038/cddis.2014.476.

Wey, A., and P.S. Knoepfler. 2010. C-myc and N-myc in the developing brain. *Aging (Albany. NY).* 2:261–262.

Whyte, W.A., D.A. Orlando, D. Hnisz, B.J. Abraham, C.Y. Lin, M.H. Kagey, P.B. Rahl, T.I. Lee, and R.A. Young. 2013. Master transcription factors and mediator establish super-enhancers at key cell identity genes. *Cell*. 153:307–319.

doi:10.1016/j.cell.2013.03.035.

Wilson, K.E., Y.W. Li, N. Yang, H. Shen, A.R. Orillion, and J. Zhang. 2014. PTPN14 forms a complex with Kibra and LATS1 proteins and negatively regulates the YAP oncogenic function. *J. Biol. Chem.* 289:23693–23700. doi:10.1074/jbc.M113.534701.

Winston Chang, Joe Cheng, JJ Allaire, Y.X. and J., and McPherson. 2017. shiny: Web Application Framework for R.

Wolfrum, C., E. Asilmaz, E. Luca, J.M. Friedman, and M. Stoffel. 2004. Foxa2 regulates lipid metabolism and ketogenesis in the liver during fasting and in diabetes. *Nature*. 432:1027–1032. doi:10.1038/nature03047.

Wu, S., J. Huang, J. Dong, and D. Pan. 2003. hippo encodes a Ste-20 family protein kinase that restricts cell proliferation and promotes apoptosis in conjunction with salvador and warts. *Cell*. 114:445–456. doi:10.1016/S0092-8674(03)00549-X.

Wu, X., D. Liu, D. Tao, W. Xiang, X. Xiao, M. Wang, L. Wang, G. Luo, Y. Li, F. Zeng, and G. Jiang. 2016. BRD4 Regulates EZH2 Transcription through Upregulation of C-MYC and Represents a Novel Therapeutic Target in Bladder Cancer. *Mol. Cancer Ther.* 15:1029–1042. doi:10.1158/1535-7163.MCT-15-0750.

Xiang, L., D.M. Gilkes, H. Hu, N. Takano, W. Luo, H. Lu, J.W. Bullen, D. Samanta, H. Liang, and G.L. Semenza. 2014. Hypoxia-inducible factor 1 mediates TAZ expression and nuclear localization to induce the breast cancer stem cell phenotype. *Oncotarget*. 5:12509–27. doi:10.18632/oncotarget.2997.

Xiao, G., S. Mao, G. Baumgarten, J. Serrano, M.C. Jordan, K.P. Roos, M.C. Fishbein, and W.R. MacLellan. 2001. Inducible Activation of c-Myc in Adult Myocardium In Vivo Provokes Cardiac Myocyte Hypertrophy and Reactivation of DNA Synthesis. *Circ. Res.* 89:1122–1129. doi:10.1161/hh2401.100742.

Xiao, H., N. Jiang, B. Zhou, Q. Liu, and C. Du. 2015. TAZ regulates cell proliferation and epithelial-mesenchymal transition of human hepatocellular carcinoma. *Cancer Sci.* 106:151–159. doi:10.1111/cas.12587.

Xiao, W., J. Wang, C. Ou, Y. Zhang, L. Ma, W. Weng, Q. Pan, and F. Sun. 2013. Mutual interaction between YAP and c-Myc is critical for carcinogenesis in liver cancer. *Biochem. Biophys. Res. Commun.* 439:167–172. doi:10.1016/j.bbrc.2013.08.071.

Xin, M., Y. Kim, L.B. Sutherland, M. Murakami, X. Qi, J. McAnally, E.R. Porrello, A.I. Mahmoud, W. Tan, J.M. Shelton, J.A. Richardson, H.A. Sadek, R. Bassel-Duby, and E.N. Olson. 2013. Hippo pathway effector Yap promotes cardiac regeneration. *Proc. Natl. Acad. Sci.* 110:13839–13844. doi:10.1073/pnas.1313192110.

Xu, J., Y. Chen, and O.I. Olopade. 2010. MYC and Breast Cancer. *Genes Cancer*. 1:629–640. doi:10.1177/1947601910378691.

Xu, M.Z., T.J. Yao, N.P.Y. Lee, I.O.L. Ng, Y.T. Chan, L. Zender, S.W. Lowe, R.T.P. Poon, and J.M. Luk. 2009. Yes-associated protein is an independent prognostic marker in hepatocellular carcinoma. *Cancer*. 115:4576–4585. doi:10.1002/cncr.24495.

Yagi, R., L.F. Chen, K. Shigesada, Y. Murakami, and Y. Ito. 1999. A WW domain-containing Yes-associated protein (YAP) is a novel transcriptional co-activator. *EMBO J.* 18:2551–2562. doi:10.1093/emboj/18.9.2551.

Yan, Y., S.P. Sung, S. Janz, and L.A. Eckhardt. 2007. In a model of immunoglobulin heavy-chain (IGH)/MYC translocation, the Igh 3′ regulatory region induces MYC

expression at the immature stage of B cell development. *Genes Chromosom. Cancer*. 46:950–959. doi:10.1002/gcc.20480.

Yang, Z., J.H.N. Yik, R. Chen, N. He, K.J. Moon, K. Ozato, and Q. Zhou. 2005. Recruitment of P-TEFb for stimulation of transcriptional elongation by the bromodomain protein Brd4. *Mol. Cell*. 19:535–545. doi:10.1016/j.molcel.2005.06.029.

Ye, T., A.R. Krebs, M.A. Choukrallah, C. Keime, F. Plewniak, I. Davidson, and L. Tora. 2011. seqMINER: An integrated ChIP-seq data interpretation platform. *Nucleic Acids Res.* 39. doi:10.1093/nar/gkq1287.

Yimlamai, D., C. Christodoulou, G.G. Galli, K. Yanger, B. Pepe-Mooney, B. Gurung, K. Shrestha, P. Cahan, B.Z. Stanger, and F.D. Camargo. 2014. Hippo pathway activity influences liver cell fate. *Cell*. 157:1324–1338. doi:10.1016/j.cell.2014.03.060.

Yimlamai, D., B.H. Fowl, and F.D. Camargo. 2015. Emerging evidence on the role of the Hippo/YAP pathway in liver physiology and cancer. *J. Hepatol.* 63:1491–1501. doi:10.1016/j.jhep.2015.07.008.

Yin, X.Y., L. Grove, N.S. Datta, K. Katula, M.W. Long, and E. V. Prochownik. 2001. Inverse regulation of cyclin B1 by c-Myc and p53 and induction of tetraploidy by cyclin B1 overexpression. *Cancer Res.* 61:6487–6493.

Yoshihama, Y., K. Chida, and S. Ohno. 2012. The KIBRA-aPKC connection: A potential regulator of membrane trafficking and cell polarity. *Commun. Integr. Biol.* 5:146–151. doi:10.4161/cib.18849.

Yu, F.X., and K.L. Guan. 2013. The Hippo pathway: Regulators and regulations. *Genes Dev.* 27:355–371. doi:10.1101/gad.210773.112.

Yu, F.X., Y. Zhang, H.W. Park, J.L. Jewell, Q. Chen, Y. Deng, D. Pan, S.S. Taylor, Z.C. Lai, and K.L. Guan. 2013. Protein kinase A activates the Hippo pathway to modulate cell proliferation and differentiation. *Genes Dev.* 27:1223–1232. doi:10.1101/gad.219402.113.

Yu, F.X., B. Zhao, and K.L. Guan. 2015. Hippo Pathway in Organ Size Control, Tissue Homeostasis, and Cancer. *Cell*. 163:811–828. doi:10.1016/j.cell.2015.10.044.

Yu, F.X., B. Zhao, N. Panupinthu, J.L. Jewell, I. Lian, L.H. Wang, J. Zhao, H. Yuan, K. Tumaneng, H. Li, X.D. Fu, G.B. Mills, and K.L. Guan. 2012. Regulation of the Hippo-YAP pathway by G-protein-coupled receptor signaling. *Cell*. 150:780–791. doi:10.1016/j.cell.2012.06.037.

Zambelli, F., G. Pesole, and G. Pavesi. 2013. PscanChIP: Finding over-represented transcription factor-binding site motifs and their correlations in sequences from ChIP-Seq experiments. *Nucleic Acids Res.* 41. doi:10.1093/nar/gkt448.

Zanconato, F., M. Cordenonsi, and S. Piccolo. 2016. YAP/TAZ at the Roots of Cancer. *Cancer Cell*. 29:783–803. doi:10.1016/j.ccell.2016.05.005.

Zanconato, F., M. Forcato, G. Battilana, L. Azzolin, E. Quaranta, B. Bodega, A. Rosato, S. Bicciato, M. Cordenonsi, and S. Piccolo. 2015. Genome-wide association between YAP/TAZ/TEAD and AP-1 at enhancers drives oncogenic growth. *Nat. Cell Biol.* 17:1218–1227. doi:10.1038/ncb3216.

Zhang, H., C.Y. Liu, Z.Y. Zha, B. Zhao, J. Yao, S. Zhao, Y. Xiong, Q.Y. Lei, and K.L. Guan. 2009a. TEAD transcription factors mediate the function of TAZ in cell growth and epithelial-mesenchymal transition. *J. Biol. Chem.* 284:13355–13362. doi:10.1074/jbc.M900843200.

Zhang, L., X. Chen, S. Stauffer, S. Yang, Y. Chen, and J. Dong. 2015a. CDK1

phosphorylation of TAZ in mitosis inhibits its oncogenic activity. *Oncotarget*. 6:31399–31412. doi:10.18632/oncotarget.5189.

Zhang, P., Z. Dong, J. Cai, C. Zhang, Z. Shen, A. Ke, D. Gao, J. Fan, and G. Shi. 2015b. BRD4 promotes tumor growth and epithelial-mesenchymal transition in hepatocellular carcinoma. *Int. J. Immunopathol. Pharmacol.* 28:36–44. doi:10.1177/0394632015572070.

Zhang, W., Y. Gao, P. Li, Z. Shi, T. Guo, F. Li, X. Han, Y. Feng, C. Zheng, Z. Wang, F. Li, H. Chen, Z. Zhou, L. Zhang, and H. Ji. 2014. VGLL4 functions as a new tumor suppressor in lung cancer by negatively regulating the YAP-TEAD transcriptional complex. *Cell Res.* 24:331–343. doi:10.1038/cr.2014.10.

Zhang, X., Y.-L. Ge, and R.-H. Tian. 2009b. The knockdown of c-myc expression by RNAi inhibits cell proliferation in human colon cancer HT-29 cells in vitro and in vivo. *Cell. Mol. Biol. Lett.* 14:305–18. doi:10.2478/s11658-009-0001-9.

Zhang, Y., T. Liu, C.A. Meyer, J. Eeckhoute, D.S. Johnson, B.E. Bernstein, C. Nussbaum, R.M. Myers, M. Brown, W. Li, and X.S. Liu. 2008. Model-based Analysis of ChIP-Seq (MACS). *Genome Biol.* 9:R137. doi:10.1186/gb-2008-9-9-r137.

Zhao, B., L. Li, Q. Lei, and K.L. Guan. 2010a. The Hippo-YAP pathway in organ size control and tumorigenesis: An updated version. *Genes Dev.* 24:862–874. doi:10.1101/gad.1909210.

Zhao, B., L. Li, Q. Lu, L.H. Wang, C.Y. Liu, Q. Lei, and K.L. Guan. 2011. Angiomotin is a novel Hippo pathway component that inhibits YAP oncoprotein. *Genes Dev.* 25:51–63. doi:10.1101/gad.2000111.

Zhao, B., L. Li, K. Tumaneng, C.Y. Wang, and K.L. Guan. 2010b. A coordinated phosphorylation by Lats and CK1 regulates YAP stability through SCFβ-TRCP. *Genes Dev.* 24:72–85. doi:10.1101/gad.1843810.

Zhao, B., X. Ye, J. Yu, L. Li, W. Li, S. Li, J. Yu, J.D. Lin, C.Y. Wang, A.M. Chinnaiyan, Z.C. Lai, and K.L. Guan. 2008. TEAD mediates YAP-dependent gene induction and growth control. *Genes Dev.* 22:1962–1971. doi:10.1101/gad.1664408.

Zhao, K., C. Shen, Y. Lu, Z. Huang, L. Li, C.D. Rand, J. Pan, X.-D. Sun, Z. Tan, H. Wang, G. Xing, Y. Cao, G. Hu, J. Zhou, W.-C. Xiong, and L. Mei. 2017. Muscle Yap Is a Regulator of Neuromuscular Junction Formation and Regeneration. *J. Neurosci.* 37:3465–3477. doi:10.1523/JNEUROSCI.2934-16.2017.

Zhou, D., C. Conrad, F. Xia, J.S. Park, B. Payer, Y. Yin, G.Y. Lauwers, W. Thasler, J.T. Lee, J. Avruch, and N. Bardeesy. 2009. Mst1 and Mst2 Maintain Hepatocyte Quiescence and Suppress Hepatocellular Carcinoma Development through Inactivation of the Yap1 Oncogene. *Cancer Cell*. 16:425–438. doi:10.1016/j.ccr.2009.09.026.

Zhou, D., Y. Zhang, H. Wu, E. Barry, Y. Yin, E. Lawrence, D. Dawson, J.E. Willis, S.D. Markowitz, F.D. Camargo, and J. Avruch. 2011. Mst1 and Mst2 protein kinases restrain intestinal stem cell proliferation and colonic tumorigenesis by inhibition of Yes-associated protein (Yap) overabundance. *Proc. Natl. Acad. Sci. U. S. A.* 108:1312–1320. doi:10.1073/pnas.1110428108.

Zuber, J., J. Shi, E. Wang, A.R. Rappaport, H. Herrmann, E.A. Sison, D. Magoon, J. Qi, K. Blatt, M. Wunderlich, M.J. Taylor, C. Johns, A. Chicas, J.C. Mulloy, S.C. Kogan, P. Brown, P. Valent, J.E. Bradner, S.W. Lowe, and C.R. Vakoc. 2011. RNAi screen identifies Brd4 as a therapeutic target in acute myeloid leukaemia. *Nature*. 478:524–528. doi:10.1038/nature10334.

Acknowledgements

I would like to thank Stefano for giving me the opportunity to work in his group.

I want to thank all the past and present members of STC group (Serena, Elisa, Francesca, Chiara, Marieta, Sara, Manuel, Deborah, Silvia, Luca, Laura, Lira) for the scientific support.

I want to thank Bruno, all the past and present members of his group (especially Chiara, Alessandro, Mirko) and the past and present members of the bioinformatics community (Luciano, Jole, Mattia, Marco, Luca, Arnaud, Kamal, Nami, Francesco, Vera, Eugenia, Valerio, Ganesh, Giorgio, Stefano, Elena, Fernando, Ines, Marco) for precious advices in bioinformatics, scientific support and for making my life at campus great.

Finally, I want to thank Francesca and Veronica for the great help in these four years.